TOWARDS THE ELECTROCATALYTIC OXIDATION OF SUGAR ALCOHOLS, SACCHARIDES AND POLYSACCHARIDES

Matthijs P. J. M. van der Ham

Propositions belonging to the thesis, entitled

TOWARDS THE ELECTROCATALYTIC OXIDATION OF SUGAR ALCOHOLS, SACCHARIDES AND POLYSACCHARIDES

1. Basic chemical knowledge of biomass-based molecules is often lacking. (this thesis)

2. The development of analytical protocols to study the conversion of biomass-based molecules is severely undervalued. (this thesis)

3. The promotion of long-term research results in more groundbreaking innovations.

4. Including science at elementary school will increase the credibility of scientific research.

5. Adding social and environmental costs to the price of goods will speed up the formation of a sustainable industry.

6. Nature can only be protected if it becomes a legal entity.

Matthijs P. J. M. van der Ham
Wageningen, 19 January 2024

TOWARDS THE ELECTROCATALYTIC OXIDATION OF SUGAR ALCOHOLS, SACCHARIDES AND POLYSACCHARIDES

Matthijs P. J. M. van der Ham

Thesis committee

Promotor

Prof. Dr. J.H. (Harry) Bitter

Professor of Biobased Chemistry & Technology

Wageningen University & Research

Co-promotors

Prof. Dr. M.T.M. (Marc) Koper

Professor of Catalysis and Surface Chemistry

Leiden University

Dr. T. (Tomas) van Haasterecht

Researcher at Biobased Chemistry & Technology

Wageningen University & Research

Other members

Prof. Dr. Ir. J. (Jasper) van der Gucht, Wageningen University & Research, NL

Prof. Dr. K.B. (Boniface) Kokoh, University of Poitiers, FR

Prof. Dr. J. (Jean-Paul) Lange, University of Twente, NL

Dr. M. (Marta) Costa Figueiredo, Eindhoven University of Technology, NL

This research was conducted under the auspices of the VLAG graduate school (Biobased, Biomolecular, Chemical, Food, and Nutrition sciences)

TOWARDS THE ELECTROCATALYTIC OXIDATION OF SUGAR ALCOHOLS, SACCHARIDES AND POLYSACCHARIDES

Matthijs P. J. M. van der Ham

Table of contents

CHAPTER 1

General Introduction

1.1 Towards a sustainable chemical industry

Fossil-based resources are currently used for most of the global energy demand (86 %) and organic chemicals (96 %).[1] However, fossil-based resources are unsustainable and lead to the emission of greenhouse and/or polluting gases, such as CO_2, CH_4, NO_X, inflicting environmental and health damage. As a result, there is an ongoing transition towards renewable energy sources and renewable carbon-based feedstocks for the production of chemicals. These energy sources and carbon-based feedstocks should be environmentally friendly, cheap, and readily available.[2,3] Carbon-based feedstocks that match these criteria include CO_2[4] and biomass derived from non-edible agricultural waste streams[3,5,6] or side streams from the food processing industry.[7,8] Renewable energy sources include wind energy, solar energy, and hydropower, while non-renewable energy sources like nuclear power might play a crucial role in the energy transition.[9] Thus to move towards a sustainable chemical industry, renewable carbon-based feedstocks are needed and conversions need to be driven by renewable energy. In this thesis, I will focus on electrochemical catalysis for (poly)saccharide oxidation.

1.2 The origin of biofeedstocks for chemical synthesis

Biofeedstocks can be processed to obtain biomass-based platform molecules such as glycerol and glucose but also larger molecules like starch are interesting. These biomass-based (platform) molecules can be modified for the synthesis of a large range of platform and speciality chemicals, such as lactic acid,[10] sorbitol,[11] gluconic acid,[12] glucaric acid,[13] and anionic starch.[14]

Glycerol can be obtained from hydrolysis fats and (waste cooking) oils.[15] This process is used for the production of bio-diesel [15] and yields approximately 4.2 million tons of glycerol annually and globally as a by-product.[16] By contrast, saccharides can be obtained from lignocellulosic biomass derived from agricultural waste, such as rice straw, wheat straw, corn straw, and bagasse. The annual global production of these agricultural waste streams amounts to 1470 million tons.[17] Thus, based on availability, saccharides hold greater potential than glycerol. Lignocellulosic biomass primarily consists of 32-47% cellulose, 19-35% hemicellulose, 5-30% lignin, and minor fractions of proteins and ash.[17,18] The two main industrial processes to obtain cellulose pulp are the Organosolv process and the Kraft process.[19]

Cellulose pulp is composed of bundles of crystalline polysaccharide fibres and can be used as such in the paper and building industry. Alternatively, cellulose pulp can be hydrolysed by an acid or an enzymatic treatment to release monosaccharides (e.g., glucose) which can be used to produce chemicals.[19,20] In addition to lignocellulosic biomass, polysaccharides and monosaccharides can also be obtained from waste streams in the food processing industry. For example, monosaccharides can be obtained from sugar beet processing,[7] while polysaccharides (e.g., starch) can be obtained from potato processing.[8]

1.3 Electrochemical conversion of biomass-based molecules

Biomass-based molecules, such as glycerol, glucose, and starch, contain a large variety of functional groups (like primary and secondary alcohols, ketones or aldehydes, ethers, and anomeric carbons), making it interesting to convert them to a wide variety of value-added platform and speciality chemicals. However, current methods for their conversion have limitations. Glucose is typically converted to gluconic acid through fermentation,[21] while the oxidation of glucose to glucaric acid and starch to anionic starch relies on nitric acid[22] and hypochlorite,[23] respectively. Unfortunately, hypochlorite and nitric acid require the use of harsh and toxic redox agents, and the use of hypochlorite results in chlorinated by-products.[13,24–27] Moreover, stoichiometric processes like hypochlorite oxidation generate substantial amounts of salts that need to be treated as waste,[26] making the process less environmentally friendly. Fermentation, on the other hand, is slow and requires complex growth media and expensive downstream processes.[21] An alternative approach lies in utilizing electrocatalytic processes, which eliminate the need for harsh redox agents by employing water as the redox agent.[28] These processes can be driven with renewable electricity, and performed under mild reaction conditions.[28]

Electrocatalytic processes are performed with electrocatalysts to lower the activation energy barrier of the reaction by reducing the electric potential required for the reaction to occur, thereby decreasing the energy input (expressed as W = V * I * t). Moreover, the decrease in activation energy barrier enhances reaction rates and allows for overcoming energy barriers that would otherwise be blocked by slow kinetics. The key challenge in (electro)catalysis is to design catalysts that are active, selective, and stable for the desired reactions.[28,29] This becomes more complicated for biofeedstocks since they are large molecules (especially starch) and have numerous functional groups whose conversion can be catalysed. Therefore, this dissertation focuses on the design of electrocatalysts that are active and selective for the conversion of biomass-based molecules to value-added chemicals.

1.4 Translating research on the electrocatalytic oxidation of sugar alcohols to saccharides

Most of the studies devoted to the selective electrocatalytic oxidation of biomass-based molecules, which are very similar to saccharides (e.g., glucose, mannose, xylose),[29–31] have been performed on sugar alcohols (e.g., glycerol, erythritol, and sorbitol).[32–38] Figure 1.1 shows the most commonly studied sugar alcohol (glycerol) and saccharide (glucose), highlighting their near similar reactive groups and the oxidation products produced from them. Glycerol has primary and secondary alcohol groups, while glucose also bears an aldehyde (i.e., anomeric carbon) group. The electrocatalytic oxidation of these functional groups enables the production of various value-added chemicals such as glyceric acid, dihydroxyacetone, and lactic acid from

glycerol, and gluconic acid, 2-keto gluconic acid, 5-keto gluconic acid and glucaric acid from glucose. The resemblance in chemical structure of sugar alcohols and saccharides allows for evaluating whether research findings on the electrochemical oxidation of glycerol can be translated to glucose and vice versa. This evaluation provides valuable insights into electrocatalyst design and the required reaction conditions for the active and selective conversion of sugar alcohols and saccharides. However, before translating research between sugar alcohols and saccharides, it is crucial to consider: 1) the impact of reaction conditions on the state of sugar alcohols and saccharides and their (intermediate) oxidation products and 2) the influence of catalyst properties and reaction conditions on the catalyst performance for the electrocatalytic oxidation of sugar alcohols and saccharides individually.
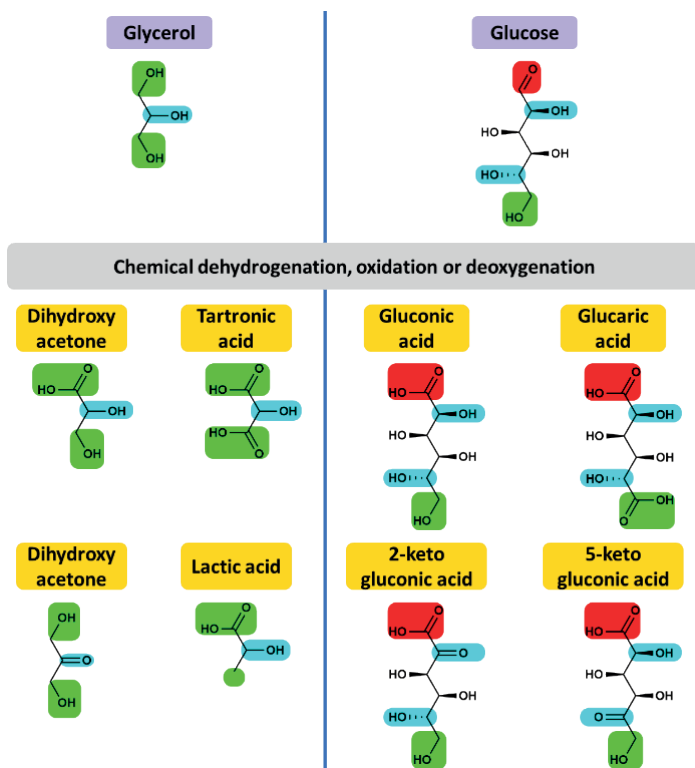
Figure 1.1. *Comparison of the chemical structure of glucose and glycerol (purple) and their oxidation, dehydrogenation, or deoxygenation oxidation products (yellow). Similar functional groups are indicated in green and light blue.*

Studies on the electrocatalytic oxidation of saccharides and sugar alcohols (e.g., glucose and glycerol) have used different reaction conditions, including pH, type of electrolyte, reactant concentration, and temperature. However, it is important to note that certain reaction conditions may induce homogeneous reactions (non-electrochemical reactions) that can change the state of the reactant or (intermediate) product, thereby affecting the overall reaction rate

and selectivity.[10,39] For instance, most studies on the electrocatalytic oxidation of sugar alcohols and saccharides have been performed under alkaline conditions since they promote the catalyst activity.[40–43] Alkaline conditions promote the deprotonation of sugar alcohols, resulting in the formation of more electroactive alkoxide species[40] that can be electrochemically oxidized to saccharides. However, under alkaline conditions, saccharides are susceptible to base-catalysed reactions, including the isomerization of saccharides (pH ≥ 10)[43,44] and retro-aldolization of >C4 saccharides (pH ≥13)[45,46]. As a result, these base-catalysed reactions affect the state of the reactant and ultimately compete with electrochemical reactions, influencing the activity and selectivity of the reaction.[10] Therefore, it is imperative to account for the competition between base-catalysed reactions and electrochemical reactions, before defining trends and translating findings between studies on the electrocatalytic oxidation of sugar alcohols and saccharides. By doing so, the effect of non-electrochemical reactions can be distinguished from electrochemical reactions, enabling accurate interpretations and comparisons of electrocatalytic oxidation processes for both sugar alcohols and saccharides.

Modifying catalyst properties (e.g., metal type, oxidation state, alloying) or adjusting reaction conditions provide strategies to control selectivity in the electrocatalytic oxidation of sugar alcohols, thereby offering potential strategies to steer selectivity in the electrocatalytic oxidation of saccharides. For instance, by modifying Pt electrodes with post-transition metals (adatoms), such as Bi and Sb the electrocatalytic oxidation of secondary alcohol groups over primary alcohol groups of sugar alcohols can be promoted.[47–49] It was proposed that Bi ad-atoms change the adsorption configuration of glycerol on the electrode surface, thereby changing the catalyst selectivity towards the electrocatalytic oxidation of the secondary alcohol group.[50] Similarly, Pt modified by Sb ad-atoms or alloyed with Sb exhibit a change in catalytic selectivity towards the secondary alcohol group of glycerol,[47–49] achieving nearly 100% selectivity towards dihydroxyacetone. These changes in catalytic selectivity induced by Bi and Sb were more dominant at $E < 0.6$ V[47–49] since Bi and Sb start to oxidize at $E > 0.6$ V and desorb at $E > 0.85$ V, losing their effect on the catalyst selectivity.[51,52] Notably, the modification of Pt with post-transition metals may also improve the catalyst selectivity towards secondary alcohol groups of glucose, enabling the selective production of 2-keto glucose or 5-keto glucose, which serve as precursors for 2-keto gluconic acid and 5-keto gluconic acid (being precursors to platform molecules like tartaric acid and ascorbic acid).[53] Additionally, the selective production of dicarboxylates from glycerol, such as tartronate (the salt form of the tartronic acid), has only been achieved on Au or Pt under highly alkaline conditions (pH ≥ 13.7).[54–58] This aligns with the electrocatalytic oxidation of glucose to glucarate (i.e., the salt form of glucaric acid) on Pt, RuO_2, and NiFe oxide (pH = 14).[13] However, an exception exists where MnO_2 was found to selectively electrocatalytically oxidize glucose to glucaric acid under acidic and neutral conditions (pH = 0.7-10).[25,59] This suggests that MnO_2 might also be able to electrocatalytically oxidize glycerol to

tartronic acid under acidic conditions, circumventing salt formation. This has the advantage that salt purification to acids can be circumvented, thereby reducing salt waste and associated purification costs.

1.5 Catalyst design for the electrocatalytic conversion of biomass-based feeds

In the chemical industry, high surface area to volume ratio catalysts are used to reduce the amount of costly and scarce metals and to reduce the reactor size needed to perform the reactions. These high surface area to volume ratio catalysts are made by decorating a high surface area porous support with metal (nanoparticles), such as refractory oxides (SiO_2, Al_2O_3, ZrO_2, etc.) or carbon. Carbon supports, in particular, have several advantages when used in electrocatalysis due to their inert and conductive nature,[60] and the potential to modify their physical[61] and chemical properties.[62] The inert properties of carbon supports make them inactive for catalytic side reactions and make them stable in a wide range of reaction conditions. Moreover, their physical properties can be modified to promote shape-selective reactions.[61] In addition, the chemical properties of the carbon support can be modified by doping the support with other elements or by introducing functional groups on the surface of the support.[62] Doping elements are used frequently in carbon-supported electrocatalysts to improve the catalyst performance,[63,64] while carbon-support functional surface group modification has been used less frequently. Although the latter approach has been used in thermal catalysis.[62]

Various functional groups, such as phosphor, sulphur, or oxygen-containing groups, have been used in carbon-supported thermocatalysts. For instance, sulphonic[65] and phosphoric[66] acid groups on carbon-supported catalysts can facilitate hydrolysis reactions, leading to the depolymerization of polysaccharides like starch or cellulose to glucose.[65] The liberated glucose can then be oxidized to various chemicals.[65] These are examples where surface groups induce additional reactivity. In addition, for oxygen groups, it has been shown that they can change the electronic properties of the metal catalyst on the carbon support[67] or affect the adsorption and desorption of products and reactants on the support in the vicinity of the metal catalyst[68]. For example, Toebes *et al.* prepared Ru on carbon nanofibers catalysts with different contents of support oxygen groups.[68] It was observed that a decrease in support oxygen groups on the Ru/CNF catalyst led to higher catalytic activity for the dehydrogenation of cinnamaldehyde. This improvement was tentatively attributed to an improved hydrophobic interaction between the reactant and the support.[68] Führer *et al.* prepared activated carbon with high and low contents of support oxygen groups, bearing different Pt of different particle sizes (Pt/AC).[69] The catalysts with 1.8 nm Pt particles and high contents of support oxygen exhibited ~3.5 times higher catalytic activity than the catalysts with 2.5 nm Pt particles and low contents of support oxygen groups. XANES and XPS measurements indicated no significant change in the electronic properties of the Pt particles induced by the support oxygen groups. Therefore, the change in catalytic activity was

attributed to an enhanced product desorption, thereby reducing catalyst deactivation.[69] Therefore, the change in catalytic activity was attributed to modifications in the desorption of products induced by support oxygen groups. In summary, carbon support oxygen groups have the potential to change the performance of thermocatalysts and may also influence the activity of electrocatalysts involved in the conversion of biomass-based molecules.

In the field of electrochemistry, the applied potential can be used to change the oxidation state of the metal, potentially influencing the catalyst activity and selectivity. Notably, on Pt electrodes, with an increase in potential, the electrocatalytic oxidation of sugar alcohols (e.g., glycerol, sorbitol) and saccharides (e.g., glucose, mannose) show two distinct peak potentials.[70–73] The first peak potential lies in the metallic Pt (< 0.9 V *vs.* RHE) region, while the second peak potential lies in the Pt oxide (> 0.9 V *vs.* RHE) region.[70–73] This shows that both metallic Pt and Pt oxide can electrocatalytically oxidize biomass-based molecules. Furthermore, chronoamperometric measurements also reveal a difference in catalytic performance between metallic Pt and Pt oxide, namely metallic Pt (at E = 0.75 V *vs.* RHE and 20% glycerol conversion) produced 90% glyceraldehyde,[74] while Pt oxide (at E = 0.9 V and 1.1 V *vs.* RHE) resulted in a higher conversion but also an increased selectivity towards glyceric acid (up to 87%).[74–76] These differences in conversion make it impossible to attribute differences in catalytic activity and selectivity to the Pt oxidation state. Therefore, the role of the Pt oxidation state on the electrocatalytic oxidation of saccharides remains to be evaluated.

1.6 Limitations in glucose oxidation product analysis

In contrast to glucose oxidation pathways,[77] the reaction pathway for the electrocatalytic oxidation of glycerol is well-described and resulted in property performance relations for the electrocatalytic oxidation of glycerol.[10] In the glycerol oxidation pathway, almost all (intermediate) oxidation products are quantified, and therefore a map can be created to evaluate which reaction pathway the catalyst favours. For example, Pt can catalyse both the oxidation of the primary and secondary alcohol groups of glycerol,[48,74,76,78] while Au can only catalyse the oxidation of the primary alcohol group of glycerol.[40,78] Moreover, in the electrocatalytic oxidation of glycerol on Pt, an increase in potential corresponds to a higher conversion of reactants and higher oxidation products, resulting in less glyceraldehyde and more glyceric acid.[74–76]

To date, for glucose oxidation, several analytical techniques, such as 2D-NMR, HPIC, HPLC, HPLC-MS, and GC-MS, have been used to attempt to quantify all (intermediate) products. However, various (intermediate) products have not been discussed or quantified, despite their expected formation during the reaction. Some examples include glucose dialdehyde (occasionally mentioned but not quantified),[22,42,79–83] 2-keto gluconic acid and 5-keto gluconic acid (rarely

quantified),[22,80,81] and guluronic acid or glucuronic acid (often only one of the two is quantified).[22,42,81–84]

To potentially quantify all reaction intermediates during glucose oxidation high-pressure anion exchange chromatography (HPAEC) holds great potential (but has not been used for this purpose yet).[85] Unlike other analytical techniques, HPAEC separates ionizable molecules based on their total charge. This approach might therefore provide the proper approach to separate and quantify all (intermediate) products of the glucose oxidation pathway. This opens new doors for systematic research on the property performance relation of (electro)catalysts for glucose oxidation, as will be shown later in this thesis (Chapter 4).

1.7 The electrocatalytic oxidation of polysaccharides

Various studies have demonstrated the feasibility of electrocatalytically oxidizing polysaccharides, including cellobiose,[86] oligosaccharides,[87] and cellulose.[88–91] However, the formation of polysaccharides with carboxylic acid groups that have not been depolymerized significantly has yet to be proven.

Kwon *et al.* investigated the electrocatalytic oxidation of cellobiose under acidic conditions (pH = 0.3, 0.5 M H_2SO_4) at various current densities ranging from 10 to 120 mA.cm^{-2}.[86] These current densities were used to promote the oxygen evolution reaction and thus the formation of acids. The acids formed at the anode led to the hydrolysis of cellobiose, which could then be electrochemically oxidized on the electrode, resulting in the formation of various smaller organic molecules through C-C cleavage reactions.[86] At mildly acidic conditions (pH = 3), Yang *et al.* studied the electrocatalytic oxidation of oligosaccharides on γ-MnO_2 on graphite electrodes at 0.42 V *vs.* RHE (-1.0 V *vs.* SCE).[87] Under these reaction conditions, γ-MnO_2 was found to be highly selective towards the cleavage of β-1,4-glycoside bonds, yielding glucose with nearly 100% selectivity.

The electrocatalytic oxidation of water-insoluble cellulose was studied under harsh alkaline conditions (pH ≥ 14)[88,89] to dissolve the cellulose followed by subsequent oxidation of the dissolved cellulose on Au,[88,89] Pt,[88] Pd[88] and Ni[88] electrodes. Au showed the highest (though still less low) catalytic activity in the lower potentials range (<1.2 V *vs.* RHE) for the electrocatalytic oxidation of cellulose, reaching 0.2 mA.cm^{-2} at E = ~1 V *vs.* RHE, based on negative going scans on a rotating disc electrode.[88] On a Pt on Ni foam at 1.1 and 1.5 V *vs.* RHE, cellulose was hydrolysed and the resulting glucose was predominantly oxidized to glucuronic acid and other smaller organic acids.[88] In an earlier study performed by Sugano *et al.*, Au was used to electrochemically oxidize cellulose by performing cyclic voltammetry between 0.6 and 1.4 V *vs.* RHE (converted from Ag/AgCl/KCl (3M)).[89] The resulting oxidized cellulose was dialyzed with a membrane having a molecular weight cut-off of 1000 Dalton, removing the NaOH causing the

water insoluble cellulose to precipitate and retaining all polysaccharides with a degree of polymerization greater than 5. The water soluble cellulose was found to be highly oxidized, while the water insoluble cellulose was not oxidized (confirmed by FTIR and ^{13}C-NMR).[89]

These studies on the electrocatalytic oxidation of polysaccharides are not conclusive on whether polysaccharides are hydrolysed first to monomers and successively oxidized or if the larger chain of the cellulose can be electrochemically oxidized without inducing severe depolymerization.[88–91] To address this, further investigation is needed, that considers the separation of oxidized starch by their molecular size (e.g., using HPSEC-RI-RALS) and the change in degree of oxidation determined by HPSEC-UV and NMR.

1.8 Research scope and outline

Biomass-based feedstocks are environmentally friendly, cheap, and readily available, and contain molecules such as glycerol, glucose, and starch that can be processed in the chemical industry for the synthesis of a broad range of platform and speciality chemicals. However, the current approach for glucose and starch oxidation to value-added chemicals relies on fermentation or the use of oxidizing agents, which have one or more limitations. These limitations include the use of harsh and toxic oxidizing agents, the formation of chlorinated by-products, and mild selectivities, requiring complex and expensive downstream processes. These limitations can potentially be resolved by using electrochemical processes. However, to establish the electrocatalytic oxidation of glucose, suitable catalysts that are active, selective, and stable need to be improved first, while electrocatalysts for the electrocatalytic oxidation of starch still need to be developed.

In this dissertation, we describe a bottom-up approach by systematically increasing the complexity of the biomass-based molecules throughout the research to explore their potential for the electrosynthesis of platform and speciality chemicals. With this approach, we aim to enhance our understanding of catalyst property performance relationships and reveal new possibilities for sustainable chemical transformations. **Chapter 2** is a review of the electrocatalytic oxidation of sugar alcohols (e.g., glycerol, erythritol, and sorbitol) and saccharides (e.g., glucose, xylose, and mannose). Sugar alcohols consist of a hydroxyl group attached to each carbon atom, while saccharides also have an aldehyde or ketone group. **Chapters 3 and 4** focus on the property performance relationships of catalysts for the electrocatalytic oxidation of glucose and **Chapter 5** evaluates the potential to electrocatalytically oxidize starch, which is a (branched) polymer of glucose.

The amount of research dedicated to the selective electrocatalytic oxidation of sugar alcohols[32–38] is significantly larger compared to that of saccharides.[29–31] Since the chemical structure of sugar alcohols and saccharides only differ in one functional group, it may be possible to translate

research from one molecule to another. Therefore, in **Chapter 2**, a critical literature review is presented on the electrocatalytic oxidation of sugar alcohols and saccharides. This enabled us to compare trends and evaluate whether research can be translated between these two molecules. The identified trends are categorized into two aspects: 1) the impact of reaction conditions on the state of the reactant and (intermediate) product and 2) the influence of reaction condition and catalyst property on the catalyst performance. The considered reaction conditions encompass pH, electrolyte type, temperature, reactant concentration, and potential, while the catalyst properties include the type of metal, metal oxidation state, facets, and bimetallic systems. Before defining trends, the effect of pH and electrolyte on the state of reactants and products is initially evaluated, enabling a more accurate differentiation between electrochemical and non-electrochemical (homogeneous) reactions.

It is well-known for thermocatalysts that the presence of support oxygen groups on carbon-supported metal catalysts can change the catalyst performance. This change in catalyst performance by support oxygen groups can either be attributed to a change in the electronic properties of the metal catalyst or to an alteration in adsorption or repulsion of the reactant on the carbon support in the vicinity of the metal catalyst. So far, the effect of support oxygen groups has not been described for electrocatalysts. Therefore, in **Chapter 3**, we aim to evaluate the effect of support oxygen groups on the performance of Pt supported on carbon nanofibers (Pt/CNF) for the electrocatalytic oxidation of glucose. For this study, we synthesized Pt/CNF catalysts with different Pt particle sizes, characterized by TEM and CO-stripping, and various contents of support oxygen groups, characterized by XPS, TGA, TPD-MS, and CV. The electronic and surface properties of the Pt particles were evaluated by *in-situ* HERFD-XANES, XPS, and CO-stripping. Subsequently, the catalytic activity of the Pt/CNF catalysts for the electrocatalytic oxidation of glucose was tested at pH = 1 (0.1 M H_2SO_4).

Although metallic Pt (Pt^0, < 0.9 V *vs.* RHE) and Pt oxide (PtO_x > 0.9 V *vs.* RHE) are known to be active for the electrocatalytic oxidation of glucose, the influence of the Pt oxidation state on the catalyst activity and selectivity for this reaction has yet to be evaluated. Thus, in **Chapter 4**, we elucidate the role of the Pt oxidation state on the catalytic activity and selectivity for the electrocatalytic oxidation of glucose. To accomplish this, a novel analytical approach that combines high-pressure liquid chromatography (HPLC) with high-pressure anion exchange chromatography (HPAEC) is employed to quantify all (intermediate) products of the glucose oxidation pathway. The electrocatalytic oxidation of glucose and glucose oxidation products, including gluconic acid and glucuronic acid, is investigated on Pt^0 and PtO_x (at E = 0.64 V and 1.2 V *vs.* RHE) to evaluate the role of Pt oxidation state on the catalyst activity and selectivity.

In **Chapter 5**, we evaluate the feasibility of electrocatalytically oxidizing industrially derived water-soluble starch as a substitute for hypochlorite-oxidized starch. First, the purification of

industrial-derived starch was discussed to remove impurities, like oligomers, thereby obtaining a high-purity starch with a degree of polymerization of ≥18. For the electrocatalytic oxidation of purified starch, Pt (at E = 0.64 V *vs.* RHE) is used in 0.1 M phosphate buffer (pH = 12). The degree of depolymerization was evaluated by HPSEC-RI and HPAEC, while the formation of oxidized groups was evaluated by HPSEC-UV and NMR.

In **Chapter 6**, the results obtained in **Chapters 2-5** are placed in a broader context, and recommendations are made for future research on the electrocatalytic oxidation of glucose and starch.

Figure 1.2 gives a schematic overview of this dissertation, illustrating the main subjects studied in this dissertation.
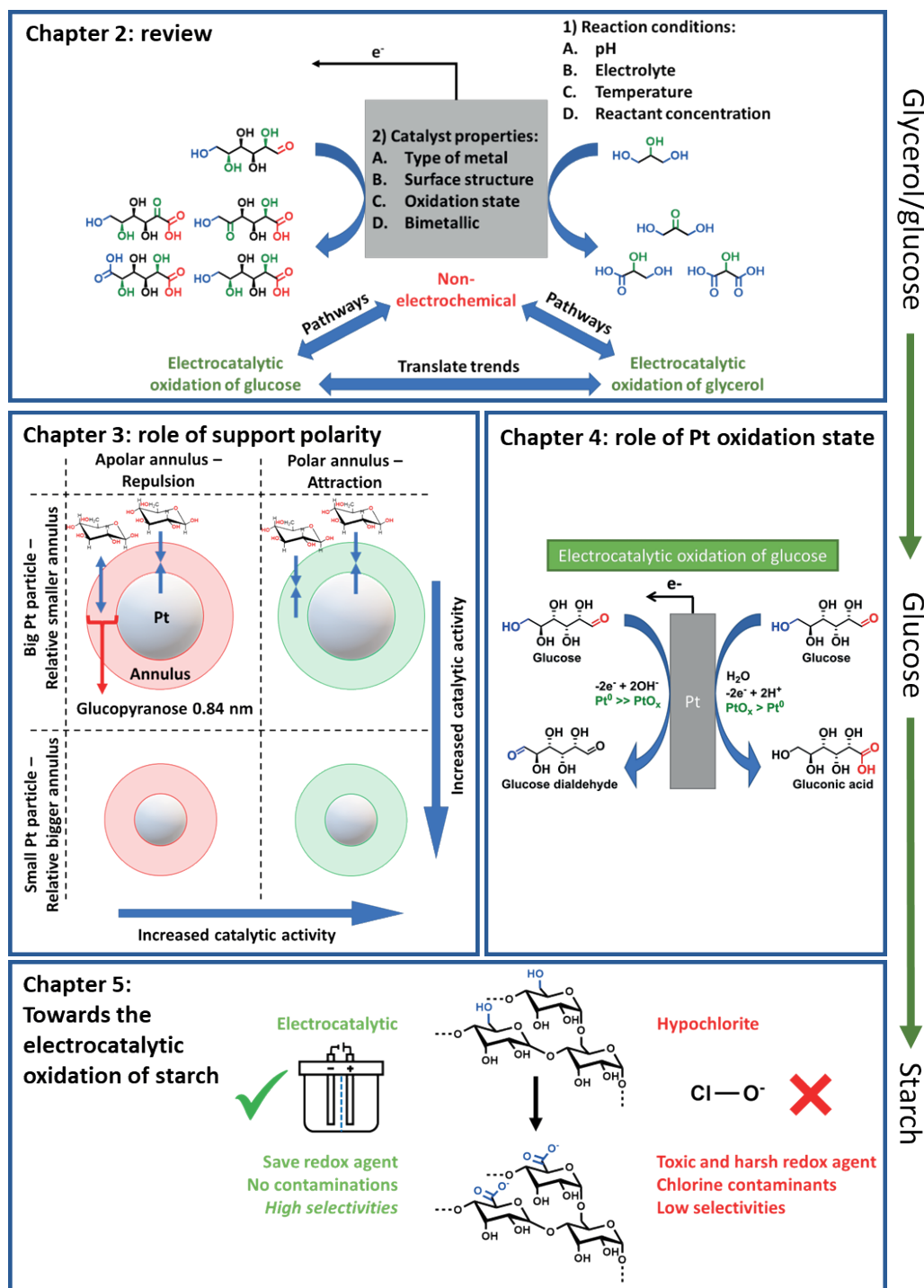
Figure 1.2. *Schematic overview of the main subjects studied in this dissertation.*

References

1. Pfaltzgraff, L. A. & Clark, J. H. Green chemistry, biorefineries and second generation strategies for re-use of waste: An overview. in *Advances in Biorefineries: Biomass and Waste Supply Chain Exploitation* 3–33 (Elsevier Ltd., 2014).

2. Li, K. & Sun, Y. Electrocatalytic Upgrading of Biomass-Derived Intermediate Compounds to Value-Added Products. *Chemistry – A European Journal* **24**, 18258–18270 (2018).

3. Gallo, J. M. R. & Trapp, M. A. The chemical conversion of biomass-derived saccharides: An overview. *J Braz Chem Soc* **28**, 1586–1607 (2017).

4. Tackett, B. M., Gomez, E. & Chen, J. G. Net reduction of CO2 via its thermocatalytic and electrocatalytic transformation reactions in standard and hybrid processes. *Nat Catal* **2**, 381–386 (2019).

5. Chen, S., Wojcieszak, R., Dumeignil, F., Marceau, E. & Royer, S. How Catalysts and Experimental Conditions Determine the Selective Hydroconversion of Furfural and 5-Hydroxymethylfurfural. *Chem Rev* **118**, 11023–11117 (2018).

6. Alonso, D. M., Wettstein, S. G. & Dumesic, J. A. Bimetallic catalysts for upgrading of biomass to fuels and chemicals. *Chem Soc Rev* **41**, 8075–8098 (2012).

7. Modelska, M. *et al.* Concept for recycling waste biomass from the sugar industry for chemical and biotechnological purposes. *Molecules* **22**, 9 (2017).

8. Torres, M. D. & Domínguez, H. Valorisation of potato wastes. *Int J Food Sci Technol* **55**, 2296–2304 (2020).

9. Duan, L., Petroski, R., Wood, L. & Caldeira, K. Stylized least-cost analysis of flexible nuclear power in deeply decarbonized electricity systems considering wind and solar resources worldwide. *Nat Energy* **7**, 260–269 (2022).

10. Dai, C. *et al.* Electrochemical production of lactic acid from glycerol oxidation catalyzed by AuPt nanoparticles. *J Catal* **356**, 14–21 (2017).

11. Creus, J., Miola, M. & Pescarmona, P. P. Unravelling and overcoming the challenges in the electrocatalytic reduction of fructose to sorbitol. *Green Chemistry* **25**, 1658–1671 (2023).

12. Todd Werpy & Gene Petersen. *Top value added chemicals from biomass: volume I--results of screening for potential candidates from sugars and synthesis gas*. http://www.osti.gov/bridge (2004).

13. Liu, W. J. *et al.* Efficient electrochemical production of glucaric acid and H2 via glucose electrolysis. *Nat Commun* **11**, 265 (2020).

14. Vanier, N. L. *et al.* Physicochemical, crystallinity, pasting and morphological properties of bean starch oxidised by different concentrations of sodium hypochlorite. *Food Chem* **131**, 1255–1262 (2012).

15. Pourzolfaghar, H., Abnisa, F., Daud, W. M. A. W. & Aroua, M. K. A review of the enzymatic hydroesterification process for biodiesel production. *Renewable and Sustainable Energy Reviews* **61**, 245–257 (2016).

16. Li, Z. *et al.* Production of value-added chemicals from glycerol using in vitro enzymatic cascades. *Commun Chem* **1**, 1–7 (2018).

17. Sarkar, N., Ghosh, S. K., Bannerjee, S. & Aikat, K. Bioethanol production from agricultural wastes: An overview. *Renew Energy* **37**, 19–27 (2012).

18. Vallejos, M. E., Zambon, M. D., Area, M. C. & Da Silva Curvelo, A. A. Low liquid-solid ratio (LSR) hot water pretreatment of sugarcane bagasse. *Green Chemistry* **14**, 1982–1989 (2012).

19. Tezcan, E. & Atıcı, O. G. A new method for recovery of cellulose from lignocellulosic bio-waste: Pile processing. *Waste Management* **70**, 181–188 (2017).

20. Ibrahim, Q. & Kruse, A. Prehydrolysis and organosolv delignification process for the recovery of hemicellulose and lignin from beech wood. *Bioresour Technol Rep* **11**, 100506 (2020).

21. Pal, P., Kumar, R. & Banerjee, S. Manufacture of gluconic acid: A review towards process intensification for green production. *Chemical Engineering and Processing: Process Intensification* **104**, 160–171 (2016).

22. Liu, W. J. *et al.* Efficient electrochemical production of glucaric acid and H2 via glucose electrolysis. *Nat Commun* **11**, 1–11 (2020).

23. Vanier, N. L. *et al.* Physicochemical, crystallinity, pasting and morphological properties of bean starch oxidised by different concentrations of sodium hypochlorite. *Food Chem* **131**, 1255–1262 (2012).

24. Genuino, H. C. *et al.* Iron Tetrasulfonatophthalocyanine-Catalyzed Starch Oxidation Using H2O2: Interplay between Catalyst Activity, Selectivity, and Stability. *ACS Omega* **6**, 13847–13857 (2021).

25. Bin, D. *et al.* Controllable oxidation of glucose to gluconic acid and glucaric acid using an electrocatalytic reactor. *Electrochim Acta* **130**, 170–178 (2014).

26. Wang, H. *et al.* Hydrogen peroxide as an oxidant in starch oxidation using molybdovanadophosphate for producing a high carboxylic content. *RSC Adv* **5**, 45725–45730 (2015).

27. Vanier, N. L., El Halal, S. L. M., Dias, A. R. G. & da Rosa Zavareze, E. Molecular structure, functionality and applications of oxidized starches: A review. *Food Chem* **221**, 1546–1559 (2017).

28. Singh, N. & Goldsmith, B. R. Role of Electrocatalysis in the Remediation of Water Pollutants. *ACS Catal* **10**, 3365–3371 (2020).

29. Vedovato, V., Vanbroekhoven, K., Pant, D. & Helsen, J. Electrosynthesis of Biobased Chemicals Using Carbohydrates as a Feedstock. *Molecules* **25**, 16 (2020).

30. Lee, J., Jung, S., Kim, Y. T., Kim, H. J. & Kim, K. H. Catalytic and electrocatalytic conversion of glucose into value-added chemicals. *Renewable and Sustainable Energy Reviews* **181**, 113337 (2023).

31. Holade, Y. *et al.* Recent advances in the electrooxidation of biomass-based organic molecules for energy, chemicals and hydrogen production. *Catal Sci Technol* **10**, 3071–3112 (2020).

32. Garlyyev, B., Xue, S., Fichtner, J., Bandarenka, A. S. & Andronescu, C. Prospects of Value-Added Chemicals and Hydrogen via Electrolysis. *ChemSusChem* **13**, 2513–2521 (2020).

33. Li, K. & Sun, Y. Electrocatalytic Upgrading of Biomass-Derived Intermediate Compounds to Value-Added Products. *Chemistry – A European Journal* **24**, 18258–18270 (2018).

34. Li, T. & Harrington, D. A. An Overview of Glycerol Electrooxidation Mechanisms on Pt, Pd and Au. *ChemSusChem* **14**, 1472–1495 (2021).

35. Coutanceau, C., Baranton, S. & Kouamé, R. S. B. B. Selective electrooxidation of glycerol into value-added chemicals: A short overview. *Front Chem* **7**, 1–15 (2019).

36. Houache, M. S. E., Hughes, K. & Baranova, E. A. Study on catalyst selection for electrochemical valorization of glycerol. *Sustain Energy Fuels* **3**, 1892–1915 (2019).

37. Du, L. *et al.* Electrocatalytic valorisation of biomass derived chemicals. *Catal Sci Technol* **8**, 3216–3232 (2018).

38. Rahim, S. A. N. M. *et al.* A review of recent developments on kinetics parameters for glycerol electrochemical conversion – A by-product of biodiesel. *Science of the Total Environment* **705**, 135137 (2020).

39. Huang, X., Zou, Y. & Jiang, J. Electrochemical Oxidation of Glycerol to Dihydroxyacetone in Borate Buffer: Enhancing Activity and Selectivity by Borate-Polyol Coordination Chemistry. *ACS Sustain Chem Eng* **9**, 14470–14479 (2021).

40. Kwon, Y., Lai, S. C. S., Rodriguez, P. & Koper, M. T. M. Electrocatalytic oxidation of alcohols on gold in alkaline media: Base or gold catalysis? *J Am Chem Soc* **133**, 6914–6917 (2011).

41. Kwon, Y. & Koper, M. T. M. Combining voltammetry with HPLC: Application to electro-oxidation of glycerol. *Anal Chem* **82**, 5420–5424 (2010).

42. Kokoh, K. B., Léger, J. M., Beden, B. & Lamy, C. 'On line' chromatographic analysis of the products resulting from the electrocatalytic oxidation of d-glucose on Pt, Au and adatoms modified Pt electrodes-Part I. Acid and neutral media. *Electrochim Acta* **37**, 1333–1342 (1992).

43. Moggia, G., Kenis, T., Daems, N. & Breugelmans, T. Electrochemical Oxidation of d-Glucose in Alkaline Medium: Impact of Oxidation Potential and Chemical Side Reactions on the Selectivity to d-Gluconic and d-Glucaric Acid. *ChemElectroChem* **7**, 86–95 (2020).

44. Takei, T. *et al.* Heterogeneous Catalysis by Gold. *Advances in Catalysis* **55**, 1–126 (2012).

45. Mäki-Arvela, P., Simakova, I. L., Salmi, T. & Murzin, D. Y. Production of lactic acid/lactates from biomass and their catalytic transformations to commodities. *Chem Rev* **114**, 1909–1971 (2014).

46. Li, L., Shen, F., Smith, R. L. & Qi, X. Quantitative chemocatalytic production of lactic acid from glucose under anaerobic conditions at room temperature. *Green Chemistry* **19**, 76–81 (2017).

47. Kwon, Y., De Jong, E., Van Der Waal, J. K. & Koper, M. T. M. Selective electrocatalytic oxidation of sorbitol to fructose and sorbose. *ChemSusChem* **8**, 970–973 (2015).

48. Kwon, Y., Birdja, Y., Spanos, I., Rodriguez, P. & Koper, M. T. M. Highly selective electro-oxidation of glycerol to dihydroxyacetone on platinum in the presence of bismuth. *ACS Catal* **2**, 759–764 (2012).

49. Kwon, Y., Hersbach, T. J. P. & Koper, M. T. M. Electro-Oxidation of Glycerol on Platinum Modified by Adatoms: Activity and Selectivity Effects. *Top Catal* **57**, 1272–1276 (2014).

50. Garcia, A. C., Birdja, Y. Y., Tremiliosi-Filho, G. & Koper, M. T. M. Glycerol electro-oxidation on bismuth-modified platinum single crystals. *J Catal* **346**, 117–124 (2017).

51. Fernandez-Vega, A., Feliu, J. M., Aldaz, A. & Clavilier, J. Heterogeneous electrocatalysis on well defined platinum surfaces modified by controlled amounts of irreversibly adsorbed adatoms. Part II. Formic acid oxidation on the Pt (100)-Sb system. *Journal of Electroanalytical Chemistry* **258**, 101–113 (1989).

52. Daniele, S., Battistel, D., Bergamin, S. & Bragato, C. Voltammetric determination of glucose at bismuth-modified mesoporous platinum microelectrodes. *Electroanalysis* **22**, 1511–1518 (2010).

53. Luo, Z., Yu, S., Zeng, W. & Zhou, J. Comparative analysis of the chemical and biochemical synthesis of keto acids. *Biotechnol Adv* **47**, 107706 (2021).

54. Qi, J. *et al.* Electrocatalytic selective oxidation of glycerol to tartronate on Au/C anode catalysts in anion exchange membrane fuel cells with electricity cogeneration. *Appl Catal B* **154–155**, 360–368 (2014).

55. Xin, L., Zhang, Z., Wang, Z. & Li, W. Simultaneous Generation of Mesoxalic Acid and Electricity from Glycerol on a Gold Anode Catalyst in Anion-Exchange Membrane Fuel Cells. *ChemCatChem* **4**, 1105–1114 (2012).

56. Ahmad, M. S. *et al.* Electro-oxidation of waste glycerol to tartronic acid over Pt/CNT nanocatalyst: study of effect of reaction time on product distribution. *Energy Sources, Part A: Recovery, Utilization, and Environmental Effects* 1–17 (2019).

57. Ahmad, M. S., Cheng, C. K., Ong, H. R., Abdullah, H. & Khan, M. R. Electro-oxidation of renewable glycerol to value added chemicals over phosphorous-doped Pt/MCNTs nanoparticles. *Materials Science and Engineering* **702**, 012025 (2019).

58. Ferreira Frota, E., Silva de Barros, V. V., de Araújo, B. R. S., Gonzaga Purgatto, Â. & Linares, J. J. Pt/C containing different platinum loadings for use as electrocatalysts in alkaline PBI-based direct glycerol fuel cells. *Int J Hydrogen Energy* **42**, 23095–23106 (2017).

59. Li, J. *et al.* Efficiently Coupled Glucose Oxidation for High-value D-glucaric Acid with Ultradurable Hydrogen via Mn (III) in Acidic Solution. *Nano Res* **16**, 10748–10755 (2023).

60. Rodriguez-Reinoso, F. The role of carbon materials in heterogeneous catalysis. *Carbon* **36**, 159–175 (1998).

61. Jiang, J. & Sandler, S. I. Shape versus inverse-shape selective adsorption of alkane isomers in carbon nanotubes. *Journal of Chemical Physics* **124**, 2 (2006).

62. Gerber, I. C. & Serp, P. A Theory/Experience Description of Support Effects in Carbon-Supported Catalysts. *Chem Rev* **120**, 1250–1349 (2020).

63. Ji, Y., Du, J. & Chen, A. Review on Heteroatom Doping Carbonaceous Materials Toward Electrocatalytic Carbon Dioxide Reduction. *Transactions of Tianjin University* **28**, 292–306 (2022).

64. Zhang, A., Liang, Y., Zhang, H., Geng, Z. & Zeng, J. Doping regulation in transition metal compounds for electrocatalysis. *Chem Soc Rev* **50**, 9817–9844 (2021).

65. Li, Z., Liu, Y., Liu, C., Wu, S. & Wei, W. Direct conversion of cellulose into sorbitol catalyzed by a bifunctional catalyst. *Bioresour Technol* **274**, 190–197 (2019).

66. Hita, I. *et al.* Phosphorus-containing activated carbon as acid support in a bifunctional Pt–Pd catalyst for tire oil hydrocracking. *Catal Commun* **78**, 48–51 (2016).

67. Shi, W. *et al.* Enhanced chemoselective hydrogenation through tuning the interaction between pt nanoparticles and carbon supports: Insights from identical location transmission electron microscopy and x-ray photoelectron spectroscopy. *ACS Catal* **6**, 7844–7854 (2016).

68. Toebes, M. L., Prinsloo, F. F., Bitter, J. H., Van Dillen, A. J. & De Jong, K. P. Influence of oxygen-containing surface groups on the activity and selectivity of carbon nanofiber-supported ruthenium catalysts in the hydrogenation of cinnamaldehyde. *J Catal* **214**, 78–87 (2003).

69. Führer, A. M. *et al.* The synergetic effect of support-oxygen groups and Pt particle size in the oxidation of α-D-glucose: a proximity effect in adsorption. *ChemCatChem* **14**, 19 (2022).

70. Kwon, Y., De Jong, E., Van Der Waal, J. K. & Koper, M. T. M. Selective electrocatalytic oxidation of sorbitol to fructose and sorbose. *ChemSusChem* **8**, 970–973 (2015).

71. Kwon, Y., Schouten, K. J. P. & Koper, M. T. M. Mechanism of the Catalytic Oxidation of Glycerol on Polycrystalline Gold and Platinum Electrodes. *ChemCatChem* **3**, 1176–1185 (2011).

72. Moggia, G., Kenis, T., Daems, N. & Breugelmans, T. Electrochemical Oxidation of d-Glucose in Alkaline Medium: Impact of Oxidation Potential and Chemical Side Reactions on the Selectivity to d-Gluconic and d-Glucaric Acid. *ChemElectroChem* **7**, 86–95 (2020).

73. Parpot, P., Santos, P. R. B. & Bettencourt, A. P. Electro-oxidation of d-mannose on platinum, gold and nickel electrodes in aqueous medium. *Journal of Electroanalytical Chemistry* **610**, 154–162 (2007).

74. Kim, H. J., Lee, J., Green, S. K., Huber, G. W. & Kim, W. B. Selective glycerol oxidation by electrocatalytic dehydrogenation. *ChemSusChem* **7**, 1051–1056 (2014).

75. Lee, S. *et al.* Highly selective transformation of glycerol to dihydroxyacetone without using oxidants by a PtSb/C-catalyzed electrooxidation process. *Green Chemistry* **18**, 2877–2887 (2016).

76. Kim, H. J. *et al.* Coproducing Value-Added Chemicals and Hydrogen with Electrocatalytic Glycerol Oxidation Technology: Experimental and Techno-Economic Investigations. *ACS Sustain Chem Eng* **5**, 6626–6634 (2017).

77. Zhang, Q., Wan, Z., Yu, I. K. M. & Tsang, D. C. W. Sustainable production of high-value gluconic acid and glucaric acid through oxidation of biomass-derived glucose: A critical review. *J Clean Prod* **312**, 127745 (2021).

78. Kwon, Y., Schouten, K. J. P. & Koper, M. T. M. Mechanism of the Catalytic Oxidation of Glycerol on Polycrystalline Gold and Platinum Electrodes. *ChemCatChem* **3**, 1176–1185 (2011).

79. Kokoh, K. B. *et al.* Selective oxidation of D-gluconic acid on platinum and lead adatoms modified platinum electrodes in alkaline medium. *Electrochim Acta* **38**, 1359–1365 (1993).

80. Armstrong, R. D., Hirayama, J., Knight, D. W. & Hutchings, G. J. Quantitative Determination of Pt-Catalyzed d-Glucose Oxidation Products Using 2D NMR. *ACS Catal* **9**, 325–335 (2019).

81. Lee, J., Saha, B. & Vlachos, D. G. Pt catalysts for efficient aerobic oxidation of glucose to glucaric acid in water. *Green Chemistry* **18**, 3815–3822 (2016).

82. Jin, X. *et al.* Synergistic Effects of Bimetallic PtPd/TiO2 Nanocatalysts in Oxidation of Glucose to Glucaric Acid: Structure Dependent Activity and Selectivity. *Ind Eng Chem Res* **55**, 2932–2945 (2016).

83. Derrien, E., Marion, P., Pinel, C. & Besson, M. Influence of Residues Contained in Softwood Hemicellulose Hydrolysates on the Catalytic Oxidation of Glucose to Glucarate in Alkaline Aqueous Solution. *Org Process Res Dev* **20**, 1265–1275 (2016).

84. Kokoh, K. B. *et al.* Selective oxidation of D-gluconic acid on platinum and lead adatoms modified platinum electrodes in alkaline medium. *Electrochim Acta* **38**, 1359–1365 (1993).

85. Wouter Huijgen, E. Cobussen-Pool, B. van Egmond & J. van Hal. Determination of carbohydrate composition of macroalgae. in *Protocols for Macroalgae Research* 200–210 (2018).

86. Kwon, Y., Kleijn, S. E. F., Schouten, K. J. P. & Koper, M. T. M. Cellobiose hydrolysis and decomposition by electrochemical generation of acid and hydroxyl radicals. *ChemSusChem* **5**, 1935–1943 (2012).

87. Yang, F., Zhang, Q., Fan, H. X., Li, Y. & Li, G. Electrochemical control of the conversion of cellulose oligosaccharides into glucose. *Journal of Industrial and Engineering Chemistry* **20**, 3487–3492 (2014).

88. Kageshima, Y. *et al.* Insights into the Electrocatalytic Oxidation of Cellulose in Solution toward Applications in Direct Cellulose Fuel Cells. *Journal of Physical Chemistry C* **125**, 14576–14582 (2021).

89. Sugano, Y., Latonen, R. M., Akieh-Pirkanniemi, M., Bobacka, J. & Ivaska, A. Electrocatalytic oxidation of cellulose at a gold electrode. *ChemSusChem* **7**, 2240–2247 (2014).

90. Sugano, Y. *et al.* Specific Electrocatalytic Oxidation of Cellulose at Carbon Electrodes Modified by Gold Nanoparticles. *ChemCatChem* **8**, 2401–2405 (2016).

91. Hao, M., Liu, X., Feng, M., Zhang, P. & Wang, G. Generating power from cellulose in an alkaline fuel cell enhanced by methyl viologen as an electron-transfer catalyst. *J Power Sources* **251**, 222–228 (2014).
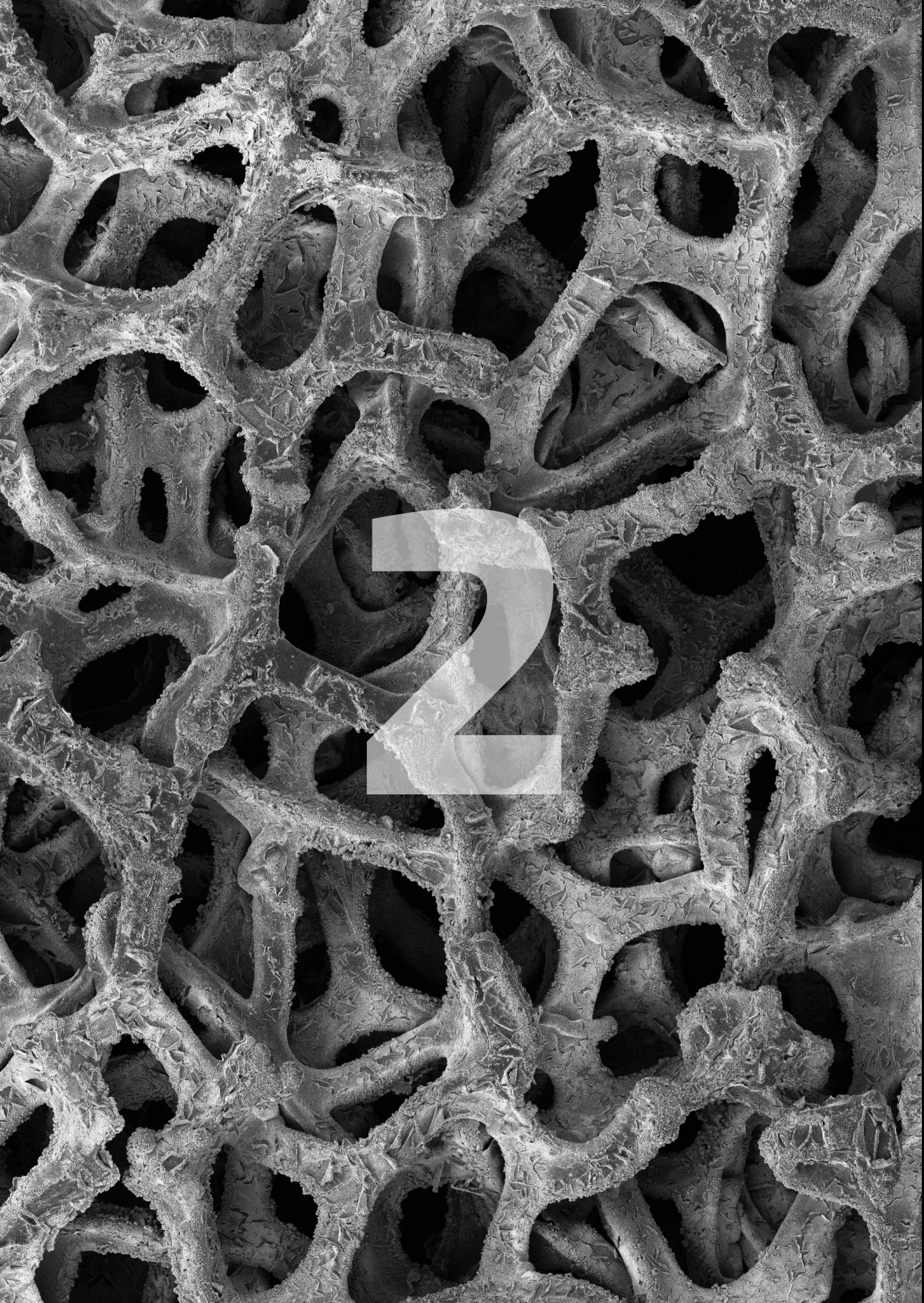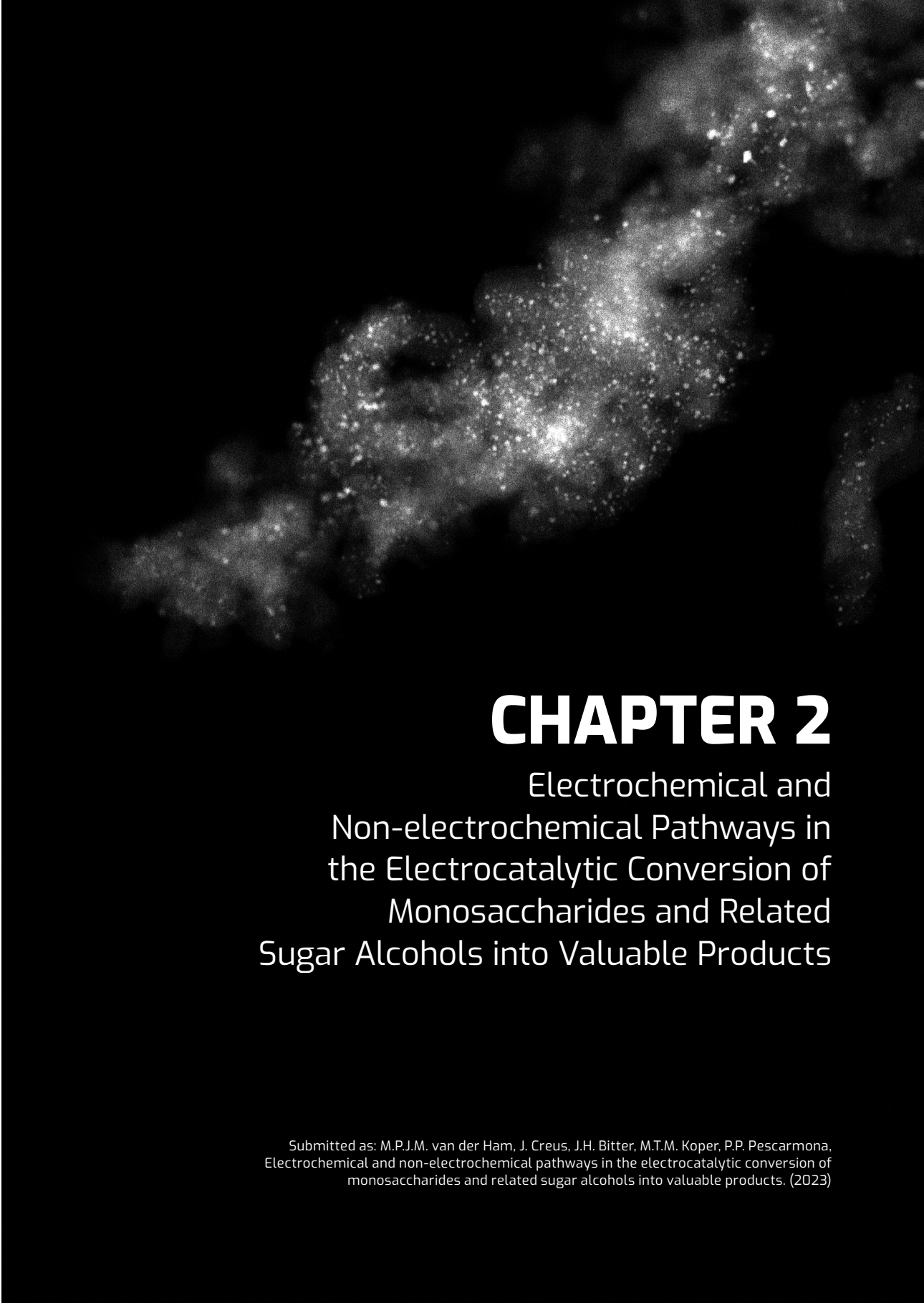
CHAPTER 2

Electrochemical and Non-electrochemical Pathways in the Electrocatalytic Conversion of Monosaccharides and Related Sugar Alcohols into Valuable Products

Abstract

In this contribution, we review the electrochemical upgrading of saccharides (e.g. glucose) and sugar alcohols (e.g. glycerol) by drawing conclusions on common trends and differences between these two important classes of bio-based compounds. For this purpose, we critically reviewed the literature on the electrocatalytic oxidation of saccharides and sugar alcohols, seeking trends in the effect of reaction conditions and electrocatalyst design on the selectivity for the oxidation of specific functional groups toward value-added compounds. Importantly, we highlighted and discussed critically the competition between electrochemical and non-electrochemical pathways. This is a crucial and yet often neglected aspect that should be taken into account and optimized for achieving the efficient electrocatalytic conversion of monosaccharides and related sugar alcohols into valuable products, which is a target of growing interest in the context of the electrification of the chemical industry combined with the utilization of renewable feedstock.
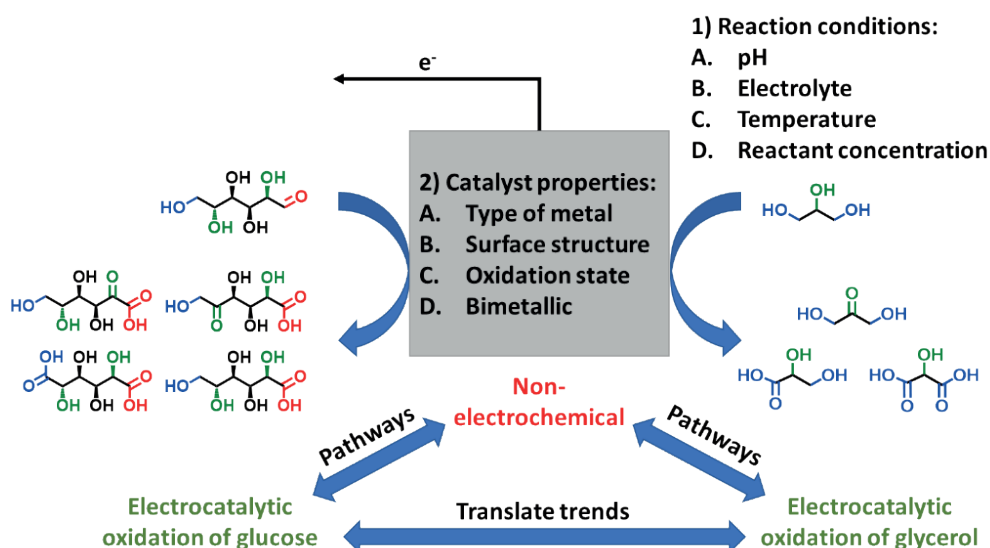
2.1 Introduction

Fossil-based resources account for 86 % of the global energy demand and a staggering 96 % of organic chemicals,[1] accounting for 614 million tons of chemicals per year in 2013.[2–4] These resources are however not sustainable and their use results in the emission of greenhouse, polluting gases (CO_2, CH_4, NO_X, etc.), inflicting environmental and health damage. This requires the search for alternative energy sources and renewable carbon-based resources, which should be environmental friendly, cheap and readily available.[3,5] In this regard, a switch from a fossil-based economy to an electrified and circular/bio-based economy could contribute to a solution.[6] In this context, electricity generated from renewable resources (e.g. wind, solar, hydropower) could serve as an energy source to drive catalytic reactions, while lignocellulosic biomass derived from non-edible agricultural waste streams could serve as a carbon source.[5,7–9] This biomass is composed of carbon-based compounds with a wide range of functionalities (e.g., alcohol, ketone/aldehyde carboxyl groups),[10–12] which offer a large range of possibilities to produce value-added (platform) chemicals.

Currently, most biomass-based feedstocks are processed on an industrial scale via fermentation, stoichiometric or thermocatalytic routes. However, these processes tend to have a substantial impact on the environment.[11] Fermentation processes are slow and require multiple expensive downstream processing steps,[13] while stoichiometric processes generate substantial amounts of waste salts. In this regard, the conversion of biomass-based feedstock via thermocatalytic routes seems an interesting alternative, considering that the catalyst, if heterogeneous, can be readily separated from the products and reused for several runs or for prolonged time on stream, and that no waste salts are generated as byproduct.[14,15] However, thermocatalysis typically requires an energy input in the form of heat to surpass the activation barrier.[16,17] Thermocatalytic redox processes may also require pressurized gaseous reactants such as O_2 or H_2. As an alternative, electrochemical routes can serve as a sustainable and clean method to carry out the conversion of biobased compounds to useful products. In these processes, a higher potential compared to what would be needed based on the thermodynamics of the reaction (i.e., an overpotential) typically needs to be applied to overcome the reaction activation barrier.[18–20] Developing electrocatalysts is crucial to minimize this overpotential and thus to optimize the energy-efficiency of the electrochemical process. In general, electrochemical routes present several potential advantages over conventional chemical production routes. First, the possibility of using ambient temperatures and pressures resulting in mild reaction conditions. Second, the use of H_2O (OH^- or H^+) as proton or oxygen source for the oxidation/reduction allows circumventing the necessity of costly oxidizing/reducing agents. Third, the ease of tuning the reaction conditions (e.g., by tuning the electrode potential) can enable easy control over the reaction rate and selectivity.[3,21] Moreover, electrosynthesis could aid in leveraging the energy surplus generated by energy suppliers, which are subject to fluctuations depending on the availability of their sources.

This is achieved by synthesizing chemicals with chemical bonds containing a high amount of energy, which can then be used as feedstock in fuel cells.[16] Electrosynthesis does not necessarily require an energy input, and if the redox reaction is thermodynamically favorable, it can be achieved in fuel cells that cogenerate electricity and chemicals.[22]

The electrocatalytic valorization of biomass-based feedstock (e.g. saccharides and sugar alcohols) derived from fats, oils and lignocellulose to obtain value-added platform molecules has been widely investigated (Figure 2.1).[23–27] Fats and oils can be obtained from edible crops, waste cooking oils or oleaginous microorganisms, and commonly consist of glycerol linked through ester groups to one to three fatty acids, forming a triglyceride.[28] These triglycerides can be subjected to hydrolysis (or transesterification) to produce free fatty acids (or esters) and glycerol. The obtained free fatty acids/esters can be used as bio-diesel, while glycerol remains a by-product,[28] accounting for 4.2 million tons per year.[29] Lignocellulosic biomass derived from agricultural waste has an even greater potential due to its abundance, accounting for 1470 million tons per year for rice straw, wheat straw, corn straw and bagasse.[30] These lignocellulosic biomass waste streams consists of three main components: cellulose (32-47%), hemicellulose (19-35%) and lignin (5-30%), with the remainder being minor fractions of proteins and ash.[30,31] Cellulose forms crystalline bundles of fibers that are intertwined by hemicellulose and lignin polymers, making it difficult to access and thus process. Hemicellulose is a branched polymer and has an amorphous structure, which makes it the easiest to hydrolyze (via an acid hydrolysis step) to yield monomeric constituents.[32] The composition of hemicellulose is highly dependent on the source and may contain various saccharides (glucose, mannose, galactose, rhamnose and xylose) and uronic acids. The fractionation of cellulose from lignocellulose is applied on an industrial scale via Organosolv and Kraft processes to obtain cellulose pulp.[33] Cellulose pulp has several commercial applications in the paper and building industry, but can also be subjected to an acid or enzymatic hydrolysis step to generate glucose monomers.[32,33] Lignin is a polymer based on phenolic units and with an amorphous structure. Its recalcitrant and complex chemical structure hinders its depolymerization and fractionation into phenolic compounds, which could be then upgraded to BTX compounds (benzene, toluene and xylene).[34] Currently, biorefinery technology is more advanced for the conversion of triglycerides and of the cellulosic and hemicellulosic fractions of lignocellulose and, therefore, the most commonly obtained platform molecules derived from biomass-based feedstock are saccharides (e.g. glucose, xylose) and sugar alcohols (e.g. glycerol).
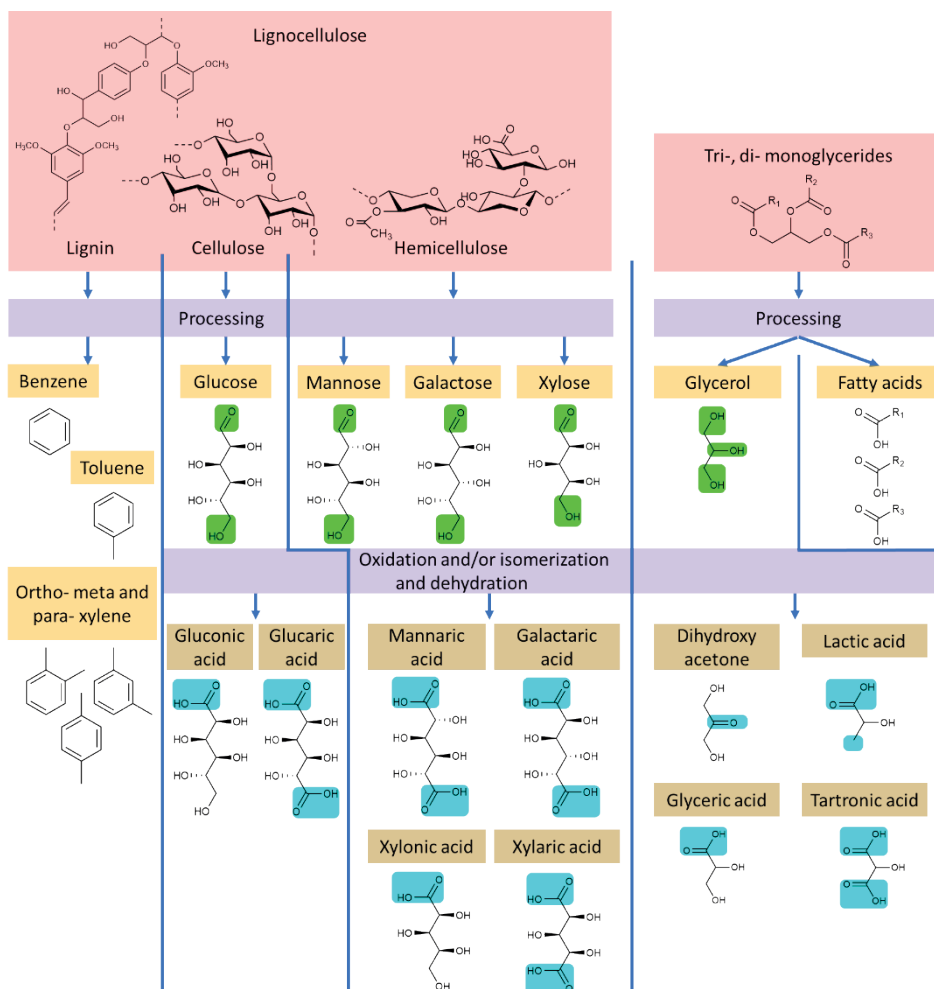
Figure 2.1. *Overview of lignocellulose and fats/oils (red) that can be fractionated to various molecules (yellow). These molecules (e.g., saccharides and sugar alcohols) have common functional groups (green) that typically can undergo oxidation and/or isomerization and dehydration (blue) to obtain value-added platform molecules (gold).*

The electrocatalytic oxidation of sugar alcohols[12,27,35–41] and saccharides[42,43] has recently gained special attention in the (electro)catalysis community, resulting in a growing number of scientific publications. However, current review papers on the electrocatalytic oxidation of sugar alcohols are limited to the selective conversion of glycerol, lacking comparison with other sugar alcohols such as erythritol,[44] arabitol[45] or sorbitol.[44,46–50] On the other hand, the selective electrocatalytic oxidation of glucose and other saccharides has been less extensively reviewed,[42,43] with most reviews on electrochemical oxidation of saccharides being focused on electrocatalyst activity for fuel cell research.[22,51,52] Sugar alcohols and saccharides both contain primary and secondary alcohol groups, while saccharides also have an aldehyde group (in the linear form) or the

corresponding anomeric carbon group (in thy cyclic form). This makes it interesting to evaluate whether the reaction conditions and/or the electrocatalyst properties affect the selective conversion of the two types of reactants in a similar way.

Here, we critically review the literature on the electrocatalytic oxidation of sugar alcohols and saccharides, seeking trends in the effect of reaction conditions and electrocatalyst design on the selectivity for the oxidation of specific functional groups toward value-added compounds. The trends have been divided according to:

a) the effect of reaction conditions on the electrocatalytic conversion of monosaccharides and sugar alcohols (section 2.2);

b) the potential-dependent state of the metal (e.g., Au and Pt) surface (section 2.3);

c) the relation between the features of the electrocatalysts (type of metal, metal oxidation state, exposed facets and mono- vs. bimetallic nature) and their performance in the oxidation of sugar alcohols and saccharides (under various reaction conditions) – see section 2.4;

d) the relation between the features of the electrocatalysts and their performance in the electrocatalytic oxidation saccharides (under various reaction conditions) – see section 2.5.

The focus is on glycerol and glucose as reference molecules to study the reactivity of C3-C6 sugar alcohols and C3-C6 saccharide reactants. Additionally, we look for trends between the two types of reactants, aiming at defining which set of reaction conditions and electrocatalyst properties can favor the selective conversion of each functional group to specific value-added products. This review also aims at providing a critical assessment of the current literature, as well as to propose alternatives for sugar alcohol oxidation based on saccharide oxidation and vice versa.

2.2 Effect of reaction conditions on the electrocatalytic conversion of monosaccharides and sugar alcohols

In this section, the influence of various reaction conditions on the electrochemical conversion of sugar alcohols and monosaccharides is discussed by comparing and rationalizing the behavior of different electrocatalysts that have been reported in the literature. The reaction parameters that have been found to influence the behavior of a certain electrocatalyst in the conversion of monosaccharides and sugar alcohols are: (a) the reaction conditions, e.g., the pH and type of ions of the electrolyte (section 2.2.1), the reaction temperature (section 2.2.2) and reactant concentration (section 2.2.3); (b) the potential-dependent state of the metal (e.g., Au and Pt) surface (section 2.3); and (c and d) the intrinsic properties of the electrocatalyst, e.g., type of metal, metal oxidation state, exposed facets and mono- vs. bimetallic nature) under various reaction conditions (section 2.4 for the oxidation of sugar alcohols; section 2.5 for the oxidation

of saccharides). First, varying these parameters can lead to a change in the configuration of the reactant, for instance by opening a pyranose ring or by forming an anionic form of a sugar alcohol. Secondly, the reactant or products can undergo non-electrochemical conversion in the bulk of the solution, through isomerization, dehydration and/or retro-aldol reactions. Thirdly, the reaction conditions can also affect the oxidation state and surface chemistry of the electrocatalyst employed, and thus its performance. Altogether, these three effects influence the interaction between the reactant and the electrocatalyst, thus contributing to its activity, selectivity and stability. Hence, it is crucial to understand the nature of such influences in order to gain control on, and thus optimize the performance of an electrocatalytic system. The observed trends in selectivity were mainly obtained from electrocatalysts based on Au and Pt. It is worth mentioning that the cell design also plays a crucial role in defining the performance of an electrocatalytic system. However, this parameter is not systematically addressed in the literature and will not be discussed further in this review.

2.2.1 Effect of pH and electrolyte ions on the state of reactant and product

2.2.1.1 Effect of pH

The pH can influence the structure and, if applicable, the neutral *vs.* ionic form of the reactant, which in turn affects the electrocatalyst performance. The pH is also related to the concentration of protons and hydroxide ions in solution, which can act as homogenous catalysts and thereby promote non-electrochemical conversion of the reactant and product in the solution. In this section, the influence of pH on the solution-phase reactions of the reactants and products is discussed, whereas its effect on the electrocatalyst selectivity will be discussed in sections 2.4 and 2.5. It is important to discuss this effect separately and at the outset of the review, as we believe the influence of (pH dependent) solution-phase reactions on activity and especially selectivity has been underestimated in many literature reports.

The electrocatalytic oxidation of sugar alcohols and monosaccharides has been studied under acidic conditions (typically at pH = 1), neutral conditions or alkaline conditions (pH > 7), with the last option being by far the most common.[46,48–50,53–55] It has been proposed that alkaline conditions are more suitable for these oxidations because a basic medium promotes the formation of electroactive species like alkoxides or enediols via non-electrochemical reactions in the electrolyte solution, which then more easily adsorb and react on the electrocatalyst surface, thereby promoting the catalytic activity.[25,55–58]

At neutral pH, the β-anomeric form of glucose is the major equilibrium species (63-67%), followed by the α-anomeric form (33-37 %) and a minor fraction of the linear form (< 0.03%).[56,59,60] The β-anomeric form is the dominant species as it has its alcohol group in the equatorial position (Scheme 2.1), which decreases the steric hindrance[61] and it has an increased number of hydrogen bonds,[59] making it thermodynamically the most stable form. Importantly, under acidic

conditions, the β-anomeric form was found to be the most reactive species for electrocatalytic oxidation reactions over Pt electrodes.[56] β-D-glucose has its anomeric C-H bond at the axial position, whereas α-D-glucose has its anomeric C-H bond at the equatorial position (Scheme 2.1). With the anomeric C-H bond at the axial position, all the OH groups remain in equatorial position, which favors a planar approach of the β-D-glucose molecule to the electrocatalyst surface due to a lower steric hindrance, thus promoting the adsorption of the reactive species and enhancing the electrocatalyst activity.[56] More recently, Holade *et al.* showed that under neutral conditions, the oxidation of the α-D-glucose on Au proceeds faster than that of β-D-glucose.[62] In contrast to Largeaud *et al.*, Holade *et al.* argue that the catalyst activity toward α-D-glucose is higher since the α-anomeric form with its C-OH bond in the axial position more easily adsorbs on the Au surface, which was based on DFT calculations.[62] The ratio between the α-anomeric form and β-anomeric form is dependent on the pH of the solution.[60] Under acidic and alkaline conditions the α-anomer:β-anomer ratio is 45:55 and 10:90, respectively.[60] Moreover, the mutarotation rate from the linear D-glucose to the β-anomer is higher under alkaline conditions, followed by acidic conditions (pH < 2) and then neutral conditions.[56,63] The fast mutarotation of glucose under alkaline conditions made it impossible to distinguish the reactivity of the different anomeric structures.[60] Hence, the time between initiation of the experiment and the addition of D-glucose might affect the catalyst activity that is measured.

In alkaline electrolytes (11 < pH < 12), a sharp increase in electrocatalytic activity was observed for the oxidation of saccharides over Cu,[64] and sugar alcohols over Au.[65,66] This effect was attributed to the formation of the anionic species upon deprotonation of glucose, yielding an enediol species (Scheme 2.1), or upon deprotonation of sugar alcohols[65] yielding an alkoxide. These anionic species are more reactive compared to their protonated counterparts. The pH at which these anionic species are formed is dependent on the pK_a of the reactant.[64] When the pH is increased above 12, a further increase in electrocatalytic activity (current density) for the oxidation of sugar alcohols and saccharides is typically observed (e.g. for electrocatalysts based on Ni, Pd, PtAu, NiPd).[67–71] At highly alkaline conditions (3 M NaOH, pH ≥ 14.5), a stagnation or a decrease in activity toward glycerol and glucose oxidation has been reported.[67,69,71] It has been suggested that the adsorption of hydroxide ions under these conditions prevents the adsorption of the reactants on the surface of the catalyst.[69,71] However, it is important to note that if hydroxide binds to the surface as neutral hydroxyl OH_{ads}, which is usually assumed, there cannot be a higher pH-dependent OH_{ads} coverage on the same potential on the RHE scale.

Depending on the pH, protons or hydroxide ions can act as homogenous catalysts and thereby induce non-electrochemical conversion of the reactants by isomerization, retro-aldol reaction, aldol condensation, dehydration, Cannizzaro rearrangement, oxidative degradation and aerobic oxidation reactions. These homogeneous reactions are also affected by the presence of oxygen

in solution, temperature, initial reactant concentration, and type of electrolyte.[46,72,73] Most electrochemical reactions are performed below 60 ˚C and under anaerobic reaction conditions. At these temperatures, under acidic conditions, most homogeneous reactions do not occur at a significant rate.[74,75] Therefore, only the homogeneous reactions that prevail under alkaline conditions are discussed here. Moreover, the effect of oxygen present in the solution, which can be formed at the anode surface or can be present in the case of incomplete deaeration before electrocatalytic experiments, must be considered as it strongly influences the products that are formed in homogeneous reactions.[46,73]

Considering isomerization reactions first, glucose tends to isomerize into the thermodynamically more stable fructose or mannose, as illustrated in Scheme 2.1.[76] The isomerization rate of glucose is higher at more alkaline conditions (becoming significant at pH ≥ 10.0) and elevated temperatures,[25,77,78] but is also highly dependent on the type of electrolyte as a combination of bromide and lithium ions can catalyze isomerization reactions in solution.[79] In line with these observations, the saccharides obtained through the electrocatalytic oxidation of sugar alcohols (e.g. glucose from sorbitol and glyceraldehyde from glycerol), can undergo these non-electrochemical isomerization reactions in alkaline media. Hence, the electrocatalytically formed glyceraldehyde (GALD) can isomerize non-electrochemically to the thermodynamically more stable dihydroxyacetone (DHA) under inert conditions,[80] while this reaction appears to be limited in oxygen rich solutions.[46,73] Therefore, the observation of a high DHA selectivity from glycerol oxidation in alkaline media is not necessarily the result of a selective catalyst; the influence of the solution-phase isomerization must be considered carefully.
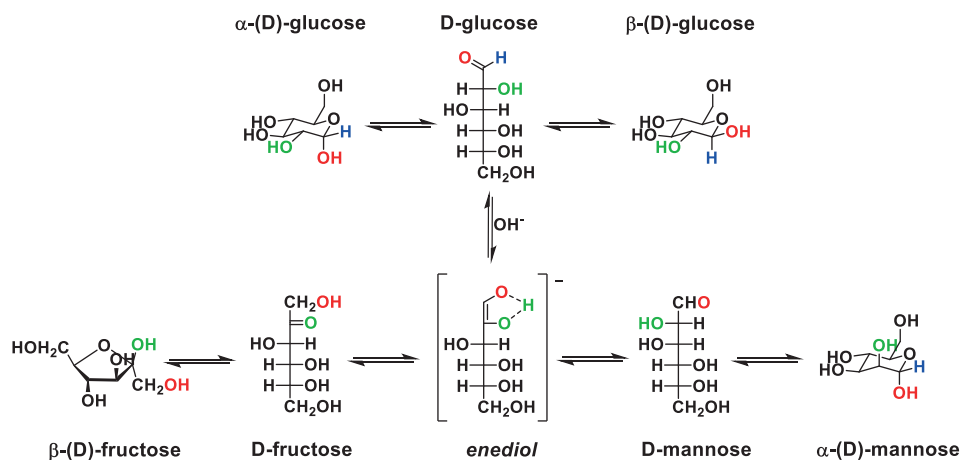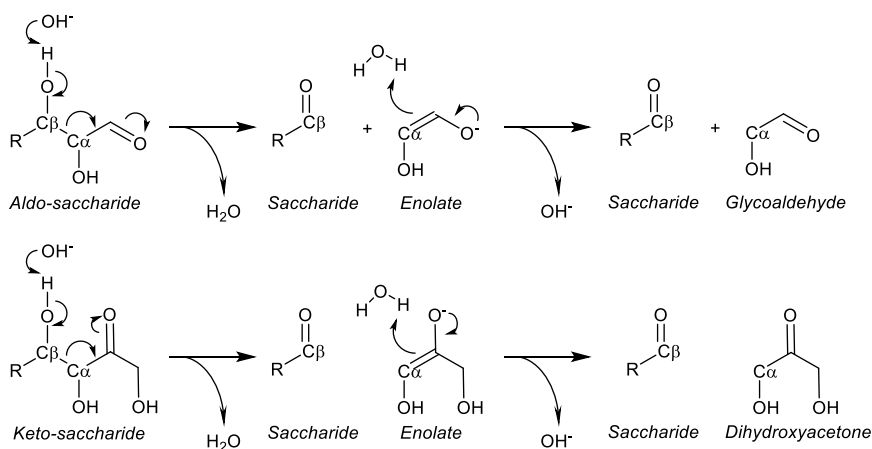

Scheme 2.1. *Reaction scheme displaying the non-electrochemical isomerization reactions taking place in the electrolyte in the presence of a base.*

An important second class of non-electrochemical homogeneous reactions are retro-aldol reactions, which result in the cleavage of the C_α-C_β bonds adjacent to a carbonyl of keto-

saccharides or an aldehyde of aldo-saccharides in alkaline solutions already at room temperature, as illustrated in Scheme 2.2.[72,73,81] More specifically, a hydroxide ion abstracts a proton from the C_β-OH group. As a result, the electrons rearrange and the C_α-C_β bond breaks, resulting in the formation of two smaller molecules. Thus, the retro-aldolization of glucose (e.g., aldo-saccharide) cleaves the C2-C3 (e.g., C_α-C_β) bond resulting in the formation of glycol aldehyde and erythrose, while the retro-aldolization of fructose (e.g., keto-saccharide) cleaves the C3-C4 bond resulting in the formation of glyceraldehyde and dihydroxyacetone.[72,73] The successive retro-aldolization of erythrose results in the formation of two glycoaldehydes.[72,81] Interestingly the retro-aldolization of glyceraldehyde was not observed under anaerobic conditions,[46] indicative that this reaction only proceeds for ≥C4 molecules. Importantly, the retro-aldol reaction is more dominant under anaerobic conditions, as oxygen rich conditions tend to enhance oxidative C-C cleavage reactions and the aerobic oxidation of aldehydes.[73] The retro-aldol reaction is in equilibrium with the aldol condensation reaction. For example, in the case of GLAD, a proton is abstracted from an hydroxide ion at C_α, resulting in an enediol which can react with a GLAD or DHA (isomers) forming glucose and fructose, respectively.

Scheme 2.2. *Reaction scheme displaying the retro-aldolization of aldo-saccharides (e.g., glucose) and keto-saccharides (e.g., fructose) taking place in the electrolyte in the presence of a base.*

A third class of relevant non-electrochemical homogeneous reactions is the dehydration of saccharides and their corresponding isomers. Under alkaline conditions, the dehydration of glyceraldehyde or dihydroxyacetone is often reported as it is a key step in the synthesis of lactate,[73] while the dehydration of glucose or fructose has been reported only under more acidic conditions at elevated temperatures,[73,82,83] since alkaline conditions promote retro-aldol reactions.[73,84] In the case of GLAD and DHA, both molecules can undergo a dehydration to form 2-hydroxypropenal, which can undergo keto-enolic tautomerization to pyruvaldehyde.[73,85,86] Successively, pyruvaldehyde can undergo an intramolecular Cannizzaro rearrangement to form

lactate (LA).[73,85] These reactions compete with aldol condensation reactions (especially at high glyceraldehyde concentrations[46]) and can be promoted under optimized reaction conditions, resulting in relatively high LA selectivities.[73] For example, the presence of divalent cations (e.g., Ba^{2+}, Cu^{2+}, Ca^{2+}, Zn^{2+} and Pb^{2+}) can redirect the pyruvaldehyde reaction toward a 1,2-hydride shift, resulting in a stabilized lactate salt, which can be acidified to produce LA.[73] Li *et al.* showed that the dehydration of DHA to pyruvaldehyde followed by a 1,2-hydride shift is the main reaction pathway for LA formation, while the pathway from GLAD to LA only plays a minor role since the LA yield was higher when starting from DHA than from GLAD.[73] Moreover, under oxygen-rich conditions the formation of LA was significantly lower,[46,73] which was attributed to the promotion of oxidative C-C cleavage reactions and the aerobic oxidation of aldehydes under these conditions.[73]

A fourth and fifth class of non-electrochemical homogeneous reactions are the oxidative C-C cleavage reactions and the oxidation of aldehydes. These reactions become dominant in alkaline solutions when oxygen is present in the electrolyte.[46,73] For example, in the presence of oxygen and at pH = 13, Kwon *et al.* showed that glyceraldehyde is predominantly converted to glycerate, glycolate and formate. In this case, the formation of glycerate is promoted by the oxidation of aldehydes mediated by molecular oxygen. In parallel, the formation of formate and glycolate is mediated by the oxidative C-C cleavage reactions in solution. In this reaction, glyceraldehyde first forms an enediol. Successively, the enediol can be attacked by the nucleophilic oxygen molecule at the C1 or C2 group to produce a hydroperoxide intermediate.[87] The resulting hydroperoxide intermediate undergoes a series of rearrangements, resulting in the formation of formate and glycolate. In the case of glucose, this reaction proceeds in a similar manner and results in the formation of formate and arabinonate.[87]

2.2.1.2 Effect of electrolyte ions

A less commonly studied topic is the effect of electrolyte ions on the catalyst selectivity.[88] A recent study on the electrocatalytic oxidation of glycerol over NiOOH researched experimentally and computationally the effect of electrolyte cations on the catalyst selectivity. It was found that the aldehyde intermediates of the electrocatalytic oxidation of glycerol (glyceraldehyde and glycolaldehyde) were stabilized more effectively in the presence of smaller cations (Li^+) than in the presence of larger cations (K^+). As a result, Li^+ inhibits the successive oxidation of the aldehydes, as was shown by chronoamperometric (CA) measurements. It was argued that the delayed oxidation of these aldehydes gives hydroxide anions more time to induce nucleophilic attacks, thereby promoting C-C cleavage reactions. This effect was substantiated by using crown ethers to coordinate the ions, thus preventing them from interacting with the aldehyde intermediates during the electrocatalytic oxidation of glycerol, which ultimately resulted in a fast decrease in the rate of C-C cleavage reactions. A related study was conducted with a cobalt borate electrode to electrocatalytically oxidize glycerol with dissolved borax ($Na_2B_4O_7$) as supporting

electrolyte.[89] The borax ions hydrolyze to form $B(OH)_4^-$, which were found to interact with the primary alcohol groups of glycerol (as revealed by NMR), consequently promoting the coordination of the secondary alcohol group with the surface of the electrode (Figure 2.2). This was suggested to enhance the electrocatalytic oxidation of the secondary alcohol group of glycerol, resulting in a high selectivity toward dihydroxyacetone, which could be further promoted from 50 to 60 % by increasing the electrolyte concentration from 0.05 M to 0.2 M borax.[89] Likewise, an increase in pH promoted the formation glycerol-borate complexes, thereby further improving the selectivity toward DHA.[89] Moreover, for the electrocatalytic oxidation of glycerol in 0.2 M $Na_2B_4O_7$, a ~250 mV lower potential resulted in the same current density (e.g., catalytic activity) when compared to 0.2 M Na_2SO_4.
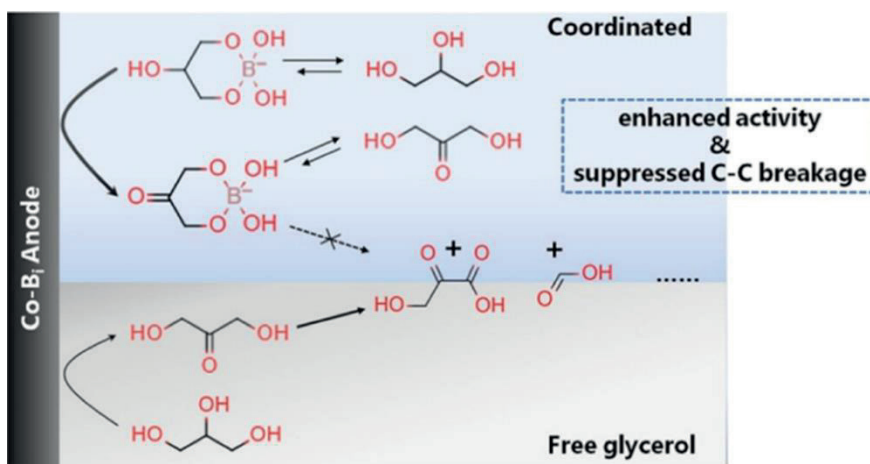

Figure 2.2. *The coordination of glycerol induced by borate ions in solution. By bonding with both primary alcohols, the secondary alcohol becomes more susceptible for the electrocatalytic oxidation promoting the formation of dihydroxyacetone and stabilizing dihydroxy-acetone through the formation of a dihydroxy-acetone-borate complex, reducing further oxidation reactions. Reprinted with permission from* [89]. *Copyright 2021 American Chemical Society.*

In conclusion, alkaline conditions promote electrocatalytic reactions by the formation of more electroactive species, but can also induce numerous non-electrochemical reactions. These non-electrochemical homogeneous reactions can be coupled with electrocatalytic reactions to steer the selectivity of the system toward a desired product. Since most electrochemical studies on the electrocatalytic oxidation of sugar alcohols[46,49,53,90–93] and saccharides[25,52,56,64] are performed under alkaline conditions, we argue that more control experiments on the reactants and the (intermediate) products should be performed to evaluate the effect of non-electrochemical reactions on the obtained product distribution, including the effect of oxygen in solution. This will give more insight on the relation between the electrocatalyst properties and the obtained selectivities and will aid in gaining insights into how the reaction pathways can be controlled. Moreover, the effect of ions present in the electrolyte should not be overlooked as they can form

complexes with the reactants or (intermediate) products and thereby affect the electrocatalyst selectivity.

2.2.2 Effect of reaction temperature

The number of publications on the effect of temperature on the electrocatalytic oxidation of sugar alcohols and saccharides is limited. Yet, the temperature becomes an increasingly important factor for large scale electrocatalytic systems, since these systems suffer more significantly from heat generated by resistances (e.g., ohmic drop). Therefore, research on the electrocatalytic oxidation of sugar alcohols and saccharides should dedicate more attention to the effect of temperature. The role of temperature on the performance of Au and Pt electrocatalysts toward the oxidation of sugar alcohols and saccharides was found to be independent of the functional groups of the reactant itself (-OH vs. C=O). It is worth highlighting that almost all the publications in which the influence of temperature was studied, were performed under alkaline conditions[25,94–102] with, to the best of our knowledge, only one paper studying temperature effects under acidic conditions.[103]

Most studies that report an effect of temperature on the electrocatalytic oxidation of sugar alcohols and saccharides, show that an increase in temperature results in an expected increase in current density, as measured by LSV (linear-sweep voltammetry) or cyclic voltammetry (CV).[94,95,97–102] In fact, several researchers have shown that there is an approximate linear relationship between the natural logarithm of the peak current density and the inverse of the temperature for the oxidation of both sugar alcohols (glycerol and sorbitol)[95,101] and saccharides (glucose),[100,102] which is in line with the Arrhenius equation. Likewise, for Pt/C at pH = 8, with increasing temperatures from 20 to 50 °C the cell potential decreased and glucose oxidation reaction rate increased.[104] By contrast, for Au-based electrocatalysts (at E = 0.4-1.3 V), in the presence of glucose and under alkaline conditions (pH = 13), when increasing the temperature from 35 to 55 °C, the catalyst activity dropped (Figure 2.3).[100] This effect was attributed to the formation of poisoning species, as was indicated by the coloration of the electrolytic solution.
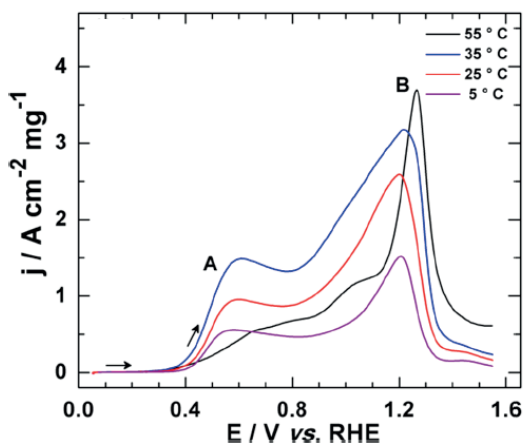
Figure 2.3. *LSV of an Au-based electrode in 0.1 M NaOH at 20 mV s^{-1} scan rate in the presence of 10 mmol·L^{-1} glucose at different temperatures in the 5-55°C range. Adapted with permission from [100]. Copyright 2015 American Chemical Society.*

The reaction temperature can have a negative effect on the selectivity, as was shown for the electrochemical oxidation of glycerol over Pt/C and PtRu/C electrocatalysts in terms of the production of tartronic acid (TA).[97,98] In this system, the selectivity toward C3 oxidation products was reduced from 96 to 91% and down to no more than 7% when the temperature was increased respectively from 30 to 60 to 90 °C, as C-C cleavage reactions were boosted at high temperature. Similarly, for the electrocatalytic oxidation of glucose to gluconic acid (GA) over Au-based electrodes, high temperatures resulted in higher concentrations of fructose (isomerization) and C-C cleavage products (degradation).[25] The C-C cleavage products prevail at high temperatures, as higher activation energy barriers are more easily surpassed. Under alkaline conditions (pH > 10), an increase in temperature can induce two effects in the conversion of glucose. First, the reactant concentration can decrease due to non-electrochemical reactions such as the isomerization of glucose (mainly to fructose) and retro-aldol reactions forming C1-C3 products. Second, an increase in the concentration of these products can induce a lower catalytic activity as they are less reactive toward oxidation, e.g. in the case of fructose when compared to glucose.[94]

Some studies also report a positive temperature effect on the electrocatalyst selectivity, as was shown for the production of gluconic acid and glucaric acid from glucose, and dihydroxyacetone or lactic acid (LA) from glycerol.[24,96,103,105] For instance, under acidic conditions (0.5 M H$_2$SO$_4$), a selectivity of 63% dihydroxyacetone was achieved at 60 °C with PtSb/C,[103] being the highest selectivity in the temperature range of 25-70 °C. Lam *et al.* achieved 34% LA selectivity with a Co-based electrocatalyst at 60 °C,[96] while only 16% LA was formed at 40 °C. According to the pH-dependent reactant reactivity, this enhanced formation of LA from dihydroxyacetone is not directly related to the electrocatalyst, but to non-electrochemical reactions (section 2.2.1.1, see

32

discussion on dehydrogenation and Cannizzaro rearrangement). Other studies show that high temperatures reduce the selectivity for the electrocatalytic conversion of sugar alcohols and saccharides.[25,97,98] For the oxidation of glucose under neutral conditions, it was shown that glucarate (Sel. = 65%) is best achieved at 15 ˚C, while at 30 ˚C the highest selectivity was obtained toward gluconate, whereas even higher temperatures resulted in a loss in selectivity toward glucarate and gluconate.[24] A possible explanation could be the use of acidic conditions in that study, which limit isomerization and C-C cleavage reactions.[96]

In summary, there is only limited research on the effect of temperature in electrosynthesis studies for sugar alcohols and saccharides oxidation. Yet, large scale electrocatalytic systems suffer not only from overpotentials but also ohmic drop, leading to heating effects, thereby affecting the temperature of the system. Hence, it is crucial to gain more insight on the effect of temperature on electrocatalytic systems. The studies that have been devoted to the effect of temperature are often performed under alkaline conditions, which are likely to be severely affected by (temperature-dependent) non-electrochemical reactions (see section 2.2.1). This issue should be addressed more carefully in future studies.

2.2.3 Effect of reactant concentration

There have been several studies on the electrocatalytic conversion of monosaccharides and sugar alcohols in which the influence of the reactant concentration was assessed.[25,48,57,68,95,106–112] Some trends can be identified by comparing the results of various systems, irrespective of the type of reactant.
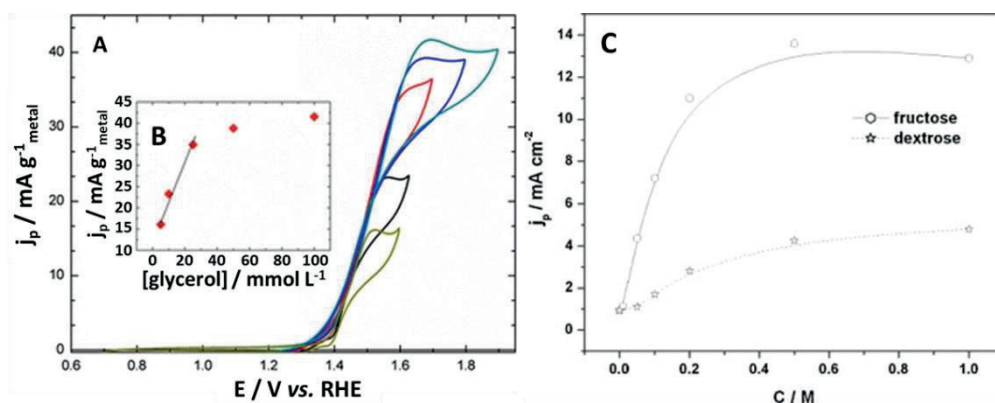
Figure 2.4. (a) CV of a Ni/C electrode in 0.1 M NaOH at different glycerol concentrations, and (b) the influence of glycerol concentration on the anodic peak current density, as derived from plot a. Adapted with permission from [68]. Copyright 2015 Springer Nature. (c) Peak current density for fructose and dextrose oxidation on a MnO_2/Pt electrode in 0.5 M Na_2SO_4, as a function of fructose and dextrose concentration. Adapted with permission from [107]. Copyright 2008 Elsevier.

If we consider the example of the oxidation of glycerol in alkaline environment (Figure 2.4a) in which the reaction is carried out with a large excess of base compared to glycerol (as it generally is the case), an approximately first order reaction kinetics in reactant concentration is observed up to a certain concentration, above which the reaction order decreased. Such a behavior has also been reported for the electrocatalytic oxidation of both monosaccharides and sugar alcohols, showing an initially linear increase in current density in cyclic voltammetry (CV) experiments with increasing reactant concentration (Figure 2.4b shows an example for fructose and dextrose, from a neutral solution).[57,68,95,106–109] At lower concentrations, the diffusion rate of the reactant from the bulk to the electrode (which depends on the reactant concentration) is lower than the rate of the conversion of the reactant at the electrode, implying that all the reactant that reaches the electrocatalyst surface is immediately converted, and first order kinetics are observed. At higher concentrations, the rate of the conversion of the reactant at the electrode becomes the limiting factor, implying that the active sites of the catalyst are saturated with the adsorbed reactant, and zeroth order kinetics are observed in the CV tests (Figure 2.4b and 2.4c).[68,107,108,110,111] It should be noted that very high concentration of saccharides can be detrimental as it can lead to an increased viscosity of the solution, which can decrease the conductivity of the electrolyte and thus result in higher ohmic losses. Moreover, the high reactant concentrations can result in an excess of (oxidized) compounds on the electrocatalyst surface, hindering the adsorption of hydroxide ions and thus decreasing the oxidation rate of adsorbed reactants.[104]

At similar reaction times in batch cells[25,48,112] and at similar hydraulic retention times in flow cells[113] but different initial reactant concentrations, the selectivities can significantly differ as different reactions may have different reaction orders. For example, low reactant concentrations tend to lead to high conversions in chronoamperometry tests (i.e., longer tests than those by CV), resulting in the coexistence of primary oxidation products (e.g., glyceraldehyde from glycerol and gluconate from glucose) with further oxidation products (e.g., glycerate in the case of glycerol and glucarate in the case of glucose).[25,48,112,113] For higher reactant concentrations, the conversion decreases, together with a rise in the selectivity toward primary oxidation products: the reactant tends to occupy the electrocatalyst surface, thereby decreasing the formation of sequential oxidation products.[25,48,112] For the electrochemical oxidation of glycerol in 0.1 M KOH on AuPt bimetallic catalysts during 12 h,[67] the overall conversion decreased from 58 to 15% when the glycerol concentration was increased from 0.1 M to 1 M, but the selectivity toward lactate (LA) remained unaltered. A possible explanation is that the initial oxidation product of glycerol, glyceraldehyde, is converted non-electrochemically in the basic solution into lactate (see section 2.2.1.1).

To conclude, the initial reactant concentration can strongly influence the reaction rate and the reaction selectivity. Studies showed that an increase in reactant concentration changes the kinetics from quasi-first order, dominated by diffusion rates of the reactant to the surface of the

catalyst, to zeroth order, dominated by intrinsic kinetic rates of the catalyst. Moreover, considering similar reaction times, low initial reactant concentrations result in multiple oxidation products, while high initial reactant concentrations results in fewer oxidation products, resulting in less complex reaction mixtures and thus easier downstream processing procedures. Hence, to compare the performance of catalysts between different studies it is recommended to perform similar conversions and use similar reactions conditions, such as initial reaction concentrations, pH, temperature, reaction times, and number of catalytic active sites.

2.3 The potential-dependent state of the Pt and Au surface

In electrocatalytic oxidation processes, the kinetics and selectivity of the reaction can be controlled by means of the applied potential. Yet, an increase in applied potential can have two effects: (1) it lowers the activation energy for electron transfer reactions and thereby increases the rate of electrocatalytic oxidation, and (2) it can change the oxidation state of the electrocatalyst surface from metallic to oxidic (i.e. metal hydroxide, oxyhydroxide or oxide), which in turn can affect the activity and selectivity of the catalyst. Therefore, in this section we distinguish between these two effects by considering the surface oxidation state of the electrocatalyst as a function of potential.
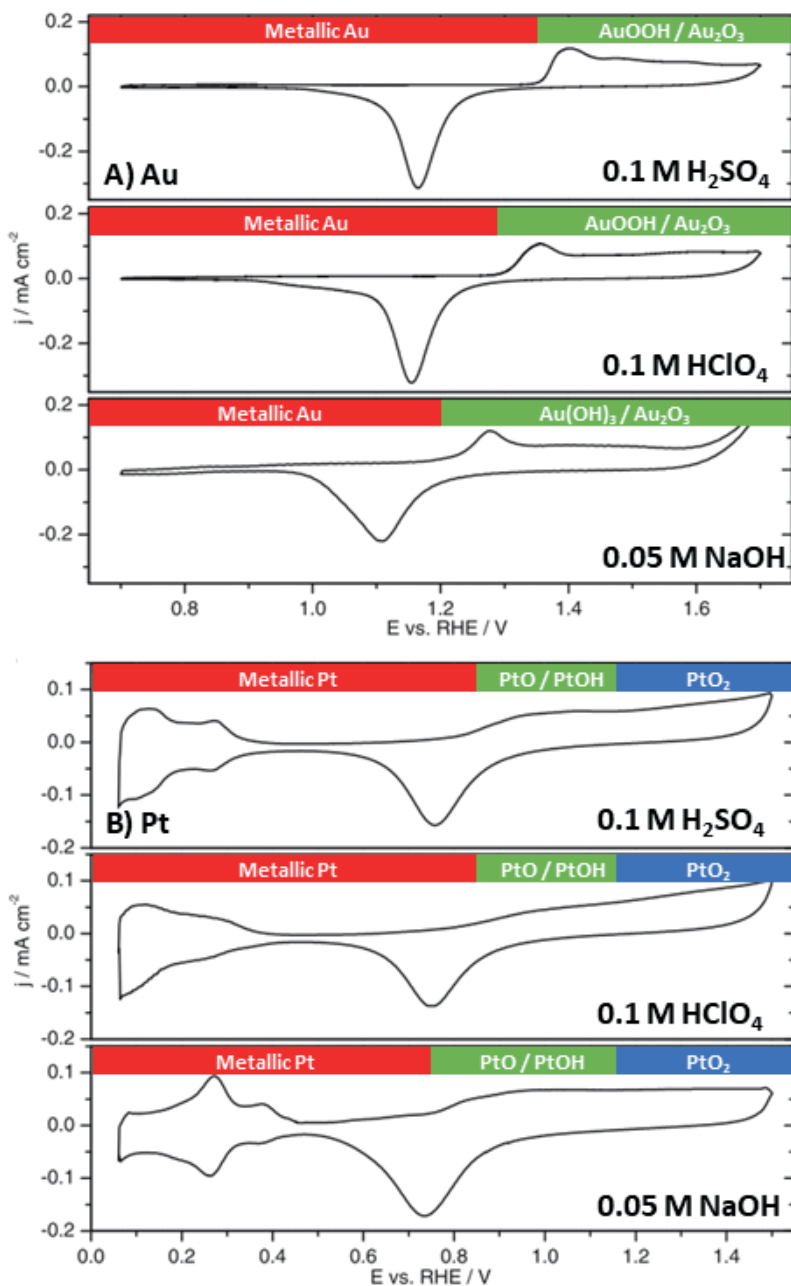
Figure 2.5. *Cyclic voltammograms of A) polycrystalline Au and B) polycrystalline Pt obtained under acidic conditions (0.1 M H2SO4 and 0.1 M HClO4) and alkaline conditions (0.05 M NaOH) measured in a flow cell at 50 mV s-1. Adapted with permission from [114]. Copyright 2014 The Electrochemical Society.*

A common approach to evaluate the oxidation state of electrodes is by deriving it from the Pourbaix diagrams. However, these diagrams do not only consider the surface oxidation state but also the bulk oxidation state. Therefore, to illustrate the effect of the potential on the state of the electrode surface, we plotted in Figure 2.5 the so-called blank cyclic voltammograms of polycrystalline Au and Pt in three representative electrolytes.

For Au, at pH = 1 in 0.1 M H_2SO_4, an increase in current density can be observed at 1.35 V vs RHE, which corresponds to the formation of gold oxyhydroxide/gold oxide ($AuOOH/Au_2O_3$), as was shown by in-situ surface-enhanced Raman spectroscopy (SERS).[115] In 0.1 M $HClO_4$, the onset potential for the formation of $AuOOH/Au_2O_3$ is ~1.28 V, based on DFT calculations[116] and in-situ SERS,[117] which is 0.07 V lower than in 0.1 M H_2SO_4 (as also deduced from the different onset potential for surface oxidation in Figure 2.5A). By contrast, at pH = 12.7 (0.05 M NaOH) an increase in current density already takes place at 1.2 V vs RHE and results in the formation of a gold hydroxide/gold oxide ($Au(OH)_3/Au_2O_3$) species.[115] This shows that metallic Au has a larger potential window under acidic conditions than under alkaline conditions[114,115] and that in acidic media anions strongly influence the surface oxidation potential.[114,115,117] The presence of Au_2O_3 at potential above 1.70 V under acidic conditions (0.1 M $HClO_4$) and above 1.57 V under alkaline conditions (0.05 M NaOH) was shown by *in situ* electrochemical surface-enhanced Raman spectroscopy.[117] The surface gold oxides reduce again with decreasing potential conditions at 1.18 V in acidic conditions and at 1.1 V in alkaline conditions.[114,115] The difference in reduction peak potential under acidic and alkaline conditions is an indication of the formation of different surface oxide species under these conditions.[114,115]

The typical CVs of Pt at different pH conditions are illustrated in Figure 2.5B. For Pt, at pH = 1 and pH = 13 the positive current from 0.1 to 0.35 V vs RHE corresponds primarily to the desorption of adsorbed hydrogen.[118–120] At step edges and corner sites, the desorbed hydrogen is replaced by adsorbed *OH species under both acidic and alkaline conditions in this potential region.[118–121] At pH = 1, for systems containing H_2SO_4 or $HClO_4$, an onset potential for surface oxidation can be observed at 0.85 V vs RHE, which is related to the chemisorption of hydroxide and/or oxygen on the Pt surface ($PtO/PtOH_{surf}$),[114,122–124] while at pH = 12.7 the onset potential for $PtO/PtOH_{surf}$ formation can be observed at 0.75 V vs RHE.[114,119] This shows that the potential window for metallic Pt is larger under acidic conditions than under alkaline conditions. Independent of the pH, above 1.15 V the place exchange of oxygen and platinum atoms occurs, and oxygen penetrates the Pt lattice up to a few monolayers to form PtO.[118,119,125,126] At 1.2-1.3 V vs RHE, PtO is converted into PtO_2 and when the potential is decreased PtO_x reduces back to metallic Pt at ~0.75 V under both acidic and alkaline conditions.[118,119,122,127,128] We note that the exact surface composition of the surface oxide is mixed and very dependent on the structure of the underlying metallic Pt. Our usage of the terms $PtO/PtOH_{surf}$, PtO and PtO_2 is therefore indicative of the

expected dominant surface oxide, but should not be taken as an accurate indication of a single Pt surface oxidation state.

The above discussion shows that the surface oxidation state of Au and Pt depends on the applied potential and pH of the electrolyte. For Au, the following surface oxidation states can be distinguished: (1) metallic Au from 0.1 to 1.28 V vs RHE under acidic conditions[116,117] and from 0.1 to 1.20 V vs RHE under alkaline conditions,[115] (2) AuOOH/Au_2O_3 above 1.28 V vs RHE under acidic conditions[116,117] and Au(OH)$_3$/Au_2O_3 above 1.20 V vs RHE under alkaline conditions.[115,117] For Pt, the following surface oxidation states can be distinguished: (1) metallic Pt from 0.1 to 0.85 V vs RHE under acidic conditions[114,122,123] and from 0.1 to 0.75 V vs RHE under alkaline conditions,[114,119] (2) PtO with possible surface hydroxide groups exists from 0.85 to 1.3 V vs RHE under acidic conditions[114,122,123] and from 0.75 to 1.3 V vs RHE under alkaline conditions,[114,118,119,125,126] and (3) PtO_2 > 1.3 V vs RHE.[118,119,122,127,128] As mentioned, in reality mixed oxidic phases are expected to exist on the surface of the electrode.

In this review, all the pH values have been calculated from the electrolyte concentrations (note that this can slightly deviate from reality) and all the reference potentials found in literature have been converted to RHE to avoid potential shifts caused by the pH of the electrolyte.[129] Therefore, the potentials reported in this paper (which are referred to RHE) may deviate from potentials in the cited articles (which are typically referred to Ag/AgCl or Hg/HgO). These calculated RHE potentials can then be used to estimate the oxidation state of the Au and Pt catalyst under acidic and alkaline conditions, based on the cyclic voltammetry shown in Fig.1. This approach enables us to group studies that have been conducted under similar reaction conditions and define trends for the electrocatalytic oxidation of sugar alcohols and saccharides. Yet, it must be noted that real surface oxidation state of Pt and Au is often not precisely known and that this approach only gives a first approximation. Other factors that might affect the surface oxidation state of Au and Pt are the type of electrolyte, the pH of the electrolyte, the adsorption of reactant/products, and (if present) the support of the metal species in the electrocatalyst. For example, a different electrolyte, such as sulphate or perchlorate, slightly changes the onset of oxidation of Au and Pt.[130] In addition, the pH affects the type surface oxide formed,[115] while the support can either withdraw or donate electrons to the supported metal,[131,132] thereby affecting the oxidation state of the catalyst. Therefore, we will consider these factors when there is evidence that they had a significant impact on catalyst performance.

## 2.4 Effect of electrocatalyst properties under various reaction conditions on the oxidation of sugar alcohols

This section presents and discusses the trends reported in the literature for the catalyst activity and selectivity in the electrocatalytic oxidation of sugar alcohols. In the majority of the studies that address this topic, Au and Pt (sections 2.4.1.1 and 2.4.1.2, respectively) were employed as

electrocatalysts, for which it has been possible to define trends with respect to the electrocatalyst properties such as the type of metal used, the oxidation state of the metal and type of bi-metallic catalyst. Au is discussed first as it is generally found to be a less active but more selective electrocatalyst for oxidation reactions when compared to Pt. Studies with other metals are scarcer, but some of them allow achieving high selectivity toward specific value-added products (see section 2.4.1.3-2.4.1.5). Before going into detail in what trends have been observed in the literature, the main mechanistic pathway for the electrocatalytic oxidation of glycerol is summarized first.

The most commonly studied sugar alcohol in electrocatalytic oxidation reactions is glycerol, which we use in this review as a basis to define trends found in literature. The trends observed with glycerol were compared to the electrocatalytic oxidation of other sugar alcohols. Scheme 2.3 gives an overview of the different reaction pathways published.[46,67] The scheme shows that glycerol can either be electrocatalytically oxidized at the primary or secondary alcohol group, forming respectively glyceraldehyde (GALD) or dihydroxyacetone (DHA). GALD and DHA inter-isomerize in the electrolyte under alkaline conditions, with DHA being the more stable isomer (see section 2.2.1.1). Under oxidative potentials, the aldehyde group of GALD can be electrocatalytically oxidized to form glyceric acid (GLA), which in turn can be further oxidized at the remaining primary alcohol group to form tartronic acid (TA). TA can also be oxidized electrocatalytically at the secondary alcohol to form mesoxalic acid (MOA). DHA can be oxidized electrocatalytically at the primary alcohol to form hydropyruvic acid (HPA). HPA could potentially be oxidized electrocatalytically to MOA, although this pathway has yet to be observed. Alternatively, under alkaline conditions GALD and DHA can be dehydrated non-electrochemically in the electrolyte to form 2-hydroxypropenal, which can undergo keto-enolic tautomerization to pyruvaldehyde (see section 2.2.1.1). Successively, pyruvaldehyde can undergo an intramolecular Cannizzaro rearrangement (see section 2.2.1.1) to form lactic acid (LA).
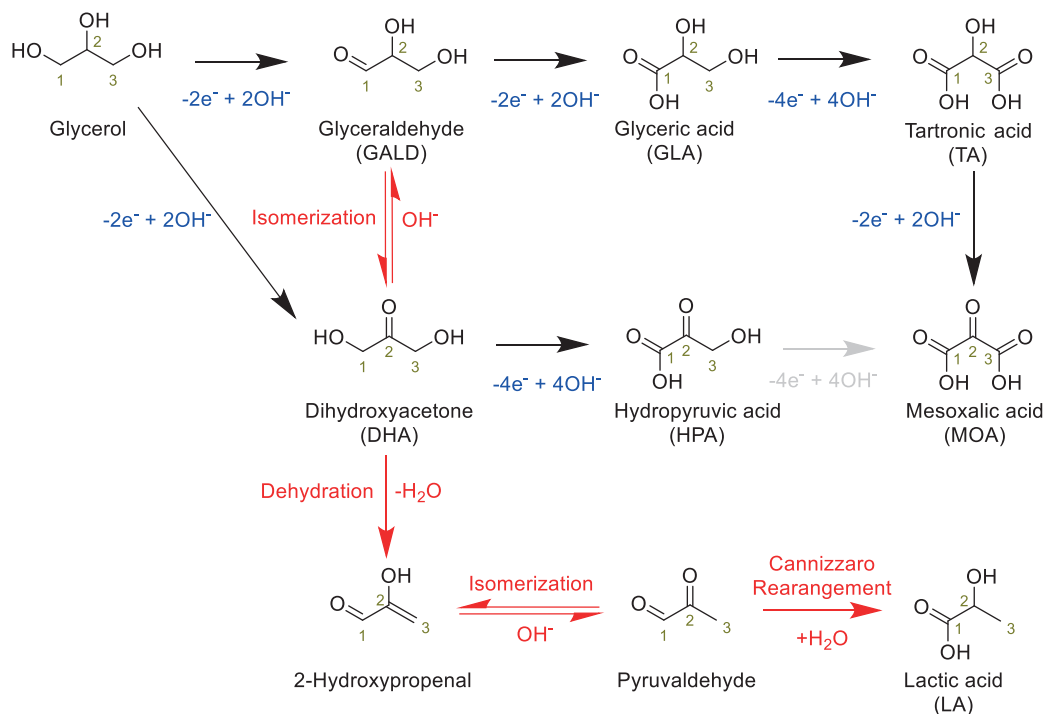
Scheme 2.3. *Main reaction pathways for the electrocatalytic oxidation (black arrows with number of electrons/hydroxides in blue), potential but non-observed electrocatalytic oxidation pathway (grey arrow) and non-electrochemical conversion (red arrows) of glycerol and derivatives observed in literature.*

2.4.1 Monometallic electrocatalysts

This section describes the trends for the selective electrocatalytic oxidation of sugar alcohols over the most studied electrocatalysts, being those based on Au (2.4.1.1) and Pt (2.4.1.2), and compares the trends with electrocatalysts based on Pd, Ir, and Ru (2.4.1.3), Ni and Co (2.4.1.4), and Cu and Mn (2.4.1.5). The trends for these electrocatalysts have been categorized based on increasing pH and potential.

2.4.1.1 Au-based electrocatalysts

This section discusses the electrocatalytic oxidation of glycerol on Au at different pH and potentials. To our knowledge, only Valter *et al.* studied the differences in activity for glycerol oxidation on different Au facets.[54] Moreover, only a few studies have reported the electrocatalytic oxidation of sugar alcohols over Au electrodes under acidic[53,54] and neutral conditions.[46] On the other hand, alkaline conditions have been widely studied, as these conditions give higher activity due to the higher reactivity of the alkoxides (see section 2.2.1.1).[46,49,53,90–93] Acidic conditions are considered first to distinguish between electrochemical and non-electrochemical reactions, even though the activity of Au is poor under acidic conditions.

Only three studies report that Au has some activity for the electrocatalytic oxidation of sugar alcohols under acidic conditions,[53,54,133] while other studies argue that Au has no appreciable activity[65] or is inactive under these conditions (based on LSV).[46,134] CV experiments on an Au electrode in 0.1 M $HClO_4$ showed that the currents are higher in the presence of glycerol than in its absence, in a broad potential range (at E = 0.55-1.65 V). However, current densities are (very) low (< 0.1 mA cm^{-2}), with somewhat higher current densities (0.4 mA cm^{-2}) obtained at $E \geq 1.30$ V.[54] Based on the range of potentials in which activity toward glycerol oxidation was observed and considering that Au is expected to be in oxidized state at $E \geq 1.30$ V (see section 2.3), it can be inferred that both metallic and oxidized Au species at the electrode surface are mildly active for glycerol oxidation, with perhaps a slightly higher activity for oxidized gold. By contrast, in 0.1 M H_2SO_4, CV experiments showed that in the presence of glycerol a significant current density was achieved only at $E \geq 1.30$ V,[54] with a ~0.1 mA cm^{-2} lower activity than in $HClO_4$. This was attributed to the stronger adsorption of the sulfate anions compared to perchlorate anions, thereby blocking active sites.[54] DFT calculations predicted that the catalytic oxidation of glycerol on Au(111) at the primary and secondary alcohol group to form DHA and 2,3-dihydroxy-2-propenal would occur at 0.39 V,[54,133] the cleavage of C-C bonds of glycerol to form CO at 0.5 V,[54] and catalytic oxidation of the primary alcohol group of glycerol to form GALD at 0.6 V,[54,133] although experimental analysis was not performed to detect these products.[54,133] Based on FTIR experiments on Au-based electrodes in 0.1 M H_2SO_4, it was argued that at $E \geq 1.20$ V Au catalyzes primary alcohol oxidation to produce TA and induces C-C cleavage reactions to form formic acid (FA) and carbon dioxide (CO_2).[53]

Kwon *et al.* reported the selectivity of the electrocatalytic oxidation of glycerol over Au electrodes under neutral conditions (0.1 M Na_2SO_4).[46] Here LSV was combined with online HPLC, showing that between 0.8-1.2 V the Au electrode performs the electrocatalytic oxidation of glycerol at the primary alcohol group with > 99% selectivity, forming GALD,[46] similarly to the results suggested by DFT calculations on Au(111).[54] At E > 1.2 V, the formation of CO_2 was observed by gas chromatography (not quantitatively determined), indicative of C-C cleavage reactions.[46]

Most studies on the electrocatalytic oxidation of sugar alcohols with Au electrodes were conducted under alkaline conditions.[46,49,53,90–93] The reason for this is that for Au catalysts, the first deprotonation step of the H_α proton of the primary alcohol of a sugar alcohol ($H_\beta R$-OH_α) is thermodynamically favorable only in alkaline media (base-promoted), while the step involving the abstraction of H_β is fast and Au-catalyzed.[65] The alkaline conditions thereby promote the formation of the alkoxide in solution (see section 2.2.1.1), which reacts at the Au catalyst surface (Scheme 2.4). The Au-based electrocatalyst abstracts the H_β from the alkoxide and acts as electron acceptor promoting the formation of the aldehyde (saccharide).[65,66] The high activities achieved under alkaline conditions with Au are therefore attributed to base-promotion and not to the catalyst-hydroxide interaction.[65] By contrast, DFT calculations do suggest that higher

activities are achieved at potentials close to the onset potential (~0.8 V *vs* RHE) for hydroxide adsorption on metallic Au.[133] The DFT calculations indicated that adsorbed OH could lower the barrier for β-elimination, suggesting that some interaction with (hydroxylated) Au surface is required.[135] However, it is likely that this adsorbed OH in the DFT calculations plays a similar role to the hydroxide in alkaline solution.
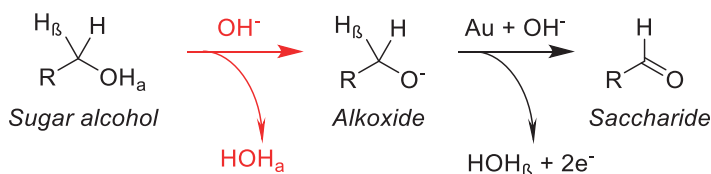
Scheme 2.4. *Mechanistic pathway described by Kwon et al. for the electrocatalytic oxidation of sugar alcohols at the primary alcohol group to the terminal aldehyde on Au and in alkaline conditions, where the first step is in solution (red arrow) and the successive step is electrochemical (black arrow). Adapted with permission from [65]. Copyright 2011, American Chemical Society.*

The selectivity for the electrocatalytic oxidation of glycerol on Au-based electrocatalysts was evaluated by LSV combined with online HPLC under alkaline conditions (pH = 13).[46,91] Under these conditions, significantly higher current densities (up to 20 mA cm^{-2}) were achieved compared to the results under acidic and neutral conditions.[46,65,91] At high potential (at E = 1.4-1.6 V), the activity of the Au electrode dropped dramatically,[46,65] due to the formation of a Au surface-oxide species (Au$_2$O$_3$, see section 2.3) that passivates the surface.[91] With Au electrode in basic medium, 20% GLA was formed with a high content of C-C cleavage products, namely 80% glycolate and FA. GALD was not detected, which indicates that this compound is quickly oxidized to GLA and successively cleaved at the C-C bond to glycolate and FA as a result of the high potentials.[46,91] Long-term electrolysis of glycerol over Au electrodes at pH = 13 were run at 1.1 V and 1.3 V.[93] After 20 h at E = 1.1 V, the conversion of glycerol was 10% and the main products were FA and glycolate (Sel. = 82 %) and to a lesser extent GLA (8%) and TA (10%).[93] At E = 1.3 V, the conversion of glycerol was slightly higher (14 %) with higher selectivity toward FA and glycolate (91%) and 9% GLA. The increase of C-C cleavage products seems to correlate with an increase in applied potential and the alkalinity of the electrolyte. Results obtained by LSV measurements at pH = 13 combined with FTIR were interpreted differently.[53] This study suggested that the oxidation of glycerol on Au electrode at 0.7 V < E < 1.2 V) could also produce DHA, while at higher potentials (E > 1.2 V) higher oxidation products were obtained, such as TA, MOA, glycolate and CO$_2$.[53] It is worth noting that the formation of DHA and MOA has not been reported in the other studies conducted under similar conditions.[46,91,93] Additionally, similar studies conducted with HPLC did not detect the formation of TA.[46,91,93] This discrepancy could potentially be attributed to the analytical method employed, where TA is an intermediate product that does not desorb from the surface (e.g., spectator molecule) and could therefore not be detected by HPLC but would be identifiable by FTIR. Moreover, the assignment of bands in FTIR spectra to specific species is not

unambiguous, creating uncertainty in the products that are being reported.[136,137] Finally, controversies exists for peak identification caused by convolution of peaks which may mask weak bands or shift the center of peaks.[138] In general, we consider product assignment based on HPLC more reliable. Therefore, this review will focus primarily on papers that use HPLC for product analysis, even though FTIR has been a main analytical technique applied to the electrocatalytic oxidation of glycerol.[138]

Under extreme alkaline conditions (pH = 14.3-14.9) and high temperatures (T = 50-60°C), 3 nm Au particles supported on a carbon (Au/C) at E < 0.9 V promote the electrocatalytic oxidation of the two primary alcohol groups of glycerol producing TA, and it can also promote the electrocatalytic oxidation of the secondary alcohol group of TA to form MOA.[90,92] This has been observed employing both a batch-electrolysis cell and an anion-exchange-membrane-based direct glycerol cell (AEM-DG cell), where the latter was operated by controlling the cell potential. In an electrolysis cell, at pH = 14.3 and 50°C, 10 % of glycerol was oxidized over an Au/C electrocatalyst (5.0 mg$_{metal}$ cm^{-2}) at E = 0.5 V to MOA (Sel. = 47%), TA (25%), GLA (14%), and oxalate (14%).[92] At higher potentials (E = 0.9-1.2 V), the formation of C-C cleavage products (glycolate, glyoxylate and oxalate) was promoted.[92] At the same pH and in an anion-exchange membrane cell, with an Au/C electrocatalyst (1.0 mg$_{metal}$ cm^{-2}) at E = 0.3 V cell potential 10% glycerol was converted to MOA with ~50% selectivity. In a follow-up study, using the same electrochemical cell, under harsher conditions (pH = 14.9 and 60°C) and with continuous flow of fresh reactant (1.0 ml min^{-1}), the Au/C electrocatalyst (0.3-0.5 V vs RHE) was able to promote the oxidation of 90% glycerol to TA (Sel. = 70%), GLA (15%, primary alcohol oxidation), LA (15%, primary or secondary alcohol oxidation), traces of MOA (primary and secondary alcohol oxidation) and of oxalate.[90] The lower selectivity toward MOA and higher selectivity toward TA in this system was attributed to the optimized reaction conditions (flow rate through the electrochemical reactor, temperature, pH, catalyst loading) to promote the successive oxidation of TA to MOA.[90] In summary, these studies show that an increase in temperature and pH at lower potentials allows to achieve a high degree of oxidation while avoiding C-C cleavage reactions.

In conclusion, Au is barely active under acidic and neutral conditions, but can selectively form GLAD under neutral conditions from glycerol. By contrast, under alkaline conditions (pH = 13), at room temperature, oxidation of glycerol on Au mainly produces C-C cleavage reactions. In general, the importance of the alkaline medium must be considered for the C-C cleavage reactions, and more clearcut data are needed to determine to what extent the medium or the electrocatalyst promote these reactions. The overall trend shows that Au is likely only able to catalyze the oxidation of primary groups of sugar alcohols. However, if the alkalinity is increased to very extreme conditions (pH ≥ 14.3) and the temperature is increased to 50-60 °C, while the potential is kept low (E ≤ 0.9 V), Au can catalyze with relative high selectivity the formation of TA or MOA, depending on the tuning of the reaction conditions.

2.4.1.2 Pt-based electrocatalysts

This section discusses the electrocatalytic oxidation of glycerol on Pt at different pH and potentials. In contrast to gold, platinum is well-known for its good electrocatalytic performance over a broad range of reaction conditions, e.g. from acidic to alkaline pH.[46,53,91,139] Therefore, Pt is one of the most widely studied metals for the electrocatalytic oxidation of sugar alcohols. In this section, the most relevant trends regarding the performance of Pt toward the electrocatalytic oxidation of glycerol (and other sugar alcohols) are summarized.

Figure 2.6 shows the relation between the activity of Pt and Au for the electrocatalytic oxidation of glycerol and the pH of the electrolyte (acidic, neutral or alkaline).[46] Pt is known to outperform Au with respect to activity for the electrocatalytic oxidation of sugar alcohols under acidic and neutral conditions, while under alkaline conditions Au can surpass the activity of Pt.[46,53] The latter observation has been attributed to the late (high-potential) surface oxidation of Au compared to Pt (see section 2.3), meaning that Au loses activity only at higher potentials. The pH and potential-dependent selectivity of Pt is outlined in this section.
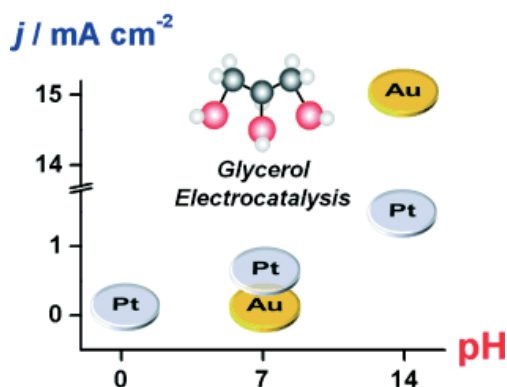

Figure 2.6. *The electrocatalytic activity of Pt and Au toward the electrocatalytic oxidation of glycerol as a function of the pH of the electrolyte. Reprinted with permission from* [46]. *Copyright 2011 WILEY-VCH Verlag GmbH & Co. KGaA, Weinheim.*

Under acidic conditions (pH = 1), Pt shows four distinct regions of activity for the catalytic oxidation of glycerol based on CV[49] and LSV combined with product analysis by online HPLC.[46,47] In the first region, where the Pt surface is metallic (at E = 0.37-0.8 V), the highest current densities and product concentrations were measured, specifically at E = 0.8 V. In the second region, where surface PtO/PtOH$_{surf}$ is expected to form (at E = 0.9-1.1 V), a substantial drop in current density accompanied by a drop in products formed was observed at E = 1.0 V,[46,47,49] indicative that the oxidized Pt surface is less active for catalyzing glycerol oxidation. In the third region, (at E = ~1.2 V), the current density and the quantity of oxidation products increase again,[46,47,49] indicative that this oxidized Pt surface species can show activity for glycerol oxidation at sufficiently high

potential. Finally, at even higher potentials ($E > 1.2$ V) the current density increases more steeply accompanied by an increase in the formation of more oxidized products (specifically glycolic acid and FA),[46,47] indicative that the interface under these conditions is more active for catalyzing C-C cleavage reactions.

Pt catalyzes the oxidation of glycerol under acidic conditions (pH = 1) between 0.37-0.6 V, primarily at the primary alcohol group, resulting in a selectivity of > 99% GALD (Scheme 2.3).[46,47] With an increase in potential to 0.6-1.1 V, the main product remains GALD, but the selectivity decreases due to the parallel oxidation of the secondary alcohol group of glycerol to form DHA (~5%) and an increase in selectivity toward GLA (i.e., the successive oxidation product of GALD) as well as the formation of CO_2.[46,47] In a chronoamperometric study at lower potentials and short reaction times (at E = 0.75 V and 20% glycerol conversion) GALD was produced with 90% selectivity,[48] while an increase in potential (at E = 0.9 V and 1.1 V) and longer reaction times (with a corresponding higher conversion of glycerol) resulted in a decrease in selectivity toward GALD and an increase in selectivity toward GLA (up to 87%).[48,50,103] These studies performed with chronoamperometry also show that over Pt-based electrocatalsyts at $E \leq 1.1$ V, only minor fractions of C-C cleavage products and higher oxidation products, such as TA and HPA, are produced.[48–50] The detection of 4% HPA after converting 69% glycerol at 0.9 V suggests that DHA is quickly oxidized to higher oxidation products during long-term electrocatalytic experiments. LSV combined with online HPLC showed that a successive increase in potential from 1.1 to 1.5 V (at which PtO_x species are expected to be present at the electrocatalyst surface) results in a gradual increase in C-C cleavage products as was shown by an increase in selectivity toward glycolic acid and FA and CO_2,[46,47] which is in agreement with chronoamperometry studies where the content of C-C cleavage products increases when the potential was increased from 1.1 V to 1.3 V (e.g. 20% at 97% glycerol conversion).[49,50] Under acidic conditions, it has been suggested that the formation of the surface platinum oxide at $E > 1.1$ V changes the adsorption of glycerol and its oxidation mechanism.[49] Scheme 2.5 illustrates that when the O/Pt ratio increases, the interaction of two Pt-O with two carbon atoms from the glycerol molecule may be favored, which changes the oxidation mechanism and results in C-C bond breaking reactions.[49] The cleavage of C-C bonds is likely catalyzed by Pt surface oxide rather than taking place via non-electrochemical reactions, since non-electrochemical reactions that induce C-C cleavage reactions, such as retro-aldol reactions only occur under alkaline conditions (see section 2.2.1.1). The detection of minor fractions of DHA or HPA indicate that Pt does not only catalyze the oxidation of the primary alcohol group, but is also able to promote the electrocatalytic oxidation of the secondary alcohol group,[46–48,50,103] in contrast to what has been observed for Au.[46,91,93] It is assumed that the electrocatalytic oxidation of the secondary alcohol group is made possible by simultaneously adsorbing the glycerol molecule through both the primary carbon and secondary carbon,[20] which is strongly dependent on the surface structure that is exposed.
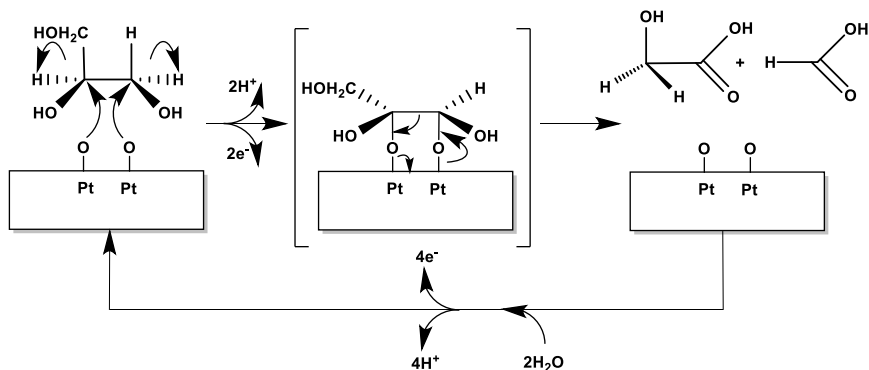
Scheme 2.5. *Proposed adsorption mechanism of glycerol on Pt surface oxide (E > 1.1 V), where both the C1-OH as well as the C2-OH groups are involved in the adsorption, resulting in C-C cleavage to glycolic acid (glycolate) and formic acid (formate). Adapted with permission from [49]. Copyright 1994 Elsevier.*

Metal-based electrocatalysts can be synthesized with different surface structures containing low-index facets (LIFs) or high-index facets (HIFs), which influence their performance. The HIFs have a higher density of edges, corners and kinks, which have a low coordination number and thus fewer bonds, generally making them catalytically more active.[140] The selectivity can be tuned by modifying the electrode so that it presents a specific crystal structure, as was shown for the selective electrocatalytic oxidation of glycerol.[20,76] The electrocatalytic oxidation of glycerol on Pt(111) and Pt(100) was investigated by combining LSV with online HPLC.[20] Scheme 2.6 illustrates the reaction pathways that were inferred for the electrocatalytic oxidation of glycerol on the different Pt facets and the resulting products. On Pt(111), several products were found, including GALD, GLA and DHA, indicative for the electrocatalytic oxidation of the primary and secondary alcohol of glycerol. On the other hand, on Pt(100) surface only GALD was detected, thus presenting a higher selectivity toward the primary alcohol group. The distinct electrochemical response on the two Pt surface structures indicates that there might be different reaction intermediates on the surface, which was supported by DFT modeling:[20] on Pt(100) the dehydrogenated glycerol intermediate binds to the surface through a Pt=C bond, while on Pt(111) the ethoxy anion intermediate is formed through the simultaneous binding of the carbon of the primary and secondary alcohol group on the surface (Pt-C bond), therefore yielding different products on the two surfaces.[20]
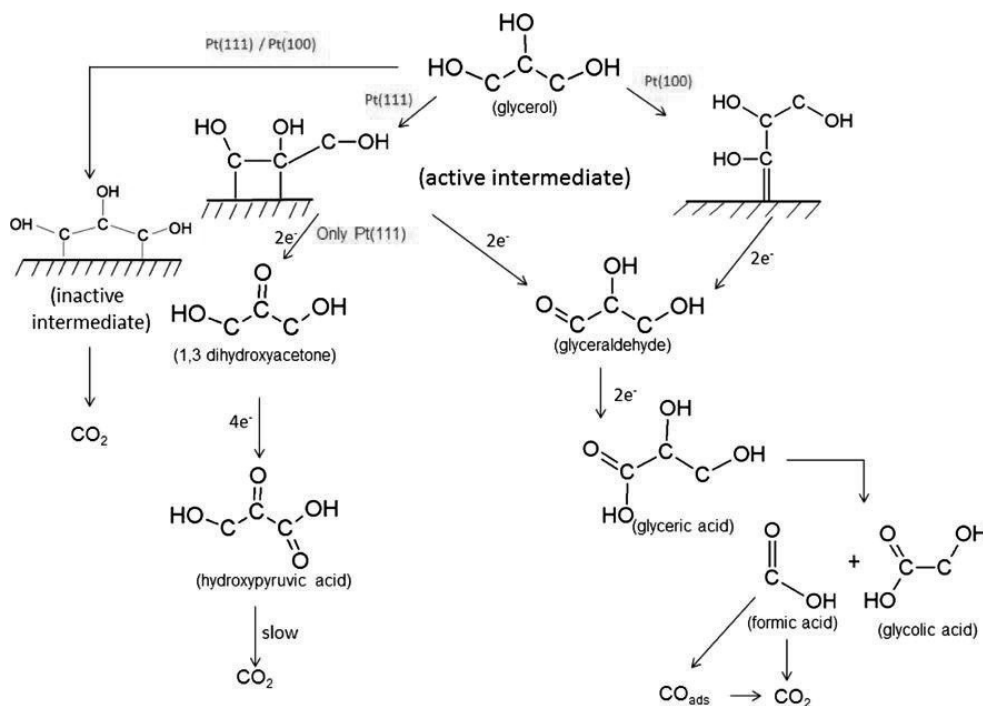
Scheme 2.6. *Proposed reaction pathways and the corresponding intermediates of the electrocatalytic oxidation of glycerol on Pt (111) and Pt (100) electrodes. Reprinted with permission from [20]. Copyright 2016, American Chemical Society.*

Polycrystalline Pt-based electrocatalysts have also been found to be selective toward the electrocatalytic oxidation of sorbitol at the primary alcohol group in acidic medium (0.1 M HClO$_4$).[141] At E = 0.55 V, the (metallic) Pt-based electrocatalyst promotes the formation of glucose and, to a lesser extent, of glucuronic acid (GLU) with traces of gluconic acid (GA) and C-C cleavage products. At slightly higher potentials (0.65 V), glucose remains the major product with a slight increase in selectivity toward the successive oxidation products, GLU and GA, and traces of C-C cleavage products. This increase in potential does not induce more C-C cleavage reactions,[141] which is in agreement with the electrocatalytic oxidation of glycerol.[46,47] At E = 1.35 V, the (oxidized) Pt-based electrocatalyst leads to the formation of glucose as the major product (Sel. = ca. 90%), but it also promotes C-C cleavage products (8% glyoxylic acid and FA) and a very small amount of GA,[141] confirming the results for the electrocatalytic oxidation of glycerol.[46,47,49,50] The formation of ketoses (secondary alcohol oxidation) was not reported, in contrast to a more recent study which proved the formation of ketoses for the electrocatalytic oxidation of glycerol, erythrol and sorbitol.[44,45] Since both studies use similar reaction conditions, this difference is tentatively explained by the difference in analytical technique (e.g., type of HPLC column and detector), as will be discussed later (*vide infra*, Section 2.5). A combination of LSV with online HPLC showed that the electrocatalytic oxidation of sorbitol in 0.5 M H$_2$SO$_4$ on Pt/C resulted in a

mixture of C1-OH/C6-OH (primary) oxidation products (glucose and gulose) and C2-OH/C5-OH (secondary) oxidation products (fructose and sorbose).[45] At $E \leq 0.9$ V primary alcohol oxidation products were observed (~90% glucose and gulose) and to a lesser extent secondary alcohol oxidation products (~5%), while at higher potentials ($E \geq 0.9$ V, where the Pt surface is expected to be oxidized) the selectivity increases toward secondary alcohol oxidation products, resulting in ~25% fructose and sorbose at $E = 1.2$ V.[45] Continuous cyclic voltammetry was employed to oxidize sugar alcohols in 0.1 M HClO$_4$ and the results were compared to long-term electrolysis at a fixed potential (at $E = 0.7$).[44] In comparison to CA, the use of cyclic voltammetry between 0.02-1.1 V was found to improve the reaction rate by a threefold and selectivity toward ketoses by a three- to fivefold, when compared to aldehydes and carboxylates, independent of the sugar alcohol (glycerol, erythritol, sorbitol) that was electrocatalytically oxidized. It was argued that the low current densities achieved during CA measurements, generally found in literature, can be related to a loss in oxidative power of Pt, as the surface reaches an oxidized (PtO$_x$) steady state.[44] As a result, Pt loses its oxidative activity for sorbitol. This hypothesis was supported by operando Raman spectroscopy and by injecting sorbitol at different time points during CA measurements. Based on Tafel slope analysis and previous research, it was postulated that the first step of sorbitol oxidation becomes rate limiting as the CA measurement proceeds. This first step involves a proton-electron transfer from an alcohol group, resulting in an oxygen bound intermediate, which can readily be achieved on non-equilibrated Pt surfaces (e.g., surfaces that have not reached an oxidized steady state). Yet, as CA measurements proceed the Pt surface reaches a oxidized steady state, which limits the first step of sorbitol oxidation. The increase in selectivity toward ketoses was attributed to a change in adsorption configuration of the reactant on the oxidized Pt surface. A metallic Pt surface enables the adsorption of sugar alcohols at the C2-OH/C5-OH (secondary) group, thereby promoting the oxidation of these groups and thus the formation of ketoses. These results on the electrocatalytic oxidation of sugar alcohols over Pt are consistent in the sense that both primary alcohol and secondary alcohol groups are catalytically oxidized for glycerol and erythrol, and the C1-OH/C6-OH (primary) groups and the C2-OH/C5-OH (secondary) groups are oxidized for sorbitol.[44,46–48,50]

The electrocatalytic oxidation of glycerol over Pt in neutral conditions (pH = 7) has been studied by LSV combined with online HPLC,[46] and follows nearly the same trends as under acidic conditions.[46,47] The catalytic oxidation of glycerol starts at 0.43 V and its activity drops when PtO/PtOH starts to form (at $E = 0.8$ V). The loss in catalytic activity continues up to $E = $ ~1.1 V, after which the activity increases again with an increase in potential.[46] The current densities under neutral conditions at $E = 0.55$-1.0 V are twice as high compared to acidic conditions, while the current densities at higher potentials ($E \geq 1.0$ V) are the same under acidic and neutral conditions.[46] Over metallic Pt at $E = 0.43$-0.7 V, GALD is the main product, which corresponds to a 0.35 V lower onset potential compared to Au under similar conditions.[46] However, when the

potential surpasses 0.6 V, C-C cleavage reactions (leading to glycolate and formate/CO_2) also start to take place, which become especially more dominant at $E \geq 1.1$ V. The formation of glycolate under neutral conditions starts at 0.6 V,[46] while C-C cleavage products under acidic conditions only become substantial at 1.1 V,[46,47,49,50] which suggests that this reaction is strongly base catalyzed.[46]

The electrocatalytic oxidation of glycerol over Pt electrodes was also studied at pH = 13 by means of LSV combined with online HPLC,[46,91] and by means of CA combined with HPLC.[49] The catalytic oxidation of glycerol over the metallic Pt electrode starts at 0.4 V, which is 0.4 V lower than over Au.[46,91] The current density increases up to 0.85 V after which it quickly drops and the electrode almost completely deactivates, which coincides with PtO/PtOH$_{surf}$ formation ($E > 0.75$ V).[46,91] This loss in catalytic activity of Pt is at much lower potential than for Au, likely due to the earlier onset for Pt oxide/hydroxide formation compared to Au hydroxide formation (see also, section 2.3 Figure 2.5).[46] HPLC samples were neutralized as soon as they were collected, avoiding non-electrochemical reactions in the vial of the fraction collector (see section 2.2.1.1 on base-catalyzed non-electrochemical reactions).[46] These studies show that over Pt at 0.4 V GALD forms selectively (> 99%),[46] while at higher potentials (0.7-1.4 V) the formation of GLA prevails (50-100%), although with low activity as the surface is deactivated in this potential window.[46,91] Additionally, at > 0.6 V the formation of C-C cleavage products becomes quantitative, as was also observed under neutral conditions.[46] Roquet *et al.* reported ~90% selectivity toward GALD and minor contents of GLA, TA and C-C cleavage products (glycolate, oxalate and formate) over Pt after 3 h of electrolysis at 0.79 V (20 % conversion).[49] CA measurements show that, as the reaction proceeds, the presence of GLA and TA increase, although GALD remains the major product.[49] Thus, it seems that at 0.79 V the sequential electrocatalytic oxidation of GALD to GLA and TA is rather slow.

Under more alkaline conditions (0.5 M NaOH), glycerol oxidation on Pt leads to 75% C3 oxidation products, where the major product was DHA (40-50%), and high contents of LA (35%) at 0.9 V (between 0.5-1.3 V vs RHE).[134] This proves that the selectivity at pH 13.7 for a Pt catalyst can avoid the formation of high quantities of C1 and C2 oxidation products. It was also shown that no C-C cleavage reactions were observed at $E = 1.3$ V (and thus over oxidized Pt). These results are in contrast to earlier studies with Pt electrodes producing residual amounts of DHA and HPA.[46–48,50,103] This discrepancy may be explained by the fact that Zhou *et al.* performed electrocatalytic oxidation reaction on systems containing 46 g.l^{-1} of glycerol and only produced 0.08 g.l^{-1} of products.[134] At these low glycerol conversions it is likely that only GLAD was formed, as was shown in earlier research,[49] which can easily undergo successive non-electrochemical reactions to form DHA and LA by dehydration and Cannizzaro rearrangement (see section 2.2.1.1) if the samples are not quenched timely.[46] Several other studies performed at 0.5-1.0 M KOH have shown that Pt is highly selective toward the formation of TA.[98,142,143] In the case of Pt/CNT in 0.5 M KOH at

0.7 V vs RHE, up to 75-95% TA was found over a 2 hour time frame,[142] while over a P-doped Pt/MWCNT catalyst in 0.5 M KOH at 0.73 V, near equimolar amounts of TA and GLA were detected, both accounting for 90% of the final products.[143] These results show that dicarboxylic acids (TA) are only produced under highly alkaline conditions, as was also shown for Au electrodes at pH ≥ 14.3.[90,92] At 1.0 M KOH, Ferreira *et al.* showed for a Pt/C catalyst that higher current densities (90 mA cm^{-2}) and hence higher overpotentials, promoted C-C cleavage reactions, whereas lower current densities (60 mA cm^{-2}) and overpotentials promoted the formation of TA and reduced the C-C cleavage.[98] Doping the Pt/MCNT with P improved the stability of the catalyst, without affecting the catalyst selectivity.[143] The increased activity was ascribed to the reduction of the accumulation of carbonaceous intermediates and an increase in the local hydroxyl concentration.[143]

In summary, the electrocatalytic oxidation of sugar alcohols under acidic and neutral conditions is substantially faster on Pt than on Au. The use of non-equilibrated Pt surfaces can be used to improve the catalyst activity further. Under acidic and neutral conditions, Pt mainly produces GLAD through the dehydrogenation of the primary alcohol groups, but also catalyzes the secondary alcohol group resulting in minor contents of DHA. The selectivity toward primary or secondary alcohol group oxidation of glycerol can be further improved with Pt electrodes that expose specific crystal structures. Moreover, surface platinum oxide has been proposed to be responsible for C-C cleavage reactions through the simultaneous adsorption of adjacent carbon groups. Finally, dicarboxylates (TA) can only be formed by Pt under highly alkaline conditions (pH ≥ 13.7). Yet, the intrinsic catalytic selectivity in alkaline media is very difficult to determine if online sample collection and immediate neutralization is not performed.

2.4.1.3 Pd-, Ir- and Ru-based electrocatalysts

This section evaluates the performance of platinum group metals for the electrocatalytic oxidation of glycerol, as they are known to have similar physical and chemical properties. Platinum group metals that have been used for the electrocatalytic oxidation of glycerol are Pd, Ru and Ir. The potential products formed with these catalysts were compared to Pt to seek for trends between platinum group metals.

Two studies have been devoted to the effect of the Pd surface structure on the selective electrocatalytic oxidation of glycerol.[144,145] Both articles show a good performance of Pd nanocubes, which predominantly expose (100) planes. In both cases, only the electrocatalytic oxidation of the primary alcohol is achieved, but the selectivity differs from one system to the other. In the first case, 99% TA was achieved after 9h electrolysis at E = 0.87 V and pH = 13,[145] which is an unusual product. TA was previously only formed through electrocatalytic reactions at pH ≥ 13.7 on Au and Pt electrodes.[90,92,98,142,143] It was argued that the high selectivity toward TA can be attributed to the high selectivity of Pd(100) toward the electrocatalytic oxidation of the

primary alcohol group (section 2.4, Scheme 2.3).[145] In the second case, at pH = 13.7 after 2h electrolysis, GALD is the main product regardless of the potential applied (55-60% at $0.6 \leq E \leq 1.2$ V), followed by a 30% of oxalate and 5-10% of glycerate.[144] Both activity and selectivity were improved when Pd(100) nanocubes were used instead of Pd nanoparticles, showing a higher oxidative current and an increased selectivity toward the primary alcohol.[144] A possible explanation for the discrepancy between these two studies could be the long reaction times (9h) applied to achieve high TA selectivity, as it requires the further electrocatalytic oxidation of GLAD.[145] The results show that the reaction pathway is shifted to the primary alcohol oxidation via the surface structure-induced selectivity of the Pd nanocubes exposing (100) planes.[144,145]

Pd nanocrystals on a carbon support were used to study the electrocatalytic oxidation of glycerol at pH = 13 and E = 0.8 V.[146] After 4h electrolysis, the reaction product selectivity was 45% glycolate, 40% GLA and some minor products (TA, oxalate and FA, 5% each), evidencing substantial cleavage of C-C bonds.[146] Under slightly more alkaline conditions (pH = 13.7), Zhou *et al.* showed that the electrocatalytic oxidation of glycerol at E = 0.8 V resulted predominantly in GLAD (45%) and oxalate (45%) with minor contents of GLA.[144] These higher selectivity toward GLAD instead of GLA indicates that the conversion was lower resulting in less oxidized species, while the opposite is expected when the selectivities of oxalate and glycolate are considered. Therefore, the difference in selectivity remains to be resolved. When the alkalinity of the electrolyte is increased further (pH = 14), at a potential of E = 0.7 V, Pd exclusively leads to the formation of GLA, while Pt leads to the formation of DHA (60%) and GLA (40%).[147] Moreover, these studies show that over Pd the primary alcohol group is exclusively oxidized,[144,146,147] while over Pt the secondary alcohol group can also be oxidized.[46–48,50,103] In contradiction to these results, Muhammed *et al.* showed that the oxidation of glycerol over Pd/CNT at E = 1 V in pH = 13.7 results in a product selectivity of DHA (65%), GALD (20%) and MOA (13%), which shows that Pd might also be able to promote the oxidation of both the secondary and primary alcohol group of glycerol.[148] Phosphorus doping of Pd/CNT further improved the catalyst selectivity by a 1.4 fold to ~93% DHA. The studies devoted to Pd were all performed at pH ≥ 13, where it is expected that GLAD isomerizes to DHA (see section 2.2.1.1). Yet, the formation of DHA was often not reported (with one exception[148]),[144–147] indicative that glycerol electrocatalytically oxidizes to GLAD to GLA without the intermediate desorption of GLAD from the electrode surface, thereby preventing the isomerization of GLAD to DHA.

RuO₂/Ti and IrO₂/Ti electrodes and a mixture of these two Dimensionally Stable Anodes (DSA) were compared with respect to selectivity and conversion at pH = 0.3 (0.5 M H_2SO_4).[149] At 1.8 V, DSA had a 30 % and 60 % higher conversion than RuO₂/Ti and IrO₂/Ti, respectively. All electrocatalysts showed similar product selectivity (~70% of the products were quantified): 40% toward GLAD and GLA, 15-18% DHA and HPA, with the remainder being C-C cleavage products. These results demonstrate that RuO₂ and IrO₂ can both catalyze the oxidation of the primary

alcohol group as well as the secondary alcohol group of glycerol,[149] similar to the results obtained with Pt electrocatalysts.[46–48,50,103]

In conclusion, further research needs to be conducted on these catalysts under acidic conditions and outside the OER region to evaluate whether Pd-, Ru- and Ir-based electrocatalysts can catalyze similar reactions for the electrocatalytic oxidation of glycerol as Pt.

2.4.1.4 Ni- and Co-based electrocatalysts

This section evaluates the electrocatalytic oxidation of glycerol on Ni oxide and Co oxide electrodes at different pH and potentials. A frequently studied metal oxide for the electrocatalytic oxidation of glycerol is Ni oxide,[105,150–153] while Co oxide is less commonly studied.[96,154] Nickel and cobalt are able to form similar metal oxyhydroxide species (e.g., NiOOH and CoOOH), which presumably catalyze similar reactions.[155] Therefore, this section discusses the mechanism through which these metal oxides catalyze glycerol oxidation and their property-performance relation.

Various studies have been devoted to nickel catalysts for the selective electrocatalytic oxidation of glycerol to value-added products.[105,150,151] Monometallic Ni catalysts have only been found to be active for glycerol oxidation in the potential region where Ni forms β-NiOOH (E ≥ ~1.3 V).[105,156] More specifically, from the potential at which β-NiOOH is formed up to the potential at which OER starts, two different mechanisms were proposed through which glycerol oxidation can proceed, being either the indirect mechanism catalyzed by β-NiOOH or the potential-dependent mechanism catalyzed by NiO_2 (Figure 2.7).[151,157] For the indirect mechanism (Figure 2.7C), $Ni(OH)_2$ is first oxidized to NiOOH and subsequently the sugar alcohol adsorbs on the surface. From this adsorbed sugar alcohol a hydrogen atom is transferred (HAT) to NiOOH to form an α-C radical and $Ni(OH)_2$. The adsorbed α-C radical successively undergoes further oxidation to form an aldehyde, GLAD in the case of glycerol. The formed $Ni(OH)_2$ undergoes oxidation to form NiOOH again which can then initiate a new cycle of indirect oxidation or potential-dependent oxidation of glycerol.[151,157] Thus, HAT reduces NiOOH to $Ni(OH)_2$,[151,157] which might explain the loss in the charge of the reduction peak for NiOOH in the presence of glycerol during the negative-going scan in the cyclic voltammogram.[156] For the potential-dependent mechanism (Figure 2.7C), $Ni(OH)_2$ is first oxidized to NiO_2. Successively, a proton is withdrawn from the primary alcohol groups of a sugar alcohol by a hydroxide ion in solution to form an alkoxide in solution. The alkoxide adsorbs on the surface of NiO_2 and loses a proton through a hydride shift, resulting in the formation of $Ni(OH)O^-$ and an aldehyde.[151,157] The $Ni(OH)O^-$ oxidizes back to NiOOH, which can catalyze the oxidation of the next sugar alcohol molecule. The indirect oxidation mechanism is pH independent, while the potential-dependent mechanism is pH dependent, as was shown by LSV under various pH conditions.[151,157] As a result, the catalytic activity observed for the oxidation of glycerol through the potential-dependent mechanism decreases severely by lowering the pH

(Figure 7A-B).[151] This decrease in catalytic activity induced by lowering the pH resembles that of Au, where the rate limiting step is base-catalyzed (section 2.4.1.1, Scheme 2.4).[65]

Goetz *et al.* also described how the pH influences the selectivity of the oxidation of glycerol.[151] At 1.52 V, with an increase in pH from 9 to 13 the electrocatalyst selectivity changes from 78% DHA to 99% FA. Likewise, at pH = 11 with an increase in potential from 1.48 to 1.57 V, the electrocatalyst selectivity changes from 40% DHA and 21% FA to 26% DHA and 30% FA. The authors found a correlation between pH, direct vs. indirect mechanism and DHA selectivity. On the basis of these considerations, they concluded that at lower pH the direct, potential-dependent mechanism is largely suppressed, and that the indirect oxidation promotes secondary alcohol oxidation leading to the observed higher DHA selectivity and avoiding C-C cleavage reactions.[151] This shows that DHA is mainly formed at relatively mild alkaline conditions, meaning that NiOOH is not the best catalyst to be combined with non-electrochemical reactions to produce LA (see section 2.2.1.1). Therefore, the formation of LA over NiOOH has been occasionally reported, but the selectivity is often relatively low[150,152,153] as the severe alkaline conditions in these studies promote the potential-dependent mechanism.[151] Alternatively, at E = 1.5 V and pH = 14.8, NiO_x embedded in oxygen-functionalized multiwalled carbon nanotubes can catalyze the oxidation of glycerol to oxalate (~60%) after 27 h, where the remaining 40% is CO_2.[153] After 27 h, the current dropped and the oxalate concentration remained unaffected, indicative that oxalate cannot be catalytically oxidized further by NiO_x.
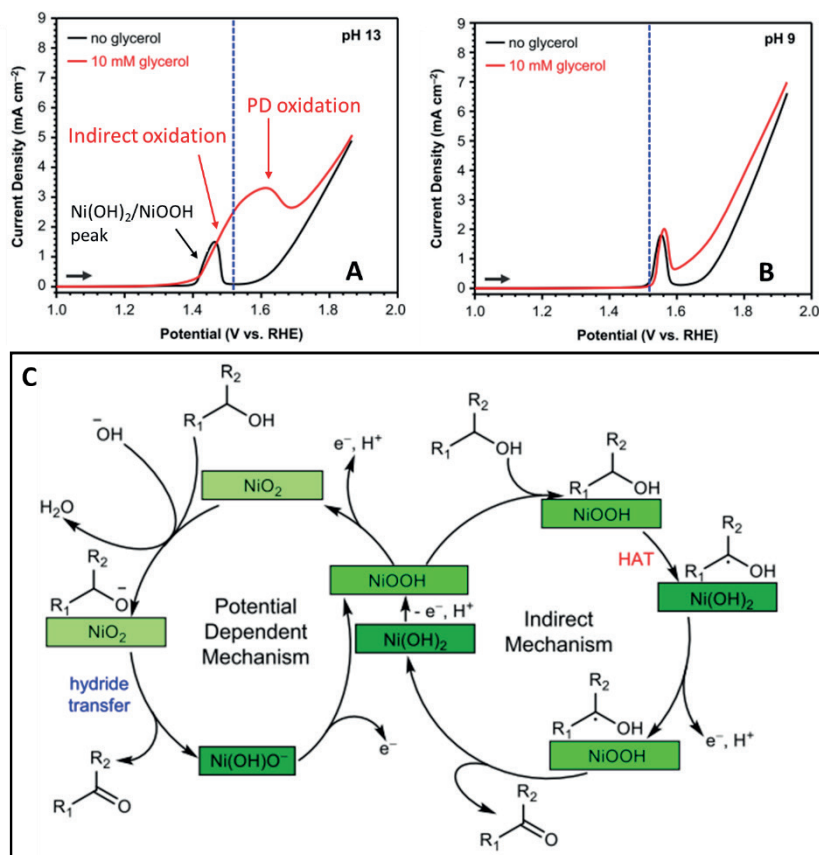
Figure 2.7. *Linear sweep voltammetry of Ni in the absence (black) and presence of 10 mM glycerol (red) obtained in an electrolyte of pH = 13 (A) and 9 (B). The dashed blue lines at 1.52 V indicate the potential at which chronoamperometric experiments were performed and the red arrows indicate the regions where NiOOH induces different reaction mechanisms. The related reaction mechanisms can be subdivided in indirect oxidation and potential-dependent oxidation (C). Adapted with permission from [151]. Copyright 2022 Springer Nature.*

A Co-based electrocatalyst was used to study the electrocatalytic oxidation of glycerol at mild alkaline conditions (pH = 10) in a borax ($Na_2B_4O_7$)[154] electrolyte and at harsh alkaline reaction conditions (pH = 13.7-14).[96] Under mild alkaline conditions, the electrocatalytic oxidation of glycerol is considered to follow two mechanisms, namely via a direct and indirect mechanism,[154] which resembles the mechanisms described for NiOOH.[151] In the indirect mechanism, the oxidation of glycerol proceeds with the simultaneous reduction of CoOOH or CoO_2 to $Co(OH)_2$, leading to the depletion of CoOOH.[154] In the direct mechanism, glycerol is incorporated in the Co hydroxide surface and oxidized by surface adsorbed OH⁻ ions, without CoOOH consumption.[154] The *operando* Raman spectra obtained at 1.5 V show high contents of $Co(OH)_2$ species, which is a relevant species in the indirect oxidation mechanism of glycerol.[154] By contrast, at 1.7 V higher contents of CoOOH species were observed by operando Raman spectroscopy, indicative that the

reaction proceeds according to the direct mechanism. After 3h chronoamperometry at $E = 1.5$ V, ~0.4% glycerol electrocatalytically oxidized, being mildly selective toward the dehydrogenation of the secondary alcohol groups of glycerol, thereby producing ~60% DHA, ~30% GLAD and ~10% FA. At $E ≥ 1.7$ V, the conversion increased to ~2.2% and the selectivity changed, reducing the dehydrogenation of the secondary alcohol (Sel. = 40% DHA) and increasing the dehydrogenation of the primary alcohol and its successive oxidation ~30% GLAD and ~5-7% GLA, as well as promoting C-C cleavage reactions ~20% FA.[154] This indicates that the indirect mechanism of CoOOH promotes the dehydrogenation of the secondary alcohol group of glycerol, leading to the formation of DHA, while the direct mechanism promotes higher oxidation products and C-C cleavage reactions. These results strongly resemble those obtained with NiOOH.[151] However, it must be noted that this study was performed in an electrolyte with borate, which might have impacted the catalyst selectivity through the formation of borate-glycerol complexes (see section 2.2.1.2).

Under harsh alkaline and optimized conditions (pH = 13.7, 20°C between 8.8-44.2 mA cm^{-2} and under continuous electrolyte mixing), Co-based electrocatalysts lead to the selective production of 50-58% GLA, while the selectivity changes to 44% LA by altering the reaction conditions (pH = 14, 60 °C at 1.8 mA cm^{-2} and under continuous mixing).[96] We argue that the higher selectivity for LA can be attributed to two effects. Firstly, the lower current densities could potentially result in a Co species that is more active for catalyzing glycerol through the direct mechanism, thereby promoting the formation of DHA. Secondly, the lower current densities reduce the sequential electrocatalytic oxidation reaction of GLAD to GLA, thereby promoting homogeneous reactions that convert GLAD to DHA to LA (see section 2.2.1.1).

In summary, Ni- and Co-based electrocatalysts appear to promote the oxidation of glycerol through similar mechanisms, thereby affecting the selectivity in a similar manner. To prove this, it would be advised to study the selectivity of Co-based electrocatalysts at various pH and E in the absence of borate electrolyte.

2.4.1.5 Cu- and Mn-based electrocatalysts

This section evaluates the electrocatalytic oxidation of glycerol at different pH and potentials on Cu- and Mn-based electrocatalyst.[158,159]

Cu-based electrodes consisting of CuO species (as determined by *operando* Raman spectroscopy and XRD), have been studied for the electrocatalytic oxidation of glycerol at pH = 9-13 and $E = 1.29$-2.06 V.[158] At pH = 13, with an increase in potential from $E = 1.29$ to $E = 1.49$-2.06 V, the catalyst selectivity changed from 70% FA, 20% GLA and 5% DHA to 98% FA and 2% glycolate. This indicates that an increase in potential improves the selectivity toward C-C cleavage reactions for CuO. Independent of the applied potential, the formation of GLAD was not detected, while GLA was detected (an oxidation product of GLAD, see Scheme 2.3). Therefore, it was argued that DHA

is isomerized to GLAD, which can more easily be oxidized by CuO, as was determined by the lower onset potential measured during CV for GLAD and DHA oxidation.[158] To evaluate this hypothesis, the electrocatalytic oxidation of glycerol was studied at pH = 9 in 0.1 M borax ($Na_2B_4O_7$) at E = 1.76 -2.06 V. Under these conditions, the selectivity changed to 50-60% DHA and 40-50% FA.[158] However, the use of borax has likely resulted in borate-glycerol complexes enabling the selective oxidation of the secondary alcohol of glycerol (see section 2.2.1.2, Figure 2.2). Moreover, the statement related to the isomerization of DHA to GLAD under alkaline conditions is rather unlikely, since ketone structures are thermodynamically favored over saccharides (see section 2.2.1.1). Therefore, the reaction pathway for glycerol oxidation catalyzed by CuO remains to be fully understood.

Mn-based electrodes consisting of MnO_2 species (as determined by *operando* Raman spectroscopy and XRD), were used to study the electrocatalytic oxidation of glycerol, GLAD and DHA at pH = 9 (0.1 M borax, $Na_2B_4O_7$) and E = 1.45-1.85 V.[159] MnO_2 exists in the α-MnO_2 phase at E = 1.45 V, while at E = 1.85 V the α-MnO_2 and δ-MnO_2 phases coexist.[159] It was shown that α-MnO_2 (at E = 1.45 V, <0.1 mA cm^{-2}) is moderately selective toward C3 oxidation products and equally selective toward the primary and secondary alcohol group of glycerol, resulting in the formation 38% FA, 33% DHA and 30% GALD. By contrast, α-MnO_2/δ-MnO_2 (at E = 1.85 V, 2.5 mA cm^{-2}) induces less C-C cleavage reactions, thereby increasing the selectivity of DHA and GALD to 45% and 40%. The electrocatalytic oxidation of DHA or GALD over α-MnO_2 (at E = 1.45 V) resulted in low selectivities toward GLA (<15%) where the remaining product was FA, indicative that α-MnO_2 favors C-C cleavage reactions. By contrast, over α-MnO_2/δ-MnO_2 (1.85 V) glycerol is oxidized to GLAD to ~75% GLA and ~25% FA; and DHA to ~60% GLA, ~30% GLAD and ~10% FA. Notably, neither δ-MnO_2 nor α-MnO_2 catalyzes the oxidation of DHA to hydroxy pyruvate, instead it promotes the isomerization of DHA to GLAD, which is then oxidized.[159] The non-electrochemical isomerization of DHA at pH = 9 was excluded by performing a stability test of DHA and GLAD in 0.1 M borax (pH = 9).[159] Finally the high selectivities toward DHA over MnO_2 can potentially also be ascribed to the type of electrolyte used, namely containing borax (see section 2.2.1.2, Figure 2.2).

To conclude, to understand the selectivity of Cu- and Mn-based electrocatalysts toward the oxidation of glycerol, research needs to be conducted in the absence of borax electrolyte as this strongly affects the catalyst selectivity. Moreover, it is strongly recommended to evaluate the effect of pH and potential on the selectivity of Cu- and Mn-based electrocatalysts to assess the possibility of different reaction mechanisms, as was also done on Ni-based electrodes.[151,157]

2.4.2 Noble bimetallic electrocatalysts

Bimetallic catalysts are generally used to improve the activity and/or selectivity of monometallic catalysts and to decrease the utilization of scarce noble metals (e.g., Au, Pt, Pd, Ir, Ru, Os, Rh).

This section has been subdivided in bimetallic catalysts that combine two noble metals (section 2.4.2), a noble metal with a non-noble metal (section 2.4.3) and a noble metal with a post-transition metal (section 2.4.4). Bimetallic systems that combine two noble metals are by far most widely studied and have therefore been subdivided again in bimetallic Ag-noble metal catalysts (2.4.2.1), bimetallic Au-noble metal catalysts (2.4.2.2), and bimetallic Pt-noble metal catalysts (2.4.2.3).

2.4.2.1 Bimetallic Ag-noble metal electrocatalysts

AgAu,[160–162] AgPt,[163] and AgPd[164,165] electrocatalysts have been used for the electrocatalytic oxidation of glycerol[160,162–165] and sorbitol[161]. These studies have all been performed under alkaline conditions (pH ≥ 13),[160–165] at which it has been shown that Ag itself has a very poor catalytic activity for the electrocatalytic oxidation of glycerol.[160,162,164] By contrast, Ag combined with Au, Pt or Pd is known to be active for the electrocatalytic oxidation of glycerol and the presence of Ag was found to affect the catalyst selectivity.

Alloying Ag with Au,[160] Pt,[163] and Pd[164,165] (the formation of the alloys was shown by XRD[160,163–165]) was found to decease the onset potential for the electrocatalytic oxidation of glycerol by ~100 mV. This indicates that Ag has a similar effect on the bimetallic catalyst activity regardless of the metal with which it is alloyed. Moreover, the addition of Ag to Au promotes C-C cleavage reactions (as evidenced by FTIR[160155] and HPLC[162]). As a result, the selectivity toward glycolate (~40%) and formate (~60%) was improved for more alloyed AuAg bimetallic systems compared to dealloyed AuAg catalysts.[162] It was argued that this is a result of the stronger interaction of the reactants with the catalyst surface due to the presence of Ag,[162157] though differences in surface roughness might have played a role too. In line with the results for AuAg electrocatalyst, the addition of Ag to Pt[163] and to Pd[164,165] was also found to improve the electrocatalyst selectivity toward C-C cleavage reactions, as was evidenced by HPLC[164] and FTIR[163,165]. For AgPt, the change in catalytic performance was attributed to a change in electronic properties of the Pt active sites induced by Ag.[163] For the study on AgPd (conducted with HPLC), an increase in Ag content in the AgPd catalyst resulted in a decrease in selectivity toward C3 oxidation products (GLA, TA, MOA) and an increase in selectivity toward C2 oxidation products (oxalate and glycolate).[164] Here the carbon balance was not closed, indicative that most likely also CO_2 was formed.

2.4.2.2 Bimetallic Au-noble metal electrocatalysts

AuPt[67,134,166] and AuPd[161,167,168] electrocatalysts have been used for the electrocatalytic oxidation of glycerol[67,134,167] and sorbitol.[161,166,168] In these studies the catalyst selectivity was almost exclusively studied under alkaline (pH ≥ 13) conditions and the products were analyzed by HPLC[67,134] and FTIR.[167]

All studies performed on AuPt/C catalysts show that both alloyed and non-alloyed bimetallic catalysts result in a similar onset potential for the electrocatalytic oxidation of sugar alcohols as on Pt, thereby being lower than that of bare Au.[67,166] By contrast, Zhou *et al.* showed a ~100 mV decrease in onset potential for their AuPt/Ag catalysts for the electrocatalytic oxidation of glycerol in comparison to Pt/C.[134] This decrease in onset potential resembles the catalysts in which Ag was alloyed with Au,[160] Pt,[163] and Pd.[164,165] This indicates that the lower onset potential observed by Zhou *et al.* is not related to the alloyed AuPt catalyst, but to an electronic effect induced by the Ag support. Under acidic conditions (pH = 1) the activity of PtAu for the electrocatalytic oxidation of glycerol was found to decrease with an increase in Au content.[134] This decrease in catalytic activity can be explained by the low activity of Au in comparison to Pt for catalyzing oxidation reactions under acidic conditions (section 2.4.1.2).[46] Zhou *et al.* showed that at $E \geq 0.8$ V in 0.5 M KOH, core-shell PtAu/Ag NPs with intermediate Pt contents (30-40%) displayed the highest current densities.[134] Yet, an explanation for the difference in electrocatalytic activity was not given.[134]

For well-alloyed AuPt catalysts, aimed at obtaining LA from glycerol, it was found that the production was predominantly dependent on the applied potential and alkalinity of the electrolyte, achieving the best LA selectivity (73%) at 0.45 V and 1 M KOH.[67] These low potentials were accompanied by low conversion, while increasing the potential resulted in a higher conversion but also a decrease in the formation of LA, due to the sequential electrocatalytic oxidation of GALD into GLA and TA or the promotion of C-C cleavage reactions.[67] Low potentials reduce the probability of sequential electrocatalytic oxidation of GALD and, therefore, enable the non-electrochemical conversion of GALD or DHA to LA (see section 2.2.1.1).[67] It has also been reported that AuPt with 90% Pt on the surface results in a lower conversion and higher selectivity toward LA than AuPt with 64% Pt on the surface. The authors attributed this difference to a modification in electronic properties of Pt caused by Au, promoting the adsorption of OH, thereby promoting oxidation reactions and thus the catalyst activity. Consequently, the enhanced catalytic activity promotes the successive oxidation of GALD to GLA, reducing non-electrochemical conversion of GLAD to LA.[67] The successive decrease in Pt surface coverage (AuPt with 15% Pt on surface) resulted in an increase in glycerol conversion and an increase in selectivity toward LA. This effect was related to insufficient Pt active sites for catalyzing dehydrogenation of the alcohol group and thus inhibits GLA formation.[67] Interestingly, under relative similar reaction conditions, Zhou *et al.* showed that $Pt_{20}Au_{80}$/Ag NPs did not achieve a high LA selectivity (<30%), but rather led to the production of DHA (40-80%).[134] This high selectivity toward DHA may perhaps be related to the high content of Pt(111) facets (section 2.4.1.2).[20] Nonetheless, it is expected that DHA would also get converted non-electrochemically to LA (see section 2.2.1.1). This discrepancy could be attributed to the low conversions over the $Pt_{20}Au_{80}$/Ag NPs reported by Zhou *et al.*, as only ~1% of glycerol was converted.[134] These low conversions are linked to short

experiments, meaning that the formed products (e.g., DHA) do not have sufficient time to undergo non-electrochemical reactions to form LA.[46,67]

An increase in catalytic activity for phase segregated PtAu electrocatalysts was also obtained for the oxidation of sorbitol in 0.3 M KOH.[166] These higher activities were attributed to the sequential electrocatalytic oxidation of glucose to gluconate and an enhancement in C-C cleavage reactions, decreasing the catalyst selectivity, as was shown by chronoamperometry at 0.9 V.[166] The observed trend of increased C-C cleavage at $E > 0.9$ V was in line with other reports.[67,134]

2.4.2.3 Bimetallic Pt-noble metal electrocatalysts

Studies devoted to bimetallic Pt-noble metal electrocatalysts evaluated the addition of Pd[144,169] and Ru[97,147,170,171] on the performance for the electrocatalytic oxidation of glycerol, where the selectivity was determined by HPLC.[97,147,169–171] The influence of Pd on PtPd electrocatalysts was exclusively studied under alkaline (pH = 13.7-14) conditions,[144,169] while the effect of Ru on PtRu electrocatalysts was studied under acidic (pH = 0.3)[171] and highly alkaline conditions at (0.5-1 M NaOH, pH = 13.7-14[147,170] and 4 M KOH pH = 14.6[97]).

Hong *et al.* studied the electrocatalytic oxidation of glycerol on PtPd alloyed nanowires in 0.5 M KOH. The alloyed structures displayed higher current densities in the CV in comparison to their monometallic counterparts, as well as a slower current decrease during chronoamperometric experiments, indicative of a higher activity and stability.[169]

Zhou *et al.* synthesized Pd nanocubes (Pd NCs) and Pd nanocubes encapsulated in Pt (Pt@Pd), as was proven by high-angle annular dark-field scanning transmission electron microscopy (HAADF-STEM) and high-resolution TEM coupled to an energy dispersive X-ray spectroscopy analyzer.[144] These electrocatalysts were compared to commercial Pt/C (10 wt.%) and Pd/C (40 wt.%) electrocatalysts for their activity toward the oxidation of glycerol in 1 M KOH. The Pt@Pd electrocatalyst displayed the highest current density during CV and was found to be the only catalyst to produce glycolate (>30% selectivity) at $E = 0.65$-1.25 V vs RHE during CA. Nonetheless, significant amounts of oxalate (> 10%) were produced over all these catalysts. This indicates that Pt@Pd suppresses the successive oxidation of glycolate to oxalate.[144]

At pH =0.3, various alloyed Pt_xRu_y/C electrocatalysts (the alloy phase was proven by XRD) were applied for the electrocatalytic oxidation of glycerol under acidic conditions (0.5 M H_2SO_4).[171] Cyclic voltammetry showed that the alloyed Pt_xRu_y/C electrocatalysts displayed ~200 mV lower onset potentials than Pt/C. Moreover, Pt_5Ru_5/C and Pt_7Ru_3/C also displayed higher current densities for glycerol oxidation at $E = $~0.85 V, in comparison to Pt/C. Pt_5Ru_5/C presented a higher stability than Pt/C, although the sequential CV experiments lead to a continuous decrease of the current density. At 1.1 V, after 7 h of electrolysis, 80% and 100% of the carbon balance was closed for Pt_5Ru_5/C and Pt/C, respectively. This indicates that the addition of Ru to Pt/C promotes C-C

cleavage reactions, resulting in the formation of CO_2. Moreover, Pt_5Ru_5/C produced based on selectivity DHA (35%) as the main product with minor fractions of GALD (17 %), glycolic acid (17 %) and GLA (11 %). By contrast, Pt/C mainly produced 42% GALD and 58% GLA with 1 % glycolic acid. This indicates that Ru addition to Pt promotes the electrocatalytic oxidation of the secondary alcohol group. DFT calculations show that the electropositive Ru atoms promote the interaction with the electronegative oxygen groups of glycerol (although the binding modes are the same).[171]

At pH = 14, the influence of Ru in bimetallic PtRu/C and PdRu/C electrocatalysts toward the electrocatalytic oxidation of glycerol was studied by Palma *et al*.[147] According to cyclic voltammetry, $Pt_{86}Ru_{14}$/C had an onset potential of 0.5 V, ~0.1 V lower than Pt/C, Pd/C and $Pd_{71}Ru_{29}$/C. The lower onset potential coincides with the study conducted on PtRu/C under acidic conditions.[171] A 60h-chronopotentiometry experiment confirmed an improved stability of the bimetallic catalysts when working at low currents (3 mA cm^{-2}) or low potentials (0.55-0.6 V), in comparison to the monometallic ones. FTIR and HPLC showed that at 0.7 V Pd/C and PdRu/C promoted exclusively the electrocatalytic oxidation of the primary alcohol group, presumably by the adsorption of this single group on the catalyst surface, generating 100% GLA (Figure 2.8). The selectivity changed when Pt/C or PtRu/C was used, resulting in the electrocatalytic oxidation of both primary and secondary alcohol groups, resulting in a product selectivity of 60% DHA and 40% GLA for Pt/C, and 44% DHA, 33% GLA and 22% TA for PtRu/C after 4h reaction time. Additionally, no carbonate was observed at the applied potential, indicative that no C-C bond breaking reactions did not occur.[147] The high selectivity toward DHA on Pt/C are somewhat surprising as most studies show that Pt is only mildly selective toward the catalytic oxidation of the secondary alcohol group.[46–48,50,103] Therefore, we believe that DHA is likely to be a product formed through non-electrochemical processes (see section 2.2.1.1). The incorporation of Ru in Pt/C appeared to promote the successive oxidation of GLA to TA,[147] which can potentially be explained by the stronger catalyst interaction with oxygen groups of glycerol, as was suggested by DFT calculations.[171] At pH = 14.6, the effect of different temperatures and current densities on the selective electrocatalytic oxidation of glycerol on a PtRu catalyst in a polybenzimidazole-based polymer electrolyte membrane reactor was investigated.[97] At 60 ºC, the main product was TA (> 60% selectivity independent of the applied current density, being 5-40 mA cm^{-2}), with GLA as second product (<30% at 20 mA cm^{-2} and decreasing at higher currents) and some glycolate. These results resemble those over Au and Pt, where similar harsh alkaline pH and temperature conditions in combination with a low applied potential resulted in an increased selectivity toward the formation of TA.[90,92,98,142,143] By increasing the current to 80 mA cm^{-2} or the temperature to 90 ºC, the electrocatalytic oxidation of TA to oxalate and FA became more prominent.[97,92]
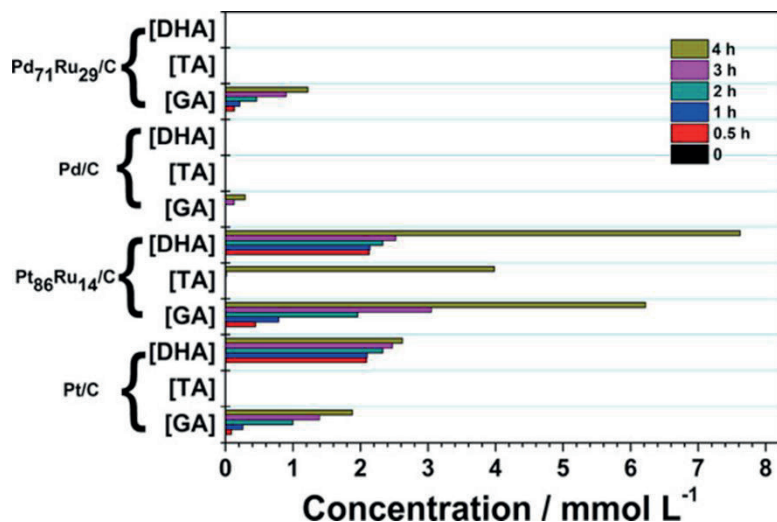
Figure 2.8. *Distribution of the glycerol oxidation products as a function of time at 0.7 V vs. RHE on the Pt-based and Pd-based electrocatalysts in 1.0 mol·L⁻¹ NaOH. GA=glycerate, TA=tartronate, DHA=1,3-dihydroxy-acetone. Reprinted with permission from [147]. Copyright 2017 Wiley-VCH Verlag GmbH & Co. KGaA, Weinheim.*

The observations discussed for bimetallic PtRu[147,171] were not in line with the results with bimetallic PtRu and PtRh on graphene nanosheets obtained by Zhou *et al*.[170] The degree of alloying was not discussed, yet the electrocatalysts had similar particle sizes to Pt/C. The onset potential of Pt was approximately 0.5 V, while the Pt-based electrocatalysts that contain Ru and Rh had a lower onset potential of 0.1 V and 0.2 V, respectively.[170] This lower onset potential for PtRu corresponds well with other studies.[147,171] The peak current density of the Rh containing catalysts was 10-times higher (> 5 mA cm⁻²) than the other catalysts, indicative of a higher catalytic activity. The specific reason of each catalytic activity is not clear, but the authors propose bi-functional, ligand and strain effects as main causes. Upon an increase in potential from 0.65 to 1.25 V, the selectivity of PtRu toward glycolate increases from 20% to >40% and the selectivity toward GALD decreases from >30% to <5%. In addition, the electrocatalyst showed the formation of ca. 15% oxalate and 30% GLA in the entire potential range. The formation of DHA was not reported,[170] in contrast with other studies conducted with PtRu[147,171] and Pt electrocatalysts.[46–48,50,103] We argue that this can be explained by the low conversions reported in that study (~0.1 %),[170] which would result in a difficulty in the detection of DHA, which often forms a minor product.[46–48,50,103] These low conversions reported by Zhou *et al*.[170] might explain why the results in other studies performed by Zhou *et al*. do not follow the trend of other studies.

2.4.3 Noble-non noble bimetallic electrocatalysts

Research devoted to bimetallic electrocatalysts that combine noble and non-noble metals for the selective electrocatalytic oxidation of glycerol includes the investigation of the effect of Ni

addition to Pt,[172] Au[150] and Pd[150]; Cu addition to Pt[173] and Pd[174]; and CeO$_2$,[175,176] Mn[177] and Fe[177] addition to Pd.

Luo *et al.* studied the selectivity of Pt/C and PtNi$_y$/C (y = 1, 2 or 3) for the electrocatalytic oxidation of glycerol at pH 14 and *E* = 0.9 V.[172] The PtNi/ C catalysts were characterized by HAADF-STEM-EDS, XPS and XANES. It was shown that PtNi$_2$/C had a homogeneous distribution of Pt and Ni on the surface and that the Pt in this bimetallic structure is less oxidized due to the electron donating nature of Ni (as determined by XANES). The addition of Ni to Pt improved the overall conversion and increased the selectivity toward oxalate, glycolate and other <C2 products, indicative for the promoting effect of Ni on C-C cleavage reactions. Operando X-ray spectroscopy and UV–vis spectroscopy were used to evaluate the effect of Ni on the PtNi catalyst. Based on these techniques, it was suggested that glycerol adsorbs strongly on the Ni(OH)$_x$ surface, preventing the oxidation of Ni. As a result, Ni is unable to catalyze glycerol oxidation (Figure 2.7). Therefore, it was suggested that the addition of Ni to Pt electrocatalysts changes the electronic properties of Pt and does not result in a bifunctional mechanism.[172] Under similar alkalinity, but higher potentials, Houache *et al.* studied the electrocatalytic oxidation of glycerol toward FA on Ni/C, Ni$_{0.9}$Au$_{0.1}$/C en Ni$_{0.8}$Pd$_{0.2}$/C electrodes.[150] Chronoamperometric measurements show that the electrocatalytic activity is significantly enhanced due to the introduction of noble metals.[150] The Faradaic efficiency (FE) at which FA was formed increased in the following order: Ni/C, Ni$_{0.9}$Au$_{0.1}$/C and Ni$_{0.8}$Pd$_{0.2}$/C.[150] Here FE was used rather than the more commonly used product selectivity. These results indicate that under the tested reaction conditions, the presence of other metals on the Ni surface improves the catalytic activity toward C-C cleavage.[150] Besides FA also traces of LA were found,[150] which can be the result of glycerol dehydrogenation by NiOOH at the secondary alcohol to DHA (section 2.4.1.4)[151] and the successive non-electrochemical conversion of DHA to LA (see section 2.2.1.1).

Mürtz *et al.* studied glycerol electrocatalytic oxidation at pH = 0.3 and *E* = 1.1 V on Pt, Pt$_8$Cu$_2$, Pt$_7$Cu$_3$, and Pt$_5$Cu$_5$. The metal particles had similar size (~2 nm, as determined by STEM), were found to be alloyed (shown by XRD) and similar metal loadings were used to study their electrocatalytic performance.[173] The current density for the electrocatalytic oxidation of glycerol was higher for PtCu electrocatalysts than for bare Pt. Moreover, the addition of Cu to Pt decreased the yield toward C-C cleavage reactions by ~10% for Pt$_8$Cu$_2$, reaching 90% C3 products, while higher Cu contents resulted in similar amounts of C-C cleavage reactions with respect to bare Pt. In comparison to bare Pt, the PtCu electrocatalysts were also not able to promote the successive oxidation of GLA to TA, resulting in high selectivity toward GLAD (60%) and GLA (30%).[173] The lower selectivity of PtCu toward C-C cleavage products and TA was attributed to a weaker adsorption strength of the intermediate products on the catalyst surface, thereby reducing successive oxidation of GLAD and GLA.[173] The lower adsorption strength of intermediate

products was inferred from the higher ratio between peak current density in the forward and backwards scan measured during cyclic voltammetry in the presence of glycerol.

Mo *et al.* studied the electrocatalytic oxidation of glycerol at pH = 14 and E = 0.8 V on $Pd_{75}Cu_{25}$, $Pd_{50}Cu_{50}$ and $Pd_{25}Cu_{75}$ electrocatalysts.[174] These catalysts were synthesized by a laser-assisted nanomaterial preparation method that does not require solvents and can be performed under atmospheric pressure and room temperature. Each electrocatalyst was prepared by coating a 10 nm layer of Cu or 10 nm Pd or a mixture of the two on a polyimide film. The resulting electrocatalysts consisted of alloyed structures as proven by XPS and HAADF-STEM-EDS. Under these reaction conditions, the current density was the highest for Pd and decreased with increasing Cu content and was zero for Cu,[174] which contrasts the results obtained with PtCu under acidic reaction conditions.[173] This indicates that the Cu oxides/hydroxides at the surface of the Cu electrode are not active for glycerol oxidation. The selectivity of the Pd electrocatalyst was ~60% GLA, ~8% GLAD, 9% TA, with the remaining products being C1 and C2 compounds, while an increase in Cu content up to $Pd_{50}Cu_{50}$ resulted in a decrease in selectivity toward C-C cleavage products down to 1% and an increase in selectivity to GLAD (~83 %), thereby reducing the rate of C-C bond breaking.[174] These results strongly resemble those of PtCu electrodes.[173] For $Pd_{25}Cu_{75}$, the only products were C1 and C2 compounds, indicative of an increase in C-C cleavage reactions. This shows that there is an optimum in Cu content in PdCu to steer the electrocatalyst selectivity toward C3 products, thereby reducing C-C cleavage reactions. The preference of PdCu for C3 products was attributed to a synergetic effect between the two metals, as supported by DFT calculations and in situ XAS experiments.[174]

Instead of alloying Pt with another metal, the effect of successive functionalization of carbon nanotubes (CNTs) with cerium oxide (CeO_2) as support for Pt nanoparticles (Pt-CeO_2/CNT) was studied.[175,176] Li *et al.* showed a uniform distribution of Pt and CeO_2 over the CNTs and claimed a ternary interaction, where the Pt-CNT interaction assures electrical conductivity and the Pt-CeO_2 interaction leads to a modification of electronic properties (as shown by an upshift in binding energy in XPS).[175] The CeO_2 also improves the dispersion of Pt particles on the CNTs, leading to an increased number of active sites.[175] Moreover, the downshift in the *d*-band center of Pt weakens the interaction with GLA during the electrocatalytic oxidation of glycerol,[178] which was claimed to lead to the observed improved recycling stability by a twofold[175] and catalyst activity by a fivefold.[176] Under relatively similar reactions conditions, Liu *et al.* showed that the selectivity of Pt is not significantly affected by CeO_2,[176] while Li *et al.* showed a higher selectivity toward TA and C-C cleavage and reduced selectivity toward LA.[175] The increased selectivity toward TA suggests that CeO_2 promotes oxidative reactions, but also causes successive C-C cleavage reactions.[175] Moreover, we argue that the reduced selectivity toward LA for Pt-CeO_2/CNT can be related to a faster oxidation of GALD preventing its desorption and the successive non-electrochemical reactions to form LA (see section 2.2.1.1). A further optimization between the

CeO_2 to Pt ratio on the CNT support decreased the selectivity toward the C-C cleavage reaction products to 4% and resulted in 64% GLA, 6% TA and 26% LA.[175]

Naik *et al.* studied the effect of the support on a Pd electrocatalyst.[179] In this case, C and TiO_{2-x} nanosheet (NS) supports were decorated with PdZn for the electrocatalytic oxidation of glycerol in 0.5 M NaOH (pH = 13.7). Here it was shown that the TiO_{2-x} NS caused a downshift in the *d*-band center. Cyclic voltammetry showed that the TiO_{2-x} NS support causes a positive shift in the PdO_x reduction peak when compared to a carbon support, suggesting that Pd binds oxygenates species less strongly on the TiO_{2-x} NS support. It was claimed that this might decrease the poisoning effect of adsorbed oxygenated species formed during the electrocatalytic oxidation of glycerol, thereby improving the electrocatalyst stability and activity, similarly to what was shown for Pt/CNT functionalized with CeO_2 (section 2.4.2.3).[175,176] The support did not show a significant effect on the catalyst selectivity, resulting in near ~45% GLA and ~45% LA. In this case glycerol is electrocatalytically oxidized to GALD and successively electrocatalytically oxidized to GLA or alternatively non-electrochemically converted to LA.

Finally the addition of Mn and Fe to Pd electrocatalysts was studied for glycerol oxidation at pH = 13. MnPd/C and FePd/C had a 2 and 1.5 fold higher current density than Pd/C.[177] Moreover, the addition of Mn or Fe to Pd changed the electrocatalyst selectivity. After CA at 0.8 V, Fe promoted the selectivity toward FA by twofold, inducing C-C cleavage reactions, while Mn promoted the selectivity toward GLA and TA by twofold, reducing C-C cleavage reactions.[177]

2.4.4 Noble-post-transition bimetallic electrocatalysts

The modification of noble metal electrocatalysts by the addition of post-transition metals and their effect on the electrocatalytic oxidation of various sugar alcohols has focused nearly exclusively on Pt electrodes,[45,47,76,103,149,180–184] with a few exceptions for Pd electrodes.[136,184] Moreover, only the studies devoted to Pt electrodes have reported the product concentrations analyzed by HPLC. Most of these studies were conducted with adatom-modified catalysts,[45,47,76,136,180–183] while few have also alloyed the noble and post-transition metals.[103,149,184] These studies were frequently performed under acidic conditions [45,47,76,103,149,180,181] and less often under alkaline conditions.[136,182–184] The most commonly studied post-transition metal is Bi,[45,47,76,103,149,181,182,184] but other post-transition metals have been also investigated, such as Sb,[45,103,181] Sn,[45,180,181] Pb[45,181,183] and In.[45,181]

The addition of Bi adatoms on Pt(111) and Pt(100) facets was studied under acidic conditions (0.5 M $HClO_4$) by LSV combined with online HPLC and *in situ* FTIR.[76] As illustrated in Figure 2.9, it was suggested that Bi on Pt(111) interacts specifically with the enediol intermediate, thereby promoting the isomerization toward DHA, and consequently steering the electrocatalyst selectivity toward the oxidation of the secondary alcohol.[76,185] On Pt(100) on the other hand, Bi decreases the activity and does not impact the formation of GALD and GLA. In the case of Pt(100),

the surface-adsorbed enediol intermediate does not exist, as glycerol only binds through a single primary carbon (see Scheme 2.6), thus leading exclusively to the electrocatalytic oxidation of the primary alcohol.[20] For Pt(111)-Bi, Bi adatoms suppress the formation of adsorbed CO and thus the catalyst poisoning.[76] For Pt(100)-Bi, Bi adatoms only partially prevent the formation of adsorbed CO species.[76] The decrease of CO poisoning induced by Bi adatoms show a resemblance to PtBi bimetallic catalysts (section 2.4.2.3).[184] These results show that the electrocatalyst structure has a strong influence on how the adatoms modify the catalyst performance.[76] A similar effect was observed in a study on the effect of Sn adatom modification of Pt(100) preferentially oriented nanoparticles in acidic media. The presence of Sn adatoms on Pt surfaces alters the adsorption of glycerol on Pt, consequently hindering the breaking of C-C bonds. As a result, the selectivity of the Sn modified Pt(100) preferentially oriented nanoparticles is diverted to C3 oxidation products, while the preference toward the electrocatalytic oxidation of the primary alcohol remained unaltered.[180]
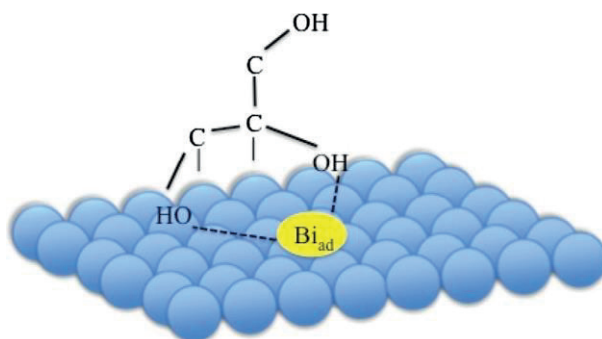

Figure 2.9. *Proposed interaction between the enediol intermediate with Bi on Pt (111) surface. Reprinted with permission from [76]. Copyright 2016 Elsevier.*

Most literature studies have been devoted to the effect of adatoms on polycrystalline Pt under acidic conditions.[45,47,181] Bi and Sb are adsorbed on Pt surfaces under acidic conditions (0.5 M H$_2$SO$_4$) at low potentials, while at E = 0.61-0.66 V both adatoms start to oxidize.[186,187] At E > 0.85 V, Bi and Sb progressively desorb.[186,187] Bearing this in mind, the highest impact on the Pt catalyst selectivity is obtained when Bi or Sb adatoms are not oxidized ($E \leq 0.6$ V).[45,47,181] In this region, Bi alters the reaction pathway: (1) by blocking the active Pt sites, which induce the electrocatalytic oxidation of the primary alcohol; (2) by changing the coordination of the adsorbed sugar alcohol on the Pt surface, which redirects the catalyst selectivity toward secondary alcohol oxidation reactions; and (3) by circumventing C-C cleavage reactions, thereby reducing CO formation.[45,47] As a result, Bi or Sb adatom modified Pt/C catalysts have been found to be highly selective toward the electrocatalytic oxidation of the secondary alcohol groups of various sugar alcohols at E < 0.6 V,[45,47,181] achieving a selectivity of nearly 100% DHA.[47,181] At E > 0.6 V, the adatoms progressively lose their effect on the selectivity due to their oxidation and desorption from the surface of

Pt.[45,47,181] Similar results were obtained with alloyed PtBi and PtSb electrocatalysts under acidic conditions (0.5 M H_2SO_4) for the oxidation of glycerol.[103,149] Briefly, at E = 0.4 V and 0.6 V (Figure 2.10), PtBi/C and PtSb/C showed similar selectivity toward the secondary alcohol group, producing DHA with 50-65% selectivity.[103] The selectivity toward DHA for PtBi/C changed at E = 0.8 V and $E \geq$ 1.0 V to 15% and 2% respectively, while the selectivity toward DHA for PtSb/C increased at E = 0.8 V first to 68% and then decreased at higher potentials to ~42%.[103] We argue that the discrepancy between research on Sb in PtSb alloyed electrodes and Sb adatom modified Pt electrodes might be related to the structural properties of the electrocatalyst, where the incorporation of Sb adatoms in the fcc Pt structure limits its desorption at E > 0.85 V (typically observed for Sb adatoms on Pt electrodes[186]). Moreover, the use of Pt_xBi_{10-x}/C (x = 1, 5 or 9) electrocatalysts for the oxidation of glycerol in 0.5 M H_2SO_4 at 1.2, 1.6 and 2.0 V vs RHE only resulted in minor contents of products obtained through secondary alcohol group dehydrogenation (~15 % DHA and HPA).[149] For Bi adatom modified Pt/C electrocatalysts, a saturation of the electrolyte with Bi further improved the selectivity toward DHA.[47] For this case it is worthwhile to study whether Bi can form a complex in solution with glycerol, as was observed for borate,[89] which can interact with the primary alcohol groups and let the secondary alcohol group coordinate towards the surface of the electrode. For Pb adatom modified Pt catalysts, a slight change in selectivity toward DHA was also induced, although the main reaction remained the electrocatalytic oxidation of the primary alcohol group, being GALD and GLA.[181] Sn and In did not appear to change the electrocatalyst selectivity significantly.[181]
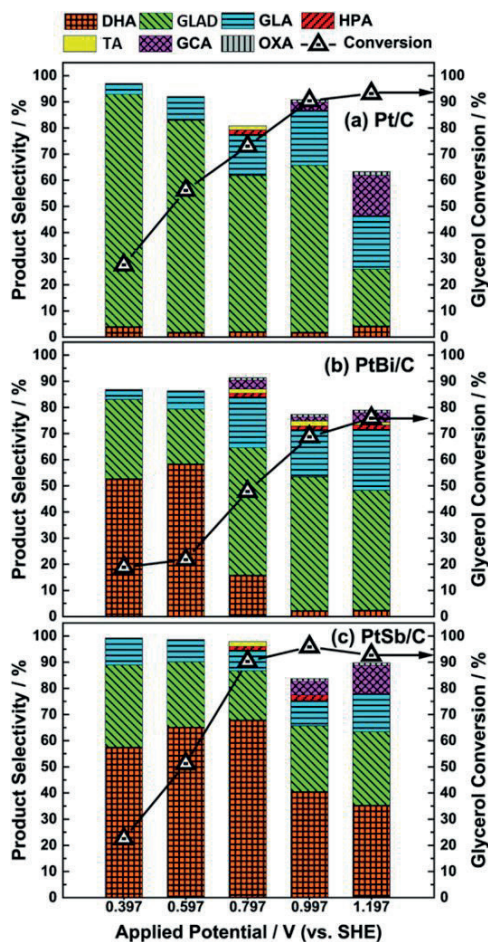
Figure 2.10. *The effect of alloying Sb or Bi with Pt/C toward the selective electrocatalytic oxidation of glycerol in 0.5 M H₂SO₄ as a function of applied potential (GCA = glycolic acid and OA = oxalic acid). Reprinted with permission from [103]. Copyright 2016 Royal Society of Chemistry.*

The effect of Bi and Sb adatoms on Pt electrodes were also studied for the electrocatalytic oxidation of C6 (sorbitol), C5 (arabitol and ribitol) and C4 (erythritol and threitol) sugar alcohols.[45] This study was devoted to the stereochemistry of C4, C5 and C6 sugar alcohols at the secondary alcohol position and how this affects the activity and selectivity of Bi and Sb adatom modified Pt/C electrodes.[45] Bi and Sb adatoms on Pt/C electrodes can direct the electrocatalytic oxidation of sugar alcohols (sorbitol and arabitol) toward the secondary alcohol at *E* < 0.6 V vs RHE under acidic conditions (0.5 M H₂SO₄), while monometallic Pt/C would mainly promote the oxidation of the primary alcohol. A general route for the electrocatalytic oxidation of sorbitol and arabitol is given in Figure 2.11. In the presence of sorbitol (C6), following Figure 2.11A, Pt/C preferably leads to oxidation of the primary alcohol groups, resulting in a mixture of glucose and gulose, while Bi- or Sb-modified Pt/C diverts the selectivity to the C2-OH and C5-OH groups, yielding a mixture of

fructose and sorbose. In the case of arabitol (C5), Figure 2.11B, which has a similar stereochemistry to sorbitol but with the C4-OH group (equivalent to the C5-OH group of sorbitol) switched, the selectivity of the electrocatalyst also changes.[45] For Pt/C, the selectivity was directed to the primary alcohol group, with a higher preference for the C1-OH group than for the C5-OH group. Bi-Pt/C on the other hand shows a preference toward both the electrocatalytic oxidation of the C2-OH and C4-OH group over the electrocatalytic oxidation of C5-OH and C2-OH group, thus diverting the selectivity of Pt/C again away from the primary alcohol groups to the C5-OH and C2-OH group. These results highlight that the selectivity of the electrocatalyst with and without adatom modification is greatly influenced by the stereochemistry of the reactant. Besides a change in selectivity, adatoms also decrease the onset potential of Pt/C. The decrease in onset potential is adatom-dependent and reactant-dependent. The decrease in onset potential for glycerol was 150 mV for Sb and Sn and 50 mV for Bi, In and Pb,[47,181] and the onset potential for sorbitol decreased 50 mV for Sn, remained unaltered for Bi, Sb and In, and increased by 50 mV for Pb.[45]
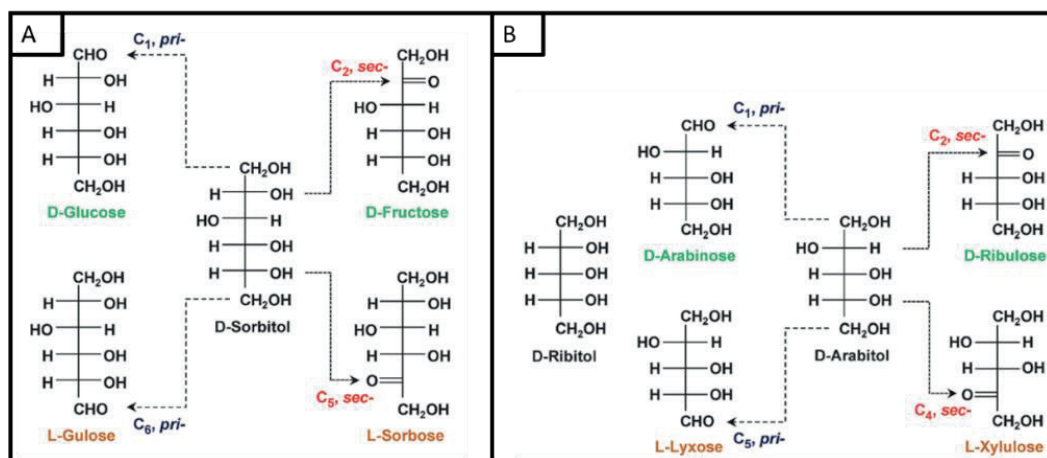

Figure 2.11. *Pathways for the electrocatalytic oxidation of sorbitol and arabitol, which can be achieved through adatom modifications of Pt electrodes. Reprinted with permission from [45]. Copyright 2015 WILEY-VCH Verlag GmbH & Co. KGaA, Weinheim.*

Under alkaline conditions (pH = 13), only Bi and Pb adatom modified Pt/C have been reported.[182,183] Bi has been shown to limit the C-C cleavage reactions $E < 0.8$ V vs RHE (based on HPLC), while at higher potentials this effect is lost,[182] possibly due to the desorption of Bi adatoms.[186,187] Unlike the studies performed with adatom modified Pt/C electrodes under acidic conditions,[45,47] the formation of DHA was not clearly detected under alkaline conditions.[182,183] The main product formed in this case was either GLA or glycolate.[182,183] It was argued that the hydroxide ions in the electrolyte can catalyze the conversion of the formed DHA into GLA.[182,183] However, this reaction is unlikely to proceed when reaction Scheme 2.3 is followed.[46] We propose

that GLA and glycolate might have formed due to the presence of oxygen in the alkaline electrolyte (see section 2.2.1.1).

Bi adatom modification of Pd did not affect the catalytic activity, but it did decrease the onset potential by ~150 mV and change the reaction pathway.[136] Here the reaction products were only determined on the surface of the catalyst by FTIR. At pH = 13 and $E \geq 0.65$ in the presence of Bi, the electrocatalytic oxidation of the secondary alcohol group of glycerol takes place, resulting in the formation of DHA. Bi adsorbs on the Pd surface decreasing the number of Pd-sites surrounded by adjacent Pd atoms, resulting in two distinct effects on the reaction pathway. Firstly, it diminishes the dissociative adsorption of glycerol (C-C cleavage) on Pd.[136] Secondly, the adsorption of the primary alcohol is limited as it requires three adjacent Pd adatoms, while the secondary alcohol requires only one or two adjacent Pd atoms. Another explanation for the enhanced formation of DHA is given by the basicity that Bi offers. In the presence of Bi, the local pH increases through the adsorption of hydroxide ions, leading to the formation of a very reactive $CH_3OH-CHO^--CH_3OH$ alcoholate that is converted into DHA.[136] This can promote the reaction pathway toward the formation of DHA, hydroxypyruvate and MOA.[136] The redirection of the selectivity toward the electrocatalytic oxidation of the secondary alcohol group of glycerol was also found for the addition of Bi or Sb adatoms on Pt electrodes under acidic conditions for the electrocatalytic oxidation of various sugar alcohols (quantified by HPLC, section 2.4.2.4).[45,47,181] However, these studies mainly show that the selectivity is improved toward DHA when Bi is not oxidized ($E \leq 0.6$). This discrepancy could potentially lie in the analytical technique that has been applied to identify the products or the use of alkaline rather than acidic reaction conditions.

2.4.5 Other electrocatalysts

Other electrocatalysts that have been used to study the oxidation of glycerol are boron doped Co (CoB)[89] and BiNi/C,[105,188] where the carbon support of BiNi/C was also doped with cerium oxide and antimony tin oxide.[105]

It has been shown that the addition of Bi to Ni can improve the catalyst activity as well as selectivity toward C3 oxidation products.[105,188] At 1.35 V and pH = 14, glycerol is oxidized over Ni/C to ~35% C3 oxidation products, whereas NiBi/C produced ~50% C3 oxidation products.[105] The effect of storing (e.g., aging) the catalyst ink used for drop casting NiBi/C on a glassy carbon electrode to perform electrochemical experiments was evaluated. Aging the NiBi/C catalyst caused structural deformations and morphological changes (as determined by HAADF-STEM, STEM-EDS and STEM-EELS), exposing more Bi-based particles on the surface. The higher percentage of exposed Bi and spatial distribution of $Ni(OH)_2$ and $Bi(OH)_3$ improved the electrocatalyst selectivity to C3 products by reducing C-C cleavage reactions.[188] Under optimized reaction conditions (pH =14, E = 1.3 V and T = 50 ˚C), the selectivity of the NiBi/C catalyst could be steered to 60% GLA, 10% TA, 5% LA and 25% C-C cleavage products, indicative of a moderate

selectivity for the electrocatalytic oxidation of the primary alcohol group.[188] The effect of doping NiBi/C and Ni/C electrocatalysts with CeO_2 and antimony tin oxide (ATO) on the selectivity was also studied at pH = 14.[105] At 1.35 V, ATO-modified Ni/C electrocatalysts displayed > 99% selectivity toward LA. On the other hand, ATO-modified NiBi/C electrocatalysts were more selective toward GLA (70%) with minor contents of TA (10%) and LA (14%). The addition of CeO_2 to Ni/C and NiBi/C catalysts gave similar results with respect to selectivity, but the addition of CeO_2 to Ni/C only gave 60% LA with 40% GLA.[105] Moreover, the catalytic activity of Ni/C and NiBi/C appears to be lower when doped with metal oxides, as was shown after 1 h of CA.[105] These results potentially indicate that the electrocatalyst primarily produces GLAD, which successively undergoes a series of non-electrochemical reactions to form LA (see section 2.2.1.1).[105] Nickel boride catalysts have also been synthesized and their composition and the reaction conditions (pH = 14.3 and E = 0.5 V) have been optimized for the electrocatalytic oxidation of glycerol to lactate, although only 9% lactate was achieved where the remainder were C-C cleavage products, being mainly FA.[152]

In another study, Co was combined with borate to yield cobalt borate and used for the electrocatalytic oxidation of glycerol at E = 1.56-1.86 V between pH = 7.6-9.6.[89] The effect of pH has been explained in section 2.2.1.1, while the effect of potential will be addressed here. With an increase in potential the selectivity toward DHA decreases, while that of HPA increases. This change in selectivity was attributed to the higher potential applied, promoting successive oxidation reaction.[89] Here we argue that higher potentials could drive the formation of more high valent redox mediator Co^{3+}/Co^{4+} species that can promote the successive oxidation of DHA to HPA.[189] Under harsh alkaline and optimized conditions (pH = 13.7, 20°C between 8.8-44.2 mA cm^{-2} and under continuous mixing) Co could selectively produce 50-58% GLA at, while the selectivity could be changed toward 44% LA by altering the reaction conditions (pH = 14, 60 °C at 1.8 mA cm^{-2} and under continuous mixing). The latter set of reaction conditions could reduce the sequential electrocatalytic oxidation reaction on Co of GLAD to GLA, while it promotes non-electrochemical reactions that convert GLAD to LA (see section 2.2.1.1).

2.5 Effect of electrocatalyst properties under various reaction conditions on the oxidation of saccharides

This section presents the literature and discusses trends of the electrocatalyst activity and selectivity for the oxidation of saccharides. To define trends for the selective electrocatalytic oxidation of the anomeric carbon in saccharide molecules, glucose is chosen as a reference compound, considering its abundance in nature and the higher number of publications about its electrochemical oxidation in comparison to other monosaccharides (e.g., fructose, xylose or mannose). Most of the studies dealing with this topic used Au and Pt (sections 2.5.1.1 and 2.5.1.2 respectively) as electrocatalysts, for which it was possible to define trends with respect to the

catalyst properties, i.e. the type of metal used, the oxidation state of the metal and type of bimetallic catalyst. Before going into detail on the trends observed in the literature, the main mechanistic pathway for the electrocatalytic oxidation of glucose is summarized. A general scheme presenting the routes in which glucose can be electrocatalytically oxidized is given in Scheme 2.7.[190] Under a broad range of pH conditions (pH = 1-13), glucose is predominantly present in its pyranose form (> 99.9 %).[56] Based on FTIR, the electrocatalytic oxidation of glucose proceeds first at the anomeric carbon by dissociative adsorption resulting in an adsorbed dehydrated intermediate.[52,58] This adsorbed intermediate can either be oxidized to gluconic acid (GA) or it can be oxidized to gluconolactone, which successively desorbs from the catalyst surface and hydrolyses non-electrochemically to form GA, as was shown by cyclic voltammetry and FTIR.[58,191] The hydrolysis of gluconolactone is dependent on the pH of the electrolyte: under acidic conditions, gluconolactone and GA are in equilibrium in the electrolyte, while in alkaline media the lactone ring of gluconolactone hydrolyses non-electrochemically to yield GA.[192] To our knowledge, gluconolactone has never been quantitatively analyzed after electrooxidizing glucose, independently of the pH used. This is believed to be a result of the fast hydrolysis of gluconolactone to gluconic acid in alkaline electrolytes, or due to the incomplete separation of analytes by chromatographic techniques. The simultaneous quantification of gluconic acid and gluconolactone can potentially be achieved by 2D-NMR.[193]

The subsequent electrocatalytic oxidation of GA can either take place though a dehydrogenation reaction at the C2-OH group or the C5-OH group, yielding 2-keto gluconic acid (2-k-GA) and 5-keto gluconic acid (5-k-GA), respectively.[57,190,194] These products have only been reported in three publications where a Pt electrode was used.[57,190,194] However, some analytical techniques do not allow discerning the presence of these products due to the strong resemblance of their chemical structure with other glucose oxidation products. Therefore, the use of ternary amine columns in HPLC or a trimethylsilylation treatment followed by gas chromatography or high-pressure anion exchange chromatography have been suggested for their separation and quantification.[57,190,194] Alternatively, the C6-OH group of GA can be oxidized to an aldehyde, forming gururonic acid (GUL), which has rarely been quantified.[104,112,190] In contrast to GUL, glucuronic acid (GLU) has been quantified more frequently,[25,77,190,195] tentatively explained by the strong resemblance in the structure of GUL and GLU (e.g., being stereoisomers),[190] hampering their separation by chromatographic techniques. Only one study enabled the discrimination of these species through the use of high-pressure anion exchange chromatography.[190] Alternatively, glucose can be dehydrogenated at the C6-OH group to form glucose dialdehyde, which has only been quantified once in literature by using high-pressure anion exchange chromatography.[190] Successively, GD can either be oxidized at C1=O or C6=O to a carboxylate yielding GUL and GLU, respectively. Finally, GUL and GLU can be oxidized at the aldehyde group to form a carboxylate, resulting in glucaric acid (GLR).

In general, several glucose oxidation products have been quantified only rarely, such as glucose dialdehyde, 2-keto gluconic acid, 5-keto gluconic acid, and either glucuronic acid or guluronic acid. This indicates that several products are likely to be overlooked. Therefore, caution should be taken in drawing conclusions from studies on the electrocatalytic oxidation of glucose and potentially also of other saccharides, such as xylose, galactose and mannose.
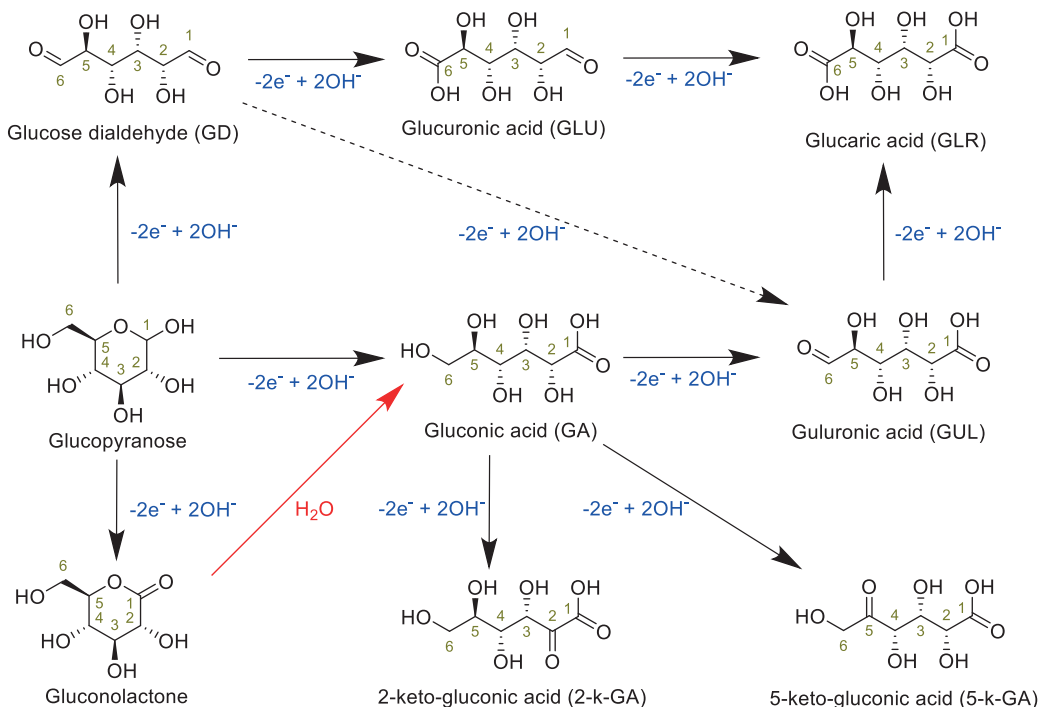
Scheme 2.7. *Main reaction pathways for the electrocatalytic oxidation (black arrows with number of electrons/hydroxides in blue), and non-electrochemical conversion (red arrow) of glucose and derivatives observed in literature.*[190]

2.5.1 Monometallic electrocatalysts

In this section the trends for the selective electrocatalytic oxidation of saccharides are discussed and compared with the trends for the electrocatalytic oxidation of sugar alcohols. The structure of this section follows the same order as in the sugar alcohol section (section 2.4), where Au (2.5.1.1) and Pt (2.5.1.2) were studied most frequently and therefore discussed first, followed by a comparison between Pd-, Ir- and Ru-based electrocatalysts (2.5.1.3), Ni- and Co- based electrocatalysts (2.5.1.4), and Cu- and Mn- based electrocatalysts (2.5.1.5).

2.5.1.1 Au-based electrocatalysts

This section evaluates the oxidation of saccharides at different pH and potentials on Au electrocatalysts. The selective electrocatalytic oxidation of saccharides, such as glucose, mannose and galactose over Au electrodes has mainly been studied under alkaline conditions (pH = 10-

13)[25,77,95,196–200] and less frequently neutral (pH = 7) conditions.[55,62] To our knowledge, only Kokoh *et al.* studied the selective oxidation of glucose on Au electrodes under acidic (pH = 1) conditions.[55] This is related to both a higher reactivity of saccharide-like reactants under alkaline conditions (see section 2.2.1.1) and low activity of Au under acidic and neutral media, as it will be further detailed.

The effect of Au (nano)particle surface shapes and sizes (rod, spherical, cuboid and polyhedron shapes) and facets on the catalyst activity has been studied for the electrocatalytic oxidation of glucose in 0.1 M NaOH.[102,201–203] Although these studies did not evaluate the effect of the different parameters on the reaction selectivity, they all converge on the higher activity (current density) of the electrocatalysts containing Au(100) facets, followed by the Au(110) facets and Au(111) being the least active. This is in line with previous research performed on single crystals studied under acidic[204] and neutral reaction conditions.[205,206]

Under acidic conditions in 0.1 M $HClO_4$ (pH = 1), polycrystalline metallic Au (at E = 0.95 V) catalyzes the oxidation of glucose in the course of 24 h to 63% GA, 29% FA, 9% glycolic acid and traces of tartaric acid (Sel. based) at a very low current density of 0.23 mA cm^{-2}.[55] In 0.1 M H_2SO_4, metallic Au does not show any clear electrocatalytic activity (~0 mA cm^{-2}) for mannose oxidation, similar to the effect of (bi)sulfate adsorption on glycerol oxidation on Au in acidic media (see section 2.4.1.1).[95] In this case, the competitive adsorption between HSO_4^- and the saccharide diminishes the catalyst activity,[204] as was also observed for the electrocatalytic oxidation of glycerol.[54]

In neutral conditions (pH = 7, 0.1 M $H_2PO_4^-$/HPO_4^{2-}), metallic Au (0.95 V) and Au(OH)$_3$ (1.35 V) both catalyze the oxidation of glucose at low currents of 0.38 mA cm^{-2} and 0.13 mA cm^{-2} respectively (cyclic voltammetry: 50 mV s^{-1} and 0.2 M glucose).[55] Under similar reaction conditions and for the electrocatalytic oxidation of glycerol on Au, comparable currents were measured.[46,65] This indicates that Au is hardly active for catalyzing saccharide and sugar alcohol oxidation under neutral reaction conditions.[55,62] By contrast, the onset potential for the electrocatalytic oxidation of saccharides over metallic Au electrodes is 0.4 V,[55] while the electrocatalytic oxidation of sugar alcohols is 0.8 V.[46] After 6 h at E = 0.87 V over an Au electrode, glucose was converted to GA (Sel. = 93%), GLR (7%) and traces of FA, glycolate and tartrate.[55] Under similar reaction conditions and after 8 h of reaction at E = 0.87 V over an Au electrode, produced GA (Sel. = 97%) and GLU (3%). This indicates that Au catalyzes the oxidation of the anomeric carbon with a highly selectively through an oxygenative or dehydrogenative step (i.e. the oxygenative oxidation of the anomeric carbon of glucose results in an adsorbed GA species, while the dehydrogenative oxidation of the anomeric carbon of glucose results in an adsorbed gluconolactone species, which can successively desorb and hydrolyze non-electrochemically to form GA, see Scheme 2.7).[55] However, the activity of Au for the electrocatalytic oxidation of glycerol[46,65] (which proceeds through the oxidation of the primary alcohol group) and glucose[55,62]

do not differ significantly. Moreover, GLU can only be formed through the electrocatalytic oxidation of GD (Scheme 2.7), which is an intermediate in the glucose oxidation pathway that is formed by the electrocatalytic dehydrogenation of the primary alcohol group of glucose. Therefore, it is likely that Au electrocatalysts can also promote the oxidation of the primary alcohol group of glucose (Scheme 2.7), resulting in the formation of GD. This might indicate that the formation of GD was overlooked and that Au is therefore much less selective toward GA than what is currently being stated in the literature. Finally, the low selectivity toward C-C cleavage products under neutral conditions is in line with the electrocatalytic oxidation of sugar alcohols (glycerol) over metallic Au (at E = 0.8-1.2 V, pH = 7, 0.1 M Na_2SO_4), where GALD was formed with 100% selectivity,[46] while $Au(OH)_3$ (E >1.2 V) promotes more C-C cleavage reactions (section 2.4.1.1).[46] These results indicate that neutral conditions and metallic Au (E < 1.2 V) is more favorable than acidic conditions for the selective conversion of saccharides and sugar alcohols.

At pH = 13 and in the metallic Au region (at E < 1.2 V), Figures 2.12A and B show that the electrocatalytic oxidation of glucose, mannose and glucuronate (GLU) over Au electrodes starts at 0.35 V.[25,77,95] The oxidation reaction at this potential corresponds to the oxygenative/dehydrogenative oxidation of the anomeric carbon (both of glucose and mannose). This low onset potential for the anomeric carbon group was also found for other molecules that bear anomeric carbon groups (xylose, 2-deoxy-d-glucose, d-glucose-6-phosphate and GLU).[196] By contrast, Figures 2.12C and D show that the electrocatalytic oxidation of the C6-OH group of GA and mannonate over Au electrodes initiates at 0.75 V,[77,95] while no clear peak for glucarate oxidation is observed in the E = 0.3-0.85 V range.[77] The onset potential for the oxidation of the C6-OH group corresponds to the onset potential of other molecules that only contain alcohol groups and no anomeric carbon or aldehyde groups (glycerol, sorbitol, GA, methyl β-d-glucopyranoside, 1,6-anhydro-β-d-glucose).[46,91,196,207] Considering the scan rates, the current densities for the electrocatalytic oxidation of glucose measured on Au in alkaline conditions (2 mA cm^{-2}, recorded in the presence of 0.04 M glucose at 10 mV s^{-1}) are of a 1-2 times higher order of magnitude than under neutral and acidic reaction conditions (0.2 mA cm^{-2}, recorded at 50 mV s^{-1} and 0.2 M glucose). A similar trend was observed for sugar alcohol oxidation on Au, which was attributed to the rate-limiting step being affected by the pH (e.g., hydroxide ion concentration) of the electrolyte (Scheme 2.4). This indicates that the rate-limiting step for the electrocatalytic oxidation of glucose on Au electrodes is determined by either (1) the hydroxide ion concentration at the interface or (2) non-electrochemical reactions that are needed for the formation of the more electroactive enediol (see section 2.2.1.1).

At pH = 13 and on a polycrystalline Au electrode Figure 2.12A and B, an increase in potential results in the electrocatalytic oxygenative/dehydrogenative oxidation of the anomeric carbon of glucose and oxidation of the aldehyde group of GLU at ~0.3 V with a peak potential at ~0.5 V.[208] A further increase in potential results in a second and third peak potential for both molecules at

~1 and ~1.25 V vs RHE. By contrast, in Figure 2.12C only two peak currents were observed for the oxidation of the C6-OH group (GA) on the Au electrode at ~1 and ~1.25 V vs RHE, while in Figure 2.12D only one peak current was observed for the oxidation GLR of at ~1.25 V vs RHE, which is likely related to C-C cleavage reactions. At higher potentials than 1.25 V vs RHE, Au passivates[77,196] through the formation of oxidized Au species, possibly in the form of $Au(OH)_3$, as was also observed for the electrocatalytic oxidation of sugar alcohols.[46,91] In the negative-going scan and in the absence of a reactant, a cathodic peak appears at E = 1 V (Figure 2.12A-C, dashed line), corresponding to the reduction of Au oxides/hydroxides to metallic Au. By contrast, in the negative-going scan and in the presence of a reactant, a sharp anodic peak appears at E = 1 V (Figure 2.12A-C, solid line), corresponding to the electrocatalytic oxidation of the reactants. This indicates that once the Au surface oxide is reduced, the oxidation of the organic molecule starts again. Finally, the measured current density and thus the electrocatalytic activity for the oxidation of saccharides over Au was higher for larger molecules going from d-allose to d-erythrose to GALD.[196] These results suggest that a higher pK_a of the molecule results in higher catalytic activity,[196] which matches the results for the electrocatalytic oxidation of sugar alcohols.[65]
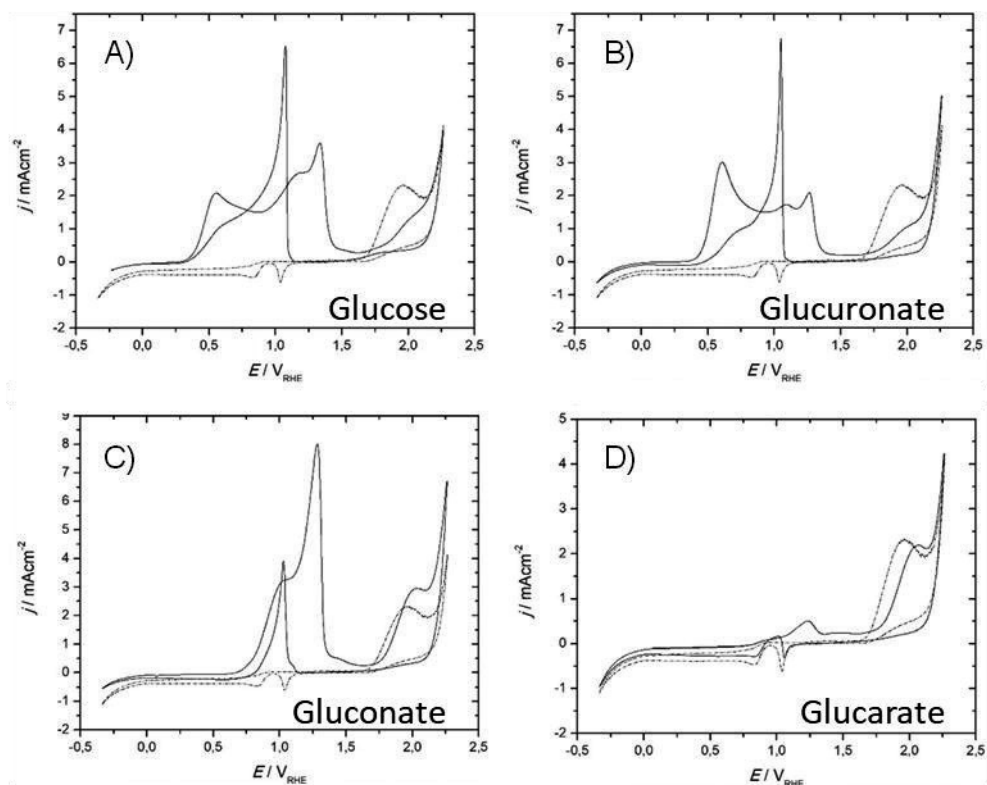
Figure 2.12. *Cyclic voltammetry of a polycrystalline Au electrode in the absence (dashed lines) and presence of (solid lines): (A) 0.04 M glucose, (B) 0.04 M glucuronate, (C) 0.04 M gluconate and (D) 0.04 M glucarate measured in 0.1 M NaOH (pH = 13) at 10 mV s^{-1}. Adapted with permission from [77]. Copyright 2020 Wiley-VCH Verlag GmbH & Co. KGaA, Weinheim.*

For long-term electrolysis, at pH = 13, after 65 h and at T = 5°C (to prevent glucose isomerization), metallic Au (at E = 0.55 V) promotes the conversion of glucose to GA (Sel. = 87%), FA (6%) and traces of GLR.[77] The detection of FA confirms that C-C cleavage does happen on Au electrodes already at E = 0.55 V.[77] In comparable studies performed at pH = 10-13 over metallic Au (at E < 0.85 V), similar results were obtained, where the oxygenative/dehydrogenative oxidation of the anomeric carbon of glucose is preferred over the electrocatalytic oxidation of the alcohol group.[25,197,198] This is in line with studies devoted to the electrocatalytic oxidation of sugar alcohols, where the onset potential over metallic Au lies close to 0.8 V.[46,91] For the electrocatalytic oxidation of glucose the selectivity toward GA ranged between 86-100%, confirming the preference of Au electrodes for the oxygenative/dehydrogenative oxidation of the anomeric carbon.[25,77,197,198] At pH = 11.3 (0.1 M Na$_2$CO$_3$), an increase in applied potential from 0.5 to 0.8 V resulted in an increase in glucose conversion from 6 to 30%, while the selectivity for GA (85%) remained unaffected.[25] At higher potentials (at E > 0.85 V), the oxidation of both the anomeric

carbon and primary alcohol groups of saccharides (mannose, galactose and glucose) are promoted over the Au electrode, resulting in the formation of C6-dicarboxylates (C1 + C6 oxidation: mannarate, galactarate and GLR) and the formation of C-C cleavage products.[25,77,95,197–199] As the potential is increased further from 0.85 V to 1.35 V, the C-C cleavage reactions are further promoted at the expense of C6-dicarboxylates.[25,95,199] These results coincide with those of sugar alcohol electro-oxidation, where E < 0.8 V over Au electrode results in minimal C-C cleavage reactions,[49] while E > 0.8 V significantly promoted C-C cleavage reactions.[46,91,92] There is one outlier in this trend for saccharide oxidation, in which it was shown that the catalytic oxidation of xylose over Au (at E = 1.1 V) did not result in the formation of xylarate (C5-dicarboxylate), but only 63% xylonate.[207] The lack of detection of C5-dicarboxylates and the effective detection of C-C cleavage products (e.g. 7.4% oxalate or 6.2% glycolate) at the very same conditions, either suggest a higher preference of C5-monocarboxylate to get degraded (C-C cleavage) rather than oxidized to C5-dicarboxylates, or that C5-dicarboxylates quickly degrade under alkaline conditions.

The selective production of glucarate (GLR) was evaluated via a sequential two-step electro-oxidation process.[25] At pH = 11 (0.1 M Na$_2$CO$_3$) and E = 0.6 V over an Au electrode, GA was selectively produced (84%),[25] avoiding the non-electrochemical reactions that would be expected at more alkaline conditions (section 2.2.1.1). The resulting mixture was oxidized for 18 h at E = 1.1 V over Au to GLR with 89% selectivity. However, the overall conversion of GA remained very low (2.4%),[25] as GLR appears to poison the catalyst surface area, independent of the pH of the electrolyte within the assessed alkaline conditions (pH = 11.5-13.5).[25,55] The electrode poisoning on Au due to the adsorption of oxidized organic products can be overcome by applying an alternating potential to refresh the electrode surface.[25,55,95,190,199] Despite the alternating potential, higher conversions for the successive electrocatalytic oxidation of GA to GLR were not achieved.[25] Alternatively, a cyclic voltammetry program can be employed to remove oxidized products and reactivate the electrocatalyst.[196] For instance, galactose was oxidized over an Au electrode at pH = 13 by applying CVs for 4h in the 0.2-0.7 V range, followed by CVs for 7h between 0.8-2.0 V. In the lower potential range, the anomeric carbon is mainly converted, while in the higher potential range, both the anomeric carbon as well as the C6-OH group are oxidized, resulting in 35% galactonate and 23% galactarate.[196] Nevertheless, C-C cleavage products such as glycolic, tartaric and oxalic acids were also observed at the end of the reaction, accounting for 40% of the initial reactant. The use of CV has been shown to overcome Au surface poisoning, as relatively high conversions (80%) were achieved. Despite this, it must be borne in mind that the employed low reactant concentrations (11 mM) may have affected the outcome of the results.[196]

In conclusion, independent of the pH, Au electrodes have only been reported to catalyze the oxidation of the primary alcohol group and anomeric carbon and not the secondary alcohol groups, in agreement with the results found for the electrocatalytic oxidation of sugar alcohols

(section 2.4.1.1). The activity of Au is highly affected by the pH of the electrolyte, resulting in activities of 1-2 orders of magnitude higher under alkaline conditions than under acidic or neutral conditions. Moreover, the saccharides with a lower pK_a are more reactive on Au electrodes. This indicates that the rate-limiting step for electrocatalytic oxidation of saccharides on Au is base-promoted, resembling that of sugar alcohol oxidation (section 2.4.1.1). To evaluate whether the rate-limiting step for the electrocatalytic oxidation of saccharides on Au is base-promoted a study is required that follows the approach of Kwon *et al.*[65] Au was found to be highly selective for the electrocatalytic oxygenative/dehydrogenative oxidation of the anomeric carbon of glucose to GA. Yet, at $E \geq 0.75$ V the formation of GD should also be considered, since this is the onset potential for the electrocatalytic oxidation of primary alcohol groups. To prove that GD is only formed at $E \geq 0.75$ V on Au, chronoamperometric measurements on the electrocatalytic oxidation of glucose over Au electrodes need to be conducted between 0.4 to 1 V at pH $\leq$ 10, and the formed products should be quantified with an analytical technique that enables the separation and quantification of GD.[190] Finally, under the studied reaction conditions at pH $\leq$ 13.5, Au was not found to be an effective electrocatalyst for the production of GLR, as the formation of low concentrations of GLR already effectively poisons the catalyst. Alternatively, an increase in pH to 14.3-15 could aid in the production of GLR, as was shown for the electrochemical oxidation of glycerol to TA and MOA over an Au elctrode.[90,92] However, this approach is likely to cause significant amounts of retro-aldol reaction products (see section 2.2.1.1).

2.5.1.2 Pt-based electrocatalysts

This section discusses the oxidation of saccharides at different pH and potentials on Pt electrocatalysts. Among the publications devoted to the oxidation of saccharides, Pt has gathered the most attention,[56,94,194] as it is known as a promising electrocatalyst to perform the oxygenative/dehydrogenative oxidation of the anomeric carbon of glucose.[57] In contrast to Au, Pt has also been shown to be active in catalyzing the oxidation of the secondary alcohol groups of glucose.[57,190,194] This section discusses the electrocatalytic oxidation of saccharides, such as glucose, mannose, xylose, over Pt electrodes.[55,57,77,95,194,207] Most studies on the selective electrocatalytic oxidation of saccharides have been performed at pH = 13,[57,77,95,194,207] while only a few studies have discussed the oxidation at neutral conditions[55,104,190] or acidic conditions.[55]

At pH = 1 (0.1 M HClO$_4$), the electrocatalytic oxidation of glucose, fructose and GA was studied over Pt(111) and Pt(100) electrocatalysts by LSV.[209] On the one hand, two peak potentials at $E =$ ~0.35 V and ~0.7 were observed over Pt(100) for the electrocatalytic oxidation of glucose, V, while only one peak potential at $E =$ ~0.5 V was observed over Pt(111). On the other hand, only one peak potential at $E =$ ~0.7 V was observed for the electrocatalytic oxidation of fructose or GA over Pt(100). This coincides with the behavior observed in the electrocatalytic oxidation of glycerol, as Pt(111) is nearly inactive for catalyzing the oxidation of primary alcohol groups, while Pt(100) can effectively catalyze this functional group (section 2.4.1.2).[20] Kokoh *et al.* studied the

electrocatalytic oxygenative/dehydrogenative oxidation of glucose in 0.1 M $HClO_4$ (pH = 1) on Pt electrodes at E = 1.1 V.[55] After 30 h, glucose was converted to GA (Sel. = > 90%), GLU (6%) and some C-C cleavage products (tartaric acid and oxalic acid).[55] The high selectivity toward GA (2e⁻ oxidation product) is in line with sugar alcohol oxidation in which Pt electrodes at $E \leq 1.1$ V mainly catalyze the formation of 2e⁻ oxidation products from glycerol, resulting in glyceraldehyde.[48–50] The formation of saccharides from sugar alcohols (Scheme 2.3) and GLU from glucose (Scheme 2.7) requires first the dehydrogenation of a primary alcohol group. Therefore, it is expected that some GD should also have been formed through the dehydrogenation of the primary alcohol group of glucose. Potentially, the formation of GD has been overlooked or this compound only forms a very minor fraction of the product mixture. Presumably, the high selectivity toward GA can be explained by the higher reactivity of the anomeric carbon of glucose than its primary alcohol group. To our knowledge, the selective electrocatalytic oxidation of saccharides over Pt electrodes at E <0.85 V has yet to be studied under acidic conditions.

Under neutral conditions (pH = 7), Pt electrodes at 0.62 V can promote the oxygenative/dehydrogenative oxidation of glucose to produce GA with > 85% selectivity and minor fractions of GLU (8%), oxalate and tartarate.[55] By contrast, under similar reaction conditions a more recent study showed that the selectivity for the oxidation over a Pt electrode is 70% GA, 23% GD and minor contents of GLU, GUL and GLR.[190] Following Scheme 2.7, these results show that metallic Pt not only catalyzes the oxygenative/dehydrogenative oxidation of the anomeric carbon of glucose but also has high activity toward the dehydrogenative oxidation of the primary alcohol group of glucose, being in line with sugar alcohol oxidation (section 2.4.1.2).[46] Under similar reaction conditions, Pt electrodes at E = 0.64 V can catalyze the dehydrogenative oxidation of gluconate at the primary alcohol group with relatively high selectivity, resulting in selectivities of 86% GUL and 10% GAR. At higher potentials (E = 1.2 V) (oxidized) Pt electrodes can catalyze glucose oxidation with high selectivity to GA (91%), and minor contents of GD, 2-k-GA, 5-k-GA, GLU, GUL and GLR.[190] The successive oxidation of GA results in selectivities of 70% GUL, 12% 2-k-GA, 6% 5-k-GA and 9% GLR, which shows that at higher potentials oxidized Pt-based electrodes also catalyze the dehydrogenation of secondary alcohol groups. In contrast, at lower potentials metallic Pt electrodes were found to be hardly active for catalyzing the oxidation of the aldehyde group of glucuronate, thereby showing poor activity for oxygen transfer reactions.[190] This is also seen for the electrocatalytic oxidation of glycerol on Pt at neutral pH, where at E < 1.2 V glyceraldehyde is formed predominantly, while at E = 1.2 V glycerate is formed more selectively.[46]

At near neutral conditions (pH = 8) and T = 50 ˚C in a paired electrochemical cell for CO_2 reduction and glucose oxidation with Pt/C as the anode, GA is produced more selectively by increasing the current density, going from 49% FE at 80 mA cm^{-2} to 58% FE at 160 mA cm^{-2}.[104] The increase in FE toward GA was mainly at the expense of GLU, which decreased from 20% FE to a few percent FE.

At 80 and 160 mA cm^{-2} the cell potential was ~1.7 and ~2.3 V, respectively, resulting in the competition between oxygen evolution reaction (OER) and the electrocatalytic oxidation of glucose. However, the sluggish nature of OER only resulted in minor rates of oxygen production, limiting the FE toward O$_2$ below 3% independent of the applied current density.[104] The increase in selectivity toward GA at higher potentials might be related to the oxidation state of the Pt electrode.[190] This indicates that it might be relevant to study the electrocatalytic oxidation of saccharides and sugar alcohols at potentials above 1.5 V in the region where competition with OER may be expected to give industrially relevant current densities (> 100 mA cm^{-2}).[104]

Under alkaline conditions in 0.1 M NaOH (pH = 13), the electrocatalytic oxidation of glucose, mannose and xylose and their oxidation products were studied by CV (see Figure 2.13) and CA.[57,77,95,194,207] Figure 2.13A and C show a typical CV of Pt in the presence of glucose and GA in 0.1 M NaOH, which are very similar to the CVs in the presence of mannose and gluconate.[77,95,194] This indicates a similar reactivity of functional groups for different reactants. The first peak at E = ~0.3 V in the presence of glucose and mannose is attributed to the dehydrogenation of the anomeric carbon, which does not require hydroxide ions and was not observed for the sequential oxidation products.[77,95] In this reaction, following Scheme 2.7, an adsorbed lactone is formed, which can desorb from the surface and react non-electrochemically with water to form a monocarboxylate such as GA or mannonate. At E = 0.5 V, the current gradually increases again in the presence of glucose, gluconate and glucuronate, while no increase in current is observed for GLR.[77] This indicates that higher potentials are required for the catalytic dehydrogenation of gluconate at the primary alcohol group (Scheme 2.7) and the electrocatalytic oxidation of the aldehyde group of GLU compared to the dehydrogenation of the anomeric carbon of glucose. As soon as the Pt surface becomes oxidized (at E = ~0.8 V), the current starts to decrease with increasing potential up to E = ~0.9 V, after which it increases again to a maximum (E = 1.15-1.2 V). When PtO$_2$ (at E > 1.2 V) is expected to become the dominant surface species, the current quickly drops again, indicative of the low activity of PtO$_2$. Interestingly, at E = 0.75 V (where the Pt surface should still be mainly metallic) higher current densities and thus reaction rates for the electrocatalytic dehydrogenation of the C6-OH group of GA were observed than on a more oxidized surface (E = 1.15-1.2 V).[77,194,210] This follows the trend for the electrocatalytic oxidation of mannonate,[95] fructose[94] and glycerol at pH = 13,[46,91] 1-O methyl glucoside (e.g., glucose with a protecting group at the anomeric carbon) at pH 10.[211] Moreover, Moggia et al. showed that the aldehyde group of glucuronate is more easily oxidized at E = 0.75 V than at E = 1.15-1.2 V,[77] confirming the results obtained by van der Ham et al. for the electrocatalytic oxidation over GLU at pH =7.[190] All this strongly indicates that metallic Pt favors dehydrogenation reactions, while PtO promotes oxygen transfer reactions.
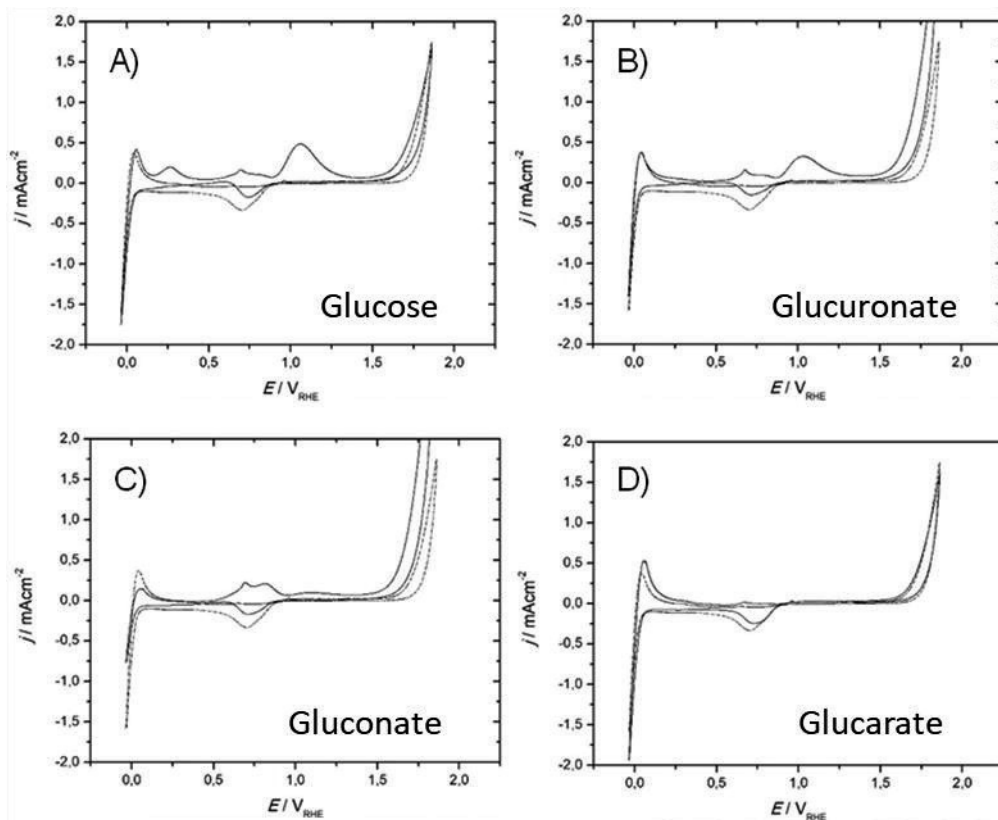
Figure 2.13. *Cyclic voltammetry of a polycrystalline Pt electrode in the absence (dashed lines) and presence of (solid lines): (A) 0.04 M glucose, (B) 0.04 M glucuronate, (C) 0.04 M gluconate and (D) 0.04 M glucarate measured in 0.1 M NaOH (pH = 13) at 10 mV s^{-1}. Adapted with permission from [77]. Copyright 2020 Wiley-VCH Verlag GmbH & Co. KGaA, Weinheim.*

The electrocatalytic oxidation of galactose was studied at pH = 13 (0.1 M NaOH) on a Pt electrode at E = 0.25 V.[199] This approach resulted in 76% conversion and yielded 34% galactonate, 1% galactarate and 24% of C-C cleavage products, composed mainly of glycolate and FA. CV scans were performed in the presence of galactose to evaluate the catalyst activity over time. It was found that the activity decreased drastically over time, indicative of strong poisoning of the Pt surface.[199] This shows that metallic Pt can already catalyze the oxygenative/dehydrogenative oxidation of the anomeric carbon at very low potentials, but also induces significant amounts of C-C cleavage reactions.

Under alkaline conditions in 0.1 M NaOH (pH = 13), the electrolytic oxidation of glucose was studied on Pt electrodes at E = 0.7 V[57,77] and at E = 1.1 V[77]. Kokoh *et al.* showed that at E = 0.7 V a conversion of 63% for glucose can be achieved in 10 h, with a selectivity of 64% toward GA, 2% toward 5-k-GA, 1% toward 2-k-GA and 1% toward GLR.[57] By contrast, Moggia *et al.* showed that at E = 0.7 V glucose can be converted (the amount was not given) over a Pt electrode giving the

following product selectivity after 64 h: 68% toward GA and 13% toward GLR.[77] The higher selectivity toward GLR can potentially be explained by the longer reaction time, resulting in products with a higher degree of oxidation. In a sequential study performed by Kokoh *et al.*, the electrocatalytic oxidation of GA was studied at pH = 13 over a Pt electrode at E = 0.7 V.[194] After 10h of electrolysis, 12% GA was converted with a FE of 95% to a large variety of products, namely 14% 5-k-GA, 11% GLU (following Scheme 2.7, this is likely to be GUL), 6% GLR and 32% C-C cleavage products.[194] These results show that the oxidation of the C5-OH is most likely achieved through the oxidation of GA. Yet, the formation of 5-keto gluconate could also originate from the isomerization of glucuronate under alkaline conditions (see section 2.2.1.1). Moggia *et al.* also showed that at E = 1.1 V Pt electrodes can catalyze the oxidation of glucose after 64 h to the following product selectivity: 78% GA and 6% GLR.[77] GLR is either formed through the oxidation of GLU or GUL at the aldehyde group via an oxygen transfer reaction (Scheme 2.7).[190] The lower selectivity of Pt electrodes toward GLR at higher potential can be explained by the high selectivity toward GA of the PtO/PtOH species that are expected to be present at the surface of the Pt electrode at such potential and their ability to successively dehydrogenate GA at the secondary alcohol groups, resulting in higher selectivity toward 2-k-GA and 5-k-GA and lower selectivity toward GLR.[57,190]

Under alkaline conditions in 0.1 M NaOH (pH = 13) at E = 1.0 V over a Pt electrode, xylose was oxidized to yield 19% xylonate and 48% C-C cleavage products (33% of the products were not analyzed).[207] These results show once more that xylose is more easily degraded to smaller molecules than galactose or glucose.[77,199,207]

Under harsh alkaline conditions in 1 M KOH (pH = 14) at E = 1.3V over Pt electrodes (with Pt species at the surface expected to be in oxidized state), the oxidation of glucose resulted in 67 % glucose conversion after 18 h and yielded 42% GA and 20% GLR.[112] Interestingly, under these harsh alkaline conditions no degradation products were observed, contrasting other studies and our discussion in section 2.2.1.1.[72,73,81] Nonetheless, the relatively high selectivity toward GLR (e.g., a dicarboxylate) indicates that dicarboxylates can only be formed at highly alkaline conditions, as was also shown for glycerol oxidation on Pt and Au (section 2.4.1.1 and 2.4.1.2).[90,92,98,142,143]

In conclusion, Pt(111) does not show appreciable activity for catalyzing the oxidation of primary alcohol groups, while Pt(100) can effectively catalyze the oxidation of this functional group. GLU is frequently reported as product but not its precursor GD (Scheme 2.7), indicating that the formation of GD might have been overlooked. GD is likely one of the main products on metallic Pt, since metallic Pt promotes dehydrogenation reactions. By contrast, PtO$_x$ is active in catalyzing oxygen transfer reactions (indirect mechanism), thereby promoting the formation of GA. Additionally, in contrast to metallic Pt, PtO$_x$ promotes the successive oxidation of the secondary

alcohol groups of GA, resulting in the formation of 2-k-GA and 5-k-GA and thus more complex reaction mixtures. The formation of GLR only seems to be feasible under harsh alkaline conditions (pH ≥ 14).

2.5.1.3 Ru-based electrocatalysts

The electrocatalytic oxidation of glucose on platinum group metals other than Pt has only been studied on Ru-based electrocatalysts in harsh alkaline conditions (pH = 14, 1 M KOH) at E = 1.3 V.[112] After 18 h 90% glucose was converted to 52% GA and 28% GLR.[112] These harsh alkaline conditions did not cause the degradation of the reactant or products,[112] opposing other studies and our discussion in section 2.2.1.1.[72,73,81] The relative high selectivity toward GLR can potentially be attributed to the high alkalinity of the electrolyte, which was also found to be crucial for the electrocatalytic oxidation of glucose on Pt and electrocatalytic oxidation of glycerol oxidation on Pt and Au.[90,92,98,142,143]

2.5.1.4 Ni- and Co-based electrocatalysts

This section evaluates the electrocatalytic oxidation of saccharides on Ni-and Co-based electrocatalysts at different pH and potentials. Ni was used to study the electrocatalytic oxidation of glucose and xylose at pH = 11[212] and mannose and galactose at pH = 13,[95,199] while Co was only used to study the electrocatalytic oxidation of glucose at harsh alkaline conditions (pH = 13.7).[85,213,214]

At pH = 11, the electrocatalytic oxidation of glucose and xylose was studied on a Ni-based electrode consisting of NiO (as determined by *ex-situ* XRD and XPS).[212] The electrocatalytic oxidation of glucose and xylose was performed at E = 1.44 V.[212] At this potential, NiOOH is expected to be present at the surface of the Ni-based electrodes,[151] coinciding with the potential at which the indirect oxidation mechanism is dominant.[151] The electrocatalytic oxidation of glucose resulted in 60% GA and 10% GLR and ~35% C-C cleavage products (equimolar amounts of oxalate and tartarate).[212] The successive electrocatalytic dehydrogenation of the primary alcohol group of GA to form GUL (mistaken by GLU in the article, see Scheme 2.7) could only be achieved effectively with the aid of TEMPO.[212] The successive oxidation of the aldehyde group of GLU could be achieved selectively with Ni based electrodes, reaching ~85% GLR.[212] This approach that combines Ni-based electrodes and TEMPO also resulted in a high selectivity for the electrocatalytic oxidation of xylose to xylarate. Following Scheme 2.7, this indicates that the indirect oxidation mechanism of β-NiOOH can effectively lead to the oxidation of aldehyde groups and oxygenative/dehydrogenative oxidation of the anomeric carbon of glucose and less effectively the dehydrogenation of the primary alcohol group of glucose.[212] This contrasts with the results for the electrocatalytic oxidation of glycerol at pH = 11 and E = 1.48 V, where glycerol was selectively dehydrogenated at the secondary alcohol group resulting in DHA as the main product.[151] This discrepancy can tentatively be explained by: 1) the higher reactivity of glucose at

the anomeric carbon group than its secondary carbon groups, thereby promoting the formation of GA over β-NiOOH, and 2) the higher activity of TEMPO for catalyzing the dehydrogenation of the primary alcohol group of GA than that of β-NiOOH for catalyzing the oxidation of the secondary alcohol group of GA, thereby promoting the formation of GUL by TEMPO.

At pH =13, the electrocatalytic oxidation of saccharides (mannose and galactose) was only feasible on Ni electrodes in the β-NiOOH region (at E > 1.2 V).[95,199] Both the electrocatalytic oxidation of galactose (at E = 1.6 and 2.3 V) and mannose (at E = 2.3 V) were studied in competition with the OER. For galactose, it was shown that a higher potential resulted in a lower conversion, which can be attributed to the competition with the OER.[199] An increase in potential from 1.6 V to 2.3 V resulted in an increase in selectivity toward the oxygenative/dehydrogenative oxidation of the anomeric carbon of galactose yielding 7% and 8.5% galactonate, respectively.[199] For mannose, the electrocatalytic oxidation at E = 2.3 V only resulted in 8% mannonate.[95] The high rate of C-C cleavage reactions was attributed to the presence of β-NiOOH at the electrode surface, consisting of a mixture of Ni hydroxide and Ni oxide in equal proportion, with the H-atom delocalized between the two species.[199] The O atoms of these two adjacent surface species have been proposed to interact with two adjacent carbon atoms, thus weakening the C-C bond and promoting the C-C bond cleavage,[199] in a similar way to the mechanism for C-C cleavage reactions on Pt oxide (Scheme 2.5). This mechanism has yet to be proven as the applied reaction conditions also promote non-electrochemical reactions, such as oxidative C-C cleavage reactions and the oxidation of aldehydes (section 2.2.1.1), thereby promoting the formation of FA.

The harsh alkaline conditions (pH = 13.7) used to study the electrocatalytic oxidation of glucose on Co-based electrodes[85,213,214] makes it complicated to distinguish between electrochemical and non-electrochemical reactions. At 10 mA cm^{-2} (cell voltage 1.46 V[85] and 1.34 V[213]) glucose was oxidized with relatively high selectivity toward LA of 45-55 % with some formation of FA 5-15% and minor contents of GA (1.5%) and GLR (1.5%). The formation of LA is likely to be induced non-electrochemically (see section 2.2.1.1),[73,85] while the Co-based electrode only catalyzes the minor fraction of glucose to GA and GLR. By contrast, at E = 1.3-1.7 V over a Co-based electrode (with μ$_1$-OH−Co^{3+} and μ$_2$-O−Co^{3+} as proposed active species based on characterization by EXAFS) FA (FE = ≥ 60%) and GA (~25%) were predominantly produced.[214] The formation of FA indicates that Co-based electrodes effectively catalyze C-C cleavage reactions since these products cannot solely be formed by non-electrochemical reactions (see section 2.2.1.1).

2.5.1.5 Cu- and Mn-based electrocatalysts

This section evaluates the oxidation of saccharides on Cu- and Mn-based electrodes at different pH and potentials. The electrocatalytic oxidation of glucose was studied at pH = 13 on Cu-based electrodes (E = 0.84-1.80 V, under which conditions Cu is expected to be in oxidized state at the surface of the electrode).[77,197] The electrocatalytic oxidation of glucose and glucuronate starts at

0.84 V, while the electrocatalytic oxidation of gluconate and glucarate is strongly promoted at E = 1.3 V.[77] This indicates that the electrocatalytic oxygenative/dehydrogenative oxidation of the anomeric carbon of glucose and the electrocatalytic oxidation of the aldehyde of GLU can selectively be achieved at E < 1.3 V.[77] This hypothesis was tested by chronoamperometric measurements on a Cu-based electrode at E = 0.84, 1.11 and 1.80 V. At E = 0.84 V, where CuO is expected to be present (though not proven by characterization),[77] and 1.11 V, where a solubilized Cu^{II} species originating from CuO were proposed to be present, glucose was mainly oxidized to GLR (Sel. = 38-27%) and GA (30-45%). By contrast, at E = 1.80 V, where solubilized CuO_2^{2-} are expected to be present, the main product was FA (54%). The high selectivity toward GLR shows that the Cu-based electrode can effectively catalyze the oxidation of the primary alcohol group of GA, which was not deducible from the CV experiments.[77] Moreover, the high selectivity toward FA at E = 1.80 V indicates that the Cu-based electrode is a good electrocatalyst for C-C cleavage reactions at sufficiently high potentials.[77,197]

A Cu-based electrode at E = 1.46-1.56 V was also used to study the electrocatalytic oxidation of glucose at harsh alkaline conditions (pH = 13.7).[215] This study aimed at maximizing LA production. Undoubtedly, the harsh alkaline conditions induce non-electrochemical production of LA (see section 2.2.1.1). The control experiment without a Cu-based electrode showed a relatively similar product distribution as the experiments where such electrode was applied. Nonetheless, it was claimed that solubilized divalent Cu species can promote C-C cleavage at the C3-C4 bond promoting the formation of GLAD and DHA, which are important intermediates for the production of LA.[215]

A MnO_2/Ti 3D anode was used for the electrocatalytic oxidation of glucose in a flow-cell reactor operated at 3 mA cm^{-2} and mild pH conditions (pH = 2-10),[24] thus minimizing the isomerization of glucose (see section 2.2.1.1).[42] Increasing the pH from 2 to 10 only increased the glucose conversion from 90% to 93%. At pH = 7, the selectivity toward GA (49%) and GLR (45%) was the highest. The high activity of the MnO_2/Ti electrode was attributed to its high stability under all pH conditions and the fast removal of oxidized products due to the supply of fresh electrolyte and reactant. Moreover, it was argued that good control of the pH is required, since alkaline conditions promote unwanted non-electrochemical reactions (see section 2.2.1.1), while acidic conditions hamper the formation of GA and GLR. Under optimized reaction conditions (retention time, initial reactant concentration, temperature, pH and MnO_2 loading), ~100% glucose was converted to 85% GLA and 15% GA, yet the faradaic efficiencies remained low (FE = 37%) as most of the current was used for water oxidation.[24] An ytterbium-doped MnO_2 electrodeposited on carbon paper (Yb-MnO_2/CP) was used to study the electrocatalytic oxidation of glucose at pH = 0.7.[216] Based on DFT calculations, it was suggested that the Yb atoms promote the adsorption and desorption process of alcohols and aldehydes on MnO_2, thereby improving the intrinsic activity of the catalyst while reducing the competing OER. After 3 h of glucose conversion at E = 1.47 V,

Yb-MnO$_2$/CP was able to catalyze the oxidation of 98 % 0.1 M glucose to 85% GLR.[216] These promising results could not be compared with the electrocatalytic oxidation of glycerol over MnO$_2$, since the study on glycerol used a borax electrolyte (see section 2.2.1.1).[159] Nonetheless, both studies on glycerol oxidation over MnO$_2$ show that high selectivity toward GLR without inducing severe amounts of C-C cleavage reactions can be achieved under acidic conditions,[159,216] thereby opening new routes for the production of glucaric acid.

2.5.2 Noble bimetallic electrocatalysts

Bimetallic formulations in electrocatalysts are generally used to improve the performance compared to monometallic electrocatalysts and to decrease the utilization of scarce precious metals. The structure of this section follows the same order as the section on glycerol oxidation on noble bimetallic catalysts (section 2.4.2), where Ag-X[198] (section 2.5.2.1) is discussed first followed by Au-X (section 2.5.2.2).[26,99,146,195,198,217–220] Pt has only been alloyed with Au and was therefore not discussed in a separate section.

2.5.2.1 Bimetallic Ag-noble metal electrocatalysts

Only Tominaga *et al.* studied the electrocatalytic oxidation of glucose on Au$_m$Ag$_{100-m}$-NPs (gold silver nanoparticles).[198] The synthesized electrocatalysts are composed of either alloys or phase-segregated structures. In this regard, it was observed that AuAg phase-segregated structures had the same onset potential as Au nanoparticles for catalyzing glucose oxidation, while AuAg alloyed structures had a 0.1 V lower onset potential.[198] This 0.1 V lower onset potential was also observed for the electrocatalytic oxidation of glycerol on alloyed Ag-noble metal (Au,[160] Pt,[163] and Pd[164]) electrocatalysts. GA was formed at 0.65-0.7 V with a ~100% Faradaic efficiency (quantified by HPLC) by using Au-NPs and AuAg-NPs.[198] At higher potentials (E = 1.25 V), the selectivity of AuAg-NPs increased toward C-C cleavage products with increasing silver content.[198] These results partially contrast the studies performed on the electrocatalytic oxidation of glycerol, where the addition of Ag to Au,[160] Pt,[163] and Pd[164,165] promoted C-C cleavage reactions independent of the applied potential. This difference can tentatively be explained by the lower potential required to oxidize the anomeric carbon group of glucose than the primary alcohol group of glycerol (see section 2.5.1.1). This would also explain the high selectivity obtained toward GA on AuAg at lower potentials.

2.5.2.2 Bimetallic Au-noble metal electrocatalysts

Au has been combined most frequently with other noble metals Ag,[198] Pt,[195,219,220] Pd[26,146,218] and PdPt.[99] Most of the studies on bimetallic Au-noble metal catalysts were performed to evaluate the electrocatalyst activity, while few also report the selectivity.[26,195,198,218] It is worth mentioning that all the papers in this section use 0.1-0.5 M NaOH/KOH electrolytes, and no studies were performed at pH < 13.

Combining Au with Pt was found to have a positive influence on the electrocatalytic oxidation of glucose at pH ≥ 13, resulting in higher electrocatalytic activities (i.e. higher currents measured by CV) and higher resistance to poisoning in the long-term electrolysis.[219,220] AuPt nanoparticles on reduced graphene oxide (AuPt/rGO) were tested in 0.1 M KOH (pH = 13) in a batch cell and a cell equipped with an anion-exchange membrane for the electrocatalytic oxidation of glucose.[195] At E = 0.65 V, $Au_{50}Pt_{50}$/rGO catalyzed the production of gluconate (GA) and glucuronate (GLU), while no GLR was found (quantified by high-performance liquid ionic chromatography). This reveals that the electrocatalyst can promote: (1) the oxygenative/dehydrogenative oxidation of the anomeric carbon of glucose and (2) the dehydrogenative oxidation of the primary alcohol of glucose (see Scheme 2.7). In the AEM cell, 90% GA was formed with a 65% FE,[195] indicating that the oxygenative/dehydrogenative oxidation of the anomeric carbon of glucose was the favored step under these conditions. This resembles the selectivity of Au electrodes at E <0.75 V (see section 2.5.1.1), which are not able to catalyze the dehydrogenation of the primary alcohol group of glucose at this potential.[25,55,77,95] Only 10% GLU was formed, which is likely attributed to Pt as it can catalyze the dehydrogenation of C6-OH of glucose at E = 0.65 V (see section 2.5.1.2).[77] After ~10 min, the produced GA and GLU amounts are almost equimolar and after ~10 min the GLU concentration remains constant, while that of GA increases linearly over time. The formation of GLU shows that glucose dialdehyde should have been formed and might therefore have been overlooked (see introductory discussion of section 2.5). Moreover, the formation of glucose dialdehyde from glucose is expected since PtAu (at E = 0.45 V) can catalyze the dehydrogenative oxidation of the primary alcohol group of glycerol to form glyceraldehyde.[67]

At pH = 13, a PdAu electrode was found to be highly active and selective for catalyzing the oxidation of xylose and glucose.[26,217,218] These studies were performed on glucose and xylose individually[26,217] and mixtures of these two saccharides.[218] From chronoamperometric measurements (at E = 0.4 V), the effect of $Pd_{30}Au_{70}$/C electrocatalyst poisoning was hardly observed after 6 h of electrolysis, and the electrocatalytic activity was restored by the introduction of fresh solution with new reactants.[26] Under these conditions, $Pd_{30}Au_{70}$/C catalyzes the conversion of 67% glucose or 12% xylose with a high selectivity toward GA (95%) and xylonate (>99%), respectively.[26] The effect of the cell potential was also studied for the electrocatalytic oxidation of glucose and xylose mixtures over $Pd_{30}Au_{70}$/C.[218] After 6 h of electrolysis, it was shown that an increase in potential from 0.4 V to 0.6 V cell potential improves the conversion from 55 to 85% (90-10% glucose xylose mixture) and from 35 to 65% (50-50% glucose xylose mixture).[218] In contrast to the results reported by the same group in 2022,[218] in 2020 Rafaïdeen *et al.* showed that an increase in cell potential from 0.4 to 0.8 V results in a decrease in Faradaic efficiency.[217] The loss in FE was attributed to the formation of C-C cleavage products,[217] which might be formed either by C-C bond cleavage reaction induced by the electrocatalyst or through retro-aldol reactions (section 2.2.1), which successively compete in the reaction on the electrocatalyst

surface. The formation of GLU was not reported, indicative that the electrocatalytic oxidation of the primary alcohol group of glucose does not take place.

Finally, Au, Pt, Pd, AuPd, and AuPdPt nanomaterials supported on reduced graphene oxide (rGO) were tested as glucose oxidation electrocatalysts in 0.1 M NaOH to evaluate the effect of alloying.[99] The prepared electrocatalysts were characterized by XRD showing that the bi- and tri-metallic systems formed alloyed particles. Chronoamperometric measurements at 0.6 V vs RHE (Figure 2.14A) show that the Pt/rGO loses its activity over time, while the other electrocatalysts reached a steady state, with $Au_{50}Pt_{25}Pd_{25}$ and $Au_{90}Pd_{10}$ displaying the highest activity (Figure 2.14B). It was suggested that Pt/rGO deactivates due to the strong adsorption of poisoning intermediates on its surface. For $Au_{50}Pt_{25}Pd_{25}$ it was found from FTIR data that CO_2 was formed, caused by C-C cleavage, but CO could not be detected. Even during chronoamperometric measurements at 0.6 V vs RHE, no CO was detected, probably due to the effectiveness of the electrocatalyst to oxidize the adsorbed CO, thus circumventing the poisoning of the electrocatalyst surface.
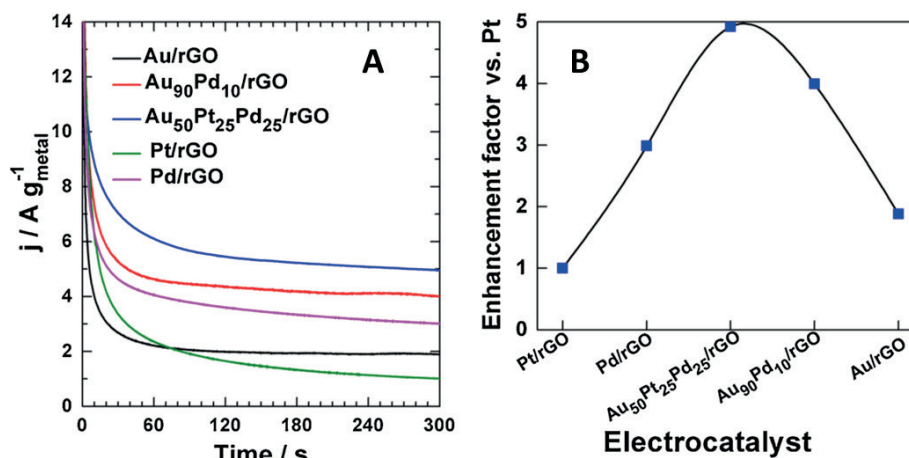
Figure 2.14. (a) Chronoamperometry experiments in 0.1 mol·L⁻¹ NaOH + 10 mmol·L⁻¹ of glucose at 0.6 V vs. RHE and (b) its corresponding Volcano plot using the catalyst composition as the descriptor of the catalytic performances, from the steady-state current density after 300 s. Reprinted with permission from [99]. Copyright 2016 Elsevier.

To conclude, AuPt electrocatalysts are likely to catalyze both the oxygenative/dehydrogenative oxidation of the anomeric carbon and the dehydrogenative oxidation of the primary alcohol of glucose. However, the oxygenative/dehydrogenative oxidation of the anomeric carbon of glucose is favored, resulting in relative high selectivity toward GA. By contrast, PdAu was only able to catalyze the oxygenative/dehydrogenative oxidation of the anomeric carbon of glucose and xylose, thereby promoting the formation of GA and xylonate. Moreover, an increase in cell

potential improves the conversion but also promotes C-C cleavage reactions, thereby decreasing the Faradaic efficiency of the electrocatalyst toward the desired undegraded larger molecules.

2.5.3 Noble-non noble bimetallic electrocatalysts

The effect of alloying Au with Cu for the electrocatalytic oxidation of glucose was assessed at 0.1 M NaOH.[197] The linear sweep voltammetry recorded in the presence of glucose for the alloyed AuCu electrocatalyst resembled that of monometallic Au.[197] On AuCu electrodes at E = 0.65-0.7 V, GA was formed with ~100% Faradaic efficiency, while at E = 1.25 V AuCu electrodes catalyzed the production of GA (FE = 35%), 2-k-GA (3%), GLR (10%) and large amounts of C-C cleavage products.[197] The high selectivity of AuCu electrodes at E = 0.65-0.7 V toward GA can be attributed to the high selectivity of Au toward the oxygenative/dehydrogenative oxidation of the anomeric carbon of glucose and its inability to catalyze the primary alcohol group of glucose at this potential (section 2.5.1.1),[77,197] and the inactivity of Cu for catalyzing glucose oxidation at this potential (section 2.5.1.5).[77] This shows that AuCu electrocatalysts might be a valuable option for the oxidation of saccharides to value-added products under alkaline conditions, especially considering that the use of Cu can allow decreasing the amount of scarce and expensive Au.

2.5.4 Noble-post-transition bimetallic electrocatalysts

Pt has frequently been combined with post-transition metals to study the selective electrocatalytic oxidation of saccharides. The most common approach was by using adatoms[55,57,95,194,199,211] and less commonly by alloying.[221] The Pt-post-transition bimetallic electrocatalysts were used to study the selectivity toward the oxidation of different saccharides, namely glucose,[55,57,194,211] mannose[95] and galactose.[199] These studies were almost all performed under alkaline (pH = 13)[57,95,194,199,221] and seldomly under mild alkaline (pH = 10)[211] and acidic conditions (pH =1)[55]. The post-transition metals that have been researched are Bi,[55,211,221] Pb,[55,57,95,194,199] Tl.[55,211]

Pt was modified with Bi, Pb and Tl adatoms to study the electrocatalytic oxidation of glucose under acidic conditions (pH = 1, 0.1 M HClO₄).[55] The effect of adatoms was investigated at various potentials, being 0.6 V for Tl, 0.7 V for Pb and 1.0 V for Bi. At E = 1 V, Bi did not affect the selectivity of Pt.[55] This can be attributed to the fact that Bi is oxidized and desorbs at these potentials (see section 2.4.4), thereby losing its effect on the electrocatalyst selectivity as was also shown for glycerol oxidation.[45,47] At pH = 1, the addition of Pb adatoms to Pt did not appear to modify the selectivity of Pt significantly, resulting in high contents of GA and minor fractions of GLU, GLR and C-C cleavage products.[95] This minor effect of Pb adatoms on Pt electrocatalysts was also shown for the oxidation of glycerol.[181] Nonetheless, Pb adatoms did show to promote the dehydrogenation of the secondary alcohol group of glycerol, which was not shown for glucose oxidation, indicative that some products might have been overlooked (see section 2.5). The addition of Tl adatoms to Pt resulted in a high selectivity toward GA (96%) by largely suppressing

the formation of C-C cleavage products (4% FA) and GLR.[55] This indicates that the addition of Tl to Pt strongly improves the catalyst selectivity toward the oxygenative/dehydrogenative oxidation of the anomeric carbon group. However, the formation of glucose dialdehyde through the dehydrogenation of the primary alcohol group of glucose or 2-k-GA and 5-k-GA through the dehydrogenation of the C2-OH and C5-OH group of glucose might have been overlooked (see section 2.5). At pH = 10, the addition of Tl adatoms on Pt was studied in the electrocatalytic oxidation of glucose.[211] With an increase in potential from 0.37 to 0.57 V, the formation of 2-keto gluconic acid became more prominent, going from 1 to 14 mM. This indicates that Tl adatoms on Pt promote the electrochemical dehydrogenation of the C2-OH group of GA (Scheme 2.7), thereby enhancing the formation of 2-k-GA.[211] These results are in strong contrast with those obtained with Pt electrodes modified with Tl adatoms under acidic conditions, for which the formation of 2-k-GA was not reported.[55] Moreover, it is interesting to note that the formation of 5-k-GA was not considered, indicative that the C5-OH group of GA is not dehydrogenated or that this product was overlooked. Tl adatoms on Pt improved the electrocatalyst activity tenfold.[211] This makes Tl adatom modified Pt electrodes interesting candidates for the production of 2-k-GA, where the Tl surface coverage could potentially be optimized to further improve the catalyst selectivity, as it has been shown for Bi adatoms in the selective oxidation of glycerol.[47]

Under alkaline conditions (pH = 13), modification of Pt electrodes with Pb adatoms do not change the catalyst selectivity in the potential window 0.5 to 0.8 V for the oxidation of mannose and glucose concerning C-C cleavage products,[57,95,194] while it does for galactose.[199] For bare metallic Pt and Pb adatom modified Pt, similar concentrations were found for mannose oxidation products and glucose oxidation products, whereas at 0.7 V Pb adatom modified Pt had a nearly 100% selectivity toward galactonate.[199] It was argued that Pb adatoms preferably occupy poisoning sites on the Pt surface and modify the adsorption coordination, enhancing the stability and altering the selectivity of the electrocatalyst.[199] Pb was also found to promote the formation of 2-k-GA and 5-k-GA.[57,194] In the presence of Pb adatoms, the coordination of GA on the Pt surface changes, thereby promoting the dehydrogenation of C2-OH and C5-OH group of GA and thus the formation of 2-k-GA (33%) and 5-k-GA (8%).[194] In line with these results, it was shown for sugar alcohol oxidation that Pb adatoms also slightly change the catalytic selectivity of Pt toward the secondary alcohol of glycerol.[181]

A non-alloyed PtBi/C catalyst was used to study the effect of Bi on the catalyst selectivity at pH = 13 (0.1 M NaOH).[221] The dilution of Pt atoms by Bi atoms decreases the likeliness of the multi-bonded adsorption mode of glucose, thus hindering C-C cleavage reactions and limiting the formation of degradation products.[221] As a result, the catalyst selectivity is improved and the stability is enhanced, as CO formation is prevented (as confirmed by FTIR) and thus the poisoning diminished. The addition of Bi to Pt reduced the onset potential for the oxidation of 1-O methyl glucoside (i.e. glucose with a protecting group at the anomeric carbon) from 0.42 to 0.22 V,

showing that it promotes the dehydrogenation of the primary alcohol group at a lower potential than monometallic Pt.[77,95,211,221] The lower onset potential for the C6-OH group can be explained by the fact that Bi atoms adsorb OH$^-$ ions at lower potentials, while Pt adsorbs the organic molecule, thus ensuring the vicinity of the two species required to initiate the oxidation of the C6-OH group of glucose.[221] This effect was also reported for PdBi/C electrocatalysts.[222] After 6 h of electrolysis at 0.4 V, PtBi/C catalyzes the conversion of glucose and 1-O methyl glucoside with nearly 100% selectivity toward GA and 1-O methyl glucuronate, respectively (as determined by MS, NMR and HPLC).[221] This makes PtBi/C an interesting candidate for electrochemically oxidizing glucose, methyl glucoside and potentially other saccharides. It is worth noting that these results do not match with those obtained for glycerol oxidation over PtBi <0.6 V, where it was reported that Bi strongly promotes the oxidation of the secondary alcohol group.[103]

At pH = 10 and 0.5 V, Tl adatom modified Pt electrodes can catalyze the selective oxidation of the C6-OH group to convert 31% of 1-O methyl glucoside to 97% methyl glucuronate (GLU).[211] Similar results were obtained at pH = 13 and 0.5 V, where metallic Pt_9Bi_1 can catalyze the selective oxidation of 40% 1-O methyl glucoside and 37% glucose with nearly 100% Faradaic efficiency and 100% selectivity to methyl glucuronate and GA.[221] Here, we argue that the high selectivity toward methyl glucuronate can be attributed to the protection of the anomeric carbon,[211,221] which can (1) steer the catalyst selectivity toward other reactive groups, and (2) prevent the mutarotation of the reactant and thus reduce the accessibility of the reactant for C-C cleavage reactions.

In summary, most studies on the effect of post-transition metals on Pt electrocatalysts for the oxidation of saccharides have been performed under alkaline conditions. However, to discriminate between base-catalyzed and electrode-catalyzed reactions more research should be conducted under acidic conditions (see section 2.2.1). In addition, the potential at which the effect of post-transition metals on Pt is studied should be chosen more carefully to avoid the oxidation/desorption of the transition metal, thereby losing its contribution to the electrocatalyst performance. Finally, and importantly, only a few studies report the formation of keto-oxidation products over Pt electrodes in the presence of Pb[57,194] or Tl adatoms,[211] while other studies neither report nor discuss the formation of these keto-oxidation products over Pt electrodes in the presence of Pb[55,95,199] or Tl[55] adatoms. Despite this, it is expected that the formation of keto-oxidation products is strongly promoted by the introduction of post-transition metals on Pt, as was shown for the electrocatalytic oxidation of sugar alcohols. This indicates that many products may have been overlooked, amongst others 2-k-GA, 5-k-GA and GD.

2.5.4.1 Au-post-transition bimetallic electrocatalysts

Very few studies describe the influence of post-transition metals on Au electrodes on the oxidation of glucose. These studies were conducted at pH = 13 with Pb,[57,223] Bi[57] and Tl[57] adatoms. It was shown that metallic Au (at E < 0.75 V) can catalyze the selective

oxygenative/dehydrogenative oxidation of the anomeric carbon of saccharides (see section 2.5.1.1), yielding predominantly monocarboxylates (e.g. GA, mannonate, galactonate).[25,77,196–199,223] At $E = 0.6$ V, the addition of Tl adatom on Au electrodes does not seem to affect the selective conversion of glucose, whereas the addition of Bi adatoms promotes the formation of GLR (12%) but also promotes C-C cleavage reactions.[57] By contrast, at $E = 0.6$ V the addition of Pb adatoms on Au improved the selectivity toward GLR to 25% without inducing more C-C cleavage reactions.[57,223] An increase in potential to 0.9 V improved the selectivity further to 35% GLR, while inducing more C-C cleavage reactions.[57,223] These results indicate Pb and Bi adatoms decrease the onset potential for the electrocatalytic oxidation of the primary alcohol group of glucose.

2.5.5 Other electrocatalysts

Li *et al.* showed that at pH = 13.7 it is possible to oxidize various saccharides (~100% conversion) to 50-40% lactate (arabinose, glucose and xylose) and 33% lactate (fructose) over hierarchical Fe-doped Ni_2P nanosheets hybridized with C on Ni foam (Fe-Ni_2P@C/NF).[224] The reaction pathway to obtain lactate is likely induced by non-electrochemical reactions (see section 2.2.1). Hence, it is difficult to attribute the reaction to electrocatalytic reactions.

Under harsh alkaline conditions (pH = 14), the selective oxidation of glucose toward GLR can be achieved with the aid of a nanostructured NiFe-based electrocatalysts on Ni foam at $E = 1.3$ V.[112] A hydrotalcite-like $NiFeO_x$ material was synthesized through a hydrothermal treatment of Ni foam with an iron precursor, resulting in $Ni(OH)_2$ and FeOOH crystalline phases (determined by XRD). This $NiFeO_x$ electrocatalyst was used to promote the conversion of 0.01 M glucose (98% conversion) to GLR with a selectivity of 83%. As a reference, a pure Ni foam catalyst was used at 1.3 V, which produced 37% GA and 17% GLR.[112] The high selectivity toward GLR obtained with the NiFe-based electrocatalyst is likely related to the harsh alkaline conditions, which were also needed for the production of dicarboxylic acids from glycerol.[90,92,98,142,143] Moreover, combining Ni with other metals/metal oxides, such as Bi, CeO_2, SbO_2, Au, Pd and Fe, dilutes the Ni surface and thereby hinders C-C cleavage reactions, as was shown for the electrocatalytic oxidation of glycerol[105,188,225] and glucose.[112] An increase in reaction time to convert higher initial glucose concentrations resulted in lower GA and GLR selectivities, namely 92% (10 mM glucose and 2 h reaction), 87% (50 mM glucose and 10 h reaction) and 71% (100 mM glucose and 18 h reaction).[112] The longer reaction times and high initial glucose concentrations are likely to induce more retro-aldol reactions under the studied harsh alkaline conditions (see section 2.2.1.1), thereby decreasing the selectivity toward C6-oxidation products. Despite this, it was claimed that no significant amount of glucose was degraded at pH = 14 after 24 h.[112]

2.6 Conclusions and considerations for future research

In this contribution, we have critically reviewed the literature on the electrocatalytic oxidation of sugar alcohols and saccharides. Trends were defined on the effect of reaction conditions and

electrocatalyst properties on the selectivity and activity for the electrocatalytic oxidation of specific functional groups of sugar alcohols and saccharides for the synthesis of value-added compounds. These trends were compared to identify the most promising routes for the selective production of value-added chemicals from the electrocatalytic oxidation of sugar alcohols and saccharides. In the next paragraphs, we highlight topics that require attention for future research and propose several avenues that are worthy of being further explored.

Main points of attention for future research on the electrocatalytic oxidation of sugar alcohols and saccharides are: (1) the type of electrolyte and the pH used in electrocatalytic experiments, specifically their influence of non-electrochemical reactions taking place in solution; (2) the analytical technique used to quantify glucose oxidation products; and (3) the use of control tests with (intermediate) products in electrocatalytic experiments.

1) Most studies on the electrocatalytic oxidation of sugar alcohols and saccharides have been performed in alkaline electrolytes. However, under these reaction conditions base-catalyzed non-electrochemical reactions compete with electrochemical reactions. As a result, it becomes nearly impossible to discriminate between base-catalyzed and electrode-catalyzed reactions, thereby making it difficult to evaluate the property-performance relationship of electrocatalysts. To properly understand the role of base-catalyzed reactions, blank experiments need to be performed with all reactants and (intermediate) products that can be formed in the electrochemical experiments. The role of time is also very important in this respect, as long reaction times are more likely to enhance the role of non-electrochemical reactions. In this context, it is strongly advised to quench (i.e. neutralize) the reaction mixtures before offline analysis (e.g. by HPLC) to minimize non-electrochemical reactions that could take place between the end of the electrochemical experiment and the analysis.[46,226]

The effect of electrolyte is not always considered to have a strong impact on the electrocatalytic oxidation of sugar alcohols and saccharides. Yet, it was shown that borax and certain cations (Li⁺) can complex with reactants or (intermediate) products, thereby stabilizing specific functional groups and thus affecting the electrocatalyst selectivity. Moreover, certain anions, such as (bi)sulfate, were found to compete with reactants for adsorption on the catalyst surface and, therefore, affect the electrocatalyst activity. Therefore, future research should make sure that the effect of certain electrolytes, like borax, is properly understood or consider the use of different anions, such as (bi)sulfate, to effectively study the property-performance relationship of electrocatalysts.

2) Studies conducted on the electrocatalytic oxidation of glucose rarely report the formation of glucose dialdehyde, 2-keto-gluconic acid and 5-keto-gluconic acid, and neither mention the formation of glucuronic acid nor guluronic acid. Thus, it is possible that many of the (intermediate) products on the glucose oxidation pathway are being overlooked and therefore

not quantified. However, to study the property-performance relationship of electrocatalysts for the oxidation of glucose it is needed to quantify (intermediate) products. Therefore, future research needs to use suitable analytical techniques, such as a combination of high pressure anion exchange chromatography with high pressure liquid chromatography,[190] to quantify all (intermediate) products of the glucose oxidation pathway.

3) The formation of dicarboxylates/dicarboxylic acids, such as tartronate and mesoxalate from glycerol or glucarate from glucose, could only be achieved under highly alkaline conditions (pH ≥ 13.7), except for MnO_2-based electrocatalysts, with which glucaric acid was produced at pH =0.7-10. This indicates that the active and selective conversion of specific intermediates is highly limited on certain electrocatalysts. Therefore, future research on the electrocatalytic oxidation of sugar alcohols and saccharides should include chronoamperometric experiments on the (intermediate) products formed. This will enable evaluating the electrocatalyst activity toward (intermediate) products (i.e. different functional groups) and thereby give better insight into the electrocatalyst selectivity and the corresponding limiting reactions.

There are several aspects of the electrocatalytic conversion of monosaccharides and sugar alcohols into valuable products that deserve to be studied in future research. Most prominent are: (1) the rate-limiting steps for the electrocatalytic oxidation of saccharides on Au; (2) the use of post-transition metals to change the catalytic selectivity of Pt for the oxidation of saccharides; (3) electrocatalysts that enable the selective production of dicarboxylic acids under acidic reaction conditions; and (4) the stability of electrocatalysts when an alternating potential is used to electrochemically oxidize sugar alcohols and saccharides.

1) It was shown that the rate-limiting step for the electrocatalytic oxidation of glycerol (i.e. primary alcohol groups oxidation) on Au is base-catalyzed. This insight can be used to tune the pH of the electrolyte in electrochemical cells to improve or limit the electrochemical oxidation of primary alcohol groups from sugar alcohols or saccharides on Au electrodes. In order to steer the reaction toward the electrocatalytic oxygenative/dehydrogenative oxidation of the anomeric carbon of saccharides on Au electrodes, it is recommended to investigate the rate-limiting step of this reaction.

2) For the electrocatalytic oxidation of sugar alcohols, post-transition metals effectively change the selectivity of Pt electrocatalysts toward the secondary alcohol groups of glycerol, promoting the formation of dihydroxyacetone. This approach was also found to promote the selective electrocatalytic oxidation of glucose or gluconic acid to 2-keto-gluconic acid and 5-keto-gluconic acid, being precursors for the synthesis of platform molecules like ascorbic acid and tartronate. Yet, few studies on post-transition metal modified Pt electrodes were devoted to the electrocatalytic oxidation of glucose, of which only one study was performed under acidic conditions. Hence, it is not yet understood whether these post-transition metals can be used to

change the selectivity of Pt toward specific secondary alcohol groups of glucose or gluconic acid. Therefore, research under acidic conditions is needed to evaluate whether these post-transition metals can be used to change the selectivity of Pt toward specific secondary alcohol groups of glucose or gluconic acid, thereby enabling the selective production of 2-keto-gluconic acid or 5-keto-gluconic acid.

3) The formation of dicarboxylates on electrodes has been achieved nearly exclusively in highly alkaline conditions (pH ≥ 13.7) over a wide range of electrocatalysts (e.g., based on Pt, Au and NiFeO$_x$), while MnO$_2$ was also reported to promote the formation of dicarboxylic acids under acidic conditions. In this case MnO$_2$-based electrocatalysts were used to promote the electrochemical oxidation of glucose to glucarate. The formation of acids is preferred as this reduces downstream processing costs and the formation of salt waste streams. Therefore, more research should be devoted to different electrocatalysts that are stable under acidic conditions for the selective production of dicarboxylic acids.

4) Multiple studies use cyclic voltammetry or an alternating potential to retain non-equilibrated metal surfaces (i.e. surfaces that do not reach an oxidized steady state), thereby improving the activity of the electrocatalyst. Yet, these alterations in potential can be detrimental for the selectivity of the electrocatalyst and can be complicated to operate in large-scale electrochemical systems. Therefore, it is recommended to evaluate the effect of an alternating potential on the electrocatalyst stability. Moreover, the feasibility of an alternating potential in large-scale electrochemical systems needs to be investigated further.

5) Most of the literature on the electrocatalytic oxidation of monosaccharides and sugar alcohols is centered on the activity and selectivity of novel electrocatalysts monitored by CV and LSV, and this was also the focus of this review. In the perspective of a practical and larger scale application of these electrochemical routes, it is important to study the electrocatalytic performance at longer reaction times (by chronoamperometry or chronopotentiometry), preferably in a flow cell configuration, and to assess the stability of the electrocatalysts under these conditions.

Chapter 2

Acronym list

Formic acid	-	FA
Glyceraldehyde	-	GALD
Dihydroxyacetone	-	DHA
Glyceric acid	-	GLA
Tartronic acid	-	TA
Mesoxalic acid	-	MOA
Hydropyruvic acid	-	HPA
Lactic acid	-	LA
Glucose dialdehyde	-	GD
Gluconic acid	-	GA
2-Keto gluconic acid	-	2-k-GA
5-keto gluconic acid	-	5-k-GA
Guluronic acid	-	GUL
Glucuronic acid	-	GLU
Glucaric acid	-	GLR
Cyclic voltammetry	-	CV
Linear sweep voltammetry	-	LSV
Chronoamperometry	-	CA
Faradaic efficiency	-	FE
Product selectivity	-	Sel.
High pressure liquid chromatography	-	HPLC
X-ray absorption near edge structure	-	XANES
X-ray absorption spectroscopy	-	XAS
X-ray photoelectron spectroscopy	-	XPS
X-ray diffraction	-	XRD
High-angle annular dark-field	-	HAADF
Scanning transmission electron microscopy	-	STEM
Energy dispersive X-ray spectroscopy	-	EDS
Electron energy loss spectroscopy	-	EELS

References

1. Pfaltzgraff, L. A. & Clark, J. H. Green chemistry, biorefineries and second generation strategies for re-use of waste: An overview. in *Advances in Biorefineries: Biomass and Waste Supply Chain Exploitation* 3–33 (Elsevier Ltd., 2014).

2. Levi, P. G. & Cullen, J. M. Mapping Global Flows of Chemicals: From Fossil Fuel Feedstocks to Chemical Products. *Environ Sci Technol* **52**, 1725–1734 (2018).

3. Li, K. & Sun, Y. Electrocatalytic Upgrading of Biomass-Derived Intermediate Compounds to Value-Added Products. *Chemistry - A European Journal* **24**, 18258–18270 (2018).

4. Védrine, J. C. Concluding remarks and challenges of heterogeneous catalysis on metal oxides. in *Metal Oxides in Heterogeneous Catalysis* 551–569 (Elsevier, 2018). doi:10.1016/B978-0-12-811631-9.00009-0.

5. Gallo, J. M. R. & Trapp, M. A. The chemical conversion of biomass-derived saccharides: An overview. *J Braz Chem Soc* **28**, 1586–1607 (2017).

6. Weiss, J., Hagerty, M. & Castañer, M. *The Coming Electrification of the North American Economy*. https://wiresgroup.com/wp-content/uploads/2020/05/2019-03-06-Brattle-Group-The-Coming-Electrification-of-the-NA-Economy.pdf (2019).

7. Chen, S., Wojcieszak, R., Dumeignil, F., Marceau, E. & Royer, S. How Catalysts and Experimental Conditions Determine the Selective Hydroconversion of Furfural and 5-Hydroxymethylfurfural. *Chem Rev* **118**, 11023–11117 (2018).

8. Li, X., Jia, P. & Wang, T. Furfural: A Promising Platform Compound for Sustainable Production of C4 and C5 Chemicals. *ACS Catal* **6**, 7621–7640 (2016).

9. Alonso, D. M., Wettstein, S. G. & Dumesic, J. A. Bimetallic catalysts for upgrading of biomass to fuels and chemicals. *Chem Soc Rev* **41**, 8075–8098 (2012).

10. Bayu, A., Abudula, A. & Guan, G. Reaction pathways and selectivity in chemo-catalytic conversion of biomass-derived carbohydrates to high-value chemicals : A review. *Fuel Processing Technology* **196**, 106162 (2019).

11. Brun, N., Hesemann, P. & Esposito, D. Expanding the biomass derived chemical space. *Chem Sci* **8**, 4724–4738 (2017).

12. Du, L. *et al.* Electrocatalytic valorisation of biomass derived chemicals. *Catal Sci Technol* **8**, 3216–3232 (2018).

13. Pal, P., Kumar, R. & Banerjee, S. Manufacture of gluconic acid: A review towards process intensification for green production. *Chemical Engineering and Processing: Process Intensification* **104**, 160–171 (2016).

14. Tong, X., Ma, Y. & Li, Y. Biomass into chemicals: Conversion of sugars to furan derivatives by catalytic processes. *Appl Catal A Gen* **385**, 1–13 (2010).

15. Gallezot, P. Conversion of biomass to selected chemical products. *Chem Soc Rev* **41**, 1538–1558 (2012).

16. Lee, J., Saha, B. & Vlachos, D. G. Pt catalysts for efficient aerobic oxidation of glucose to glucaric acid in water. *Green Chemistry* **18**, 3815–3822 (2016).

17. Villa, A. *et al.* Glycerol oxidation using gold-containing catalysts. *Acc Chem Res* **48**, 1403–1412 (2015).

18. Kwon, Y., Schouten, K. J. P., Van Der Waal, J. C., De Jong, E. & Koper, M. T. M. Electrocatalytic Conversion of Furanic Compounds. *ACS Catal* **6**, 6704–6717 (2016).

19. Kwon, Y. & Koper, M. T. M. Electrocatalytic hydrogenation and deoxygenation of glucose on solid metal electrodes. *ChemSusChem* **6**, 455–462 (2013).

20. Garcia, A. C. *et al.* Strong Impact of Platinum Surface Structure on Primary and Secondary Alcohol Oxidation during Electro-Oxidation of Glycerol. *ACS Catal* **6**, 4491–4500 (2016).

21. May, A. S. & Biddinger, E. J. Strategies to Control Electrochemical Hydrogenation and Hydrogenolysis of Furfural and Minimize Undesired Side Reactions. *ACS Catal* **10**, 3212–3221 (2020).

22. Holade, Y. *et al.* Recent advances in the electrooxidation of biomass-based organic molecules for energy, chemicals and hydrogen production. *Catal Sci Technol* **10**, 3071–3112 (2020).

23. Yang, C., Maldonado, S. & Stephenson, C. R. J. Electrocatalytic Lignin Oxidation. *ACS Catal* **11**, 10104–10114 (2021).

24. Bin, D. *et al.* Controllable oxidation of glucose to gluconic acid and glucaric acid using an electrocatalytic reactor. *Electrochim Acta* **130**, 170–178 (2014).

25. Moggia, G., Schalck, J., Daems, N. & Breugelmans, T. Two-steps synthesis of D-glucaric acid via D-gluconic acid by electrocatalytic oxidation of D-glucose on gold electrode: Influence of operational parameters. *Electrochim Acta* **374**, 137852 (2021).

26. Rafaïdeen, T., Baranton, S. & Coutanceau, C. Highly efficient and selective electrooxidation of glucose and xylose in alkaline medium at carbon supported alloyed PdAu nanocatalysts. *Appl Catal B* **243**, 641–656 (2019).

27. Alaba, P. A. *et al.* A review of recent progress on electrocatalysts toward efficient glycerol electrooxidation. *Reviews in Chemical Engineering* **37**, 779–811 (2020).

28. Pourzolfaghar, H., Abnisa, F., Daud, W. M. A. W. & Aroua, M. K. A review of the enzymatic hydroesterification process for biodiesel production. *Renewable and Sustainable Energy Reviews* **61**, 245–257 (2016).

29. Li, Z. *et al.* Production of value-added chemicals from glycerol using in vitro enzymatic cascades. *Commun Chem* **1**, 71 (2018).

30. Sarkar, N., Ghosh, S. K., Bannerjee, S. & Aikat, K. Bioethanol production from agricultural wastes: An overview. *Renew Energy* **37**, 19–27 (2012).

31. Vallejos, M. E., Zambon, M. D., Area, M. C. & Da Silva Curvelo, A. A. Low liquid-solid ratio (LSR) hot water pretreatment of sugarcane bagasse. *Green Chemistry* **14**, 1982–1989 (2012).

32. Ibrahim, Q. & Kruse, A. Prehydrolysis and organosolv delignification process for the recovery of hemicellulose and lignin from beech wood. *Bioresour Technol Rep* **11**, 100506 (2020).

33. Tezcan, E. & Atıcı, O. G. A new method for recovery of cellulose from lignocellulosic bio-waste: Pile processing. *Waste Management* **70**, 181–188 (2017).

34. Du, X., Zhang, H., Sullivan, K., Gogoi, P. & Deng, Y. Electrochemical Lignin Conversion. *ChemSusChem* **13**, 4318–4343 (2020).

35. Rahim, S. A. N. M. *et al.* A review of recent developments on kinetics parameters for glycerol electrochemical conversion – A by-product of biodiesel. *Science of the Total Environment* **705**, 135137 (2020).

36. Carneiro, J. & Nikolla, E. Electrochemical conversion of biomass-based oxygenated compounds. *Annu Rev Chem Biomol Eng* **10**, 85–104 (2019).

37. Simões, M., Baranton, S. & Coutanceau, C. Electrochemical valorisation of glycerol. *ChemSusChem* **5**, 2106–2124 (2012).

38. Wu, J., Yang, X. & Gong, M. Recent advances in glycerol valorization via electrooxidation: Catalyst, mechanism and device. *Chinese Journal of Catalysis* **43**, 2966–2986 (2022).

39. Ahmad, M. S. *et al.* A review on advances in green treatment of glycerol waste with a focus on electro-oxidation pathway. *Chemosphere* **276**, 130128 (2021).

40. Li, T. & Harrington, D. A. An Overview of Glycerol Electrooxidation Mechanisms on Pt, Pd and Au. *ChemSusChem* **14**, 1472–1495 (2021).

41. Zhang, W. Y., Ma, X. Y., Zou, S. Z. & Cai, W. Bin. Recent Advances in Glycerol Electrooxidation on Pt and Pd: from Reaction Mechanisms to Catalytic Materials. *Journal of Electrochemistry* **27**, 233–256 (2021).

42. Vedovato, V., Vanbroekhoven, K., Pant, D. & Helsen, J. Electrosynthesis of Biobased Chemicals Using Carbohydrates as a Feedstock. *Molecules* **25**, 16 (2020).

43. Lee, J., Jung, S., Kim, Y. T., Kim, H. J. & Kim, K. H. Catalytic and electrocatalytic conversion of glucose into value-added chemicals. *Renewable and Sustainable Energy Reviews* **181**, 113337 (2023).

44. Kim, D., Zhou, C., Zhang, M. & Cargnello, M. Voltage cycling process for the electroconversion of biomass-derived polyols. *Proceedings of the National Academy of Sciences* **118**, e2113382118 (2021).

45. Kwon, Y., De Jong, E., Van Der Waal, J. K. & Koper, M. T. M. Selective electrocatalytic oxidation of sorbitol to fructose and sorbose. *ChemSusChem* **8**, 970–973 (2015).

46. Kwon, Y., Schouten, K. J. P. & Koper, M. T. M. Mechanism of the Catalytic Oxidation of Glycerol on Polycrystalline Gold and Platinum Electrodes. *ChemCatChem* **3**, 1176–1185 (2011).

47. Kwon, Y., Birdja, Y., Spanos, I., Rodriguez, P. & Koper, M. T. M. Highly selective electro-oxidation of glycerol to dihydroxyacetone on platinum in the presence of bismuth. *ACS Catal* **2**, 759–764 (2012).

48. Kim, H. J. *et al.* Coproducing Value-Added Chemicals and Hydrogen with Electrocatalytic Glycerol Oxidation Technology: Experimental and Techno-Economic Investigations. *ACS Sustain Chem Eng* **5**, 6626–6634 (2017).

49. Roquet, L., Belgsir, E. M., Léger, J. M. & Lamy, C. Kinetics and mechanisms of the electrocatalytic oxidation of glycerol as investigated by chromatographic analysis of the reaction products: Potential and pH effects. *Electrochim Acta* **39**, 2387–2394 (1994).

50. Kim, H. J., Lee, J., Green, S. K., Huber, G. W. & Kim, W. B. Selective glycerol oxidation by electrocatalytic dehydrogenation. *ChemSusChem* **7**, 1051–1056 (2014).

51. Holade, Y. *et al.* Advances in Electrocatalysis for Energy Conversion and Synthesis of Organic Molecules. *ChemPhysChem* **18**, 2573–2605 (2017).

52. Brouzgou, A. & Tsiakaras, P. Electrocatalysts for Glucose Electrooxidation Reaction: A Review. *Top Catal* **58**, 1311–1327 (2015).

53. Gomes, J. F. & Tremiliosi-Filho, G. Spectroscopic Studies of the Glycerol Electro-Oxidation on Polycrystalline Au and Pt Surfaces in Acidic and Alkaline Media. *Electrocatalysis* **2**, 96–105 (2011).

54. Valter, M. *et al.* Electrooxidation of Glycerol on Gold in Acidic Medium: A Combined Experimental and DFT Study. *Journal of Physical Chemistry C* **122**, 10489–10494 (2018).

55. Kokoh, K. B., Léger, J. M., Beden, B. & Lamy, C. 'On line' chromatographic analysis of the products resulting from the electrocatalytic oxidation of d-glucose on Pt, Au and adatoms modified Pt electrodes-Part I. Acid and neutral media. *Electrochim Acta* **37**, 1333–1342 (1992).

56. Largeaud, F., Kokoh, K. B., Beden, B. & Lamy, C. On the electrochemical reactivity of anomers: electrocatalytic oxidation of α- and β-d-glucose on platinum electrodes in acid and basic media. *Journal of Electroanalytical Chemistry* **397**, 261–269 (1995).

57. Kokoh, K. B., Léger, J. M., Beden, B., Huser, H. & Lamy, C. 'On line' chromatographic analysis of the products resulting from the electrocatalytic oxidation of d-glucose on pure and adatoms modified Pt and Au electrodes-Part II. Alkaline medium. *Electrochim Acta* **37**, 1909–1918 (1992).

58. Beden, B., Largeaud, F., Kokoh, K. B. & Lamy, C. Fourier transform infrared reflectance spectroscopic investigation of the electrocatalytic oxidation of D-glucose: Identification of reactive intermediates and reaction products. *Electrochim Acta* **41**, 701–709 (1996).

59. Schmidt, R. K., Karplus, M. & Brady, J. W. The anomeric equilibrium in D-xylose: Free energy and the role of solvent structuring. *J Am Chem Soc* **118**, 541–546 (1996).

60. Sugiyama, H. & Usui, T. The anomeric equilibrium of glucose in acidic and basic media. *Agric Biol Chem* **44**, 3001–3002 (1980).

61. Kaufmann, M., Mügge, C. & Kroh, L. W. NMR analyses of complex D-glucose anomerization. *Food Chem* **265**, 222–226 (2018).

62. Holade, Y. *et al.* Deciphering the Electrocatalytic Reactivity of Glucose Anomers at Bare Gold Electrocatalysts for Biomass-Fueled Electrosynthesis. *ACS Catal* **12**, 12563–12571 (2022).

63. Rittenberg, D. & Graff, C. A Comparison of the Rate of Mutarotation and O18 Exchange of Glucose1. *J Am Chem Soc* **80**, 3370–3372 (1958).

64. Marioli, J. M. & Kuwana, T. Electrochemical characterization of carbohydrate oxidation at copper electrodes. *Electrochim Acta* **37**, 1187–1197 (1992).

65. Kwon, Y., Lai, S. C. S., Rodriguez, P. & Koper, M. T. M. Electrocatalytic oxidation of alcohols on gold in alkaline media: Base or gold catalysis? *J Am Chem Soc* **133**, 6914–6917 (2011).

66. Lai, S. C. S. *et al.* Effects of electrolyte pH and composition on the ethanol electro-oxidation reaction. *Catal Today* **154**, 92–104 (2010).

67. Dai, C. *et al.* Electrochemical production of lactic acid from glycerol oxidation catalyzed by AuPt nanoparticles. *J Catal* **356**, 14–21 (2017).

68. Oliveira, V. L. *et al.* Kinetic Investigations of Glycerol Oxidation Reaction on Ni/C. *Electrocatalysis* **6**, 447–454 (2015).

69. Habibi, E. & Razmi, H. Glycerol electrooxidation on Pd, Pt and Au nanoparticles supported on carbon ceramic electrode in alkaline media. *Int J Hydrogen Energy* **37**, 16800–16809 (2012).

70. Torigoe, K. *et al.* High-Power Abiotic Direct Glucose Fuel Cell Using a Gold-Platinum Bimetallic Anode Catalyst. *ACS Omega* **3**, 18323–18333 (2018).

71. Tao, B., Miao, F. & Chu, P. K. Preparation and characterization of a novel nickel-palladium electrode supported by silicon nanowires for direct glucose fuel cell. *Electrochim Acta* **65**, 149–152 (2012).

72. Mäki-Arvela, P., Simakova, I. L., Salmi, T. & Murzin, D. Y. Production of lactic acid/lactates from biomass and their catalytic transformations to commodities. *Chem Rev* **114**, 1909–1971 (2014).

73. Li, L., Shen, F., Smith, R. L. & Qi, X. Quantitative chemocatalytic production of lactic acid from glucose under anaerobic conditions at room temperature. *Green Chemistry* **19**, 76–81 (2017).

74. Choudhary, V. *et al.* Insights into the interplay of lewis and Brønsted acid catalysts in glucose and fructose conversion to 5-(hydroxymethyl)furfural and levulinic acid in aqueous media. *J Am Chem Soc* **135**, 3997–4006 (2013).

75. Wrigstedt, P., Keskiväli, J., Leskelä, M. & Repo, T. The role of salts and Brønsted acids in lewis acid-catalyzed aqueous-phase glucose dehydration to 5-hydroxymethylfurfural. *ChemCatChem* **7**, 501–507 (2015).

76. Garcia, A. C., Birdja, Y. Y., Tremiliosi-Filho, G. & Koper, M. T. M. Glycerol electro-oxidation on bismuth-modified platinum single crystals. *J Catal* **346**, 117–124 (2017).

77. Moggia, G., Kenis, T., Daems, N. & Breugelmans, T. Electrochemical Oxidation of d-Glucose in Alkaline Medium: Impact of Oxidation Potential and Chemical Side Reactions on the Selectivity to d-Gluconic and d-Glucaric Acid. *ChemElectroChem* **7**, 86–95 (2020).

78. Takei, T. *et al.* Heterogeneous Catalysis by Gold. in *Advances in Catalysis* vol. 55 1–126 (Academic Press, 2012).

79. Yoo, C. G., Li, N., Swannell, M. & Pan, X. Isomerization of glucose to fructose catalyzed by lithium bromide in water. *Green Chemistry* **19**, 4402–4411 (2017).

80. Bricotte, L., Chougrani, K., Alard, V., Ladmiral, V. & Caillol, S. Dihydroxyacetone: A User Guide for a Challenging Bio-Based Synthon. *Molecules* **28**, (2023).

81. Wu, L., Moteki, T., Gokhale, A. A., Flaherty, D. W. & Toste, F. D. Production of Fuels and Chemicals from Biomass: Condensation Reactions and Beyond. *Chem* **1**, 32–58 (2016).

82. Kluster, B. F. M. & van der Baan, H. S. The Dehydration of fructose. (1975). doi:10.6100/IR33489.

83. Chheda, J. N., Román-Leshkov, Y. & Dumesic, J. A. Production of 5-hydroxymethylfurfural and furfural by dehydration of biomass-derived mono- and poly-saccharides. *Green Chemistry* **9**, 342–35 (2007).

84. Asghari, F. S. & Yoshida, H. Acid-catalyzed production of 5-hydroxymethyl furfural from D-fructose in subcritical water. *Ind Eng Chem Res* **45**, 2163–2173 (2006).

85. Li, D. *et al.* Deep eutectic solvents derived carbon-based efficient electrocatalyst for boosting H2 production coupled with glucose oxidation. *Chemical Engineering Journal* **430**, 132783 (2022).

86. Tang, Z. *et al.* Base-free conversion of glycerol to methyl lactate using a multifunctional catalytic system consisting of Au-Pd nanoparticles on carbon nanotubes and Sn-MCM-41-XS. *Green Chemistry* **21**, 4115–4126 (2019).

87. Arts, S. J. H. F., Mombarg, E. J. M., van Bekkum, H. & Sheldon, R. A. Hydrogen peroxide and oxygen in catalytic oxidation of carbohydrates and related compounds. *Synthesis (Stuttg)* **6**, 597–613 (1997).

88. Wu, J. *et al.* Steering the Glycerol Electro-Reforming Selectivity via Cation–Intermediate Interactions. *Angewandte Chemie - International Edition* **61**, e202113362 (2022).

89. Huang, X., Zou, Y. & Jiang, J. Electrochemical Oxidation of Glycerol to Dihydroxyacetone in Borate Buffer: Enhancing Activity and Selectivity by Borate-Polyol Coordination Chemistry. *ACS Sustain Chem Eng* **9**, 14470–14479 (2021).

90. Qi, J. *et al.* Electrocatalytic selective oxidation of glycerol to tartronate on Au/C anode catalysts in anion exchange membrane fuel cells with electricity cogeneration. *Appl Catal B* **154**, 360–368 (2014).

91. Kwon, Y. & Koper, M. T. M. Combining voltammetry with HPLC: Application to electro-oxidation of glycerol. *Anal Chem* **82**, 5420–5424 (2010).

92. Xin, L., Zhang, Z., Wang, Z. & Li, W. Simultaneous Generation of Mesoxalic Acid and Electricity from Glycerol on a Gold Anode Catalyst in Anion-Exchange Membrane Fuel Cells. *ChemCatChem* **4**, 1105–1114 (2012).

93. Yongprapat, S., Therdthianwong, A. & Therdthianwong, S. Au/C catalyst prepared by polyvinyl alcohol protection method for direct alcohol alkaline exchange membrane fuel cell application. *J Appl Electrochem* **42**, 483–490 (2012).

94. Yei, L. H. E., Beden, B. & Lamy, C. Electrocatalytic oxidation of glucose at platinum in alkaline medium: on the role of temperature. *Journal of Electroanalytical Chemistry* **246**, 349–362 (1988).

95. Parpot, P., Santos, P. R. B. & Bettencourt, A. P. Electro-oxidation of d-mannose on platinum, gold and nickel electrodes in aqueous medium. *Journal of Electroanalytical Chemistry* **610**, 154–162 (2007).

96. Lam, C. H., Bloomfield, A. J. & Anastas, P. T. A switchable route to valuable commodity chemicals from glycerol via electrocatalytic oxidation with an earth abundant metal oxidation catalyst. *Green Chemistry* **19**, 1958–1968 (2017).

97. De Paula, J., Nascimento, D. & Linares, J. J. Electrochemical reforming of glycerol in alkaline PBI-based PEM reactor for hydrogen production. *Chem Eng Trans* **41**, 205–210 (2014).

98. Ferreira Frota, E., Silva de Barros, V. V., de Araújo, B. R. S., Gonzaga Purgatto, Â. & Linares, J. J. Pt/C containing different platinum loadings for use as electrocatalysts in alkaline PBI-based direct glycerol fuel cells. *Int J Hydrogen Energy* **42**, 23095–23106 (2017).

99. Ghosh, S. *et al.* One-pot synthesis of reduced graphene oxide supported gold-based nanomaterials as robust nanocatalysts for glucose electrooxidation. *Electrochim Acta* **212**, 864–875 (2016).

100. Hebié, S. *et al.* Advanced Electrocatalysts on the Basis of Bare Au Nanomaterials for Biofuel Cell Applications. *ACS Catal* **5**, 6489–6496 (2015).

101. Oyarce, A. *et al.* Direct sorbitol proton exchange membrane fuel cell using moderate catalyst loadings. *Electrochim Acta* **116**, 379–387 (2014).

102. Hebié, S., Napporn, T. W., Morais, C. & Kokoh, K. B. Size-Dependent Electrocatalytic Activity of Free Gold Nanoparticles for the Glucose Oxidation Reaction. *ChemPhysChem* **17**, 1454–1462 (2016).

103. Lee, S. *et al.* Highly selective transformation of glycerol to dihydroxyacetone without using oxidants by a PtSb/C-catalyzed electrooxidation process. *Green Chemistry* **18**, 2877–2887 (2016).

104. Xie, K. *et al.* Eliminating the need for anodic gas separation in CO2 electroreduction systems via liquid-to-liquid anodic upgrading. *Nat Commun* **13**, 3070 (2022).

105. Shubair, A. Tuning the selectivity of bimetallic NiBi catalysts for glycerol electrooxidation into value-added chemicals. (2021). doi:10.20381/ruor-26104.

106. Lyons, M. E. G., Fitzgerald, C. A. & Smyth, M. R. Glucose Oxidation at Ruthenium Dioxide Based Electrodes. *Analyst* **119**, 855–861 (1994).

107. Das, D., Sen, P. K. & Das, K. Mechanism of potentiostatic deposition of MnO2 and electrochemical characteristics of the deposit in relation to carbohydrate oxidation. *Electrochim Acta* **54**, 289–295 (2008).

108. Das, D., Sen, P. K. & Das, K. Carbohydrate electro-oxidation on chemically prepared MnO2. *Journal of Electroanalytical Chemistry* **611**, 19–25 (2007).

109. Zalineeva, A., Baranton, S. & Coutanceau, C. Bi-modified palladium nanocubes for glycerol electrooxidation. *Electrochem commun* **34**, 335–338 (2013).

110. Yan, L. *et al.* Efficient and poison-tolerant PdxAuy/C binary electrocatalysts for glucose electrooxidation in alkaline medium. *Appl Catal B* **150**, 268–274 (2014).

111. Tung, S. P., Huang, T. K., Lee, C. Y. & Chiu, H. T. Electrochemical growth of gold nanostructures on carbon paper for alkaline direct glucose fuel cell. *RSC Adv* **2**, 1068–1073 (2012).

112. Liu, W. J. *et al.* Efficient electrochemical production of glucaric acid and H2 via glucose electrolysis. *Nat Commun* **11**, 265 (2020).

113. Zhang, Z., Xin, L. & Li, W. Electrocatalytic oxidation of glycerol on Pt/C in anion-exchange membrane fuel cell: Cogeneration of electricity and valuable chemicals. *Appl Catal B* **119**, 40–48 (2012).

114. Cherevko, S., Zeradjanin, A. R., Keeley, G. P. & Mayrhofer, K. J. J. A Comparative Study on Gold and Platinum Dissolution in Acidic and Alkaline Media. *J Electrochem Soc* **161**, H822–H830 (2014).

115. Yang, S. & Hetterscheid, D. G. H. Redefinition of the Active Species and the Mechanism of the Oxygen Evolution Reaction on Gold Oxide. *ACS Catal* **10**, 12582–12589 (2020).

116. Diaz-Morales, O., Calle-Vallejo, F., De Munck, C. & Koper, M. T. M. Electrochemical water splitting by gold: Evidence for an oxide decomposition mechanism. *Chem Sci* **4**, 2334–2343 (2013).

117. Suzuki, K., Li, X., Wang, Y., Nagasawa, F. & Murakoshi, K. Active Intermediates in Plasmon-Induced Water Oxidation at Au Nanodimer Structures on a Single Crystal of TiO2. *ACS Energy Lett* **5**, 1252–1259 (2020).

118. Hersbach, T. J. P. *et al.* Base-Accelerated Degradation of Nanosized Platinum Electrocatalysts. *ACS Catal* **11**, 9904–9915 (2021).

119. Kusano, S., Matsumura, D., Ishii, K., Tanaka, H. & Mizuki, J. Electrochemical adsorption on Pt nanoparticles in alkaline solution observed using in situ high energy resolution X-ray absorption spectroscopy. *Nanomaterials* **9**, 642 (2019).

120. McCrum, I. T., Chen, X., Schwarz, K. A., Janik, M. J. & Koper, M. T. M. Effect of Step Density and Orientation on the Apparent pH Dependence of Hydrogen and Hydroxide Adsorption on Stepped Platinum Surfaces. *Journal of Physical Chemistry C* **122**, 16756–16764 (2018).

121. Chen, X., McCrum, I. T., Schwarz, K. A., Janik, M. J. & Koper, M. T. M. Co-adsorption of Cations as the Cause of the Apparent pH Dependence of Hydrogen Adsorption on a Stepped Platinum Single-Crystal Electrode. *Angewandte Chemie - International Edition* **56**, 15025–15029 (2017).

122. Jerkiewicz, G., Vatankhah, G., Lessard, J., Soriaga, M. P. & Park, Y. S. Surface-oxide growth at platinum electrodes in aqueous H2SO 4 Reexamination of its mechanism through combined cyclic-voltammetry, electrochemical quartz-crystal nanobalance, and Auger electron spectroscopy measurements. *Electrochim Acta* **49**, 1451–1459 (2004).

123. Rahman, M. R., Awad, M. I., Kitamura, F., Okajima, T. & Ohsaka, T. A comparative study of ORR at the Pt electrode in ammonium ion-contaminated H2SO4 and HClO4 solutions. *J Power Sources* **220**, 65–73 (2012).

124. Angerstein-Kozlowska, H., Conway, B. E. & Sharp, W. B. A. The real condition of electrochemically oxidized platinum surfaces: Part I. Resolution of component processes. *Electroanalytical Chemistry and Interfacial Electrochemistry* **43**, 9–36 (1973).

125. Drnec, J., Harrington, D. A. & Magnussen, O. M. Electrooxidation of Pt(111) in acid solution. *Curr Opin Electrochem* **4**, 69–75 (2017).

126. Deng, X., Galli, F. & Koper, M. T. M. In Situ AFM Imaging of Platinum Electrode Surface during Oxidation-Reduction Cycles in Alkaline Electrolyte. *ACS Appl Energy Mater* **3**, 597–602 (2020).

127. Shrestha, B. R., Yadav, A. P., Nishikata, A. & Tsuru, T. Application of channel flow double electrode to the study on platinum dissolution during potential cycling in sulfuric acid solution. *Electrochim Acta* **56**, 9714–9720 (2011).

128. Huang, Y. F., Kooyman, P. J. & Koper, M. T. M. Intermediate stages of electrochemical oxidation of single-crystalline platinum revealed by in situ Raman spectroscopy. *Nat Commun* **7**, 12440 (2016).

129. Li, Y. *et al.* Cobalt phosphate-modified barium-doped tantalum nitride nanorod photoanode with 1.5% solar energy conversion efficiency. *Nat Commun* **4**, 2566 (2013).

130. Silva, F. & Martins, A. Surface structural effects on specific adsorption of oxoanions on gold single crystal electrodes. *Journal of Electroanalytical Chemistry* **467**, 335–341 (1999).

131. Mahmoodinia, M., Åstrand, P. O. & Chen, D. Tuning the Electronic Properties of Single-Atom Pt Catalysts by Functionalization of the Carbon Support Material. *Journal of Physical Chemistry C* **121**, 20802–20812 (2017).

132. Van der Ham, M. P. J. M. *et al.* Improved electrocatalytic activity of Pt on carbon nanofibers for glucose oxidation mediated by support oxygen groups in Pt perimeter. *Appl Catal B* **338**, 123046 (2023).

133. Verma, A. M., Laverdure, L., Melander, M. M. & Honkala, K. Mechanistic Origins of the pH Dependency in Au-Catalyzed Glycerol Electro-oxidation: Insight from First-Principles Calculations. *ACS Catal* **12**, 662–675 (2022).

134. Zhou, Y., Shen, Y. & Xi, J. Seed-mediated synthesis of PtxAuy@Ag electrocatalysts for the selective oxidation of glycerol. *Appl Catal B* **245**, 604–612 (2019).

135. Zope, B. N., Hibbitts, D. D., Neurock, M. & Davis, R. J. Reactivity of the gold/water interface during selective oxidation catalysis. *Science (1979)* **330**, 74–78 (2010).

136. Zalineeva, A., Baranton, S. & Coutanceau, C. How do Bi-modified palladium nanoparticles work towards glycerol electrooxidation? An in situ FTIR study. *Electrochim Acta* **176**, 705–717 (2015).

137. Scachetti, T. P. & Angelo, A. C. D. Ordered Intermetallic Nanostructured PtSb/C for Production of Energy and Chemicals. *Electrocatalysis* **6**, 472–480 (2015).

138. Li, T. & Harrington, D. A. An Overview of Glycerol Electrooxidation Mechanisms on Pt, Pd and Au. *ChemSusChem* **14**, 1472–1495 (2021).

139. dos Santos, E. C. *et al.* Efficient Screening of Bi–Metallic Electrocatalysts for Glycerol Valorization. *Electrochim Acta* **398**, 139283 (2021).

140. Poerwoprajitno, A. R., Gloag, L., Cheong, S., Gooding, J. J. & Tilley, R. D. Synthesis of low- and high-index faceted metal (Pt, Pd, Ru, Ir, Rh) nanoparticles for improved activity and stability in electrocatalysis. *Nanoscale* **11**, 18995–19011 (2019).

141. Proença, L. *et al.* Electrocatalytic oxidation of D-sorbitol on platinum in acid medium: Analysis of the reaction products. *Journal of Electroanalytical Chemistry* **432**, 237–242 (1997).

142. Ahmad, M. S. *et al.* Electro-oxidation of waste glycerol to tartronic acid over Pt/CNT nanocatalyst: study of effect of reaction time on product distribution. *Energy Sources, Part A* 1–17 (2019).

143. Ahmad, M. S., Cheng, C. K., Ong, H. R., Abdullah, H. & Khan, M. R. Electro-oxidation of renewable glycerol to value added chemicals over phosphorous-doped Pt/MCNTs nanoparticles. *Materials Science and Engineering* **702**, 012025 (2019).

144. Zhou, Y. & Shen, Y. Selective electro-oxidation of glycerol over Pd and Pt@Pd nanocubes. *Electrochem commun* **90**, 106–110 (2018).

145. Guima, K. E., Alencar, L. M., Da Silva, G. C., Trindade, M. A. G. & Martins, C. A. 3D-Printed Electrolyzer for the Conversion of Glycerol into Tartronate on Pd Nanocubes. *ACS Sustain Chem Eng* **6**, 1202–1207 (2018).

146. Holade, Y., Servat, K., Napporn, T. W. & Kokoh, K. B. Electrocatalytic properties of nanomaterials synthesized from 'Bromide Anion Exchange' method - Investigations of glucose and glycerol oxidation. *Electrochim Acta* **162**, 205–214 (2015).

147. Palma, L. M. *et al.* Effect of Co-catalyst on the Selective Electrooxidation of Glycerol over Ruthenium-based Nanomaterials. *ChemElectroChem* **4**, 39–45 (2017).

148. Ahmad, M. S. *et al.* Glycerol electro-oxidation to dihydroxyacetone on phosphorous-doped Pd/CNT nanoparticles in alkaline medium. *Catal Commun* **139**, 105964 (2020).

149. Guschakowski, M. & Schröder, U. Direct and Indirect Electrooxidation of Glycerol to Value-Added Products. *ChemSusChem* **14**, 5216–5225 (2021).

150. Houache, M. S. E. *et al.* Selective Electrooxidation of Glycerol to Formic Acid over Carbon Supported Ni 1– x M x (M = Bi, Pd, and Au) Nanocatalysts and Coelectrolysis of CO2. *ACS Appl Energy Mater* **3**, 8725–8738 (2020).

151. Goetz, M. K. K., Bender, M. T. & Choi, K. S. Predictive control of selective secondary alcohol oxidation of glycerol on NiOOH. *Nat Commun* **13**, 5848 (2022).

152. Brix, A. C. *et al.* Electrocatalytic Oxidation of Glycerol Using Solid-State Synthesised Nickel Boride: Impact of Key Electrolysis Parameters on Product Selectivity. *ChemElectroChem* **8**, 2336–2342 (2021).

153. Morales, D. M. *et al.* Electrocatalytic Conversion of Glycerol to Oxalate on Ni Oxide Nanoparticles-Modified Oxidized Multiwalled Carbon Nanotubes. *ACS Catal* **12**, 982–992 (2022).

154. Vo, T. G., Ho, P. Y. & Chiang, C. Y. Operando mechanistic studies of selective oxidation of glycerol to dihydroxyacetone over amorphous cobalt oxide. *Appl Catal B* **300**, 120723 (2022).

155. Taitt, B. J., Nam, D. H. & Choi, K. S. A Comparative Study of Nickel, Cobalt, and Iron Oxyhydroxide Anodes for the Electrochemical Oxidation of 5-Hydroxymethylfurfural to 2,5-Furandicarboxylic Acid. *ACS Catal* **9**, 660–670 (2019).
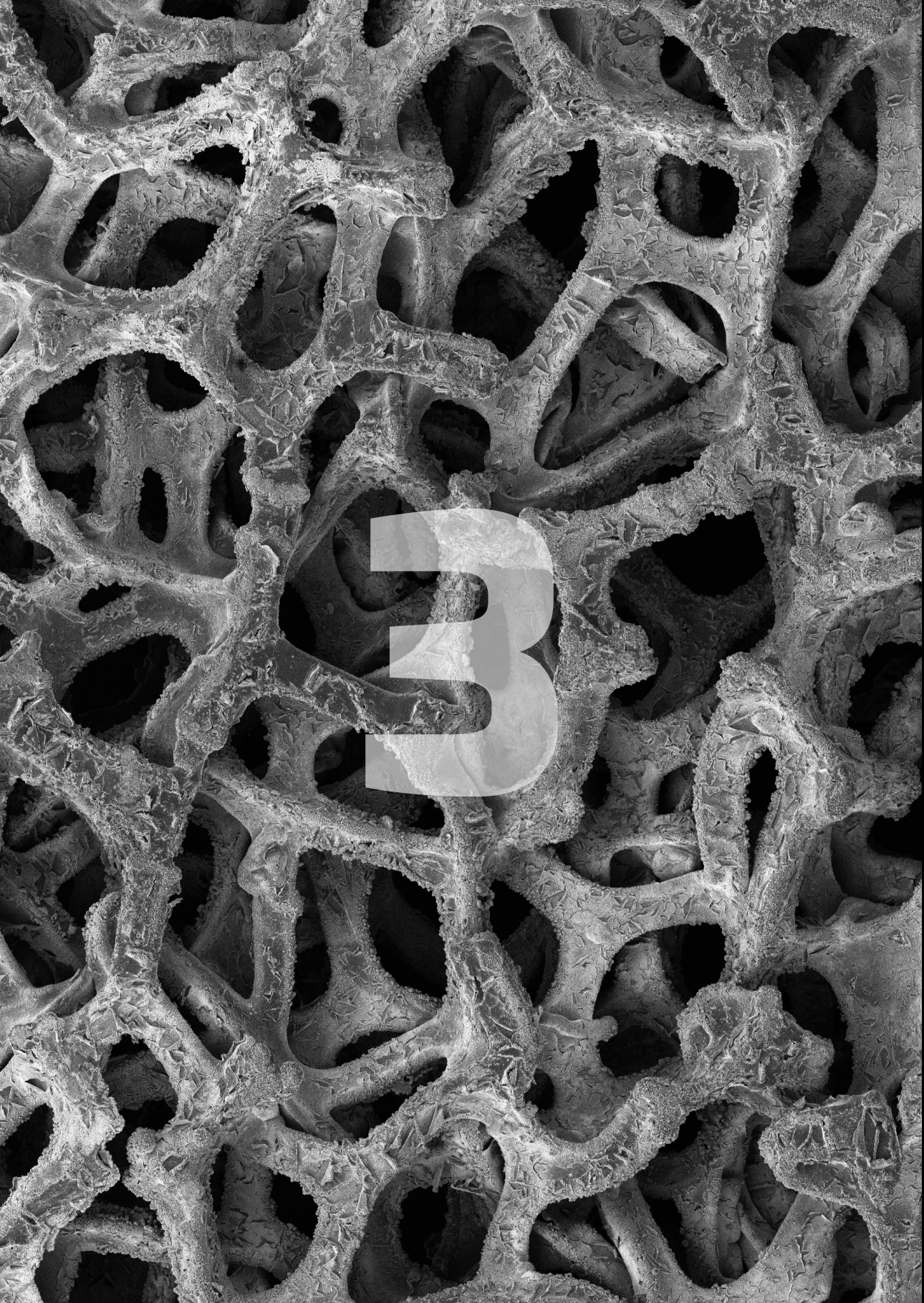
156. Houache, M. S. E. *et al.* Electrochemical Valorization of Glycerol on Ni-Rich Bimetallic NiPd Nanoparticles: Insight into Product Selectivity Using in Situ Polarization Modulation Infrared-Reflection Absorption Spectroscopy. *ACS Sustain Chem Eng* **7**, 14425–14434 (2019).

157. Bender, M. T., Warburton, R. E., Hammes-Schiffer, S. & Choi, K. S. Understanding Hydrogen Atom and Hydride Transfer Processes during Electrochemical Alcohol and Aldehyde Oxidation. *ACS Catal* **11**, 15110–15124 (2021).

158. Liu, C. *et al.* Selective electro-oxidation of glycerol to dihydroxyacetone by a non-precious electrocatalyst – CuO. *Appl Catal B* **265**, 118543 (2020).

159. Tran, G. S., Vo, T. G. & Chiang, C. Y. Earth-abundant manganese oxide nanoneedle as highly efficient electrocatalyst for selective glycerol electro-oxidation to dihydroxyacetone. *J Catal* **404**, 139–148 (2021).

160. Gomes, J. F. *et al.* Influence of silver on the glycerol electro-oxidation over AuAg/C catalysts in alkaline medium: A cyclic voltammetry and in situ FTIR spectroscopy study. *Electrochim Acta* **144**, 361–368 (2014).

161. Torres-Pacheco, L. J. *et al.* Effect of AuM (M: Ag, Pt & Pd) bimetallic nanoparticles on the sorbitol electro-oxidation in alkaline medium. *Fuel* **274**, 117864 (2020).

162. Thia, L., Xie, M., Kim, D. & Wang, X. Ag containing porous Au structures as highly selective catalysts for glycolate and formate. *Catal Sci Technol* **7**, 874–881 (2017).

163. Garcia, A. C., Ferreira, E. B., Silva de Barros, V. V., Linares, J. J. & Tremiliosi-Filho, G. PtAg/MnOx/C as a promising electrocatalyst for glycerol electro-oxidation in alkaline medium. *Journal of Electroanalytical Chemistry* **793**, 188–196 (2017).

164. Benipal, N., Qi, J., Liu, Q. & Li, W. Carbon nanotube supported PdAg nanoparticles for electrocatalytic oxidation of glycerol in anion exchange membrane fuel cells. *Appl Catal B* **210**, 121–130 (2017).

165. Inoue, H. *et al.* Mechanism of glycerol oxidation reaction on silver-modified palladium electrode in alkaline medium. *Int J Hydrogen Energy* **43**, 18664–18671 (2018).

166. Torres-Pacheco, L. J., De Leon-Rodriguez, A., Álvarez-Contreras, L., Guerra-Balcázar, M. & Arjona, N. Sorbitol electro-oxidation reaction on sub<10 nm PtAu bimetallic nanoparticles. *Electrochim Acta* **353**, 136593 (2020).

167. Ottoni, C. A., da Silva, S. G., De Souza, R. F. B. & Neto, A. O. Glycerol oxidation reaction using PdAu/C electrocatalysts. *Ionics* **22**, 1167–1175 (2016).

168. Torres-Pacheco, L. J. *et al.* Electrocatalytic evaluation of sorbitol oxidation as a promising fuel in energy conversion using Au/C, Pd/C and Au–Pd/C synthesized through ionic liquids. *Fuel* **250**, 103–116 (2019).

169. Hong, W., Shang, C., Wang, J. & Wang, E. Bimetallic PdPt nanowire networks with enhanced electrocatalytic activity for ethylene glycol and glycerol oxidation. *Energy Environ Sci* **8**, 2910–2915 (2015).

170. Zhou, Y., Shen, Y. & Piao, J. Sustainable Conversion of Glycerol into Value-Added Chemicals by Selective Electro-Oxidation on Pt-Based Catalysts. *ChemElectroChem* **5**, 1636–1643 (2018).

171. Kim, Y. *et al.* The Role of Ruthenium on Carbon-Supported PtRu Catalysts for Electrocatalytic Glycerol Oxidation under Acidic Conditions. *ChemCatChem* **9**, 1683–1690 (2017).

172. Luo, H. *et al.* Role of Ni in PtNi Bimetallic Electrocatalysts for Hydrogen and Value-Added Chemicals Coproduction via Glycerol Electrooxidation. *ACS Catal* **12**, 14492–14506 (2022).

173. Mürtz, S. D., Musialek, F., Pfänder, N. & Palkovits, R. Bimetallic PtCu/C Catalysts for Glycerol Assisted Hydrogen Evolution in Acidic Media. *ChemElectroChem* **10**, e202300193 (2023).

174. Mo, X. *et al.* Direct 3D Printing of Binder-Free Bimetallic Nanomaterials as Integrated Electrodes for Glycerol Oxidation with High Selectivity for Valuable C3Products. *ACS Nano* **16**, 12202–12213 (2022).

175. Li, J. *et al.* Tuning the Product Selectivity toward the High Yield of Glyceric Acid in Pt-CeO2/CNT Electrocatalyzed Oxidation of Glycerol. *ChemCatChem* **14**, e202200509 (2022).

176. Liu, X. & Yang, C. Electrocatalytic selective oxidation of glycerol to glyceric acid over efficient Pt/CNTs-CeO2 catalysts. *Mater Lett* **324**, 132658 (2022).

177. Palma, L. M. *et al.* Identification of chemicals resulted in selective glycerol conversion as sustainable fuel on Pd-based anode nanocatalysts. *RSC Adv* **4**, 64476–64483 (2014).

178. Zhang, X. *et al.* Overcoming the Deactivation of Pt/CNT by Introducing CeO2 for Selective Base-Free Glycerol-to-Glyceric Acid Oxidation. *ACS Catal* **10**, 3832–3837 (2020).

179. Naik, K. M., Hashisake, K., Hamada, T., Higuchi, E. & Inoue, H. Intermetallic PdZn nanoparticles loaded on deficient TiO 2 nanosheets as a support: a bifunctional electrocatalyst for oxygen reduction in PEMFCs and the glycerol oxidation reactions . *J Mater Chem A Mater* **10**, 13987–13997 (2022).

180. Araujo, H. R. *et al.* How the adsorption of Sn on Pt (100) preferentially oriented nanoparticles affects the pathways of glycerol electro-oxidation. *Electrochim Acta* **297**, 61–69 (2019).

181. Kwon, Y., Hersbach, T. J. P. & Koper, M. T. M. Electro-Oxidation of Glycerol on Platinum Modified by Adatoms: Activity and Selectivity Effects. *Top Catal* **57**, 1272–1276 (2014).

182. De Souza, M. B. C. *et al.* Bi-modified Pt Electrodes toward Glycerol Electrooxidation in Alkaline Solution: Effects on Activity and Selectivity. *ACS Catal* **9**, 5104–5110 (2019).

183. De Souza, M. B. C. *et al.* Pb- And Bi-Modified Pt Electrodes toward Glycerol Electrooxidation in Alkaline Media. Activity, Selectivity, and the Importance of the Pt Atoms Arrangement. *ACS Catal* **10**, 2131–2137 (2020).

184. Simões, M., Baranton, S. & Coutanceau, C. Enhancement of catalytic properties for glycerol electrooxidation on Pt and Pd nanoparticles induced by Bi surface modification. *Appl Catal B* **110**, 40–49 (2011).

185. Nagorski, R. W. & Richard, J. P. Mechanistic imperatives for aldose - Ketose isomerization in water: Specific, general base- and metal ion-catalyzed isomerization of glyceraldehyde with proton and hydride transfer. *J Am Chem Soc* **123**, 794–802 (2001).

186. Fernandez-Vega, A., Feliu, J. M., Aldaz, A. & Clavilier, J. Heterogeneous electrocatalysis on well defined platinum surfaces modified by controlled amounts of irreversibly adsorbed adatoms. Part II. Formic acid oxidation on the Pt (100)-Sb system. *Journal of Electroanalytical Chemistry* **258**, 101–113 (1989).

187. Daniele, S., Battistel, D., Bergamin, S. & Bragato, C. Voltammetric determination of glucose at bismuth-modified mesoporous platinum microelectrodes. *Electroanalysis* **22**, 1511–1518 (2010).

188. Houache, M. S. E., Hughes, K., Safari, R., Botton, G. A. & Baranova, E. A. Modification of Nickel Surfaces by Bismuth: Effect on Electrochemical Activity and Selectivity toward Glycerol. *ACS Appl Mater Interfaces* **12**, 15095–15107 (2020).

189. Huang, X., Guo, Y., Zou, Y. & Jiang, J. Electrochemical oxidation of glycerol to hydroxypyruvic acid on cobalt (oxy)hydroxide by high-valent cobalt redox centers. *Appl Catal B* **309**, 121247 (2022).

190. van der Ham, M. P. J. M., van Keulen, E., Koper, M. T., Tashvigh, A. A. & Bitter, J. H. Steering the Selectivity of Electrocatalytic Glucose Oxidation by the Pt Oxidation State. *Angewandte Chemie - International Edition* **62**, e202306701 (2023).

191. Aoun, S. Ben *et al.* Effect of metal ad-layers on Au(1 1 1) electrodes on electrocatalytic oxidation of glucose in an alkaline solution. *Journal of Electroanalytical Chemistry* **567**, 175–183 (2004).

192. Cañete-Rodríguez, A. M. *et al.* Gluconic acid: Properties, production methods and applications—An excellent opportunity for agro-industrial by-products and waste bio-valorization. *Process Biochemistry* **51**, 1891–1903 (2016).

193. Armstrong, R. D., Hirayama, J., Knight, D. W. & Hutchings, G. J. Quantitative Determination of Pt- Catalyzed d - Glucose Oxidation Products Using 2D NMR. *ACS Catal* **9**, 325–335 (2019).

194. Kokoh, K. B. *et al.* Selective oxidation of D-gluconic acid on platinum and lead adatoms modified platinum electrodes in alkaline medium. *Electrochim Acta* **38**, 1359–1365 (1993).

195. Lemoine, C. *et al.* New insights on the selective electroconversion of the cellulosic biomass-derived glucose at PtAu nanocatalysts in an anion exchange membrane fuel cell. *Journal of Electroanalytical Chemistry* **887**, 115162 (2021).

196. Parpot, P., Nunes, N. & Bettencourt, A. P. Electrocatalytic oxidation of monosaccharides on gold electrode in alkaline medium: Structure-reactivity relationship. *Journal of Electroanalytical Chemistry* **596**, 65–73 (2006).

197. Tominaga, M., Taema, Y. & Taniguchi, I. Electrocatalytic glucose oxidation at bimetallic gold–copper nanoparticle-modified carbon electrodes in alkaline solution. *Journal of Electroanalytical Chemistry* **624**, 1–8 (2008).

198. Tominaga, M., Shimazoe, T., Nagashima, M. & Taniguchi, I. Composition-activity relationships of carbon electrode-supported bimetallic gold-silver nanoparticles in electrocatalytic oxidation of glucose. *Journal of Electroanalytical Chemistry* **615**, 51–61 (2008).

199. Parpot, P., Pires, S. G. & Bettencourt, A. P. Electrocatalytic oxidation of D-galactose in alkaline medium. *Journal of Electroanalytical Chemistry* **566**, 401–408 (2004).

200. Tominaga, M., Shimazoe, T., Nagashima, M. & Taniguchi, I. Electrocatalytic oxidation of glucose at gold nanoparticle-modified carbon electrodes in alkaline and neutral solutions. *Electrochem commun* **7**, 189–193 (2005).

201. Hebié, S., Kokoh, K. B., Servat, K. & Napporn, T. W. Shape-dependent electrocatalytic activity of free gold nanoparticles toward glucose oxidation. *Gold Bull* **46**, 311–318 (2013).

202. Wang, J. *et al.* Shape-dependent electrocatalytic activity of monodispersed gold nanocrystals toward glucose oxidation. *Chemical Communications* **47**, 6894–6896 (2011).

203. Hebié, S., Cornu, L., Napporn, T. W., Rousseau, J. & Kokoh, B. K. Insight on the surface structure effect of free gold nanorods on glucose electrooxidation. *Journal of Physical Chemistry C* **117**, 9872–9880 (2013).

204. Hsiao, M. W., Adzic, R. R. & Yeager, E. B. The effects of adsorbed anions on the oxidation of D-glucose on gold single crystal electrodes. *Electrochim Acta* **37**, 357–363 (1992).

205. Adzic, R. R., Hsiao, M. W. & Yeager, E. B. Electrochemical oxidation of glucose on single crystal gold surfaces. *Journal of Electroanalytical Chemistry* **260**, 475–485 (1989).

206. Hsiao, M. W., Adii, R. R. & Yeager, E. B. Electrochemical Oxidation of Glucose on Single Crystal and Polycrystalline Gold Surfaces in Phosphate Buffer. *J. Electrochem. Soc* **143**, 759–767 (1996).

207. Governo, A. T., Proença, L., Parpot, P., Lopes, M. I. S. & Fonseca, I. T. E. Electro-oxidation of D-xylose on platinum and gold electrodes in alkaline medium. *Electrochim Acta* **49**, 1535–1545 (2004).

208. Mello, G. A. B., Cheuquepán, W., Briega-Martos, V. & Feliu, J. M. Glucose electro-oxidation on Pt(100) in phosphate buffer solution (pH 7): A mechanistic study. *Electrochim Acta* **354**, 136765 (2020).

209. Popović, K. D., Tripković, A. V. & Adžić, R. R. Oxidation of d-glucose on single-crystal platinum electrodes: A mechanistic study. *Journal of Electroanalytical Chemistry* **339**, 227–245 (1992).

210. Faverge, T. *et al.* In Situ Investigation of d-Glucose Oxidation into Value-Added Products on Au, Pt, and Pd under Alkaline Conditions: A Comparative Study. *ACS Catal* **13**, 2657–2669 (2023).

211. Bamba, K., Kokoh, K. B., Servat, K. & Léger, J. M. Electrocatalytic oxidation of monosaccharides on platinum electrodes modified by thallium adatoms in carbonate buffered medium. *J Appl Electrochem* **36**, 233–238 (2006).

212. Zhang, K. *et al.* An efficient electrocatalytic system composed of nickel oxide and nitroxyl radical for the oxidation of bio-platform molecules to dicarboxylic acids. *Journal of Energy Chemistry* **80**, 58–67 (2023).

213. Wu, M., Zhao, J., Li, C. & Liu, R. Heterogeneity in a metal–organic framework in situ guides engineering Co@CoO heterojunction for electrocatalytic H 2 production in tandem with glucose oxidation . *J Mater Chem A Mater* **10**, 4791–4799 (2022).

214. Zhu, Y. *et al.* Identification of Active Sites Formed on Cobalt Oxyhydroxide in Glucose Electrooxidation. *Angewandte Chemie* **135**, e202219048 (2023).

215. Ostervold, L., Perez Bakovic, S. I., Hestekin, J. & Greenlee, L. F. Electrochemical biomass upgrading: degradation of glucose to lactic acid on a copper (II) electrode. *RSC Adv* **11**, 31208–31218 (2021).

216. Li, J. *et al.* Efficiently coupled glucose oxidation for high-value D-glucaric acid with ultradurable hydrogen via Mn (III) in acidic solution. *Nano Res* **16**, 10748–10755 (2023).

217. Rafaïdeen, T., Neha, N., Kouamé, B. R. S., Baranton, S. & Coutanceau, C. Electroreforming of Glucose and Xylose in Alkaline Medium at Carbon Supported Alloyed Pd3Au7 Nanocatalysts: Effect of Aldose Concentration and Electrolysis Cell Voltage. *Clean Technologies* **2**, 184–203 (2020).

218. Rafaïdeen, T., Baranton, S. & Coutanceau, C. Electroreforming of Glucose/Xylose Mixtures On PdAu Based Nanocatalysts. *ChemElectroChem* **9**, e202101575 (2022).

219. Basu, D. & Basu, S. Synthesis and characterization of Pt-Au/C catalyst for glucose electro-oxidation for the application in direct glucose fuel cell. *Int J Hydrogen Energy* **36**, 14923–14929 (2011).

220. Tonda-Mikiela, P. *et al.* Synthesis of Gold-Platinum Nanomaterials Using Bromide Anion Exchange-Synergistic Electroactivity toward CO and Glucose Oxidation. *J Electrochem Soc* **159**, H828–H833 (2012).

221. Neha, N., Kouamé, B. S. R., Rafaïdeen, T., Baranton, S. & Coutanceau, C. Remarkably Efficient Carbon-Supported Nanostructured Platinum-Bismuth Catalysts for the Selective Electrooxidation of Glucose and Methyl-Glucoside. *Electrocatalysis* **12**, 1–14 (2021).

222. Chen, C. C., Lin, C. L. & Chen, L. C. A binary palladium-bismuth nanocatalyst with high activity and stability for alkaline glucose electrooxidation. *J Power Sources* **287**, 323–333 (2015).

223. Belgsir, E. M. *et al.* Electrosynthesis in aqueous medium: a kinetic study of the electrocatalytic oxidation of oxygenated organic molecules. *Electrochim Acta* **36**, 1157–1164 (1991).

224. Li, D. *et al.* Coupling overall water splitting and biomass oxidation via Fe-doped Ni2P@C nanosheets at large current density. *Appl Catal B* **307**, 121170 (2022).

225. Houache, M. S. E. *et al.* Influence of Pd and Au on electrochemical valorization of glycerol over Ni-rich surfaces. *J Catal* **396**, 1–13 (2021).

226. Creus, J., Miola, M. & Pescarmona, P. P. Unravelling and overcoming the challenges in the electrocatalytic reduction of fructose to sorbitol. *Green Chemistry* **25**, 1658–1671 (2023).

CHAPTER 3

Improved electrocatalytic activity of Pt on carbon nanofibers for glucose oxidation mediated by support oxygen groups in Pt perimeter

Abstract

Support effects in supported metal catalysts are well studied for thermocatalytic reactions, but less studied for electrocatalytic reactions. Here, we prepared a series of Pt supported on carbon nanofiber catalysts which vary in their Pt particle size and the content of oxygen groups on the surface of the CNF. We show that the activity of these catalysts for electrocatalytic glucose oxidation relates linearly with the content of support oxygen groups. Since the electronic state of Pt (XAS) and Pt surface structure (CO-stripping) were indistinguishable for all materials, we conclude that sorption effects of glucose play a crucial role in catalytic activity. This was further confirmed by establishing a relation between the annulus of the Pt particles and the activity.
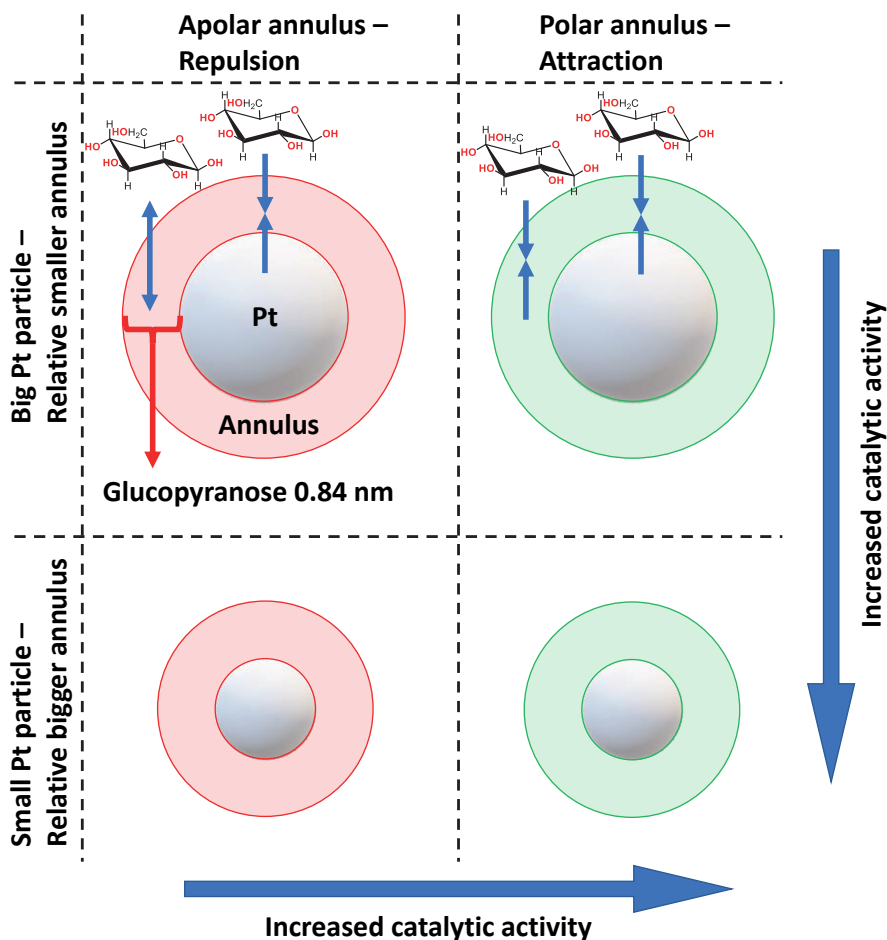
3.1 Introduction

The most promising method for the oxidation of saccharides to various carboxylates is through stoichiometric processes (e.g., with nitric acid), despite the moderate selectivity and emission of hazardous NO_x compounds.[1,2] The development of a green and sustainable production route for the selective oxidation of saccharides has therefore gained great interest. In this regard, electrocatalytic processes have attracted increasing attention, as they can operate under mild reaction conditions (room temperature, neutral pH) and do not require hazardous redox agents.[2] Moreover, in paired electrolysis, the oxidation of saccharides at the anode can be achieved at low potentials and consequently reduce the energy input for hydrogen evolution or CO_2 reduction at the cathode.[3–6] These advances in paired electrolysis are promising for cogenerating energy carriers and value-added platform chemicals, yet significant further steps need to be made to improve the heterogeneous electrocatalyst performance at the anode to bring paired electrolysis for large-scale chemical production a step closer to reality.

There are two distinct approaches to improving the electrocatalyst performance, namely by tuning the properties of the supported catalyst or the properties of the support itself. The former can be tuned by tweaking, among others, the catalyst particle size,[7] modifying the catalyst surface structure,[8,9] encapsulating the catalyst within a polymer layer,[10] adding adatoms[9] or changing the type of metal.[8,11] The second approach involves changing the type of support,[12] modifying the support morphology,[13] doping the support with hetero-atoms,[14] introducing support functionalities.[15] Support functionalities have been widely studied, especially in the field of thermocatalysis, where it has been shown that they can induce various effects on the catalyst properties and consequently its performance.[16]

Thermocatalytic studies have shown that support functionalities can affect the catalyst performance via multiple mechanisms. For example, support functionalities have been shown to affect the support polarity and thus influence the adsorption/desorption rate and the adsorption mode of the reactant on the active phase of the supported catalyst.[17–21] Thereby, it affects the catalyst activity and selectivity, as was shown for the dehydrogenation of cinnamaldehyde over Pt on carbon nanofibers upon removal of acidic support groups.[17,18] Besides, functional groups on carbon supports can change the electron density of the supported catalyst.[22] Similar results were obtained for doping carbon supports with various elements.[23] This change in electron density of the supported catalyst changes in its turn the adsorption/desorption rate of reactants, consequently altering the catalyst performance.[22,23]

On the other hand, support functionalities can play a crucial role in catalytic reactions, as was shown for bifunctional catalysis,[24,25] cooperative catalysis,[26,27] and hydrogen spillover.[28] Bifunctional catalysis on metal-baring carbon supports can occur when support functionalities have their own catalytic role in the chemical reaction.[24,25,29] In contrast, in cooperative catalysis,

the support functionalities can function as a promotor. The promotor can reduce the activation energy barrier of the rate-limiting step, thereby improving the catalyst activity.[26,30] An increase in hydrogen spillover was related to a higher content of quinone groups on the Co/CNT catalyst support and consequently improved the catalyst for Fischer-Tropsch synthesis.[28]

In contrast to this wealth of thermocatalytic studies, the field of electrocatalysis has yielded fewer studies elucidating the role of support functionalities on the performance of supported electrocatalysts.[16] Some effects induced by support functionalities on the electrocatalyst performance have been attributed to a change in charge transfer resistance for heteroatom-doped carbon,[31] a change in proton conductivity and wettability for sulfonated carbon,[32] and an improved adsorption of reactants for nitrogen functionalized carbon.[33] More studies have attempted to elucidate the effect of support oxygen groups on the performance of supported electrocatalysts.[34–39] However, these studies were less systematic, as the support oxygen groups have been modified by (harsh) acid or gas-phase treatments before impregnation.[34–39] This does not only result in the modification of the type and content of support oxygen groups but also other properties of the support and the supported catalyst properties. These multiple modifications made it impossible to relate the effect of support oxygen groups on the catalytic performance of the catalyst.

Therefore, the purpose of the study is to evaluate the effect of support oxygen groups on the performance of supported electrocatalysts, by comparing self-synthesized Pt/CNF catalysts with different types and contents of support oxygen groups and by studying how these support-oxygen groups affect the catalyst activity towards the oxidation of glucose. Additionally, *in-situ* XANES, *ex-situ* XPS, and CO-stripping are performed to determine how these support oxygen groups affect the performance of the supported electrocatalyst.

3.2 Experimental Section

3.2.1 Preparation of carbon nanofibers (CNF)

Ni/SiO$_2$ to be used for the CNF growth (5 wt.% Ni) was synthesized via homogeneous deposition precipitation based on a protocol described by Dillen et al.[40] A slurry of 20 g silica (aerosol 300, Evonik), 5.23 g nickel(II) nitrate hexahydrate (Sigma-Aldrich) and 3.23 g urea (Acros) in 1 L miliQ (MQ) water was acidified to pH = 3 with 68% HNO$_3$ (Merck). The slurry was then stirred at 850 rpm for 18 h at 363 K to yield a gel. The gel was washed three times with MQ water before drying in static air at 383 K for 18 h. The collected material was crushed with a mortar and pestle and sieved to obtain 425-800 µm particles. The resulting material was subsequently calcined in static air at 873 K for 18 h, yielding NiO/SiO$_2$.

The NiO/SiO$_2$ was used to synthesize CNF as described by Toebes et al.[17] 3 g of NiO/SiO$_2$ were placed in a quartz boat in a tubular oven and reduced to Ni/SiO$_2$ at 1 bar and 973 K in 240

ml.min^{-1} N$_2$ and 60 ml.min^{-1} H$_2$ for 2 h (heating ramp 5 K.min^{-1}). After cooling to 823 K the gas flow was switched to 38 ml.min^{-1} H$_2$, 100 ml.min^{-1} CO and 168 ml.min^{-1} N$_2$ for 26 h to grow the CNF. The obtained material was washed three times with 1 M KOH to remove the SiO$_2$. This synthesis methodology by chemical vapor deposition yields high purity CNF supports that are uniform in their porosity, are mesoporous and have a high surface area.[41,42] After washing with water, the material was refluxed in 68% HNO$_3$ for 1.5 h to remove exposed Ni and introduce oxygen-containing groups on the CNF surface, yielding a CNF-ox support. The support material was crushed with a mortar and pestle and sieved to obtain a 90-210 µm particle size fraction, which was used for impregnation.

3.2.2 Impregnation of CNF with Pt

Incipient wetness impregnation was used to load 5 wt.% of Pt on the CNF-ox support. Tetraamine platinum(II) nitrate ([Pt(NH$_3$)$_4$](NO$_3$)$_2$) (Merck) was dissolved in MQ and added dropwise to the support to incipient wetness. In between additions, the sample was vigorously mixed. After impregnation, the catalyst was dried at 383 K and successively calcined at 523 K for 2 h to yield the PtO$_x$/CNF-ox catalyst.

3.2.3 Removal of surface oxygen-containing groups

Pt/CNF catalysts with different amounts of surface oxygen-containing groups were prepared by heat treatments at different temperatures. First, PtO$_x$/CNF-ox (1.0 g) was placed in a quartz boat inside a tubular oven. The oven tube was flushed with H$_2$/N$_2$ (100 ml H$_2$.min^{-1} and 209 ml.min^{-1} N$_2$) for 30 min and heated to 523K for 2 hours (heating ramp 5 K.min^{-1}) to reduce the catalyst. The resulting catalyst is denoted as Pt/CNF-R523. The reduced catalyst was then heat treated in a N$_2$ flow of 266 ml.min^{-1} for 2 h at 573 K or 773 K or 973 K (heating ramp 5 K.min^{-1}), generating Pt/CNF-R573, Pt/CNF-R773, and Pt/CNF-R973, respectively. Finally, the catalysts were ground to a fine powder <75 µm with a mortar and pestle.

3.2.4 Electrode preparation

A glassy carbon electrode (GCE) was used as support. The GCE was polished successively with 3 and 1 µm diamond polish (Buehler) to a mirror finish.[43] Between steps the GCE was sonicated successively in MQ and ethanol and finally washed thoroughly with MQ to remove any organic and inorganic material. After these treatments, the GCE weight was determined accurately on a microbalance. Next, a catalyst ink was prepared by suspending 50 mg Pt/CNF in 200 µl Nafion 1100 W (Sigma-Aldrich, 5 wt. % in lower aliphatic alcohols and water) and 800 µl anhydrous THF (Merck). 30 µl of catalyst ink was drop cast on the GCE. The electrode was air-dried for 5 min and oven dried for another 10 min at 333 K and weighed again (aiming at a 1.5 ± 0.15 mg loading).

3.2.5 Electrochemical oxidation of Pt/CNF

The effect of electrochemical oxidation of the support of Pt/CNF-R523, Pt/CNF-R773 and Pt/CNF-R973 was studied by holding the potential at 1.4 V *vs.* RHE for 30 min in 0.1M H_2SO_4, generating Pt/CNF-R523-EO, Pt/CNF-R773-EO and Pt/CNF-R973-EO (EO = electrochemically oxidized). After this electrochemical glucose oxidation experiments were performed below at $E \leq 1.0$ V *vs.* RHE to avoid the electrochemical oxidation of the CNF support, since the electrochemical oxidation of amorphous and graphitic carbon starts at 0.95 V[44] and 1.2 V *vs.* RHE[45], respectively. Moreover, Pt can accelerate the electrochemical oxidation of graphitic carbon in its annulus.[46,47]

3.2.6 Catalyst characterization

N_2-physisorption was performed at 77 K using a Micromeritics Tristar II Plus to determine the BET surface area, pore volume, and average pore size. The samples were vacuum-dried at 373 K for 2 h before analysis.

Temperature-programmed decomposition coupled to a mass spectrometer (TPD-MS) was performed with a Micromeritics Autochem II 2920 to qualitatively determine the functional groups (surface oxygen-containing groups) of the synthesized catalysts. 100 mg of catalyst was heated to 1173 K at 10 K.min^{-1} under 20 ml.min^{-1} He gas flow. The gasses were analyzed with a THERMOStarTM mass spectrometer from Pfeiffer.

The content of oxygen groups was determined by thermogravimetric analysis (TGA) using a Mettler Toledo TGA/DSC 1. 50 mg of catalyst was placed in a 70 ul alumina crucible and exposed to a 130 ml.min^{-1} N_2 flow. As a reference a N_2 flow of 20 ml.min^{-1} was used. The temperature program consisted of a 5 K.min^{-1} ramp to 373 K, an isothermal period of 30 min followed by a ramp of 5 K.min^{-1} to 1173 K, and a final isothermal period of 5 min. The thermogravimetric curves were processed to obtain the derivative of the thermogravimetric curve (DTG) and used for comparison with TPD-MS data.

X-ray diffraction (XRD) measurements were recorded with a Bruker D8 Advance to characterize the graphitic nature of the CNF support. The system was equipped with an Lynxeye-XE-T PSD detector and a Cu-K$\alpha_{1,2}$ tube generating X-rays with $\lambda = 1.542$ Å. The scans were recorded from $2\theta = 10°$ to $2\theta = 90°$ with a step size of 0.05°.[48]

The Pt loading was quantified thermogravimetrically using the same Mettler Toledo TGA/DSC by complete combustion of the carbon support in air (80 ml.min^{-1}) with a reference gas flow of 20 ml.min^{-1} and temperature program of a ramp of 10 K.min^{-1} to 373 K, an isotherm of 30 min and a ramp of 10 K.min^{-1} to 1173 K. At 1173 K and under air Pt is retained in its metallic state with few oxygen species (5-10%) on the grain boundaries and defective sites.[49]

X-ray photoelectron spectroscopy (XPS) analysis was performed with a Thermo Scientific K-Alpha, equipped with a 180° double-focusing hemispherical analyzer, a 128-channel detector, and a monochromatic small-spot X-ray source. The spectra were collected at a spot size of 400 µm with an aluminum anode (Al Kα=1486.6 eV) operated at 72 W. The data were analyzed with CasaXPS. Two different approaches were used for the wide scans and narrow scans. The wide scans were measured at 200 eV to determine the atomic composition of the Pt/CNF catalysts. For the wide scans, the samples were reduced first in a plug flow reactor at 523 K while keeping it in place with quartz wool (SiO_2) for 2 h under a 209 ml.min^{-1} N_2 flow and a 100 ml.min^{-1} H_2 flow to remove chemisorbed water.[50] The Pt_{4f} and O_{1s} arrow scans were measured at 50 eV to identify the Pt oxidation state present on the support and to determine the relative contribution of different types of support oxygen groups present on the support. For the narrow scans, the samples were characterized without pretreatment to avoid the contamination of the O1s peak with SiO_2.

All the samples were characterized by high resolution transmission electron microscopy (HRTEM) and scanning transmission electron microscopy-high angle annular dark field (STEM-HAADF) using an aberration-corrected FEI Titan^3 Themis 60–300 microscope. The Pt particle size distribution was obtained by counting a minimum of 100 particles. Both the number average Pt particle size and the surface area average Pt particle size were used.

The specific capacitance of the Pt/CNF, an indicator for the content of support oxygen groups, was characterized by cyclic voltammetry (CV).[51] The CVs were recorded between 0.1 and 1.0 V in 0.1 M H_2SO_4 (Merck, Suprapur) solutions at a scan rate of 5 mV.s^{-1}. All electrochemical measurements were performed at room temperature and under oxygen-free conditions in a three-electrode glass cell in which the reference was a RHE, separated from the work compartment by a Luggin capillary.[52] The specific capacitance was calculated from the CV curve according to the following equation:[53,54]

$$C = \frac{\int IEdE}{vm\Delta E}$$

I (A) and E (V) are the current measured and applied potential during the CV, v (V.s^{-1}) is the scan rate, m is the mass of the Pt/CNF loaded on the GCE and ΔE is the potential window of interest.[51]

CO-stripping from Pt/CNF was performed both to clean the catalyst surface from any possible contaminants and to measure the electrochemical surface area (ECSA) of the prepared electrocatalysts before testing their catalytic performance. CO-stripping was performed in 0.1M H_2SO_4 (calculated pH = 1) by holding the potential at 0.1 V *vs.* RHE for 30 min while purging the solution with CO to saturate the Pt surface with CO, after which the solution was purged another 30 min with Ar to remove any dissolved CO. Successively 5 CVs were recorded up to 1.0 V to

avoid dissolution of Pt,[55,56] to avoid restructuring of the Pt particles,[55,56] and to prevent the oxidation of the carbon support.[45] The contribution of CO oxidation from other electrochemical processes was differentiated by subtracting the second anodic scan from the first anodic scan.[57]

In-situ Pt L_{III}-edge HERFD-XANES spectra were collected at beamline 15-2 of the Stanford Synchrotron Radiation Lightsource using a liquid nitrogen-cooled Si(311) double-crystal monochromator. A configuration of two Rh-coated Kirkpatrick–Baez mirrors delivered at the sample position an incident X-ray beam with a full width at half maximum (FWHM) of ~130 x 860 μm^2 (vertical x horizontal) and a photon flux of ~$4x10^{12}$ photons/sec was used. The beam energy was calibrated by assigning a value of 11563.7 eV to the first inflection of a Pt reference metallic foil. The fluorescent X-rays were detected with a high energy resolution using a seven-crystal Johann-type spectrometer.[58] The spectrometer detected the maxima of Pt $L_{\alpha1}$ emission line at a Bragg angle of ~79.95^o and an energy resolution of ~0.8eV by using seven Ge(660) crystals of 100mm diameter, spherically bent with a 1-meter radius of curvature. The advantage of this method has been described before.[48]

The aforementioned protocol was used to acquire *operando* spectra in a homemade, 25-mL volume polystyrene electrochemical cell to which a 0.5-mm thick glassy carbon electrode (HTW-Germany, Sigradur G) working electrode was affixed using a 5-mm diameter hole in the side of the cell. The working electrode contained a small amount of catalyst ink, which was prepared by mixing 30 mg catalyst powder with 200 µL Nafion 1100 W (Sigma-Aldrich, 5 wt. % in lower aliphatic alcohols and water), 480 µL ethanol (Merck, Uvasol) and 320 µL isopropanol (Sigma-Aldrich, for HPLC). Before each experiment, this catalyst ink was ultrasonicated for 1 minute, after which 4 µL was drop cast on the working electrode and air-dried. In addition to this working electrode, the electrochemical cell contained a HydroFlex reversible hydrogen reference electrode (Gaskatel), and a glassy carbon counter electrode (Alfa Aesar, type 1, 5 mm diameter, 100 mm length). Once assembled, the cell was filled with 0.1 M H_2SO_4 (Merck, Suprapur), and the catalyst was cleaned and characterized in a fume hood with carbon monoxide as described in the "Catalyst Characterization" section. Following these steps, the cell was moved to the beamline to collect in-situ X-ray absorption spectra at various electrode potentials. The small (sub-0.2 eV) gradual energy drifts of the monochromator occurred along the multiple days of the experimental study and were accurately corrected by aligning a fixed glitch feature of the monochromator crystals throughout all collected spectra. The collected spectra were successively averaged, flattened, and normalized in ATHENA.[59] Because the spectra were normalized by setting the edge jump to 1, all absorption intensities will be reported in units of 'edge fraction'.[60]

Using HERFD-XANES, the potential-dependent adsorbate coverage on the Pt electrocatalyst surface was calculated using the spectral features caused by each adsorbate. To do so, four

spectral components were defined. The first of these is the spectrum of each catalyst at 0.4 V *vs.* RHE in absence of glucose: this spectrum corresponds as closely as possible to a Pt surface without adsorbates and is therefore referred to as the 'base spectrum'.[61] The remaining three components are the difference spectra that are obtained by subtracting the base spectrum from another spectrum. Specifically, the *OH adsorbate was defined by subtracting the base Pt spectrum from the spectrum obtained at 0.78 V *vs.* RHE (without glucose present). At this potential, Pt is covered by *OH,[61] such that the resulting difference spectra can be taken as the fingerprint for adsorbed *OH. The *glucose adsorbate was defined by subtracting the base Pt spectrum from the spectrum at 0.1 V *vs.* RHE in the presence of 0.1 M glucose. Under these conditions, the Pt surface is likely to be fully covered by *glucose and its decomposition products.[62–64] Therefore, the resulting difference spectrum is a proxy for the coverage of glucose-derived species. Finally, the PtO_x species was defined as the difference spectra taken from Pt at 1.0 V *vs.* RHE (with glucose present), whence the Pt surface is free of adsorbates.[64] The Pt adsorbate coverages were extracted by fitting a combination of the base spectrum, the *OH difference spectrum, the *glucose difference spectrum, and the PtO_x difference spectrum to the experimental XANES spectra. This approach, also known as linear combination analysis (LCA), yields an estimate of the relative coverages of each adsorbate.

3.2.7 Performance testing

The performance of the catalyst, after CO-stripping (described in the "Catalyst Characterization" section), was studied by linear sweep voltammetry (LSV) and by chronoamperometry (CA) in 0.1M H_2SO_4. LSV was conducted from 0.1 to 1.0 V vs RHE with a scan rate of 1 $mV.s^{-1}$. First a blank (i.e., all components except glucose were present in the reactor) LSV was measured, after which 0.1M glucose (99.5%, Merck) was added. The system was purged for 30 min with Ar to ensure a homogeneous solution before repeating the LSV with glucose. The currents measured for glucose oxidation reported in this study for LSV are an average of two experiments and have been corrected by the blank for surface charging.[65] A similar procedure was used for CA as was used for LSV, namely a blank measurement, followed by 0.1M glucose addition, purging the system for 30 min, and another measurement in the presence of glucose.

3.3 Results & Discussion

The results and discussion section has been subdivided into three individual sections that discuss the characterization of the support oxygen groups on the different Pt/CNF catalysts (3.3.1) and the characterization of the platinum supported on the carbon nanofiber catalysts (3.3.2). These sections were used as a basis to evaluate the performance of the different Pt/CNF catalysts for the electrocatalytic oxidation of glucose (3.3.3).

3.3.1 Characterization of support oxygen groups on different Pt/CNF catalysts

Table 3.1 shows a summary of the content of support oxygen groups determined by TGA (weight %, see Figure S3.1 for details) and XPS (O/C ratios, see Table S3.1 and Figure S3.2 for details) and the number of oxygen groups normalized per surface area (atoms.nm^{-2}, using the BET surface area of 187 m^2.g^{-1} for bare CNF-ox, see Table S3.2 and Figure S3.3 for details) as has been done before.[66] The BET surface area of Pt/CNF-ox and Pt/CNF-R973 are similar (Table S3.2), indicative that the heat treatment does not affect the surface structure of the synthesized catalysts.[18]

TGA shows that the number of support oxygen groups decreased from 6.6 oxygen atoms.nm^{-2} for PtO$_x$/CNF-ox to 5.0 oxygen atoms.nm^{-2} for Pt/CNF-R523. Successive heat treatment steps resulted in a gradual decrease in support oxygen groups to 1.5 oxygen atoms.nm^{-2} for the sample heat-treated at 973 K which is in line with earlier studies.[54,66]

XPS shows a decrease in support oxygen groups from 6.8 oxygen atoms.nm^{-2} for Pt/CNF-R523 to 4.1 oxygen atoms.nm^{-2} for Pt/CNF-973 K. XPS and TGA show a difference in absolute values for the support oxygen groups content, which can be explained by the difference in analytical technique (e.g., probing depth). As a result, XPS is less affected by the decomposable surface oxygen groups.[67,68] Nonetheless, XPS shows a similar trend to that observed by TGA, namely a decrease in support oxygen group content for catalysts exposed to higher thermal treatments.

Table 3.1. *The total number of oxygen groups on the support (O-atoms.nm^{-2}) of the synthesized Pt/CNF catalysts as a function of reduction treatment (Pt/CNF-R523) and heat treatment (Pt/CNF-R523 to Pt/CNF-R973) determined by TGA and XPS and the weight fraction of oxygen groups (wt. %) decomposed above 673 K determined by TGA.*

Catalyst	TGA			XPS	
	Weight loss (%)		O-atoms. nm^{-2}	O/C atomic ratio	O-atoms. nm^{-2}
	Total	> 673 K	Total	Total	Total
PtO$_x$/CNF-ox	5.8	4.1 ± 0.1	6.6 ± 0.1	-	-
Pt/CNF-R523	4.4	3.5 ± 0.1	5.0 ± 0.3	0.054	6.8 ± 0.6
Pt/CNF-R573	4.2	3.3 ± 0.0	4.9 ± 0.0	0.037	4.9 ± 0.7
Pt/CNF-R773	3.3	2.6 ± 0.1	3.8 ± 0.4	0.030	3.8 ± 0.6
Pt/CNF-R973	1.3	0.9 ± 0.1	1.5 ± 0.3	0.032	4.1 ± 0.0

The nature of the support oxygen groups on the Pt/CNF catalysts was characterized by TPD-MS (Figure S3.4), DTG (Figure S3.5), and O$_{1s}$ XPS spectra (Figure S3.6 and Table S3.3). The parent catalyst, PtO$_x$/CNF-ox, was found to bear carboxylic acids, anhydrides, lactones, phenols and carbonyls/quinones.[28,50,54] After a reduction step at 523 K, the carboxylic acids, anhydrides,

carbonyl groups adjacent to ketones and aldehydes are removed,[28,50,54] indicative that Pt/CNF-R523 only bares lactone, phenol and carbonyl/quinone surface groups. With an increase in the heat treatment step, the content of lactone, phenol and carbonyl/quinone surface groups is gradually reduced.[28,50,54]

The graphitic nature of the bare CNF-ox support and of Pt/CNF-R573 and Pt/CNF-R973 (e.g., subjected to mild and high heat treatment temperatures) was characterized by XRD (Figure S3.7). No significant difference was found between the graphitic nature of Pt/CNF-R573 and Pt/CNF-R973, indicative that it was not affected by the heat treatment.[48] The electrochemical properties of the support oxygen groups were studied by CV in 0.1M H_2SO_4. Figure 3.1A shows the weight normalized steady-state CV (the fourth CV after CO-stripping) for the different catalysts. For PtO_x/CNF-ox, in the forward scan, three oxidative peak currents can be observed, while in the backward scan, only two cathodic peak currents can be observed. In the forward scan, peak 1 from 0.1 to 0.3 V *vs.* RHE is attributed to the desorption of hydrogen from Pt,[55] while peak 2 from 0.4 to 0.8 V *vs.* RHE represents the oxidation of phenol/hydroquinone surface groups to lactone and carbonyl/quinone groups,[54,69] and peak 3 from 0.8 to 1.0 V *vs.* RHE is related to the oxidation of metallic Pt to PtO_x.[55] In the backward scan, peak 4 from 0.8 to 0.4 V *vs.* RHE represents both the reduction of PtO_x to metallic Pt[55] and the reduction of lactone and carbonyl/quinone support oxygen groups to phenol/hydroquinone groups,[69] while peak 5 below 0.4 V *vs.* RHE is related to hydrogen adsorption on Pt.[55] The redox reaction of carboxylic acid groups could not be observed from the CV of PtO_x/CNF-ox since the redox potential of these groups is between 1.1 to 1.6 V *vs.* RHE.[69] Thus, from the CVs it can be concluded that all catalysts bare electroactive Pt nanoparticles and redox-active phenol and hydroquinone support oxygen groups, confirming the results obtained by TGA, XPS, and TPD-MS.

The CV in Figure 3.1A shows that peak 2 and peak 4 are similar in intensity for PtO_x/CNF-ox and Pt/CNF-R523, thereby indicating that the reduction step at 523 K does not change the content of lactone, phenol and carbonyl/quinone groups on the catalyst support. The successive heat treatment step, going from Pt/CNF-R523 to Pt/CNF-R973, results in a gradual decrease of peaks 2 and peak 4. This shows the gradual removal of lactone, phenol and carbonyl/quinone groups from the support as a result of increasing treatment temperature. The charge related to the oxidation of these support oxygen groups[55,69] is also known as the pseudocapacitance and can increase the specific capacitance (e.g., pseudocapacitance plus double layer charging) of the Pt/CNF catalysts.[51,70]
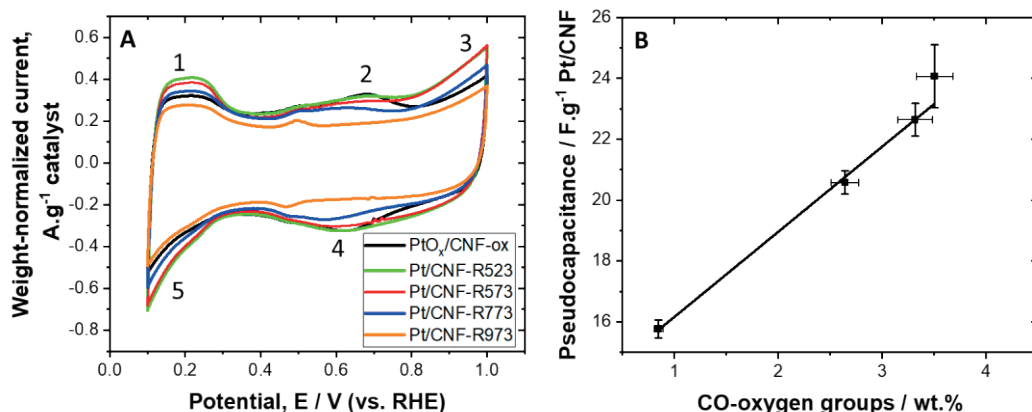
Figure 3.1. *A) Cyclic voltammograms of Pt/CNF catalysts in 0.1 M H_2SO_4 at a scan rate of 5 mV.s^{-1} and B) the relation between the pseudocapacitance of the Pt/CNF catalysts derived from CV as a function of the content of CO-oxygen groups (phenols and carbonyls/quinones) determine by TGA (R^2 = 0.99).*

It has been shown before that the specific capacitance is related to the content of phenol and carbonyl/quinone groups present on the support.[51,70] To study this relation the specific capacitance was derived from the currents measured at peak 2 (0.4-0.8 V *vs.* RHE) from the anodic scan[54] was plotted as a function of the content of lactone, phenol and carbonyl/quinone support groups (thermogravimetrically measured oxygen groups decomposed above 673 K, given in Table 3.1) in Figure 3.1B.[70] This graph shows a linear correlation between the specific capacitance and the number of oxygen groups that decompose above 673 K (lactone, phenol and carbonyl/quinone groups), confirming the presence of these support oxygen groups under electrochemical conditions.

3.3.2 Characterization of platinum supported on carbon nanofiber catalysts

In addition to the change in CV features related to the content of oxygen groups on the carbon support, also a change in CV features related to Pt on the carbon support can be observed (Figure 3.1A, peaks 1, 3 and 5). After the first reduction step, going from PtO$_x$/CNF-ox to Pt/CNF-R523, an increase in these peaks can be observed. This indicates that for Pt/CNF-R523 there is a larger exposed Pt surface area available for hydrogen adsorption/desorption or that the PtO$_x$/CNF-ox bears a certain amount of electrochemically inactive Pt which is still partially oxidized (Figure S3.8) and therefore exposes fewer metallic Pt sites for hydrogen adsorption/desorption, even after several oxidative and reductive cycles. A similar low uptake for a low-temperature reduced Pt/CNF was found by Toebes et al. and low-temperature heat-treated Pt/CNT was found by Jiang et al.[66,71] The difference in Pt oxidation state between PtO$_x$/CNF-ox and Pt/CNF-R523 makes it

impossible to relate changes in support oxygens between these two catalysts to a change in catalyst performance. Therefore, PtO_x/CNF-ox has been omitted from further discussions.

In Figure 3.1A it can also be observed that an increase in heat treatment temperature, going from Pt/CNF-R523 to Pt/CNF-R973, results in a decrease of peaks 1, 3 and 5. The decrease in these peaks suggests that the exposed Pt surface area gradually decreases with increasing heat treatment temperature.[71,72] This can be explained by sintering of Pt particles at elevated temperatures, thereby increasing the average Pt particle size,[72] as will be discussed now (Table 3.2).

Table 3.2 shows the metal loading determined by TGA, the ECSA of the synthesized catalysts determined by CO-stripping, and the average Pt particle size derived from the ECSA and HAADF-STEM.[56]

The metal loading of the catalysts was determined by TGA using combustion up to 1173 K. For all the catalysts the metal loading was found to be between 5.2-5.6 wt.%, thus showing that the metal loading is consistent.

The ECSA of the catalysts were calculated from CO-stripping curves, as will be discussed later (*vide infra*, Figure 3.4), assuming a charge of 420 mC.cm^{-2} for the oxidation of a monolayer of linearly adsorbed CO.[73] With an increase in heat treatment, going from Pt/CNF-R523 to Pt/CNF-R973, the ECSA decreases gradually from 215 to 138 cm^2 Pt.g^{-1} Pt/CNF, corresponding to an increase in average Pt particle size from 1.5 to 2.3 nm.[72] These results coincide with the observations made for the decrease in hydrogen adsorption/desorption and platinum oxidation peaks (Figure 3.1A).

The surface area average Pt particle size derived from HAADF-STEM images shows an increase in surface area average Pt particle size for Pt/CNF-R523 from 1.7 nm to 2.3 nm for the sample heat-treated at 973 K. The surface area average Pt particle size determined by HAADF-STEM matches well with the ECSA derived by CO-stripping. This shows that the Pt/CNF catalysts were well wetted, otherwise the values from Pt particle size derived from ECSA should have been significantly larger than from HAADF-STEM.

Table 3.2. *The Pt load, the surface area average Pt particle size based on HAADF-STEM imaging, the average Pt particle size derived from the ECSA, and the ECSA of the synthesized Pt/CNF catalysts.*

Catalyst	TGA	CO-stripping		HAADF-STEM
	Pt loading	Pt surface area	Pt particle size	Surface based Pt particle size
	(wt.%)	(cm^2 Pt.g^{-1} Pt/CNF)	(nm) [a]	(nm)
Pt/CNF-R523	5.5	215 ± 4	1.5	1.7
Pt/CNF-R573	5.6	219 ± 2	1.5	-
Pt/CNF-R773	5.2	187 ± 2	1.7	2.2
Pt/CNF-R973	5.4	138 ± 6	2.3	2.3

[a] The average Pt particle size was calculated from the ECSA based on the relation d = 6 x 10^3 / (ECSA x ρ), where ρ is the density of Pt (21.45 g/cm^3).

HAADF-STEM images were analyzed to evaluate the surface area average and number average Pt particle sizes including Pt particles < 1.5 nm. The HAADF-STEM images (Figure 3.2A and Figure S3.9A-B) reveal that the Pt particles are homogeneously distributed over the carbon nanofiber support. The number average Pt particle size distribution in Figure 3.2B shows a log-normal distribution for the Pt particle with a size range between 0.5-3 nm and a few particles >3.5 nm. With increasing heat treatment temperature, a shift in the log-normal distribution towards larger Pt particles can be observed, caused by sintering of Pt.[74]
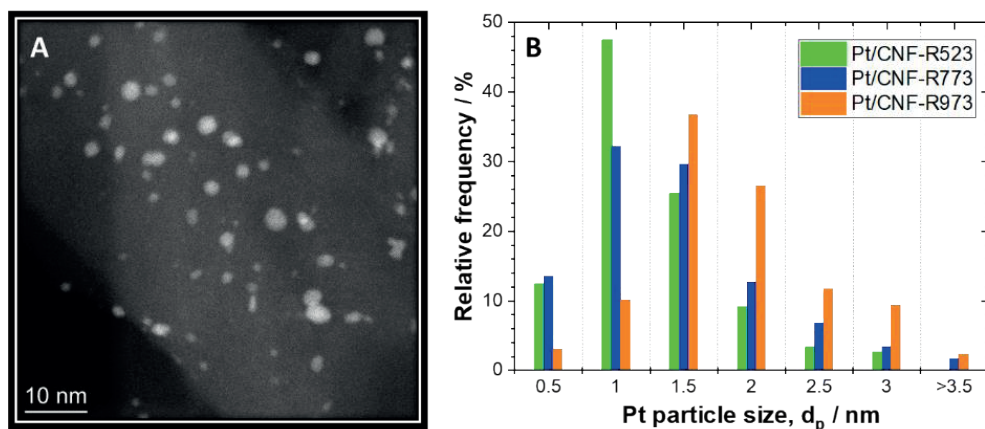
Figure 3.2. *A) HAADF-STEM images of Pt/CNF-R523 and B) the relative frequency of the number average Pt particle size measured on the CNF supports for various catalysts.*

Besides the ECSA, CO-stripping was performed to determine the surface properties of the different Pt/CNF electrocatalysts. The background corrected CO-stripping curves are given in Figure 3.3.[57]

The CO-stripping curves in Figure 3.3 show for all the catalysts one main peak around 0.8 V, while for Pt/CNF-R973 there is also a preceding plateau between 0.4 V and 0.7. This plateau is related to CO oxidation at surface defects (kinks and step sites),[75,76] indicative that the high temperatures to which Pt/CNF-R973 has been exposed resulted in some surface defects on the Pt surface. The main peak is by far the main contributor to CO oxidation and appears to compose of a single peak, which indicates that the Pt nanoparticles of all the catalysts have a similar surface structure.[75–77]
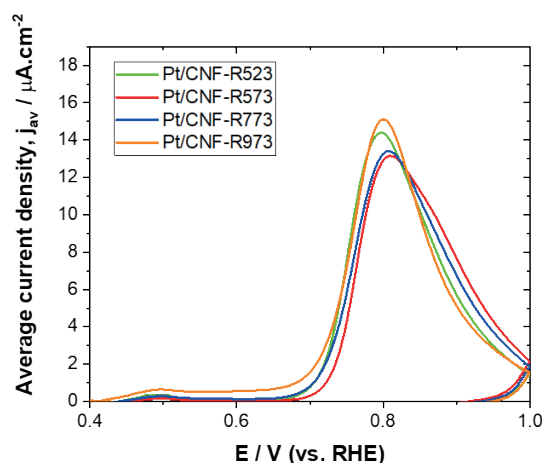
Figure 3.3. *Background corrected CO-stripping curves corrected for of Pt/CNF catalysts obtained in 0.1 M H₂SO₄ recorded at 5 mV.s⁻¹.*

Figure 3.4 displays the *in situ* HERFD-XANES spectra of Pt/CNF-R523, Pt/CNF-R773, and Pt/CNF-R973 recorded at 0.4 V *vs.* RHE in 0.1 M H_2SO_4. All XANES spectra show similar features and Pt/CNF-R523 will be discussed in detail as a representative example. The spectrum of Pt/CNF-R523 shows the main adsorption peak (the whiteline) at 11564.5 eV, which is typical for Pt.[61] The absorption intensity increases from 2.23 to 2.48 when stepping the electrode (Figure S3.10A) from 0.1 to 0.78 V *vs.* RHE. This corresponds to an increase in unoccupied d-character states of the Pt catalyst and can be related to the adsorbed species on Pt at various potentials.[61,78,79] At 0.1 V *vs.* RHE, Pt is covered with *H, which causes antibonding states, yielding a broadened and lowered whiteline.[61] As the potential is increased to 0.4 V *vs.* RHE, this *H is replaced by *OH adsorbed at the top of Pt step edges and corners.[61,78] With a further increase in potential to 0.64 V and 0.78 V *vs.* RHE, the surface coverage of *OH increases through adsorption at the bottom of step edges and concave sites, thereby increasing absorption.[61,79] Thus, the replacement of *H

with *OH and the successive gradual increase in *OH coverage increases the number of unoccupied d-states of the Pt catalyst.

For the different Pt/CNF catalysts, the whiteline gives a similar trend (Figure 3.4A), as a function of the applied potential (Figure S3.10A-C), and therefore shows a similar oxidation state. The similarity in the Pt oxidation state on the CNF support functionalized with various amounts of support oxygen groups and different Pt particle sizes are in accordance with XPS Pt_{4f} scan (Figure S3.11 and Table S3.4). This similarity in the Pt oxidation state for the different Pt/CNF catalysts indicates that the electronic property of Pt is not significantly affected by the Pt particle size or by the presence of lactone, phenol and carbonyl/quinone support oxygen groups, which is in line with thermocatalytic research.[78,79]

Moreover, Pt/CNF-R523 has a significant amount of reduced support oxygen groups (hydroxyls) at 0.4 V *vs.* RHE and oxidized support oxygen groups (carbonyls) at 0.78 V *vs.* RHE present on the support (discussed in Figure 3.2A), while Pt/CNF-R973 bears hardly any support oxygen groups. Therefore, the agreement between the Pt spectral shapes of those two catalysts recorded at 0.4 V *vs.* RHE and 0.78 V *vs.* RHE, as well as the close resemblance of their corresponding Δμ spectra (S10G and S10I) indicates that the electronic structure of the electrochemically accessible Pt species is not affected by the oxidized nor the reduced state of the lactone, phenol and carbonyl/quinone oxygen groups present on the support.
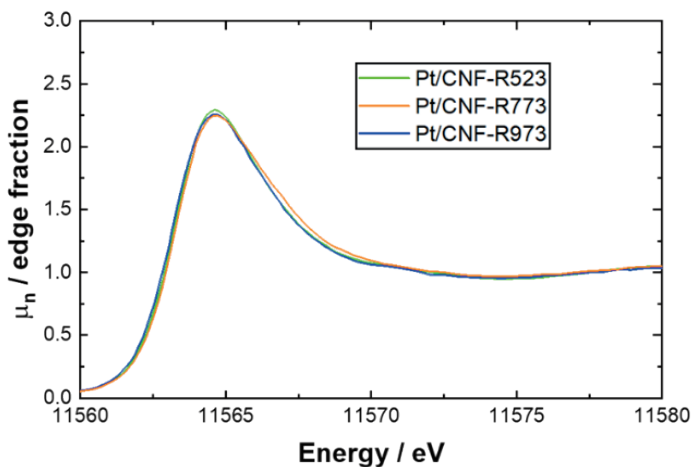
Figure 3.4. *Pt L$_{III}$-edge HERFD-XANES spectra of Pt/CNF catalysts measured in 0.1M H$_2$SO$_4$ at 0.4 V vs. RHE hold potential.*

3.3.3 Electrocatalytic oxidation of glucose
The four different Pt/CNF catalysts were tested for their activity toward the electrocatalytic oxidation of glucose. Linear sweep voltammetries of a bare CNF support in the absence and

presence of glucose can be found in Figure S3.12, which shows that bare CNF is inactive for catalyzing glucose oxidation reactions. The catalyst activity for the electrocatalytic oxidation of glucose was studied by background-corrected linear sweep voltammetry in 0.1M H_2SO_4 (Figure 3.5A). The background-corrected linear sweep voltammetries were derived from the linear sweep voltammetries in the presence and absence of glucose (Figure S3.13).

The linear sweeps of the different Pt/CNF catalysts show three oxidation peaks at 0.45 V (peak 1), 0.62 V (peak 2) 0.78 V (peak 3). Peak 1 is related to dehydrogenative adsorption of glucose at the anomeric carbon (RCHOH → $R\dot{C}OH_{ads}Pt + H^+ + e^-$) as was shown for alkaline and acidic media.[80–82] Peaks 2 and 3 have been attributed to the electrocatalytic oxidation of glucose oxidation products,[83] which can either be the oxidation of the adsorbed glucose to an adsorbed gluconolactone ($R\dot{C}OH_{ads}Pt \rightarrow R\dot{C}=O_{ads}Pt$)[84] or the oxidation of gluconolactone itself.[82] Alternatively, these two peaks also suggest that there are glucose oxidation products weakly (peak 2) and strongly (peak 3) adsorbed to the Pt surface, which is indicative of the presence of different Pt facets.[83,85,86] From the linear sweep voltammograms and up to 0.5 V it can be observed that the current densities are similar for all catalysts. This indicates that the catalyst activity is similar for all the catalysts up to this point and that the catalyst activity towards glucose dehydrogenation is not affected by the difference in catalyst properties. Above 0.5 V and up to 0.9 V, going from Pt/CNF-R523 to Pt/CNF-R973, a gradual decrease in current density is observed. This points to a decrease in catalytic activity for catalysts that have been exposed to higher heat treatment temperatures.
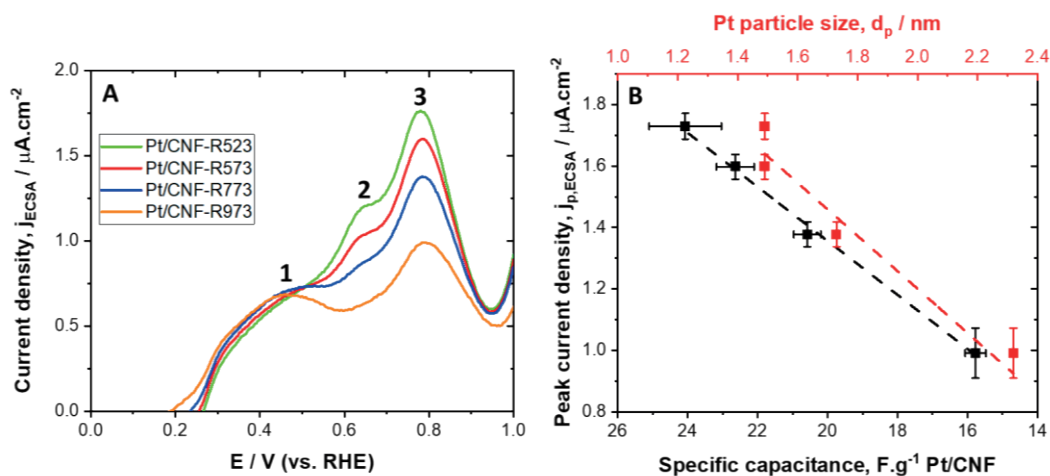
Figure 3.5. *A) Background corrected linear sweep voltammetry measured in 0.1M H_2SO_4 in the presence of 0.1M glucose at 1 mV.s^{-1} and B) the corresponding peak current density measured by LSV at 0.78 V vs. RHE as a function of the specific capacitance (R^2 = 0.99) and Pt particle size (R^2 = 0.90) of the Pt/CNF electrocatalysts.*

To evaluate whether the change in catalytic activity does not originate from diffusion limitation a similar experiment was performed, but then under convection with increased glucose concentration (Figure S3.14). Under these reaction conditions, the current density went up by the same order of magnitude (2.7 and 3.5-fold for Pt/CNF-R523 and Pt/CNF-R973 respectively), which indicates that both systems suffer from similar extents of diffusion limitations which thus still allows us to compare catalytic activities.

To evaluate where the difference in catalytic activity originates from, the peak current densities measured by LSV at 0.78 V (j_p, Figure 3.5B) have been plotted against the specific capacitance and the average Pt particle diameter (derived from the ECSA) of the Pt/CNF catalysts. Both the Pt particle size and the specific capacitance show a linear correlation with the peak current density. This indicates that both changes in catalyst properties might affect the catalyst activity. However, a change in ECSA-normalized catalytic activity induced by a difference in particle size would require a difference in electronic properties of the Pt particles or a difference in Pt surface structure for the different Pt/CNF catalysts. Yet, a difference in electronic properties was not found by *in-situ* HERFD-XANES (Figure 3.4) and Pt_{4f} XPS (Figure S3.11 and Table S3.4), nor was a difference in Pt surface structure found by CO-stripping (Figure 3.3). Therefore, a change in catalytic activity should be related to a change in specific capacitance which in turn influences reactant/product adsorption. Since the specific capacitance is strongly related to the lactone, phenol, and carbonyl/quinone groups present on the support (Figure 3.1B),[51,70] we argue that the presence of these support oxygen groups influences the catalytic performance. The fact that this increase in activity can only be seen at $E \geq 0.5$ V *vs.* RHE might originate from the nature of the support oxygen groups, namely, at $E \geq 0.5$ V *vs.* RHE (determined by CV, Figure 3.1A) the support oxygen groups are oxidized to C=O groups.[69] These C=O groups could promote the formation of hydrogen bridges with the C-H and C-OH groups of glucose and thereby improve the adsorption of glucose in the annulus of the Pt nanoparticles, consequently increasing the catalyst activity. Therefore, we argue that the enhanced adsorption of glucose mediated by oxidized support oxygen groups increases the number of glucose molecules in vicinity of the Pt catalysts and thereby improves the catalyst activity.

Chronoamperometry was performed at 0.78 V *vs.* RHE to evaluate whether the difference in catalytic activity observed by LSV is not a temporary effect but also remains during longer reaction times (Figure 3.6A) and to gain initial insights on the catalyst selectivity. Regarding the catalyst selectivity, preliminary results indicate that all catalysts predominantly form gluconic acid (>80 %).[87] After 30 min and going from Pt/CNF-R523 to Pt/CNF-R973, a gradual decrease in current density can be observed. This decrease in current density shows that catalysts exposed to higher heat treatment temperatures have lower catalytic activity, confirming the results made by LSV. Moreover, this difference in current densities after 30 min of CA shows that the variance in catalytic activity is not a temporary effect.
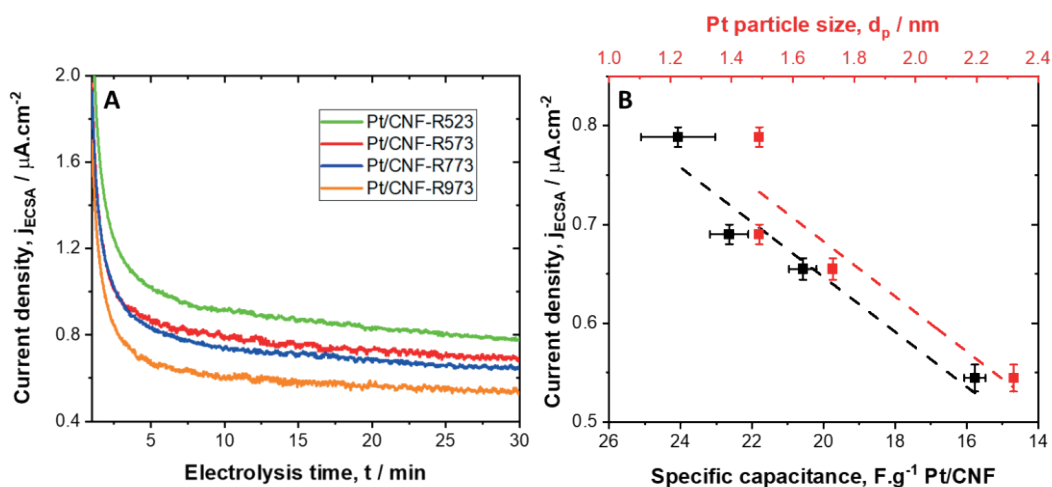
Figure 3.6. *A) Background-corrected current densities measured in 0.1M H_2SO_4 in the presence of 0.1M glucose at 0.78 V vs. RHE and B) the corresponding current density measured after 30 min chronoamperometry as a function of the specific capacitance ($R^2 = 0.91$) and Pt particle size ($R^2 = 0.76$) of the Pt/CNF electrocatalysts.*

The current densities measured after 30 min CA have been plotted against the specific capacitance and the Pt particle size for the Pt/CNF catalysts in Figure 3.6B to re-evaluate the origin of the difference in catalytic activity. Once again, the specific capacitance (e.g., the content of lactone, phenol and carbonyl/quinone support oxygen groups) has a linear correlation with the catalyst activity, thereby confirming the results obtained by LSV.

The most accepted reaction mechanism requires both the adsorption of glucose and hydroxyls on the Pt surface before glucose can be catalytically oxidized by Pt. The ratio between different adsorbates can influence the catalyst activity. This adsorbate coverage can be estimated from the XANES spectra and the associated difference XANES spectra[64,88] by using LCA, which is based on Figure S3.10A-L. The estimate of the relative coverages of each adsorbate for three different Pt/CNF catalysts is shown in Figure 3.7A-C.
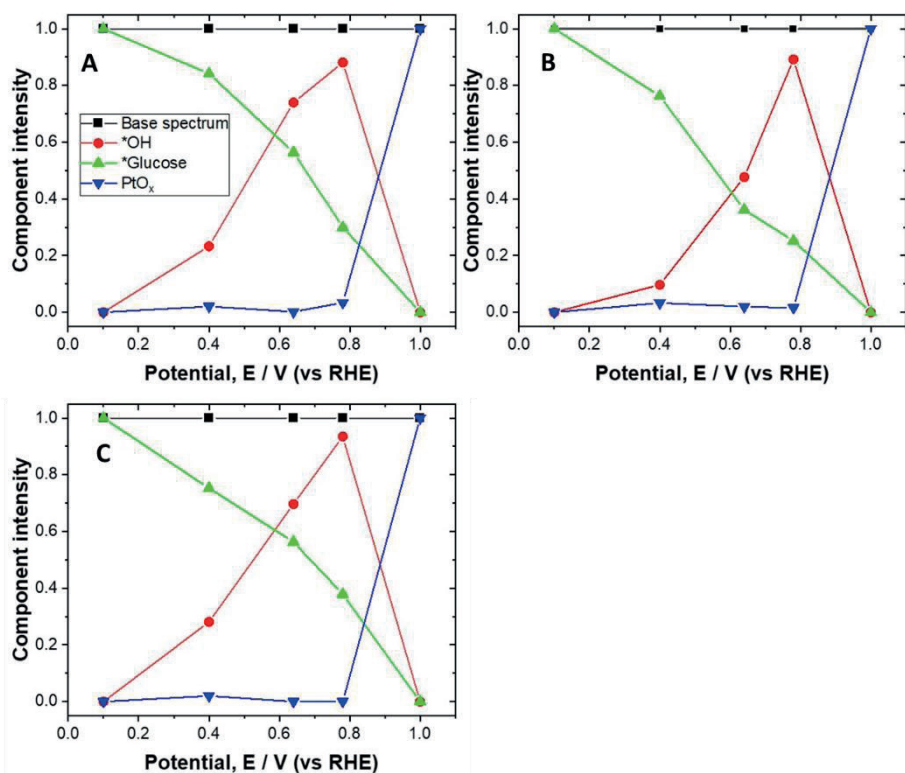
Figure 3.7. *Results of LCA of HERFD-XANES spectra at Pt L$_{III}$-edge obtained at various hold potentials in 0.1M H$_2$SO$_4$ and 0.1 M glucose for Pt/CNF-R523 (A), Pt/CNF-773 (B) and Pt/CNF-R973 (C).*

Figure 3.7A compares the calculated intensity for each adsorbate component in the fitting results of a Pt/CNF-R523 catalyst as a function of potential. At 0.1 V *vs.* RHE and in the presence of 0.1M glucose, the surface of Pt is free of adsorbed *OH and completely covered with adsorbed *glucose. This is a direct result of the methodology for estimating the coverage of species since the spectrum at 0.1V *vs.* RHE in the presence of glucose corresponds to the base spectrum of Pt and the *glucose difference spectrum. As the potential is increased to 0.78 V *vs.* RHE, the content of adsorbed *glucose gradually decreases, while the content of *OH increases. This indicates that *OH adsorbates replace the adsorbed *glucose at higher potentials, which agrees with the results reported for the adsorbate coverage in ethanol oxidation of Pt electrodes. [64,88] A successive increase in potential to 1.0 V results in a loss of adsorbates due to the formation of a PtO$_x$ species. Also, this is a direct result of the methodology for estimating the coverage of species, since the spectrum at 1.0 V *vs.* RHE in the presence of glucose corresponds to the base spectrum of Pt and PtO$_x$ difference spectrum. [64] Here it is argued that the PtO$_x$ species causes the

desorption of adsorbates, resulting in a loss in catalytic activity of Pt in acidic media, which coincides with a decrease in catalytic activity as was shown in Figure 3.5A.[89]

A similar trend of adsorbates as a function of potential for Pt/CNF-R523 can be observed for Pt/CNF-R773 and Pt/CNF-R973 (Figure 3.7A-C), which indicates that the potential-dependent adsorbate coverage is similar between these Pt/CNF catalysts. Hence, the ratio between adsorbates present on the Pt surface for the Pt/CNF electrocatalysts is not affected by the content of lactone, phenol and carbonyl/quinone support oxygen groups. In other words, the steady state of the Pt surface is the same for all measured catalysts. Nonetheless, an increase in catalytic activity was observed for Pt/CNF catalysts with higher contents of lactone, phenol and carbonyl/quinone support oxygen groups (Figure 3.5B and 3.6B). This indicates that the improved catalytic activity induced by support oxygen groups is likely to originate from improved glucose turnover. We suggest that this improvement stems from accelerated reactant adsorption in the annulus of the Pt particles, caused by the formation of hydrogen bridges between C=O support groups ($E \geq 0.5$ V $vs.$ RHE) and C-H and C-OH groups of glucose. As a result, the content of reactive species increases in the annulus of the Pt particles. This hypothesis will be quantified in the following section, where electrochemically oxidized Pt/CNF-R523 and Pt/CNF-R973 will be used as a base case scenario.

Pt/CNF-R523, Pt/CNF-R773 and Pt/CNF-R973 were electrochemically oxidized to Pt/CNF-R523-EO, Pt/CNF-R773-EO and Pt/CNF-R973-EO to re-introduce support oxygen on the carbon support. On the one hand, CO-stripping (Figure S3.15) showed that the electrochemical oxidization of the catalysts did not induce significant changes in the ECSA and resulted in catalysts with similar Pt surface structures. On the other hand, CV (Figure S3.16) showed that the specific capacitance increased sufficiently to oxidize the carbon support in the annulus of the Pt particles.

The activity towards the electrooxidation of glucose was evaluated by LSV for Pt/CNF-R523, Pt/CNF-R773 and Pt/CNF-R973 before and after electrochemical oxidation (Figure 3.8). After electrochemical oxidation, all three catalysts show a significant increase in current density above 0.5 V $vs.$ RHE compared to their non-oxidized counterparts. At 0.78 V $vs.$ RHE going from Pt/CNF-R523 to Pt/CNF-R523-EO, the current density increases from 1.8 to 3.0 $\mu A.cm^{-2}$, while the current density from Pt/CNF-R773 to Pt/CNF-R773-EO increases from 1.4 to 2.7 $\mu A.cm^{-2}$, and the current density from Pt/CNF-R973 to Pt/CNF-R973-EO increases from 1.0 $\mu A.cm^{-2}$ to 2.4 $\mu A.cm^{-2}$. For Pt/CNF-R523, Pt/CNF-R773 and Pt/CNF-R973, this increase in current density corresponds to an increase in catalytic activity of 72, 93 and 144 % respectively. This increase in catalytic activity after electrochemical oxidation of the Pt/CNF catalyst indicates that the introduction of support oxygen groups improves the catalyst activity. The increasing trend in catalytic activity (e.g., 72 to 93 to 144 %) induced by electrochemical oxidation can be attributed to the decreasing content

in support oxygen groups before electrochemical oxidation, going from Pt/CNF-R973 to Pt/CNF-R523.
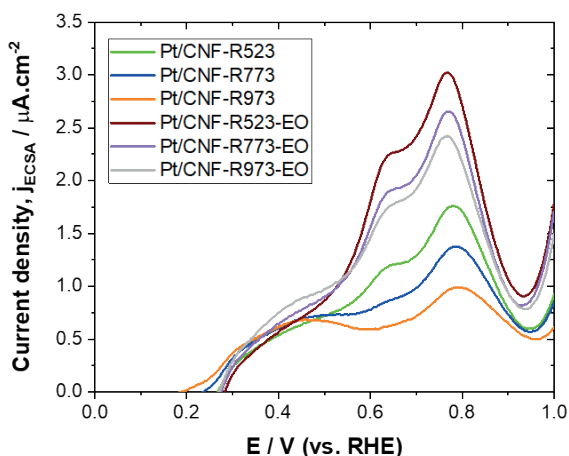
Figure 3.8. *Background corrected linear sweep voltammetry measured at 1 mV.s⁻¹ in 0.1M H₂SO₄ and 0.1M glucose for pristine Pt/CNF-R523, Pt/CNF-R773 and Pt/CNF-R973 and Pt/CNF-R523-EO, Pt/CNF-R773-EO and Pt/CNF-R973-EO.*

Table 3.3 gives an overview of the reaction conditions and the measured current densities for the electrocatalytic oxidation of glucose on Pt electrodes in acidic medium reported in this study and literature.[87,90,91] Considering the difference in scan rates, the current density reported in this study of Pt/CNF-R523-EO corresponds well with the current densities (e.g., catalytic activity) reported in the literature.

Table 3.3. *Summary of current densities reported in the literature for the electrocatalytic oxidation of glucose on Pt in acidic medium.*

Catalyst	Technique	Electrolyte	Glucose conc. M	Scan rate mV.s⁻¹	Current density µA.cm⁻²	Reference
Pt/CNF-R523-EO	LSV	0.1 M H₂SO₄	0.1	1	3	This work
Pt/C	CV	0.1 M HClO₄	0.1	20	18	[90]
Pt	CV	0.1 M HClO₄	0.1	50	55	[91]
Pt	CV	0.1 M HClO₄	0.2	50	55	[87]

Generally, the measured current is normalized by the active surface area of the supported metallic catalyst (ECSA), to compare the catalytic activity of two different catalysts. However, the

presence of oxygen groups on the carbon support can facilitate the adsorption of reactants in the annulus of the Pt particles,[19,68] which increases available species in proximity of the metal catalyst that are susceptible to conversion (Figure 3.9) and can thereby improve the catalyst activity. In line with this reasoning, the measured currents were normalized by both the active surface area of the metallic catalyst and the annulus around the perimeter of the catalyst nanoparticles (ASA = ECSA + annulus area). The surface area of the annulus can be calculated with the inner radius of the annulus (r) and the outer radius of the annulus (R), where r = Pt nanoparticle radius and R = Pt nanoparticle radius + length of glucopyranose (0.84 nm) (calculations in supporting information "Current normalization by adsorbable surface area"). Based on these considerations, the ASA changes with the radius of the Pt nanoparticles, where smaller Pt nanoparticles (Pt/CNF-R523-EO) are more influenced by the annulus surface area than larger Pt particles (Pt/CNF-R973-EO), illustrated in Figure 3.9.
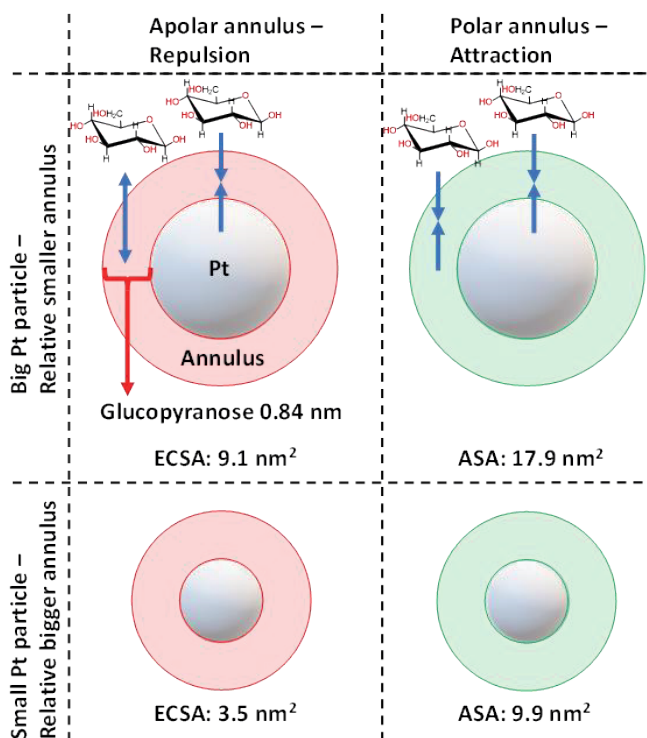
Figure 3.9. Top view of a small (1.5 nm) and (2.4 nm) big Pt particle on a carbon support. The annulus of the Pt particle is either non-functionalized (red) or functionalized with support oxygen groups (green), resulting in the repulsion or adsorption of a substrate (e.g. glucopyranose) respectively. The electrochemical active surface area (ECSA) of the Pt particles are given in grey, while the adsorbable surface area (ASA) of glucopyranose is given in grey and green.

Figure 3.10 shows the background-corrected LSV at E = 0.5-1.0 V *vs.* RHE for the electrocatalytic oxidation of glucose over Pt/CNF-R523-EO, Pt/CNF-R773-EO and Pt/CNF-R973-EO and the related currents densities normalized by the ECSA (j_{ECSA}) and ASA (j_{ASA}), to evaluate how this affects the current densities. The j_{ECSA} is higher than the I_{ASA} for all catalysts since the ECSA is smaller than the ASA (Figure 3.9). Going from Pt/CNF-R523-EO to Pt/CNF-R973-EO, the j_{ECSA} decreases , while the j_{ASA} is nearly identical for all catalysts. Moreover, the relative difference between j_{ECSA} and j_{ASA} decreases from Pt/CNF-R523-EO to Pt/CNF-R973-EO. The increasing difference between the j_{ECSA} and j_{ASA} when going from Pt/CNF-R523-EO to Pt/CNF-R973-EO can be explained by the larger contribution of the annulus for catalysts that bare smaller Pt particles. In this case, the Pt particles are 1.6, 1.8 and 2.2 nm for Pt/CNF-R523-EO, Pt/CNF-R773-EO and Pt/CNF-R973-EO respectively. More remarkable is that the current density based on ASA is nearly the same for all catalysts, indicative that the catalyst activity can best be described by the adsorbable surface area on the metal surface and in the annulus of the metal particles.
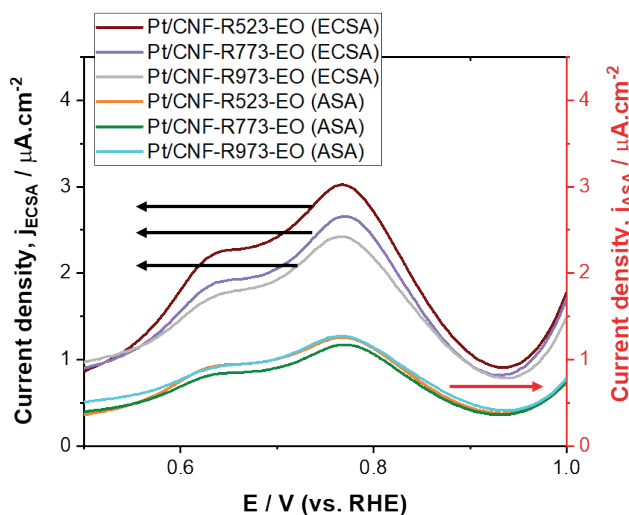
Figure 3.10. *Background-corrected linear sweep voltammetry measured at 1 mV.s^{-1} in 0.1M H$_2$SO$_4$ and 0.1M glucose, with currents normalized by the ECSA and ASA for Pt/CNF-R523-EO, Pt/CNF-R773-EO and Pt/CNF-R973-EO.*

3.4 Conclusion

We observed that the heat treatment of Pt/CNF functionalized with support oxygen groups (e.g., lactone, phenol and carbonyl/quinone groups) resulted in a gradual increase in Pt particle size and a gradual decrease in the content of support oxygen groups. As a result, catalysts were obtained with different Pt particle sizes and different contents of support oxygen groups. The difference in Pt particle size and content of support oxygen groups did not affect the Pt surface structure, the Pt electronic properties, and the ratio between adsorbates on the Pt surface during the electrocatalytic oxidation of glucose. Despite this, the catalytic activity evaluation showed a direct correlation between the activity and the support oxygen group content. More specifically, the introduction of support oxidation groups in the annulus of the Pt particles by electrochemical oxidation resulted in an approximately 2.5-fold increase in catalytic activity. This increase in catalytic activity was found to be higher for electrochemically oxidized Pt/CNF functionalized with smaller Pt particles. In this case, we argue that the annulus for smaller Pt particles plays a more significant role in the adsorption of reactants in the vicinity of the Pt catalyst. Therefore, we conclude that support oxygen groups improve the adsorption of reactants in vicinity of the Pt catalyst and thereby improve the catalyst activity.

Declaration of competing interest

The authors declare that they have no known competing financial interests or personal relationships that could have appeared to influence the work reported in this paper.

Author contribution

The authors are grateful for the assistance in drafting the manuscript under the supervision of Marc Koper and Harry Bitter. Marlene Führer taught me how to synthesize Pt/CNF catalysts. Tomas van Haasterecht contributed to the analysis of TPD-MS and N_2-physisorption. Thomas Hersbach and Dimosthenis Sokaras performed the in-situ x-ray spectroscopy study, data analysis, and interpretation. Tiny Verhoeven and Emiel Hensen performed XPS measurements and assisted in data interpretation. The HAADF-STEM measurements were performed by Juan José.

Acknowledgment

measurements were financed by MINECO (Spain) and Junta de Andalucia through projects PID2020-113809RB-C33 and PY18-2727.

References

1.	Derrien, E. *et al.* Aerobic Oxidation of Glucose to Glucaric Acid under Alkaline-Free Conditions: Au-Based Bimetallic Catalysts and the Effect of Residues in a Hemicellulose Hydrolysate. *Ind Eng Chem Res* **56**, 13175–13189 (2017).

2.	Bin, D. *et al.* Controllable oxidation of glucose to gluconic acid and glucaric acid using an electrocatalytic reactor. *Electrochim Acta* **130**, 170–178 (2014).

3.	Verma, S., Lu, S. & Kenis, P. J. A. Co-electrolysis of CO2 and glycerol as a pathway to carbon chemicals with improved technoeconomics due to low electricity consumption. *Nat Energy* **4**, 466–474 (2019).

4.	Liu, W. J. *et al.* Efficient electrochemical production of glucaric acid and H2 via glucose electrolysis. *Nat Commun* **11**, 1–11 (2020).

5.	Rafaïdeen, T., Baranton, S. & Coutanceau, C. Highly efficient and selective electrooxidation of glucose and xylose in alkaline medium at carbon supported alloyed PdAu nanocatalysts. *Appl Catal B* **243**, 641–656 (2019).

6.	Zheng, D. *et al.* Three-birds-with-one-stone electrolysis for energy-efficiency production of gluconate and hydrogen. *Appl Catal B* **277**, (2020).

7.	Hayden, B. E., Pletcher, D. & Suchsland, J.-P. Enhanced Activity for Electrocatalytic Oxidation of Carbon Monoxide on Titania-Supported Gold Nanoparticles. *Angewandte Chemie* **119**, 3600–3602 (2007).

8.	Barbosa, J. R. *et al.* PtSnO2/C and Pt/C with preferential (100) orientation: High active electrocatalysts for ammonia electro-oxidation reaction. *Appl Catal B* **264**, 118458 (2020).

9.	Garcia, A. C., Birdja, Y. Y., Tremiliosi-Filho, G. & Koper, M. T. M. Glycerol electro-oxidation on bismuth-modified platinum single crystals. *J Catal* **346**, 117–124 (2017).

10.	Fu, Q. & Bao, X. Confined microenvironment for catalysis control. *Nat Catal* **2**, 834–836 (2019).

11.	Kwon, Y. & Koper, M. T. M. Electrocatalytic hydrogenation and deoxygenation of glucose on solid metal electrodes. *ChemSusChem* **6**, 455–462 (2013).

12.	Feng, W. *et al.* Impacts of Support Properties on the Vacuum Residue Slurry-Phase Hydrocracking Performance of Mo Catalysts. *Pet Sci* (2023) doi:10.2139/ssrn.3983894.

13.	Kourtelesis, M. *et al.* The effects of support morphology on the performance of Pt/CeO2 catalysts for the low temperature steam reforming of ethanol. *Appl Catal B* **284**, (2021).

14.	Audevard, J. *et al.* Multifunctional Catalytic Properties of Pd/CNT Catalysts for 4-Nitrophenol Reduction. *ChemCatChem* **14**, (2022).

15.	Chen, J., Wu, Z., Liu, H., Bao, X. & Yuan, P. A Surface-Cofunctionalized Silica Supported Palladium Catalyst for Selective Hydrogenation of Nitrile Butadiene Rubber with Enhanced Catalytic Activity and Recycling Performance. *Ind Eng Chem Res* **58**, 11821–11830 (2019).

16.	Gerber, I. C. & Serp, P. A Theory/Experience Description of Support Effects in Carbon-Supported Catalysts. *Chem Rev* **120**, 1250–1349 (2020).

17.	Toebes, M. L., Prinsloo, F. F., Bitter, J. H., Van Dillen, A. J. & De Jong, K. P. Influence of oxygen-containing surface groups on the activity and selectivity of carbon nanofiber-supported ruthenium catalysts in the hydrogenation of cinnamaldehyde. *J Catal* **214**, 78–87 (2003).

18.	Plomp, A. J., Vuori, H., Krause, A. O. I., de Jong, K. P. & Bitter, J. H. Particle size effects for carbon nanofiber supported platinum and ruthenium catalysts for the selective hydrogenation of cinnamaldehyde. *Appl Catal A Gen* **351**, 9–15 (2008).

19.	Gosselink, R. W., Xia, W., Muhler, M., De Jong, K. P. & Bitter, J. H. Enhancing the activity of Pd on carbon nanofibers for deoxygenation of amphiphilic fatty acid molecules through support polarity. *ACS Catal* **3**, 2397–2402 (2013).

20.	Makowski, P., Demir Cakan, R., Antonietti, M., Goettmann, F. & Titirici, M. M. Selective partial hydrogenation of hydroxy aromatic derivatives with palladium nanoparticles supported on hydrophilic carbon. *Chemical Communications* 999–1001 (2008).

21. Dong, Z. *et al.* Efficient Pd on carbon catalyst for ammonium formate dehydrogenation: Effect of surface oxygen functional groups. *Appl Catal B* **321**, (2023).

22. Shi, W. *et al.* Enhanced chemoselective hydrogenation through tuning the interaction between pt nanoparticles and carbon supports: Insights from identical location transmission electron microscopy and x-ray photoelectron spectroscopy. *ACS Catal* **6**, 7844–7854 (2016).

23. Ning, X. *et al.* Electron transfer dependent catalysis of Pt on N-doped carbon nanotubes: Effects of synthesis method on metal-support interaction. *J Catal* **348**, 100–109 (2017).

24. Contreras, R. C. *et al.* Effect of mesoporous carbon support nature and pretreatments on palladium loading, dispersion and apparent catalytic activity in hydrogenation of myrcene. *J Catal* **372**, 226–244 (2019).

25. Van De Vyver, S. *et al.* Tuning the acid/metal balance of carbon nanofiber-supported nickel catalysts for hydrolytic hydrogenation of cellulose. *ChemSusChem* **5**, 1549–1558 (2012).

26. Dai, J. *et al.* Janus N-Doped Carbon@Silica Hollow Spheres as Multifunctional Amphiphilic Nanoreactors for Base-Free Aerobic Oxidation of Alcohols in Water. *ACS Appl Mater Interfaces* **10**, 33474–33483 (2018).

27. Markus, H. *et al.* Hydrogenolysis of hydroxymatairesinol over carbon-supported palladium catalysts. *Catal Letters* **103**, 125–131 (2005).

28. Ghogia, A. C. *et al.* Beyond confinement effects in Fischer-Tropsch Co/CNT catalysts. *J Catal* **397**, 156–171 (2021).

29. Li, B. & Su, D. The nucleophilicity of the oxygen functional groups on carbon materials: A DFT analysis. *Chemistry - A European Journal* **20**, 7890–7894 (2014).

30. Han, X. *et al.* N-doped carbon supported Pt catalyst for base-free oxidation of 5-hydroxymethylfurfural to 2,5-furandicarboxylic acid. *Appl Catal A Gen* **526**, 1–8 (2016).

31. Peng, Y., Lu, B., Wang, N., Li, L. & Chen, S. Impacts of interfacial charge transfer on nanoparticle electrocatalytic activity towards oxygen reduction. *Physical Chemistry Chemical Physics* **19**, 9336–9348 (2017).

32. Gharibi, H., Yasi, F., Kazemeini, M., Heydari, A. & Golmohammadi, F. Fabrication of MEA based on sulfonic acid functionalized carbon supported platinum nanoparticles for oxygen reduction reaction in PEMFCs. *RSC Adv* **5**, 85775–85784 (2015).

33. Yang, H. P. *et al.* Platinum/nitrogen-doped carbon/carbon cloth: A bifunctional catalyst for the electrochemical reduction and carboxylation of CO2 with excellent efficiency. *Chemical Communications* **54**, 4108–4111 (2018).

34. Wang, Z. B., Yin, G. P. & Shi, P. F. Effects of ozone treatment of carbon support on Pt-Ru/C catalysts performance for direct methanol fuel cell. *Carbon N Y* **44**, 133–140 (2006).

35. Salgado, J. R. C. *et al.* Effect of functionalized carbon as Pt electrocatalyst support on the methanol oxidation reaction. *Appl Catal B* **102**, 496–504 (2011).

36. Alegre, C. *et al.* Influence of support's oxygen functionalization on the activity of Pt/carbon xerogels catalysts for methanol electro-oxidation. in *International Journal of Hydrogen Energy* vol. 37 7180–7191 (Pergamon, 2012).

37. Muthuswamy, N. *et al.* Towards a highly-efficient fuel-cell catalyst: Optimization of Pt particle size, supports and surface-oxygen group concentration. *Physical Chemistry Chemical Physics* **15**, 3803–3813 (2013).

38. Alegre, C. *et al.* Oxygen-functionalized highly mesoporous carbon xerogel based catalysts for direct methanol fuel cell anodes. *Journal of Physical Chemistry C* **117**, 13045–13058 (2013).

39. Sebastián, D. *et al.* Oxidized carbon nanofibers supporting PtRu nanoparticles for direct methanol fuel cells. *Int J Hydrogen Energy* **39**, 5414–5423 (2014).

40. Dillen, A. J., Geus, J. W., Hermans, L. A. M. & Meijden, J. Production of supported copper and nickel catalysts by deposition-precipitation. *Proceedings of the 6th International Conference on Catalysis* **11**, 677–685 (1977).

41. De Jong, K. P. & Geus, J. W. Carbon Nanofibers: Catalytic Synthesis and Applications. *Catal Rev Sci Eng* **42**, 481–510 (2000).

42. Bitter, J. H. Dark material with a bright future: Carbon as support in future heterogeneous catalysis – A short personal perspective. *Catal Today* **423**, (2023).

43. Monteiro, M. C. O. & Koper, M. T. M. Alumina contamination through polishing and its effect on hydrogen evolution on gold electrodes. *Electrochim Acta* **325**, 134915 (2019).

44. Fang, H. T. *et al.* Purification of single-wall carbon nanotubes by electrochemical oxidation. *Chemistry of Materials* **16**, 5744–5750 (2004).

45. Yi, Y. *et al.* Electrochemical corrosion of a glassy carbon electrode. *Catal Today* **295**, 32–40 (2017).

46. Kou, Z. *et al.* Observable Electrochemical Oxidation of Carbon Promoted by Platinum Nanoparticles. *ACS Appl Mater Interfaces* **8**, 3940–3947 (2016).

47. Lia, M. F. *et al.* Oxidation of carbon supports at fuel cell cathodes: Differential electrochemical mass spectrometric study. *Chinese Journal of Chemical Physics* **23**, 442–446 (2010).

48. Führer, M., van Haasterecht, T. & Bitter, J. H. Cinnamaldehyde hydrogenation over carbon supported molybdenum and tungsten carbide catalysts. *Chemical Communications* **58**, 13608–13611 (2022).

49. Salanov, A. N. *et al.* Oxidation and recrystallization of platinum group metals (Pt, Pd, Rh) in oxygen. Surface and subsurface reconstruction of polycrystalline platinum during annealing in the O2 atmosphere over the temperature range of 600–1400 K. *Appl Surf Sci* **490**, 188–203 (2019).

50. Göckeler, M. *et al.* Surface reactions during temperature-programmed desorption and reduction experiments with oxygen-functionalized carbon blacks. *Appl Surf Sci* **561**, 150044 (2021).

51. Śliwak, A., Grzyb, B., Ćwikła, J. & Gryglewicz, G. Influence of wet oxidation of herringbone carbon nanofibers on the pseudocapacitance effect. *Carbon* **64**, 324–333 (2013).

52. Monteiro, M. C. O. *et al.* Absence of CO2 electroreduction on copper, gold and silver electrodes without metal cations in solution. *Nat Catal* **4**, 654–662 (2021).

53. Zhang, L. & Gong, H. Improvement in flexibility and volumetric performance for supercapacitor application and the effect of Ni-Fe ratio on electrode behaviour. *J Mater Chem A Mater* **3**, 7607–7615 (2015).

54. Jovanovic, Z. *et al.* The role of surface chemistry in the charge storage properties of graphene oxide. *Electrochim Acta* **258**, 1228–1243 (2017).

55. Sandbeck, D. J. S. *et al.* Particle Size Effect on Platinum Dissolution: Practical Considerations for Fuel Cells. *ACS Appl Mater Interfaces* **12**, 25718–25727 (2020).

56. Sandbeck, D. J. S. *et al.* Particle Size Effect on Platinum Dissolution: Considerations for Accelerated Stability Testing of Fuel Cell Catalysts. *ACS Catal* **10**, 6281–6290 (2020).

57. Dix, S. T., Lu, S. & Linic, S. Critical Practices in Rigorously Assessing the Inherent Activity of Nanoparticle Electrocatalysts. *ACS Catal* **10**, 10735–10741 (2020).

58. Sokaras, D. *et al.* A seven-crystal Johann-type hard x-ray spectrometer at the Stanford Synchrotron Radiation Lightsource. *Review of Scientific Instruments* **84**, (2013).

59. Ravel, B. & Newville, M. ATHENA, ARTEMIS, HEPHAESTUS: Data analysis for X-ray absorption spectroscopy using IFEFFIT. in *Journal of Synchrotron Radiation* vol. 12 537–541 (2005).

60. Calvin, S. *XAFS for Everyone*. (CRC Press, 2013). doi:10.1201/b14843.

61. Hersbach, T. J. P. *et al.* Base-Accelerated Degradation of Nanosized Platinum Electrocatalysts. *ACS Catal* **11**, 9904–9915 (2021).

62. Busó-Rogero, C. *et al.* Surface structure and anion effects in the oxidation of ethanol on platinum nanoparticles. *J Mater Chem A Mater* **1**, 7068–7076 (2013).

63. Neha, N. *et al.* Revisited Mechanisms for Glucose Electrooxidation at Platinum and Gold Nanoparticles. *Electrocatalysis* **14**, 121–130 (2022).

64. Melke, J. *et al.* Ethanol oxidation on carbon-supported Pt, PtRu, and PtSn catalysts studied by operando X-ray absorption spectroscopy. *Journal of Physical Chemistry C* **114**, 5914–5925 (2010).

65. Holade, Y. *et al.* Deciphering the Electrocatalytic Reactivity of Glucose Anomers at Bare Gold Electrocatalysts for Biomass-Fueled Electrosynthesis. *ACS Catal* **12**, 12563–12571 (2022).

66. Toebes, M. L. *et al.* Support effects in the hydrogenation of cinnamaldehyde over carbon nanofiber-supported platinum catalysts: Characterization and catalysis. *J Catal* **226**, 215–225 (2004).

67. Gosselink, R. W. *et al.* Gas phase oxidation as a tool to introduce oxygen containing groups on metal-loaded carbon nanofibers. *Carbon* **50**, 4424–4431 (2012).

68. Führer, A. M. *et al.* The synergetic effect of support-oxygen groups and Pt particle size in the oxidation of α-D-glucose: a proximity effect in adsorption. *ChemCatChem* **14**, 19 (2022).

69. Reid, L. M., Li, T., Cao, Y. & Berlinguette, C. P. Organic chemistry at anodes and photoanodes. *Sustain Energy Fuels* **2**, 1905–1927 (2018).

70. Bleda-Martínez, M. J. *et al.* Role of surface chemistry on electric double layer capacitance of carbon materials. *Carbon* **43**, 2677–2684 (2005).

71. Jiang, X. *et al.* Effects of heat treatment temperature and atmosphere on electrocatalytic properties of platinum nanocrystals. *Journal of Electroanalytical Chemistry* **729**, 53–60 (2014).

72. Santos, L. G. R. A., Freitas, K. S. & Ticianelli, E. A. Heat treatment effect of Pt-V/C and Pt/C on the kinetics of the oxygen reduction reaction in acid media. *Electrochim Acta* **54**, 5246–5251 (2009).

73. Maillard, F. *et al.* Influence of particle agglomeration on the catalytic activity of carbon-supported Pt nanoparticles in CO monolayer oxidation. *Physical Chemistry Chemical Physics* **7**, 375–383 (2005).

74. Datye, A. K., Xu, Q., Kharas, K. C. & McCarty, J. M. Particle size distributions in heterogeneous catalysts: What do they tell us about the sintering mechanism? *Catal Today* **111**, 59–67 (2006).

75. Cuesta, A. *et al.* Potential dependence of the saturation CO coverage of Pt electrodes: The origin of the pre-peak in CO-stripping voltammograms. Part 3: Pt(poly). *Journal of Electroanalytical Chemistry* **586**, 184–195 (2006).

76. García, Gonzalo; Koper, M. T. M. Stripping voltammetry of carbon monoxide oxidation on stepped platinum single-crystal electrodes in alkaline solution. *Physical Chemistry Chemical Physics* **10**, 3802–3811 (2008).

77. Ciapina, E. G., Santos, S. F. & Gonzalez, E. R. Electrochemical CO stripping on nanosized Pt surfaces in acid media: A review on the issue of peak multiplicity. *Journal of Electroanalytical Chemistry* **815**, 47–60 (2018).

78. Chen, X., McCrum, I. T., Schwarz, K. A., Janik, M. J. & Koper, M. T. M. Co-adsorption of Cations as the Cause of the Apparent pH Dependence of Hydrogen Adsorption on a Stepped Platinum Single-Crystal Electrode. *Angewandte Chemie - International Edition* **56**, 15025–15029 (2017).

79. Ramaker, D.; Koningsberger, D. The atomic AXAFS and Δl XANES techniques as applied to heterogeneous catalysis and electrocatalysis. *Physical Chemistry Chemical Physics* **12**, 5503–5513 (2010).

80. Moggia, G., Kenis, T., Daems, N. & Breugelmans, T. Electrochemical Oxidation of d-Glucose in Alkaline Medium: Impact of Oxidation Potential and Chemical Side Reactions on the Selectivity to d-Gluconic and d-Glucaric Acid. *ChemElectroChem* **7**, 86–95 (2020).

81. Parpot, P., Santos, P. R. B. & Bettencourt, A. P. Electro-oxidation of d-mannose on platinum, gold and nickel electrodes in aqueous medium. *Journal of Electroanalytical Chemistry* **610**, 154–162 (2007).

82. Vassilyev, Y. B., Khazova, O. A. & Nikolaeva, N. N. Kinetics and mechanism of glucose electrooxidation on different electrode-catalysts. Part I. Adsorption and oxidation on platinum. *Journal of Electroanalytical Chemistry* **196**, 105–125 (1985).

83. Castro Luna, A. M., Bolzán, A. E., De Mele, M. F. L. & Arvia, A. J. The Voltammetric Electrooxidation of Organic Residues Produced From Glucose Electroadsorption on Platinum Electrodes with Different Preferred Crystallographic Orientations. *Zeitschrift fur Physikalische Chemie* **160**, 25–43 (1988).

84. Popović, K. D., Tripković, A. V. & Adžić, R. R. Oxidation of d-glucose on single-crystal platinum electrodes: A mechanistic study. *Journal of Electroanalytical Chemistry* **339**, 227–245 (1992).

85. Luna, A. M. C., Bolzán, A. E., de Mele, M. F. & Arvia, A. J. The voltammetric electrooxidation of glucose and glucose residues formed on electrodispersed platinum electrodes in acid electrolytes. *Pure and Applied Chemistry* **63**, 1599–1608 (1991).

86. Popović, K., Tripković, A., Marković, N. & Adžić, R. R. Structural effects in electrocatalysis: oxidation of glucose on single-crystal platinum electrodes. *Journal of Electroanalytical Chemistry* **295**, 79–94 (1990).

87. Kokoh, K. B., Léger, J. M., Beden, B. & Lamy, C. 'On line' chromatographic analysis of the products resulting from the electrocatalytic oxidation of d-glucose on Pt, Au and adatoms modified Pt electrodes-Part I. Acid and neutral media. *Electrochim Acta* **37**, 1333–1342 (1992).

88. Dixon, D. *et al.* Space resolved, in operando X-ray absorption spectroscopy: Investigations on both the anode and cathode in a direct methanol fuel cell. *Journal of Physical Chemistry C* **116**, 7587–7595 (2012).

89. Kwon, Y., Schouten, K. J. P. & Koper, M. T. M. Mechanism of the Catalytic Oxidation of Glycerol on Polycrystalline Gold and Platinum Electrodes. *ChemCatChem* **3**, 1176–1185 (2011).

90. Kanninen, P. & Kallio, T. Activation of commercial Pt/C catalyst toward glucose electro-oxidation by irreversible Bi adsorption. *Journal of Energy Chemistry* **27**, 1446–1452 (2018).

91. Largeaud, F., Kokoh, K. B., Beden, B. & Lamy, C. On the electrochemical reactivity of anomers: electrocatalytic oxidation of α- and β-d-glucose on platinum electrodes in acid and basic media. *Journal of Electroanalytical Chemistry* **397**, 261–269 (1995).

92. Göckeler, M. *et al.* Surface reactions during temperature-programmed desorption and reduction experiments with oxygen-functionalized carbon blacks. *Appl Surf Sci* **561**, (2021).

93. Toebes, M. L., Van Heeswijk, J. M. P., Bitter, J. H., Jos van Dillen, A. & De Jong, K. P. The influence of oxidation on the texture and the number of oxygen-containing surface groups of carbon nanofibers. *Carbon N Y* **42**, 307–315 (2004).

94. Mom, R. *et al.* The Oxidation of Platinum under Wet Conditions Observed by Electrochemical X-ray Photoelectron Spectroscopy. *J Am Chem Soc* **141**, 6537–6544 (2019).

95. Rajala, T. *et al.* A platinum nanowire electrocatalyst on single-walled carbon nanotubes to drive hydrogen evolution. *Appl Catal B* **265**, 118582 (2020).

96. Plomp, A. J., Su, D. S., Jong, K. P. D. & Bitter, J. H. On the nature of oxygen-containing surface groups on carbon nanofibers and their role for platinum depositionsan XPS and titration study. *Journal of Physical Chemistry C* **113**, 9865–9869 (2009).

97. Rizo, R., Sebastián, D., Rodríguez, J. L., Lázaro, M. J. & Pastor, E. Influence of the nature of the carbon support on the activity of Pt/C catalysts for ethanol and carbon monoxide oxidation. *J Catal* **348**, 22–28 (2017).

98. Psofogiannakis, G. M. & Froudakis, G. E. DFT study of hydrogen storage by spillover on graphite with oxygen surface groups. *J Am Chem Soc* **131**, 15133–15135 (2009).

99. Prins, R. Hydrogen spillover. Facts and fiction. *Chem Rev* **112**, 2714–2738 (2012).

Supporting information

The relative weight retained by the Pt/CNF catalysts as a function of temperature under N_2 is given in Figure S3.1. The weight loss with an increase in temperature was related to the decomposition of support oxygen groups (CO_2 and CO) from the CNF. The weight loss was used to quantify the content of support oxygen groups (Table 3.1). This figure shows that catalysts that have been exposed to higher temperatures during catalyst preparation have a lower content of support oxygen groups present on the CNF support.
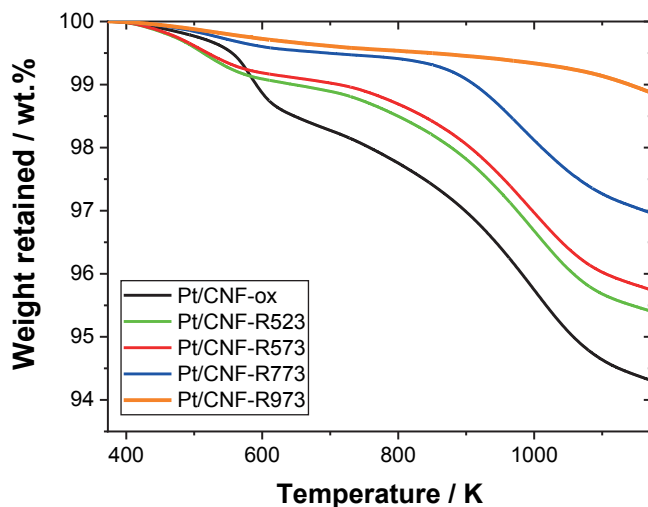
Figure S3.1. *The thermogravimetric curves of the Pt/CNF catalysts were obtained under a N_2 flow.*

XPS-wide scans were made to quantify the atomic composition of the Pt/CNF catalysts (Figure S3.2). The Pt/CNF catalysts were reduced first at 523 K to remove chemisorbed water and CO_2 from the support.[92] This reduction step was performed in a plug flow reactor and required the use of quartz wool (SiO_2). A small fraction of SiO_2 contaminated the catalysts. Therefore, a correction was applied to the atomic composition to subtract the contribution of SiO_2. Table S3.1 shows the atomic composition of the Pt/CNF catalysts before correction for the SiO_2.
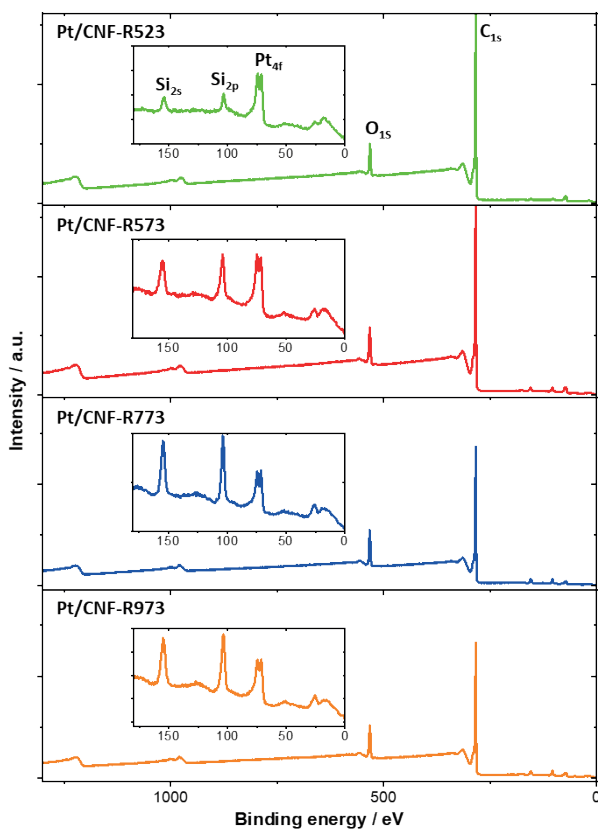
Figure S3.2. *Wide-scan XPS with accompanying insets for Pt/CNF catalysts.*

Table S3.1. *The atomic composition of Pt/CNF catalysts contaminated with SiO_2.*

Catalyst	Atomic composition (%)				
	O_{1s}	C_{1s}	Si_{s2}	Si_{2p}	Pt_{4f}
Pt/CNF-R523	8.2	88	1.7	1.4	0.28
Pt/CNF-R573	10.3	82	4.0	3.8	0.24
Pt/CNF-R773	9.2	85	2.8	3.2	0.28
Pt/CNF-R973	10.4	81	3.8	4.1	0.29

Nitrogen physisorption was used to assess the textural properties of bare CNF-ox support, PtO$_x$/CNF-ox and Pt/CNF-R973. Their corresponding adsorption and desorption isotherms are given in Figure S3.3. The isotherms show multilayer adsorption and desorption combined with capillary condensation in the large mesopores, resulting in a hysteresis loop. Moreover, the isotherms show a similar trend, indicative that the catalysts have similar textural properties.

The isotherms of the support and the catalysts were used to derive the textural characteristics, the BET-surface area, and pore volume, and are given in Table S3.2. Both CNF-ox and PtO$_x$/CNF-ox have a BET-surface area and pore volume that are in the same order of magnitude, indicative that the surface area does not differ after functionalizing the support with platinum. Moreover, PtO$_x$/CNF-ox and Pt/CNF-R973 show a similar BET-surface area and pore volume, suggesting that the reduction and heat treatment does not cause a change in the textural properties of the catalyst, being in line with earlier research.[93]
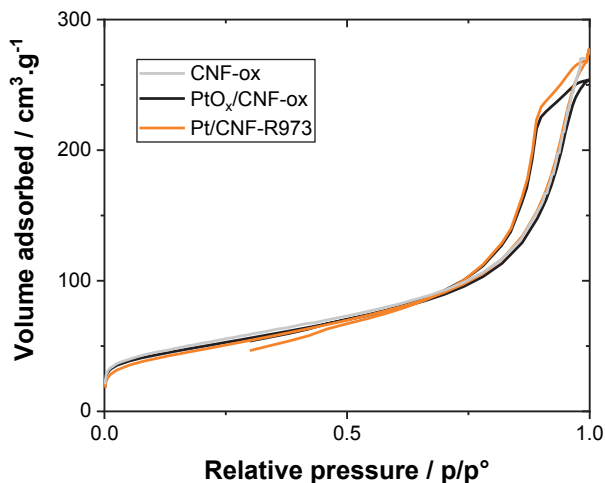
Figure S3.3. *Adsorption-desorption isotherms of N$_2$ for CNF-ox, PtO$_x$/CNF-ox and Pt/CNF-R973.*

Table S3.2. *BET surface area (S$_{BET}$) and total pore volume (V$_{total}$) of CNF-ox, PtO$_x$/CNF-ox and Pt/CNF-R973.*

Catalyst	S$_{BET}$ (m^2/g)	V$_{total}$ (cm^3/g)
CNF-ox	187	0.25
PtO$_x$/CNF-ox	178	0.24
Pt/CNF-R973	171	0.25

Typical TPD-MS and DTG curves, exemplified for the parent catalyst PtOx/CNF-ox, are given in Figures S3.4A and S3.4B. The MS data (Figure S3.4A) shows one main peak at 543 K (1) for CO_2 (m/z=44), followed by two shoulders at 634 K (2) and 851 K (3), and two minor peaks for CO (m/z=28) at 543 K (4) and 634 K (5) followed by one major peak from 673-1073 K (6). The CO_2 peaks 1, 2 and 3 can be attributed to the decomposition of carboxylic acid, anhydride, and lactone surface groups respectively, while the CO peaks 4, 5 and 6 can be attributed to the decomposition of carbonyl groups adjacent to ketones and aldehydes, anhydride, and phenol and carbonyl/quinone surface groups respectively.[28,54,92] Thus, in the case of PtOx/CNF-ox, there are carboxylic acids, anhydrides, lactones, carbonyl groups adjacent to ketones and aldehydes, phenols and carbonyls/quinones present on the carbon support.
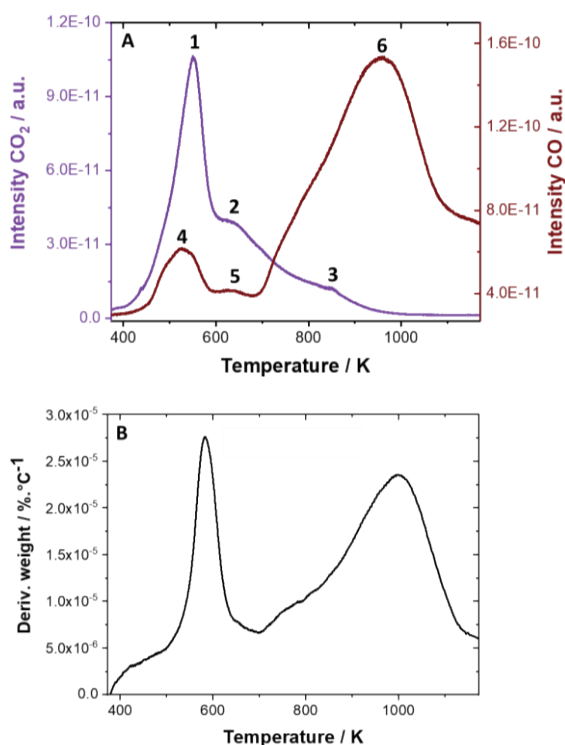
Figure S3.4. A) MS patterns measured during TPD for PtOx/CNF-ox and B) the DTG curves for the Pt/CNF catalysts.

The DTG curve (Figure S3.4B) of PtOx/CNF-ox shows one major peak at 583 K followed by a shoulder at 680 K and a broad peak ranging from 705-1120 K. The DTG curve of PtOx/CNF-ox follows the same pattern as the combined CO and CO_2 signal measured by TPD-MS for PtOx/CNF-ox though with a 50 K temperature shift. The shift is most likely the result of differences in the experimental setups (i.e., the gas flows through the sample for TPD and flows over the sample for DTG).

After the reduction of PtO$_x$/CNF-ox to Pt/CNF-523, the DTG curve (Figure S3.5) shows a new peak at 500 K and the loss of two peaks at 583 K and 680 K. The appearance of the new peak can be attributed to chemisorbed water present on the sample,[92] while the loss of the two peaks can be related to the loss of carboxylic acid and carbonylic acids adjacent to ketones and aldehydes and anhydride surface groups.[28] This indicates that Pt/CNF-523 only bears chemisorbed water, and lactone, phenol, and carbonyl/quinone surface groups. A consecutive and gradual increase in heat treatment, going from Pt/CNF-523 to Pt/CNF-923, results in a steady decrease in the peak at 500 K and the peak between 705-1120 K. It can therefore be concluded that the heat treatment results in a gradual removal of chemisorbed water, and lactone, phenol and carbonyl/quinone surface groups.[28,54,92]
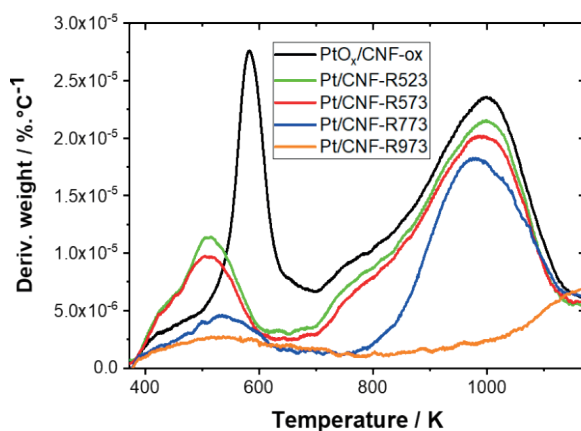
Figure S3.5. *The DTG curves for the Pt/CNF catalysts.*

The O_{1s} XPS spectra (Figure S3.6) show signals at 529.7-530.0 eV, 531.3-531.5 eV, 532.7-532.9 eV, and a shoulder at 535.2-534.9 eV, which have been attributed to covalent platinum oxide bonds (Pt-O),[94,95] carbonyl (C=O),[48,68,96,97] phenol/ether (C-O),[48,68,96,97] and chemisorbed water (H_2O)[48,68,96,97] respectively. The contribution of different oxygen groups to the total amount of oxygen groups (Table S3.3) was investigated to evaluate whether the nature of the oxygen groups changed by the heat treatment. On Pt/CNF-R523 phenol/ethers (47%) and carbonyls (46%) were present in a one-to-one ratio. With an increase in heat treatment, the contributions of the different oxygen groups present on Pt/CNF remain similar for all catalysts. Thus, both XPS and DTG show that the heat treatment does not change the ratio of the different oxygen groups present on the support and only decreased the total amount of oxygen groups.
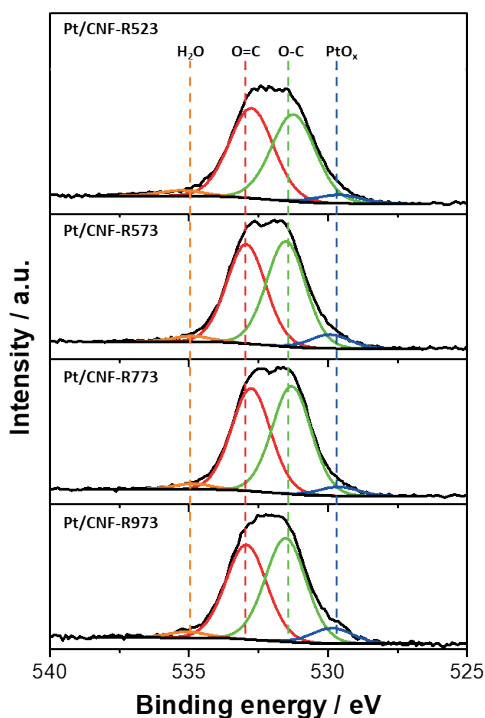
Figure S3.6. *O_{1s} XPS spectra of the Pt/CNF catalysts.*

Table S3.3. *The relative contribution of oxygen groups present on the Pt/CNF catalysts.*

Catalyst	Pt-O (~529.8 eV)	C-O (531.4 eV)	C=O (532.8 eV)	H_2O (535.5 eV)
Pt/CNF-R523	4%	47%	46%	3%
Pt/CNF-R573	6%	44%	47%	3%
Pt/CNF-R773	4%	46%	48%	3%
Pt/CNF-R973	7%	43%	47%	3%

Figure S3.7 shows the X-ray diffractograms of a bare CNF-ox support, Pt/CNF-R573 and Pt/CNF-R973. All samples show 2θ signals at 28, 43, 53 and 78˚, which correspond to the (002), (101), (004) and (110) reflections of the CNF.[48] The addition of Pt resulted in the appearance of new 2θ signals at 39, 46, 68, 82 and 86˚, which represent the (111), (200), (220), (311) and (222) planes of Pt respectively.[97] With an increase in heat treatment temperature, going from Pt/CNF-R573 to Pt/CNF-R973 the 2θ signals of the CNF do not alter, indicative that the graphitic nature of the CNF support is unaffected. In contrast, the 2θ signals of Pt increase, which can be related to an increase in Pt particle size, which is discussed in Table 3.2.
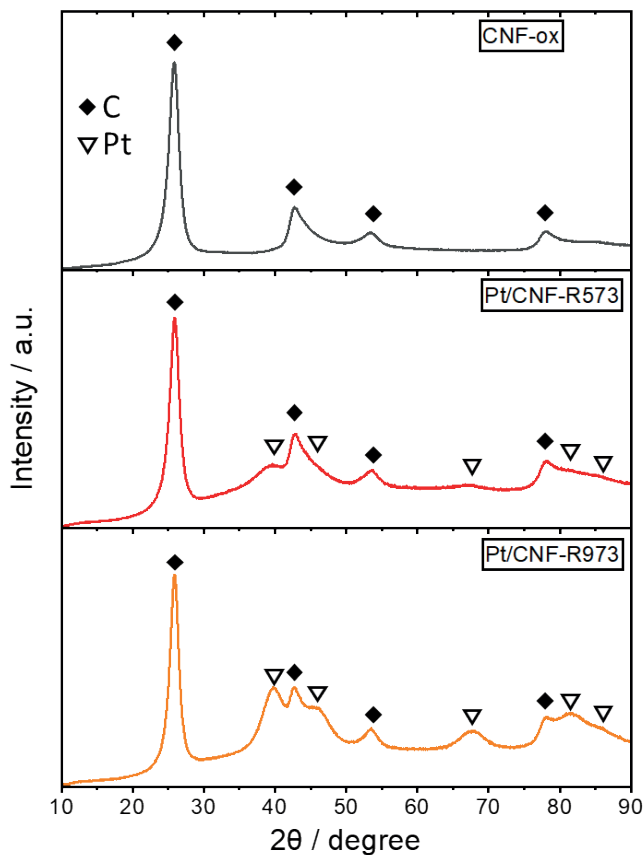
Figure S3.7. X-ray diffractograms of bare CNF-ox, Pt/CNF-R573 and Pt/CNF-R973.

Figure S3.8 shows the Pt L_{III}-edge HERFD-XANES spectra at a hold potential of 0.4 V *vs.* RHE of the parent catalyst (PtO$_x$/CNF-ox) and of the catalyst that has been reduced at 523 K, Pt/CNF-R523. After reducing the catalyst, the whiteline shifts from 11565.2 to 11564.6 eV, and the intensity decreases from 2.51 to 2.29, indicative that PtO$_x$/CNF-ox is more oxidized than Pt/CNF-R523.
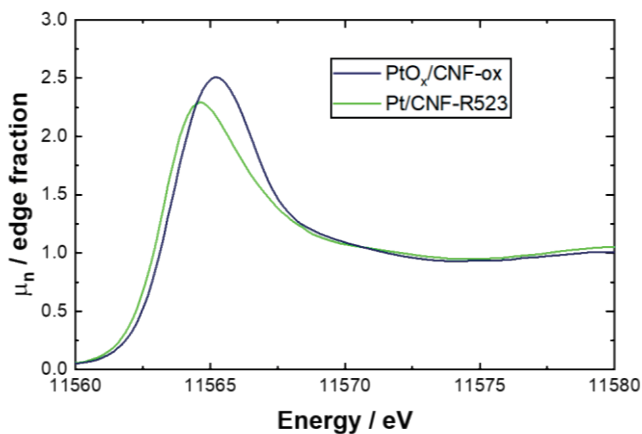
Figure S3.8. *Pt L_{III}-edge HERFD-XANES spectra of PtO$_x$/CNF-ox and Pt/CNF-R523 measured in 0.1M H_2SO_4 at 0.4 V vs. RHE hold potential.*

HAADF-STEM images of Pt/CNF-R773 and Pt/CNF-R973 are given in Figures S3.9A-B. These figures were used to estimate the number average and surface average Pt particle sizes, and evaluate the distribution of the Pt particles on the CNF.
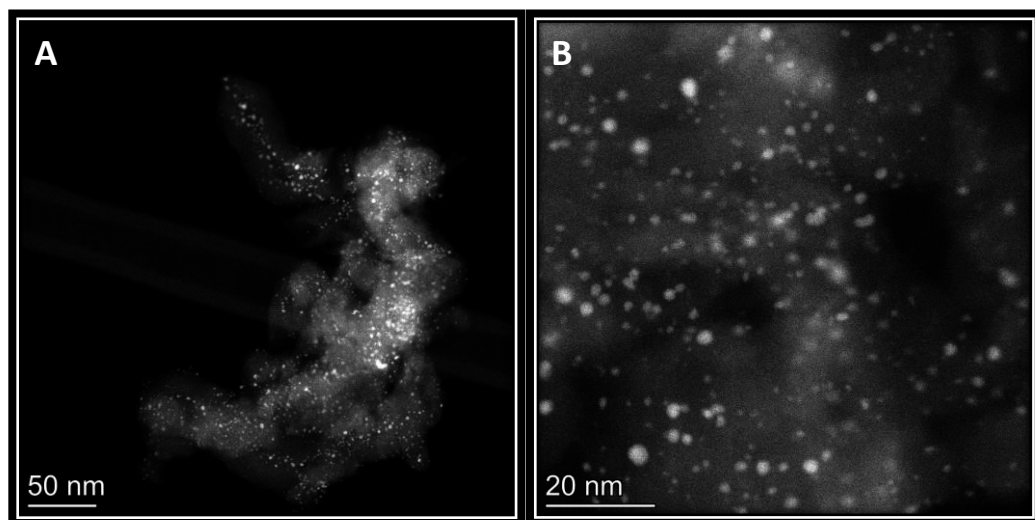
Figure S3.9. *HAADF-STEM images of A) Pt/CNF-R773 and B) Pt/CNF-R973.*

Figure S10 shows the XANES spectra of Pt/CNF-523, Pt/CNF-R773 (B, E), and Pt/CNF-973 (C, F) obtained at various potentials in the absence (A, B, C) and the presence of glucose (D, E, F), and the corresponding difference spectra in the absence (G, H, I) and presence of glucose (J, K, L).
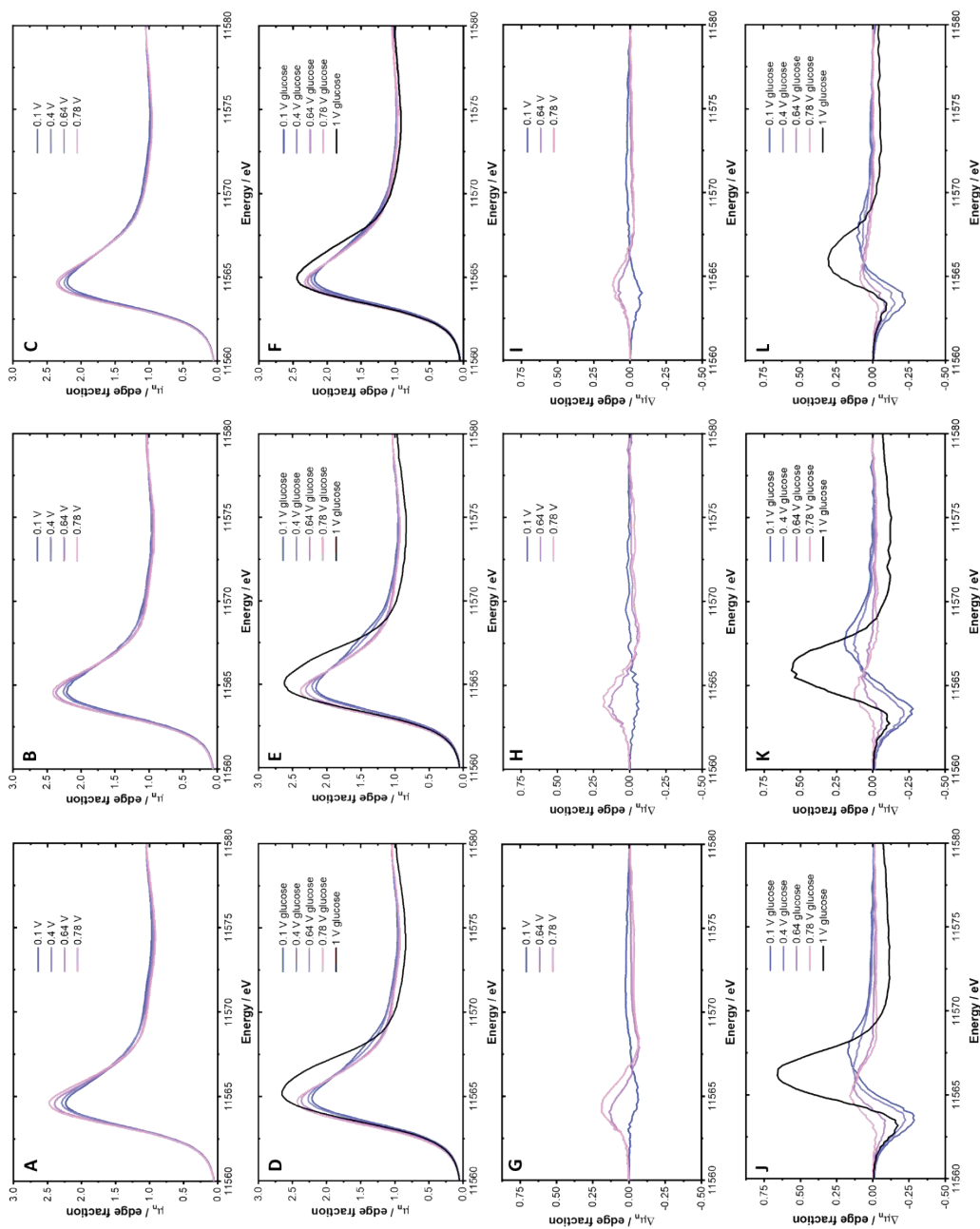
Figure S3.10. *Pt L_III-edge HERFD-XANES spectra of Pt/CNF-523 (A, D, G), Pt/CNF-R773 (B, E, H) and Pt/CNF-973 (C, F, I) at various hold potentials in 0.1M H_2SO_4 in the absence (A, B, C) and presence of 0.1 M glucose (D, E, F) and the difference spectra in the absence (G, H, I) and presence (J, K, L) of 0.1 M glucose obtained by Δμ(x) = μ(x) − μ(clean, 0.4V).*

Pt$_{4f}$ XPS spectra (Figure S3.11) were made for the Pt/CNF catalysts to quantify the relative atomic composition of the oxidation state of the Pt nanoparticles. The results of peak deconvolution of the Pt$_{4f5/2}$ and Pt$_{4f7/2}$ peaks are given in Table S3.4. From the table, a gradual increase in Pt^0 bulk can be observed accompanied by a gradual decrease in Pt^0 NP with increasing heat treatment steps. This indicates that the Pt particle size gradually increases with higher heat treatment steps, which is in accordance with the average Pt particle size determined by TEM and CO-stripping. The relative abundance of Pt^0 is 87 % to 90 % for all the catalysts. These percentages are in the same order of magnitude and therefore demonstrate that the relative abundance of Pt species in a specific oxidation state is similar for the Pt/CNF catalysts. This indicates that the oxidation state of the Pt catalyst is not affected by the presence of support oxygen groups.
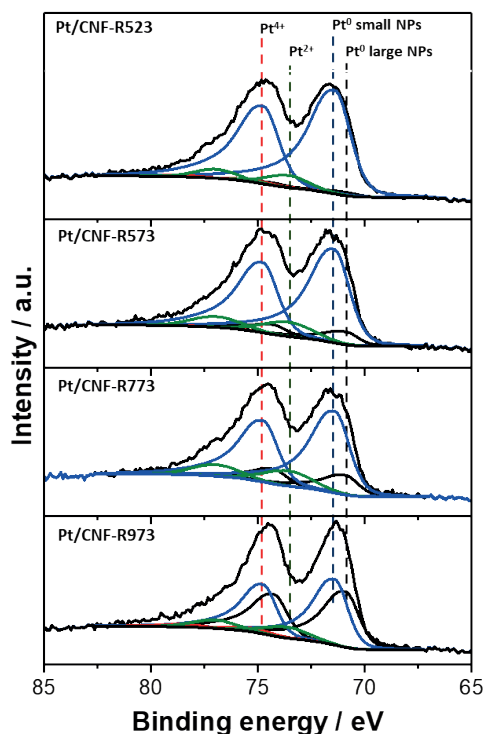
Figure S3.11. *Pt$_{4f}$ XPS spectra of the Pt/CNF catalysts.*

Table S3.4. *Relative abundance of Pt species determined by peak deconvolution of the Pt$_{4f}$ XPS spectra.*

Catalyst	Pt^0 bulk (70.9 / 74.3 eV)	Pt^0 small NPs (71.4 / 74.8 eV)	Pt^0 total	PtO$_2$ (75.3 / 78.7 eV)	PtO (73.6 / 77.0 eV)
Pt/CNF-R523	1.5 / 1.1	50 / 37	90	0.8 / 0.6	4.8 / 3.6
Pt/CNF-R573	5.5 / 4.1	45 / 34	88	0.2 / 0.1	6.9 / 5.2
Pt/CNF-R773	8.9 / 6.7	41 / 30	87	0.0 / 0.0	7.6 / 5.7
Pt/CNF-R973	24 / 18	27 / 20	89	1.5 / 1.1	4.8 / 3.6

Figure S3.12 shows the linear sweep voltammetries of bare CNF in 0.1 M H_2SO_4 in the absence and presence of 0.1 M glucose. In the absence of glucose and with an increase in potential an anodic current was measured with a main peak between 0.4 and 0.8 V *vs.* RHE. The anodic current measured throughout the LSV can be related to double-layer charging, while the main peak can be attributed to the oxidation of phenol/hydroquinone surface groups to lactone and carbonyl/quinone groups.[54,69] The same experiment in the presence of glucose resulted in a similar current profile, indicative that bare CNF is not active for the electrocatalytic oxidation of glucose.
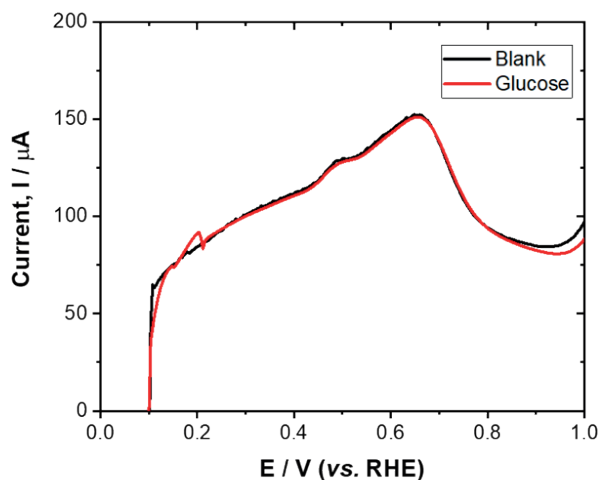
Figure S3.12. Linear sweep voltammetry of bare CNF measured in 0.1M H_2SO_4 in the absence and presence of 0.1M glucose at 1 mV.s^{-1}.

Figure S3.13 shows the linear sweep voltammetries of Pt/CNF-R523 in 0.1 M H_2SO_4 in the absence and presence of 0.1 M glucose. In the absence of glucose and with an increase in potential, a current was measured that relates to several electrochemical processes that take place on the electrode surface: 0.1-0.3 V vs. RHE hydrogen desorption and double layer charging,[55] 0.4-0.5 V vs. RHE double layer charging, 0.4-0.8 V vs. RHE the oxidation of phenol/hydroquinone surface groups to lactone and carbonyl/quinone groups and double layer charging,[54,69] and 0.8-1.0 V vs. RHE oxidation of metallic Pt to PtO_x and double layer charging.[55] In the presence of glucose and below 0.28 V vs. RHE the current is lower than in the absence of glucose. This indicates that glucose adsorbs on the surface of the Pt catalyst, thereby suppressing hydrogen adsorption. In the presence of glucose and above 0.28 V vs. RHE the current is higher than in the absence of glucose. This indicates that Pt is catalyzing the oxidation of glucose. Yet, electrochemical processes related to double layer charging, oxidation of phenol/hydroquinone surface groups to lactone and carbonyl/quinone groups, and Pt oxidation, partially contribute to the current that is measured for glucose oxidation. Therefore, the current measured for the electrocatalytic oxidation of glucose was corrected for other electrochemical processes that might take place on the electrode surface.
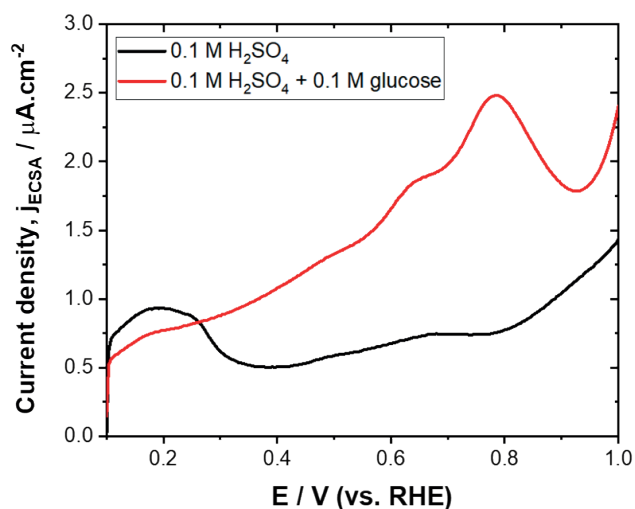
Figure S3.13. Linear sweep voltammetry of a Pt/CNF-R523 measured at 1 $mV.s^{-1}$ in 0.1M H_2SO_4 in the absence and presence of 0.1M glucose.

Figure S3.14 shows the electrocatalytic oxidation of glucose studied under static conditions in the presence of 0.1 M glucose and under convection in the presence of 0.5 M glucose. This experiment was performed to evaluate whether the differences in catalytic activity arise from mass transport limitations. Under convection and in the presence of higher concentrations of glucose the current densities go up at 0.78 V *vs.* RHE from 1.8 mA.cm^{-2} to 4.8 mA.cm^{-2} for Pt/CNF-R973 and from 1 mA.cm^{-2} to 3.4 mA.cm^{-2} for Pt/CNF-R973. This increase in current density corresponds to an increase in catalytic activity due to a higher concentration of reactant being available for catalytic conversions and improved diffusion due to convection. Yet, the increase in current density is in the same order of magnitude for Pt/CNF-R523 (2.7x) and Pt/CNF-R973 (3.5x). This indicates that both catalysts suffer similar diffusion limitations.
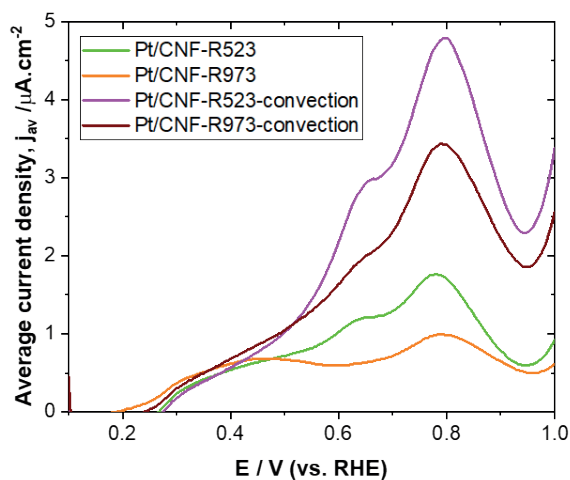
Figure S3.14. *Background corrected linear sweep voltammetry measured at 1 mV.s^{-1} in 0.1 M H$_2$SO$_4$ in the presence of 0.1 M glucose under static conditions and the presence of 0.5 M glucose under convection.*

CO-stripping was performed on Pt/CNF-R523-EO, Pt/CNF-R773-EO and Pt/CNF-R973-EO (Figure S3.15) to evaluate the effect of electrochemical oxidation on the properties and ECSA of the Pt particles. After electrochemical modification, the current measured at 0.8 V *vs.* RHE increases slightly, while the current measured below 0.72 V *vs.* RHE and above 0.85 V *vs.* RHE decreases slightly for all three catalysts. This indicates that the Pt surface structure changes slightly after electrochemical oxidation. However, after electrochemical oxidation, the CO-stripping curves are very similar and therefore indicate that the surface structure of the Pt particles is nearly identical. Moreover, the ECSA of Pt/CNF-R523 and Pt/CNF-R773 decreased by 15 and 7 % respectively, while the ECSA of Pt/CNF-R973 increased by 2 %. The decrease in ECSA of Pt/CNF-R523 could be attributed to the small Pt particles on this catalyst, making it more susceptible to leaching.[55,56]
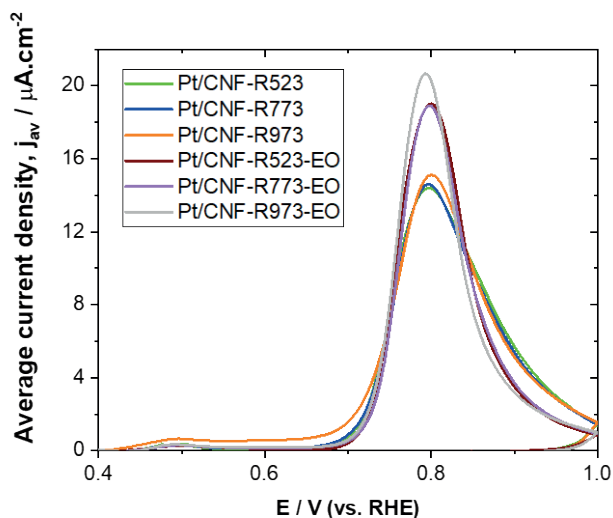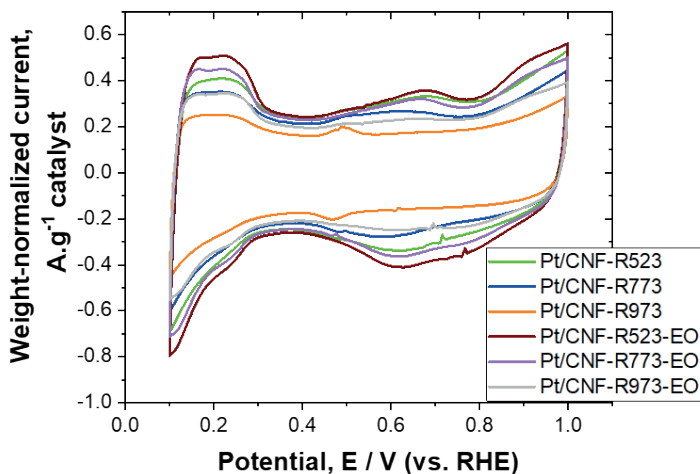

Figure S3.15. CO-stripping curves of Pt/CNF-R523, Pt/CNF-R773 and Pt/CNF-R973 (before electrochemical oxidation) and Pt/CNF-R523-EO, Pt/CNF-R773-EO and Pt/CNF-R973-EO (after electrochemical oxidation) obtained in 0.1 M H_2SO_4 recorded at 5 mV.s^{-1}.

Pt/CNF-R523-EO, Pt/CNF-R773-EO and Pt/CNF-R973-EO were characterized by CV (Figure S3.16) to evaluate the specific capacitance of the catalyst. After electrochemical modification and based on the CV, the specific capacitance (e.g., the content of phenol and carbonyl/quinones groups present on the support) increased only slightly for Pt/CNF-R523 (3 %), while it increased more significantly for Pt/CNF-R773 (13 %) and Pt/CNF-R973 (27 %). The increase in specific capacitance can be related to an increase in pseudo capacitance and is much more severe for Pt/CNF-R973 and Pt/CNF-R773 than for Pt/CNF-R523 since Pt/CNF-R523 already contains many support oxygen groups while Pt/CNF-R973 and Pt/CNF-R773 does not/barely contains any support oxygen groups. Even though the 3% increase in specific capacitance for Pt/CNF-R523 appears to be minimal, it is already sufficient to electrocatalytically oxidize the first three adjacent carbon atoms (0.33 nm) of the annulus of the Pt particles (calculations given in the Supporting Excel file). In contrast after electrochemical modification, the hydrogen underpotential deposition region from the CVs did increase significantly for Pt/CNF-R523, Pt/CNF-R773 and Pt/CNF-R973. Potentially hydrogen can get adsorbed on the Pt particles and migrate to adjacent support oxygen groups, where it gets stored.[98,99]

Figure S3.16. *Cyclic voltammograms of Pt/CNF-R523, Pt/CNF-R773 and Pt/CNF-R973 (before electrochemical oxidation) and Pt/CNF-R523-EO, Pt/CNF-R773-EO and Pt/CNF-R973-EO (after electrochemical oxidation) in 0.1 M H_2SO_4 at a scan rate of 5 mV.s^{-1}.*

Current normalization by adsorbable surface area

The currents measured during the electrocatalytic oxidation of glucose over Pt/CNF-R523-EO and Pt/CNF-R973-EO were normalized by the ASA (j_{ASA}). The ASA was determined through the summation of the ECSA and the surface area in the annulus of the Pt particles. The ECSA was derived from CO-stripping experiments based on the Pt/CNF loading on GCE, while the surface of the annulus ($A_{annulus}$) was calculated according to the following equation:

$$A_{annulus} = \left(\pi \left(r_p + \delta \right)^2 - \pi\, r_p^2 \right) * n_p$$

In this equation r_p, δ and n_p are related to the radius of the Pt particle, the width of the annulus, and the number of Pt particles present on 1.5 mg Pt/CNF. The width of the annulus is based on the diameter of glucopyranose (0.86 nm).
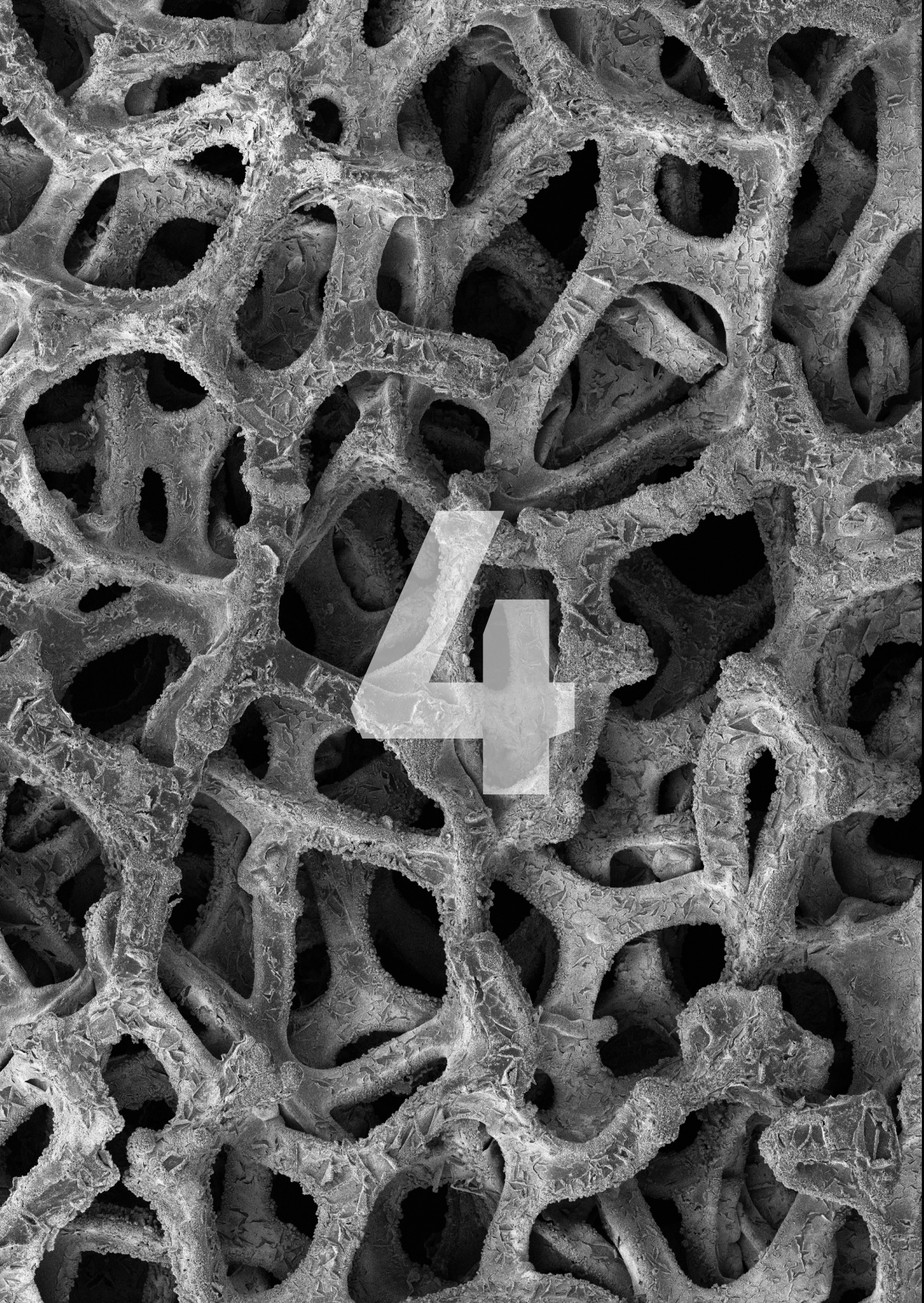
CHAPTER 4

Steering the Selectivity of Electrocatalytic Glucose Oxidation by the Pt Oxidation State

Abstract

Electrocatalytic glucose oxidation can produce high value chemicals, but selectivity needs to be improved. Here we elucidate the role of the Pt oxidation state on the activity and selectivity of electrocatalytic oxidation of glucose with a new analytical approach, using high-pressure liquid chromatography and high-pressure anion exchange chromatography. It was found that the type of oxidation, i.e. dehydrogenation of primary and secondary alcohol groups or oxygen transfer to aldehyde groups, strongly depends on the Pt oxidation state. Pt^0 has a 7-fold higher activity for dehydrogenation reactions than for oxidation reactions, while PtO_x is equally active for both reactions. Thus, Pt^0 promotes glucose dialdehyde formation, while PtO_x favors gluconate formation. The successive dehydrogenation of gluconate is achieved selectively at the primary alcohol group by Pt^0, while PtO_x also promotes the dehydrogenation of secondary alcohol groups, resulting in more complex reaction mixtures.
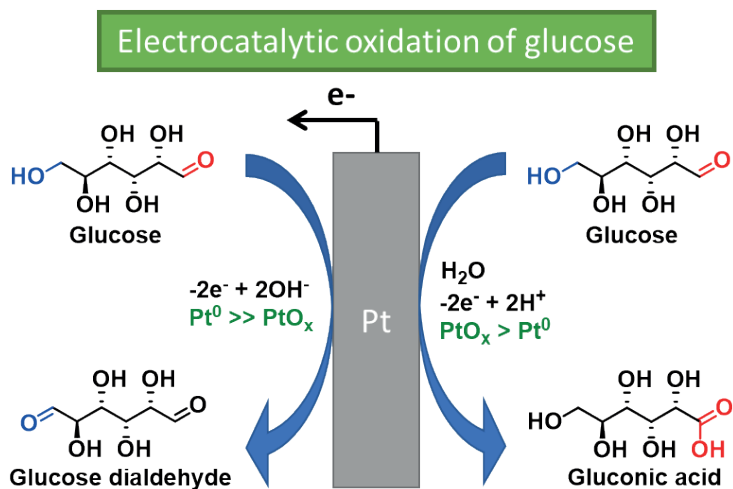
4.1 Introduction

Glucose is a widely abundant biomass-based feedstock, that can be electrocatalytically oxidized by (or cogenerate) renewable electricity to yield numerous chemicals that are of great interest in the chemical industry.[1,2] The most relevant products are glucaric acid and gluconic acid, which are among the top value-added chemicals mentioned by the National Renewable Energy Laboratory.[2,3] Other glucose oxidation products include 2-keto gluconic acid,[4] 5-keto gluconic acid,[5] and glucuronic acid.[6] These glucose oxidation products are (precursors to) platform molecules and specialty chemicals that are used as building blocks or as additives in pharmaceuticals, food, feed, and materials.[2–9]

However, currently the mechanism behind the catalyst selectivity for the (electro-)oxidation of glucose and how to steer it to a desired product is not yet fully understood. To steer the selectivity it is essential to understand the reaction pathway, which requires the quantification of all (intermediate) products during the glucose oxidation reaction. Several chemocatalytic[10–13] and electrocatalytic[4,14,15] studies have investigated the glucose oxidation pathway, where different analytical techniques (e.g., 2D-NMR,[10] HPIC,[12,15] and HPLC,[4,11,12,14] HPLC-MS,[11] and GC-MS[4]) have been applied in an attempt to quantify the (intermediate) glucose oxidation products. Still, various (intermediate) products have not been addressed even though they are expected to be formed during the reaction. Some examples include glucose dialdehyde (only mentioned, but never quantified),[4,10–15] guluronic acid or glucuronic acid (often only one or the other is quantified),[4,11–15] and 2-keto gluconic acid and 5-keto gluconic acid (seldomly quantified).[10,11,14]

The similarity in the structures of glucose oxidation products poses a challenge in their differentiation and may result in inadequate separation by the analytical technique employed. This problem in correctly identifying glucose oxidation products can be observed for guluronic acid and glucuronic acid, which are stereoisomers.[10] As a result, it has been claimed that gluconic acid can be oxidized to glucuronic acid,[4,12] while guluronic acid is expected based on the stereochemistry of the molecules. Moreover, for an adequate separation of guluronic acid and glucuronic acid, other techniques than HPLC or GC are required, as has been shown for the compositional analysis of seaweed (e.g., consisting of guluronic acid and glucuronic acid).[16]

Here, we address this challenge by introducing a new analytical approach that combines high-pressure liquid chromatography (HPLC)[17,18] with high-pressure anion exchange chromatography (HPAEC)[16]. Unlike other analytical techniques, HPAEC separates ionizable molecules based on their total charge. This analytical approach enables us to quantify all (intermediate) products in the glucose oxidation pathway, allowing us to 1) simultaneously quantify guluronic acid, glucuronic acid, 2-keto gluconic acid, and 5-keto gluconic acid and 2) quantify glucose dialdehyde. With this analytical approach in hand, we can draw a complete map of the reaction pathway for

the electrocatalytic oxidation of glucose and show how in detail the Pt oxidation state affects the selectivity.

4.2 Experimental Procedures

4.2.1. Chemicals and materials preparation

Potassium permanganate (≥ 99%) and Sulfuric acid (96%) were purchased from Sigma-Aldrich; and Hydrogen peroxide (30%) was purchased from VWR and used for cleaning the glassware. The chemicals used for preparing the electrolyte were sodium phosphate dibasic (≥ 99.99%, Sigma-Aldrich) and sodium phosphate monobasic (≥ 99.999%, Honeywell). Gucose (≥ 99.5%), gluconic acid sodium salt (≥ 99%), glucuronic acid sodium salt monohydrate (97.5-102.5%), 5-keto-gluconic acid potassium salt (≥ 98%), glucaric acid potassium salt (≥ 98%), arabinose (≥ 98%), oxalic acid (98%) and formic acid (≥ 95%) were purchased from Sigma-Aldrich; guluronic acid sodium salt (≥ 98.0%) and 2-Keto-D-gluconic acid (≥ 98.0%) were obtained from Biosynth/Carbosynth; and glucose dialdehyde was purchased from Cymit Quimica S.L and used as reactants and for product analysis.

The glassware used in this study was stored in a 1 g.L^{-1} permanganate and 0.5 M sulfuric acid solution. Before use, the glassware was rinsed with a dilute sulfuric acid and hydrogen peroxide solution. Successively, the glassware was rinsed multiple times with MiliQ. [1]

A 50·50 mm Pt gauze (3600 mesh/cm2, 0.04 mm wire diameter, 99.9%) was woven around a Pt wire (1 mm wire diameter, 99.95%) and used as the anode and cathode. An Ag/AgCl (saturated KCl) electrode was used as the reference electrode. All measured potentials in this study have been converted to RHE, according to the Nernstian equation (equation S2), where the standard equilibrium potential of Ag/AgCl ($E^0_{Ag/AgCl}$) at 25°C equals 0.198.

$$E_{RHE} = E_{Ag/AgCL} + 0.059pH + E^0_{Ag/AgCl}$$ Eq. S1

All electrochemical experiments were conducted in an H-cell divided by a Nafion™ 117 membrane (0.180 mm thick, >0.90 meq/g exchange capacity). Each compartment contained 37 ml of electrolyte and was purged 30 min with Ar before conducting electrochemical experiments.

4.2.2. Electrochemical measurements

The electrochemical surface area (ECSA) of the Pt electrode was determined from the hydrogen underpotential deposition method from the hydrogen desorption peak obtained by cyclic voltammetry.[2] 20 continuous CVs were made in Ar-saturated 0.1 M H_2SO_4 between 0.1 V and 1.5 V *vs.* RHE at a scan rate of 50 mV.s^{-1}. From the final scan, the ECSA was calculated according to equation S2, where Q_r is the charge of the hydrogen underpotential corrected for double-layer surface charging and 210 µC.cm^{-2} is the charge capacity of hydrogen desorption from Pt. The derived ECSA was used to normalize all measured currents in this study.

$$ECSA = \frac{Q_r}{210}$$

<div align="right">Eq. S2</div>

All other electrochemical experiments were conducted in 0.2 M phosphate buffer solution (PBS, pH = 6.8). Before each experiment, the potential was cycled 20 times between 0.1 V and 1.5 V *vs.* RHE at a scan rate of 50 mV.s^{-1} to check that the system was free from any contaminants. Successively, a specific amount of reactant was added to the anode compartment and purged for 30 min with Ar to assure a homogenous and Ar-saturated solution.

Linear sweep voltammetry (LSV) was used to derive the peak potentials for the electrocatalytic oxidation of 0.1 M glucose, which were used for chronoamperometric measurements. LSV was conducted by increasing the potential with 1 mV.s^{-1} from 0.07 V to 1.45 V *vs.* RHE.

Chronoamperometry (CA) was performed with a 400 ml.min^{-1} Ar flow through the solution to induce convection unless stated otherwise, and a potential program.[3] The potential program includes two short potential pulses followed by a potential plateau that is repeated during the experiment to retain an electroactive catalyst. Without this potential program, the catalyst would deactivate rapidly due to the strong adsorption of oxidized species.[3] The first two short pulses consisted of 2.0 V *vs.* RHE for 0.5 s and 0.2 V *vs.* RHE for 5 s, corresponding to the desorption of oxidized species (E_{des}), and the reduction of the catalyst followed by the dissociative adsorption of glucose ($E_{red/ads}$). The potential plateau was held for 500 s and corresponds to the peak potentials required for electrocatalytically oxidizing glucose (E_{ox}), which were derived from the LSV experiment. The potential program was optimized to maximize the oxidation of the reactants at E_{ox}. During CA measurements 0.5 ml samples were collected and analyzed by two chromatographic techniques.

4.2.3. Sample analysis

High-pressure anion exchange chromatography (HPAEC, Thermo Fischer Scientific Dionex ICS 3500) was performed with a Carbopac PA-1 guard column (1 x 50 mm) and a Dionex CarboPac PA-1 IC Column (2 x 250 mm) coupled to an electrochemical pulsed amperometric detector (PAD, Dionex ICS-5000 ED). HPAEC-PAD was performed based on a protocol described by Huijgen et al.[4] Chromatography was conducted at 20 ˚C with a 0.3 ml.min^{-1} eluent flow, composed of three different eluents: 0.1 M NaOH, 1 M NaOAC in 0.1 M NaOH, and De-ionized water. The gradient applied in this study is described in Table 4.1. Before HPAEC analysis the samples were filtered over a 0.2 µm syringe filter and diluted to prevent a detector overload for the oxidized glucose species while retaining a 25 mM glucose and 50 mM PBS concentration. A 10 µl injection volume was used.

Table 4.1. *HPAEC-PAD gradient profile used for the eluent.*

Reactant	Eluent		
	0.1 M NaOH	1 M NaOAC in 0.1 M NaOH	De-ionized water
	%	%	%
0	15	0	85
17.0	15	0	85
17.5	16	11	73
29.5	40	15	45
34.9	25	65	10
35.0	0	100	0
45.0	0	100	0
45.1	15	0	85

High-pressure liquid chromatography (HPLC, Dionex UltiMate 3000 RS) was performed with a Biorad HPX-87H column (300 x 7.8 mm) coupled to a UV detector (Ultimate 3000 RS VW) and RI detector (Shodex RI-101). Chromatography was conducted at 50 ˚C with a 0.5 ml.min^{-1} 5 mM sulfuric acid eluent flow.[5] The injection volume was 10 μl. For product analysis, the UV detector was set at 210 nm and the RI detector was thermostated at 50 ˚C.

The molar concentration of the products were normalized to the moles of carbon product formed according to equation S3 and thereby expressed as mol carbon ($M_{c,x}$, mol$_c$.l^{-1}). The moles of carbon product was calculated by multiplying the product concentration of each products (c_x, mol.l^{-1}) by the carbon atoms present in its molecular structure (CF_x, -).

$$M_{c,x} = c_x * CF_x$$

Eq. S3

The carbon balance (C_{bal}, %) was calculated to evaluate the reliability of the analytical method according to equation S4. The product concentration of the individual products was multiplied by the carbon atoms present in its molecular structure and summed up. This value was divided by the glucose concentration (c_g, mol.l^{-1}) and multiplied by the number of carbons atoms present in glucose (CF_g, -).

$$C_{bal} = \frac{\sum c_x * CF_x}{c_g * CF_g} * 100\%$$

Eq. S4

The overall faradaic efficiency ($FE_{ov,t = 6h}$, %) was calculated to determine the efficiency of charge transfer for the electrocatalytic oxidation of glucose according to equation S5. The charge produced for the formation of the individual products was determined by multiplying the product concentration of the individual products (c_x, mol.l^{-1}) with the electrolyte volume (V, l), the number of electrons required to form the specific product from the reactant that is

164

electrocatalytically oxidized (z_x, -) and the Faraday constant (F, 96.485 C.mol^{-1}). These values for the different products were summed up and divided by the measured charge transferred (C).

$$FE_{ov,t = 6h} = \frac{\sum c_x * V * z_x * F}{C} * 100\%$$ Eq. S5

This study aims to evaluate the effect of the Pt oxidation state on the electrocatalytic oxidation of glucose at different potentials. Despite this, an alternating potential was applied to reactivate the catalyst (see Electrochemical measurements), which might result in the formation of products at E_{des} rather than E_{ox} (the potential of interest). Hence, the measured charge at the desorption potential at time point t (C_{des}) was compared to the theoretical charge required from each product (C_x), which was determined with equation S6. C_x was calculated by multiplying c_x with V, z_x, and F.

$$C_x = c_x * V * z_x * F$$ Eq. S6

The turnover frequency (TOF, s^{-1}) was calculated to evaluate the catalyst activity according to equation S7. The individual product concentration (c_x) was multiplied by V, the number of reaction steps needed to go from the initial reactant to the product measured (rs_x, -), and Avogadro's number (N_A, $6.022*10^{23}$ mol^{-1}). The summation of these values for the different products was divided by the total reaction time (t) multiplied by the surface density of Pt atoms (N_{Pt}, $1.3*10^{15}$ atoms.cm^{-2}) and the active surface area of the Pt electrode (ECSA, cm^2).

$$TOF = \frac{\sum c_x * V * rs_x * A_N}{t * N_{Pt} * ECSA}$$ Eq. S7

The catalyst selectivity towards a specific product at t = 6h (S_x, %) was evaluated according to equation S8. Here c_x was multiplied by CF_x and divided summation of the different products formed.

$$S_x = \frac{c_x * CF_x}{\sum c_x * CF_x} * 100\%$$ Eq. S8

4.3 Results & Discussion

Figure 4.1A shows the linear sweep voltammograms (LSV) of glucose oxidation and of the oxidation of the main glucose oxidation products (gluconate and glucuronate) on a polycrystalline Pt electrode in a pH = 6.8 buffer solution (0.2 M phosphate buffer solution, PBS). These reaction conditions were chosen to avoid non-electrochemical side reactions, such as isomerization, retro-aldol and aldol condensation reactions.[19] 0.1M reactant concentrations were used to avoid the overload of the detectors of the chromatographic equipment and to prevent high conversions of the reactants. This all enables the discrimination between catalytic activities towards different reactants. Figure 4.1B displays the dominant structures of glucose,[20]

gluconate,[21] and glucuronate[22] under the studied reaction conditions and highlights the most reactive groups of these species.

For glucose oxidation, Figure 4.1A shows two oxidation peaks, at 0.64 V and 1.2 V *vs.* RHE respectively.[23] This characteristic LSV is common for the electrochemical oxidation of small organic molecules, indicating the presence of two reaction pathways for oxidation.[23–26] Since the first anodic peak is below the Pt surface oxidation potential, Pt is expected to be mainly in its metallic state (Pt^0, though steps and defects sites are likely mildly oxidized[27]), while the second anodic peak is above the surface oxidation potential of Pt and hence the surface is in a more oxidized state (referred to as PtO_x).[24,28] Figure S4.1 shows the CV of Pt in 0.2 M PBS to give a better understanding of its surface structure and its oxidation state as a function of the applied potential. The LSV of glucose shows a peak potential at 0.64 V *vs.* RHE, corresponding well to the LSV of Pt(110)-type sites.[29] For Pt^0, an anodic current density of ca. 50 $\mu A.cm^{-2}$ can be observed for the electrocatalytic oxidation of glucose, while a much lower current density is observed for gluconate and glucuronate oxidation (4 $\mu A.cm^{-2}$). PtO_x shows an anodic current density for the electrocatalytic oxidation of glucose of ca. 70 $\mu A.cm^{-2}$ and also a lower anodic current density for gluconate (10 $\mu A.cm^{-2}$) and glucuronate (20 $\mu A.cm^{-2}$) oxidation, but the difference is less pronounced than on Pt^0.[30] This indicates that the catalytic activity of Pt^0 follows glucose >> gluconate ~ glucuronate, while the activity of PtO_x follows glucose > glucuronate > gluconate.
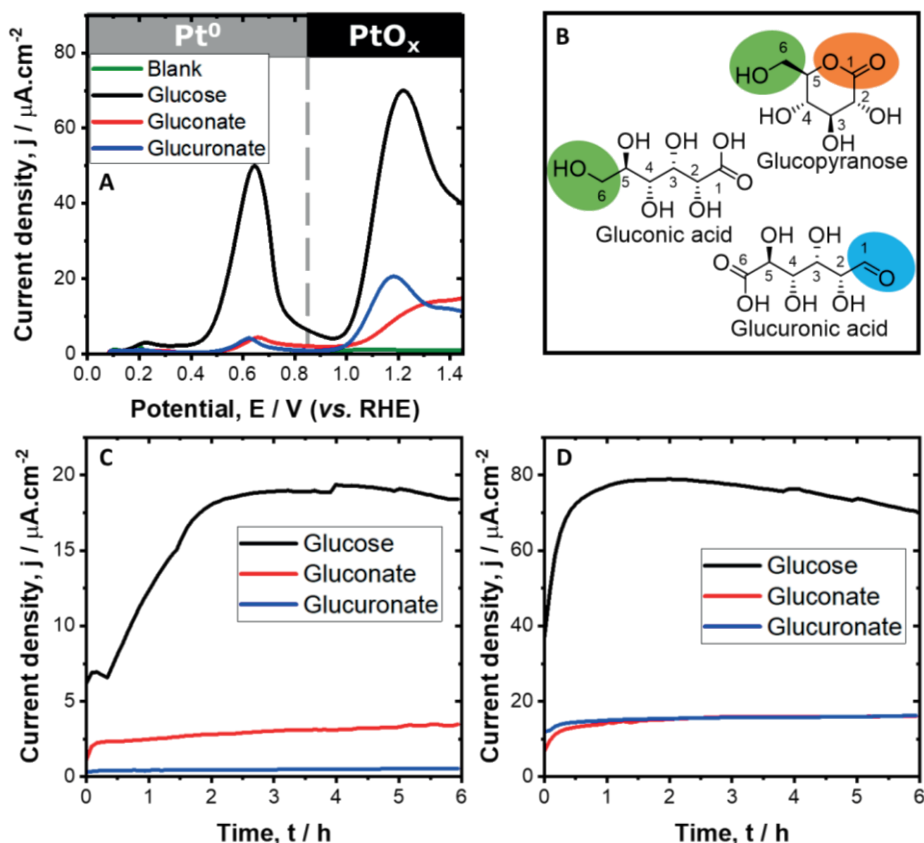
Figure 4.1. A) Blank LSV and LSV of 0.1 M glucose, 0.1 M gluconate, and 0.1 M glucuronate in 0.2 M PBS (pH = 6.8) on a polycrystalline Pt electrode recorded at a scan rate of 1 mV.s⁻¹. The potential windows 0-0.85 V and > 0.85 V vs. RHE correspond to Pt^0 and PtO_x, respectively. B) The dominant structures of glucose (e.g., glucopyranose), gluconate and glucuronate at the studied reaction conditions (for simplicity the structures have been drawn in protonated form) in which the main reactive groups are highlighted. Current-time curves for the electrocatalytic oxidation of 0.1 M glucose, 0.1 M gluconate, and 0.1 M glucuronate in 0.2 M PBS over Pt^0 (0.64 V vs. RHE, C) and PtO_x (1.2 V vs. RHE, D).

For chronoamperometric measurements, the applied reaction conditions were optimized to limit mass transport limitations by applying convection (Figure S4.2), to retain a constant pH by buffering with 0.2 M PBS (Figure S4.3), and to retain an active catalyst by applying a potential program (Figure S4.3).[15,30]

Figures 4.1C and 4.1D show the chronoamperometric measurements for the electrocatalytic oxidation of glucose, gluconate, and glucuronate on Pt^0 (0.64 V vs. RHE) and PtO_x (1.2 V vs. RHE), respectively. The current densities do not significantly change from 2 to 6 h, indicating that the formation of (intermediate) products do not significantly affect the catalyst activity. After 6 h of reaction on Pt^0 (0.64 V vs. RHE), the current density for the electrocatalytic oxidation of glucose

(18 µA.cm^{-2}) is a 5-fold higher than for gluconate (3.5 µA.cm^{-2}) and a 12-fold higher than for glucuronate (0.5 µA.cm^{-2}). By contrast, after 6 h of oxidation on PtO$_x$ (1.2 V vs. RHE), the current densities for the electrocatalytic oxidation of glucose (70 µA.cm^{-2}) is a 4-fold higher than for gluconate and glucuronate (16 µA.cm^{-2} each). The overall lower catalytic activity of Pt^0 compared to PtO$_x$ can be attributed to the lower applied potential for Pt^0 and a partial CO poisoning of Pt^0.[29,31,32] These results indicate that both Pt^0 and PtO$_x$ exhibit higher catalytic activity in the oxidation of glucose as compared to gluconate or glucuronate oxidation. By contrast, PtO$_x$ is equally active for catalyzing the oxidation of gluconate and glucuronate, while Pt^0 is more active for catalyzing the oxidation of gluconate than glucuronate. This shows that Pt^0 is more active for catalyzing the dehydrogenation of C6-OH of gluconate than for catalyzing the oxidation of C1=O of glucuronate, while PtO$_x$ is equally active for both reactions.[25,33] Moreover, this reveals that PtO$_x$ is more active than Pt^0 for catalyzing oxygen transfer reactions. These results are in agreement with results of the electrocatalytic oxidation of methanol and glycerol.[25,32–34] Those studies showed that Pt-Pt pair sites stabilize and dehydrogenate primary alcohols and Pt-OH sites are required for oxygen transfer reactions.[32,34]

All (intermediate) products formed by the electrocatalytic oxidation of glucose were quantified to establish the reaction pathway and product selectivity as a function of Pt oxidation state. Here we have developed a new analytical approach, in which high pressure anion exchange chromatography-pulsed amperometric detection (HPAEC-PAD, Figure S4.5A-B) and high pressure liquid chromatography-refractive index-ultraviolet (HPLC-RI-UV, Figure S4.6A-B) were combined, to separate the different intermediates and products (e.g., glucose dialdehyde, gluconate, guluronate, glucuronate 2-keto gluconate, 5-keto gluconate, and glucarate), enabling their quantification. The carbon balance was close to 100% for the electrocatalytic oxidation of glucose over Pt^0 and PtO$_x$, indicating that all products were accurately quantified.

Figure 4.2A-F shows the concentrations of products as a function of time during the electrocatalytic oxidation of glucose over Pt^0 and PtO$_x$, evidencing a significant effect of the Pt oxidation state on the selectivity for catalyzing different functional groups.
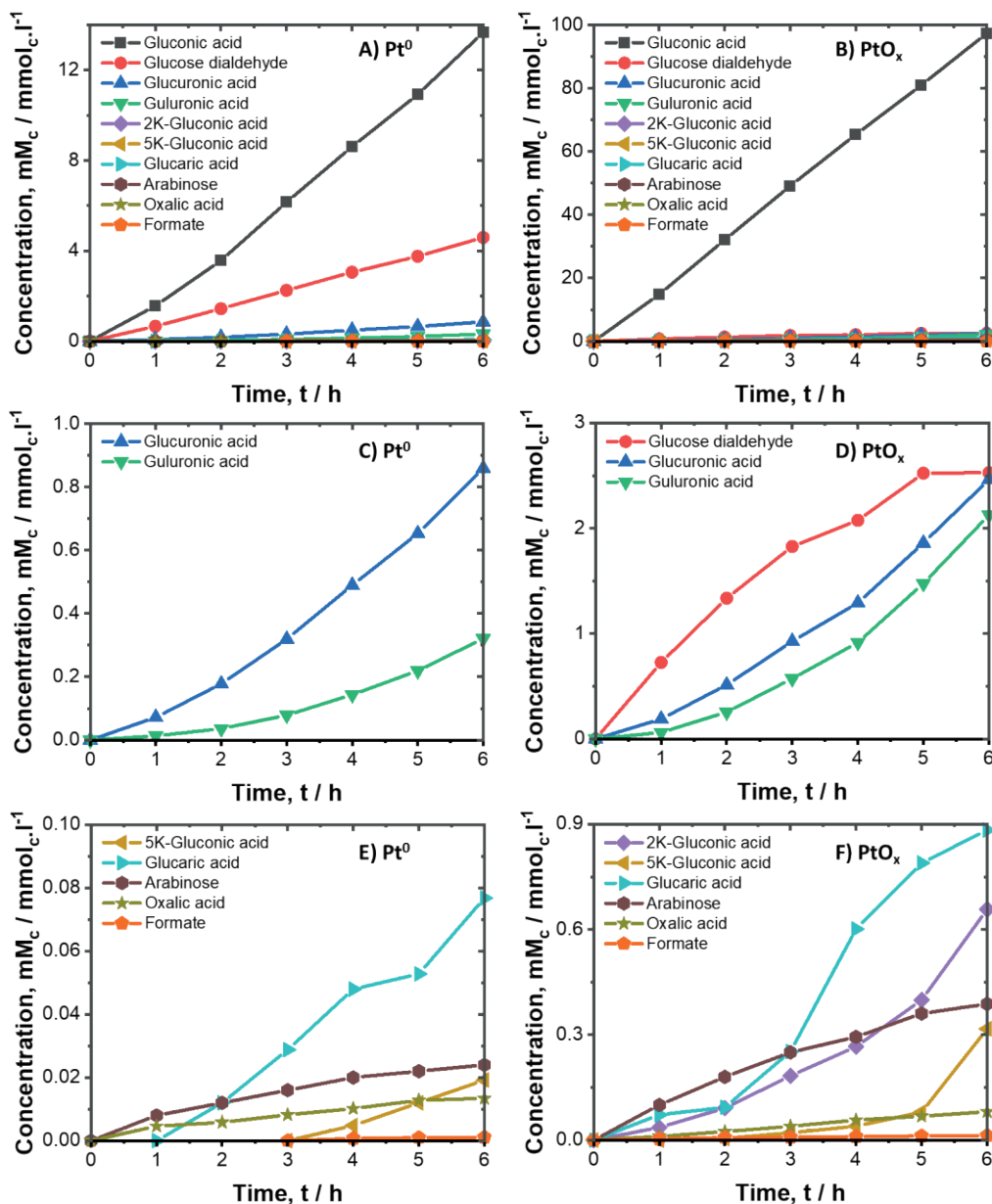
Figure 4.2. *Major (A-B), secondary (C-D) and minor (E-F) product concentration-time curves for the electrocatalytic oxidation of glucose on Pt⁰ and PtOₓ in 0.2 M PBS (pH = 6.8).*

For glucose oxidation over Pt^0, Figure 4.2A shows a linear increase in gluconate and glucose dialdehyde concentration over time. This suggests that these products are formed at a constant rate, exhibiting an approximately zero-order kinetics, reaching concentrations of 13.5 and 4.6 mmolc.l^{-1} respectively. By contrast, PtO_x (Figure 4.2B) is much more active for gluconate

production (reaching 98 mmolc.l^{-1}), while the production of glucose dialdehyde (Figure 4.2D) only reaches 2.5 mmolc.l^{-1}. This reveals that Pt^0 is more active towards the electrocatalytic dehydrogenation of the C6-OH of glucose, while PtO$_x$ favors the electrocatalytic dehydrogenation/oxidation of glucose, in line with the electrocatalytic oxidation of methanol and glycerol over Pt^0 and PtO$_x$.[32,34]

As for the secondary products, Figure 4.2C shows that the electrocatalytic oxidation of glucose on Pt^0 results in a faster exponential increase in glucuronate concentration compared to guluronate concentration. For PtO$_x$, Figure 4.2D reveals that the exponential increase in glucuronate and guluronate concentration proceed at a similar rate. The observed exponential increase in concentration suggests that guluronate and glucuronate are formed according to first-order kinetics, originating from gluconate/glucose dialdehyde and glucose dialdehyde respectively. As a result, the higher selectivity of Pt^0 towards glucuronate can be related to the higher selectivity towards glucose dialdehyde of Pt^0 compared to PtO$_x$.

In Figure 4.2E and F we illustrate the formation rates of other minor products. The electrocatalytic oxidation of glucose on Pt^0 shows an increase in 5-keto gluconate concentration (Figure 4.2E), while for PtO$_x$ (Figure 4.2F) an increase in 2-keto gluconate and 5-keto gluconate concentration is observed. To observe these products, the application of a desorption potential (2V vs RHE) was needed. That desorption potential also reactivated the catalyst (Figure S4.3). To evaluate whether these products are indeed formed during normal operation on Pt^0 (0.64 V *vs.* RHE) and PtO$_x$ (1.2 V *vs.* RHE) and not at the desorption potential (2.0 V *vs.* RHE), the theoretical coulombs required to form these products were compared to the coulombs measured at the desorption potential (all values are given in Table S4.1). From these results, it is clear that PtO$_x$ forms 2-keto gluconate and 5-keto, but it is uncertain whether Pt^0 forms 5-keto gluconate. This implies that PtO$_x$ is more active for the dehydrogenation of the secondary alcohol groups of gluconate, which is similar to the dehydrogenation of glycerol to dihydroxyacetone under neutral conditions[25] or sorbitol to fructose under acidic conditions.[35]

The concentration profiles of glucarate over Pt^0 and PtO$_x$ as shown in Figure 4.2E-F suggest that its formation involves multiple pathways. Specifically, glucarate can be formed through the electrocatalytic oxidation of both guluronate and glucuronate.

Finally, the concentration profiles of arabinose, oxalate and formate (e.g., C$_5$-C$_1$ products) over Pt^0 and PtO$_x$ increase gradually over time, revealing that C-C cleavage reactions are being catalyzed, but only at very low rates.

Table 4.2 summarizes the selectivity of the products, faradaic efficiency (FE), and turnover frequency (TOF) for the electrocatalytic oxidation of glucose, gluconate, and glucuronate on Pt^0 and PtO$_x$.

Table 4.2. *Faradaic efficiency, TOF and product selectivity, for the electrocatalytic oxidation of 0.1M glucose, gluconate, and glucuronate in 0.2 M PBS (pH = 6.8) on Pt^0 and PtO_x. A color code was added to guide the eye, going from high (green) to low (red) selectivities. The description of the abbreviations of the (intermediate) products are given in the footnote.*

Reactant	Catalyst	FE	TOF	Product selectivities (%)[a]							
		%	(10^{-3} s^{-1})	GA	GD	GUL	GLU	2-kGA	5-kGA	GAR	C_5-C_1
Glucose	Pt^0	105	36	70	23	2	4	-	0.1	0.4	0.2
GA	Pt^0	101	6	-	-	86	-	-	3	10	1
GLU	Pt^0	141	1	-	-	-	-	-	-	98	2
Glucose	PtO_x	105	210	91	2	2	2	0.6	0.3	0.8	0
GA	PtO_x	114	36	-	-	70	-	12	6	9	2
GLU	PtO_x	101	40	-	-	-	-	-	-	100	0

[a] GA = gluconate, GD = glucose dialdehyde, GUL = guluronate, GLU = glucuronate, 2-kGA = 2-keto gluconate, 5-kGA = 5-keto gluconate, GAR = glucarate, AR = arabinose, OA = oxalate, FA = formate

The low conversions of gluconate and glucuronate during electrocatalytic oxidation made it difficult to accurately determine the carbon balance closure for these reactions. Therefore, in Table 4.2 the product selectivities are based on the products formed (CO and CO_2/HCO_3^- cannot be detected by the chromatographic techniques). However, the FE is close to 100% for all reactions and therefore shows that all products formed during CA were quantified, except for the electrocatalytic oxidation of glucuronate on Pt^0, likely due to the low concentrations of glucarate.

The TOF for the electrocatalytic oxidation of glucose, gluconate, and glucuronate on Pt^0 (0.64 V *vs.* RHE) are 0.036, 0.006 and 0.001 s^{-1} and on PtO_x (1.2 V *vs.* RHE) are 2.1, 0.36 and 0.040 s^{-1}. PtO_x has a similar TOF for the electrocatalytic oxidation of gluconate and glucuronate, while Pt^0 has a lower activity for the electrocatalytic oxidation of glucuronate. This reveals that PtO_x is equally active for catalyzing the dehydrogenation of C_6-OH of gluconate as it is for oxidation of C_1=O of glucuronate. while Pt^0 is more active for catalyzing the dehydrogenation of C_6-OH of gluconate than it is for oxidation of C_1=O of glucuronate (Figure 4.1C).

As shown in Table 4.2, glucose is more selectively converted to glucose dialdehyde by Pt^0 (23%) than by PtO_x (2%), suggesting that Pt^0 favors the dehydrogenation of C_6-OH of glucose. By contrast, PtO_x is more selective towards gluconate (91%), indicating that it promotes the dehydrogenation/oxidation of the anomeric carbon of glucose. In line with these results, gluconate was selectively converted to guluronate (86%) by Pt^0, which shows the high selectivity of Pt^0 towards C_6-OH dehydrogenation. By contrast, PtO_x also promotes the formation of 2-keto gluconate (12%) and 5-keto gluconate (6%), revealing that PtO_x also promotes secondary alcohol

dehydrogenation, resulting in a loss in selectivity towards gluconate. Finally, glucuronate can be converted with similar selectivity towards glucarate (~100%) by Pt^0 and PtO_x, indicative that they both are highly selective for the electrocatalytic oxidation of $C_1=O$ of glucuronate.

Scheme 4.1 illustrates the electrocatalytic oxidation pathways of glucose over Pt in neutral reaction conditions. It is expected that gluconate and glucose dialdehyde are primary products, while guluronate and glucuronate are secondary products. To verify this, an experiment was conducted with different initial glucose concentrations (Figure S4.7). This experiment revealed that a reduction in initial glucose concentration corresponds with decreased selectivity towards primary oxidation products (gluconate and glucose dialdehyde) and an increase in selectivity towards secondary oxidation products (guluronate and glucuronate).
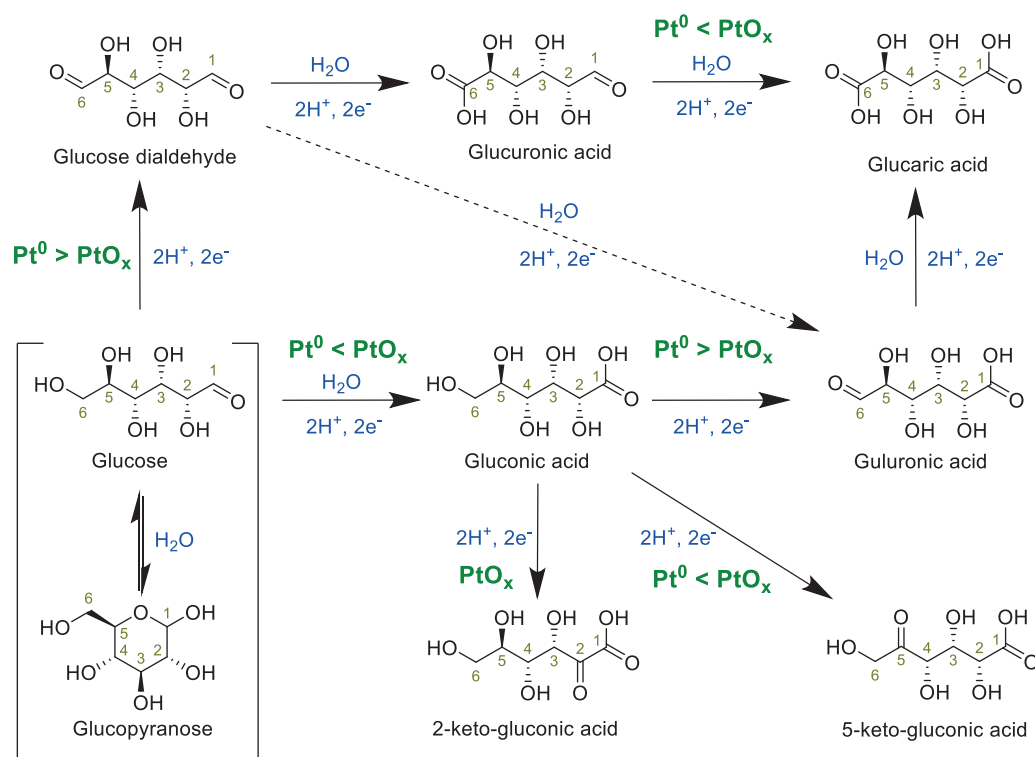
Scheme 4.1. Reaction pathways for the electrocatalytic oxidation of glucose on Pt^0 and PtO_x in neutral solution (for simplicity the structures have been drawn in protonated form).

The scheme also highlights the preferred pathways for Pt^0 and PtO_x. Firstly, glucose can either be dehydrogenated at the C_6-OH to glucose dialdehyde or dehydrogenated/oxidized at the anomeric carbon to gluconate. In this case, Pt^0 promotes the dehydrogenation of C_6-OH of glucose and therefore drives the selectivity towards glucose dialdehyde. By contrast, PtO_x can promote both dehydrogenation and oxidation (e.g., oxygen transfer) reactions and therefore

172

favors the dehydrogenation/oxidation of the anomeric carbon of glucose, resulting in a high selectivity towards gluconate. Secondly, gluconate can either be dehydrogenated at the primary alcohol group (C_6-OH) to guluronate or at the secondary alcohol group (C_2-OH and C_5-OH) to 2-keto gluconate and 5-keto gluconate. Pt^0 promotes the dehydrogenation of C_6-OH of gluconate and might have some activity for the dehydrogenation of the C_5-OH, resulting in minor contents of 5-keto gluconate. In addition, PtO_x can dehydrogenate both the primary and secondary alcohol groups of gluconate, resulting in a complex mixture of products containing amongst others guluronate, 2-keto gluconate, and 5-keto gluconate. Finally, glucuronate can be oxidized at C_1=O to glucarate. Both Pt^0 and PtO_x are selective for this reaction. Yet, PtO_x has a considerably higher activity for this reaction than Pt^0, which indicates that Pt needs to be oxidized to promote oxidation/oxygen-transfer reactions under neutral conditions.

4.4 Conclusion

In conclusion, we have developed a new analytical approach to identify and quantify all glucose oxidation products and investigate the influence of Pt oxidation state on the selectivity and activity of the catalyst for the electrocatalytic oxidation of glucose. We found that Pt^0 is more active for primary alcohol dehydrogenation than aldehyde oxidation, promoting the formation of glucose dialdehyde from glucose and guluronate from gluconate. Hence, Pt^0 drives the selectivity towards the dehydrogenation of primary alcohol groups at the expense of aldehyde oxidation reactions and anomeric carbon dehydrogenation/oxidation. On the other hand, PtO_x is equally active for catalyzing aldehyde oxidation and primary alcohol dehydrogenation, thereby promoting the formation of gluconate from glucose and glucarate from glucuronate. Hence, PtO_x increases the selectivity towards the electrocatalytic dehydrogenation/oxidation of the anomeric carbon at the expense of primary alcohol dehydrogenation. Despite the high selectivity of PtO_x towards gluconate, it also promotes its successive dehydrogenation of secondary alcohol groups, leading to complex reaction mixtures. This role of the Pt oxidation state on the catalyst selectivity and activity for the electrocatalytic oxidation of glucose illustrates how the catalyst properties can crucially affect product distribution.

Acknowledgements

References

1. Xie, K. *et al.* Eliminating the need for anodic gas separation in CO2 electroreduction systems via liquid-to-liquid anodic upgrading. *Nat Commun* **13**, 1–9 (2022).

2. Werpy, T. & Petersen, G. *Top Value Added Chemicals from Biomass Volume I-Results of Screening for Potential Candidates from Sugars and Synthesis Gas*. http://www.osti.gov/bridge (2004).

3. Li, Y., Wei, X., Chen, L. & Shi, J. Electrocatalytic Hydrogen Production Trilogy. *Angewandte Chemie International Edition* **60**, 19550–19571 (2021).

4. Kokoh, K. B. *et al.* Selective oxidation of D-gluconic acid on platinum and lead adatoms modified platinum electrodes in alkaline medium. *Electrochim Acta* **38**, 1359–1365 (1993).

5. Luo, Z., Yu, S., Zeng, W. & Zhou, J. Comparative analysis of the chemical and biochemical synthesis of keto acids. *Biotechnol Adv* **47**, 107706 (2021).

6. Amaniampong, P. N. *et al.* Selective and Catalyst-free Oxidation of D-Glucose to D-Glucuronic acid induced by High-Frequency Ultrasound. *Sci Rep* **7**, 40650 (2017).

7. Deng, W. *et al.* Efficient Catalysts for the Green Synthesis of Adipic Acid from Biomass. *Angewandte Chemie - International Edition* **60**, 4712–4719 (2021).

8. Chheda, J. N., Huber, G. W. & Dumesic, J. A. Liquid-phase catalytic processing of biomass-derived oxygenated hydrocarbons to fuels and chemicals. *Angewandte Chemie - International Edition* **46**, 7164–7183 (2007).

9. Ishida, T. & Haruta, M. Gold catalysts: Towards sustainable chemistry. *Angewandte Chemie - International Edition* **46**, 7154–7156 (2007).

10. Armstrong, R. D., Hirayama, J., Knight, D. W. & Hutchings, G. J. Quantitative Determination of Pt- Catalyzed d - Glucose Oxidation Products Using 2D NMR. *ACS Catal* **9**, 325–335 (2019).

11. Lee, J., Saha, B. & Vlachos, D. G. Pt catalysts for efficient aerobic oxidation of glucose to glucaric acid in water. *Green Chemistry* **18**, 3815–3822 (2016).

12. Jin, X. *et al.* Synergistic Effects of Bimetallic PtPd/TiO2 Nanocatalysts in Oxidation of Glucose to Glucaric Acid: Structure Dependent Activity and Selectivity. *Ind Eng Chem Res* **55**, 2932–2945 (2016).

13. Derrien, E., Marion, P., Pinel, C. & Besson, M. Influence of Residues Contained in Softwood Hemicellulose Hydrolysates on the Catalytic Oxidation of Glucose to Glucarate in Alkaline Aqueous Solution. *Org Process Res Dev* **20**, 1265–1275 (2016).

14. Liu, W. J. *et al.* Efficient electrochemical production of glucaric acid and H2 via glucose electrolysis. *Nat Commun* **11**, 265 (2020).

15. Kokoh, K. B., Léger, J. M., Beden, B., Huser, H. & Lamy, C. 'On line' chromatographic analysis of the products resulting from the electrocatalytic oxidation of d-glucose on pure and adatoms modified Pt and Au electrodes- Part II. Alkaline medium. *Electrochim Acta* **37**, 1909–1918 (1992).

16. Wouter Huijgen, E. Cobussen-Pool, B. van Egmond & J. van Hal. Determination of carbohydrate composition of macroalgae. in *Protocols for Macroalgae Research* 200–210 (2018).

17. Wan, Y. *et al.* One-pot synthesis of gluconic acid from biomass-derived levoglucosan using a Au/Cs2.5H0.5PW12O40 catalyst. *Green Chemistry* **21**, 6318–6325 (2019).

18. Solmi, S., Morreale, C., Ospitali, F., Agnoli, S. & Cavani, F. Oxidation of d-Glucose to Glucaric Acid Using Au/C Catalysts. *ChemCatChem* **9**, 2797–2806 (2017).

19. Moggia, G., Schalck, J., Daems, N. & Breugelmans, T. Two-steps synthesis of D-glucaric acid via D-gluconic acid by electrocatalytic oxidation of D-glucose on gold electrode: Influence of operational parameters. *Electrochim Acta* **374**, 137852 (2021).

20. Largeaud, F., Kokoh, K. B., Beden, B. & Lamy, C. On the electrochemical reactivity of anomers: electrocatalytic oxidation of α- and β-d-glucose on platinum electrodes in acid and basic media. *Journal of Electroanalytical Chemistry* **397**, 261–269 (1995).

21. Van Dijken, J. P., Van Tuijl, A., Luttik, M. A. H., Middelhoven, W. J. & Pronk, J. T. Novel pathway for alcoholic fermentation of δ-gluconolactone in the yeast Saccharomyces bulderi. *J Bacteriol* **184**, 672–678 (2002).

22. Dowben, R. On the hydrolysis and oxidation of glucuronolactone. *Biochim. Biophys. Acta* **31**, 454–458 (1959).

23. Kokoh, K. B., Léger, J. M., Beden, B. & Lamy, C. 'On line' chromatographic analysis of the products resulting from the electrocatalytic oxidation of d-glucose on Pt, Au and adatoms modified Pt electrodes-Part I. Acid and neutral media. *Electrochim Acta* **37**, 1333–1342 (1992).

24. Li, N.-H., Sun, S.-G. & Chen, S.-P. Studies on the role of oxidation states of the platinum surface in electrocatalytic oxidation of small primary alcohols. *Journal of Electroanalytical Chemistry* **430**, 57–67 (1997).

25. Kwon, Y., Schouten, K. J. P. & Koper, M. T. M. Mechanism of the Catalytic Oxidation of Glycerol on Polycrystalline Gold and Platinum Electrodes. *ChemCatChem* **3**, 1176–1185 (2011).

26. Xin, L., Zhang, Z., Qi, J., Chadderdon, D. & Li, W. Electrocatalytic oxidation of ethylene glycol (EG) on supported Pt and Au catalysts in alkaline media: Reaction pathway investigation in three-electrode cell and fuel cell reactors. *Appl Catal B* **125**, 85–94 (2012).

27. Chen, X., McCrum, I. T., Schwarz, K. A., Janik, M. J. & Koper, M. T. M. Co-adsorption of Cations as the Cause of the Apparent pH Dependence of Hydrogen Adsorption on a Stepped Platinum Single-Crystal Electrode. *Angewandte Chemie - International Edition* **56**, 15025–15029 (2017).

28. Imai, H. *et al.* In situ and real-time monitoring of oxide growth in a few monolayers at surfaces of platinum nanoparticles in aqueous media. *J Am Chem Soc* **131**, 6293–6300 (2009).

29. A.B. Mello, G., Cheuquepán, W. & Feliu, J. M. Investigation of reactivity of Pt basal planes towards glucose electro-oxidation in neutral solution (pH 7): structure-sensitivity dependence and mechanistic study. *Journal of Electroanalytical Chemistry* **878**, 114549 (2020).

30. Moggia, G., Kenis, T., Daems, N. & Breugelmans, T. Electrochemical Oxidation of d-Glucose in Alkaline Medium: Impact of Oxidation Potential and Chemical Side Reactions on the Selectivity to d-Gluconic and d-Glucaric Acid. *ChemElectroChem* **7**, 86–95 (2020).

31. Farias, M. J. & Feliu, J. M. Determination of Specific Electrocatalytic Sites in the Oxidation of Small Molecules on Crystalline Metal Surfaces. *Topics Curr. Chem.* **377**, 5 (2019).

32. Kunimatsu, K., Hanawa, H., Uchida, H. & Watanabe, M. Role of adsorbed species in methanol oxidation on Pt studied by ATR-FTIRAS combined with linear potential sweep voltammetry. *Journal of Electroanalytical Chemistry* **632**, 109–119 (2009).

33. Kwon, Y., Birdja, Y., Spanos, I., Rodriguez, P. & Koper, M. T. M. Highly selective electro-oxidation of glycerol to dihydroxyacetone on platinum in the presence of bismuth. *ACS Catal* **2**, 759–764 (2012).

34. Nonaka, H. & Matsumura, Y. Electrochemical oxidation of carbon monoxide, methanol, formic acid, ethanol, and acetic acid on a platinum electrode under hot aqueous conditions. *Journal of Electroanalytical Chemistry* **520**, 101–110 (2002).

35. Kwon, Y., De Jong, E., Van Der Waal, J. K. & Koper, M. T. M. Selective electrocatalytic oxidation of sorbitol to fructose and sorbose. *ChemSusChem* **8**, 970–973 (2015).

36. Arulmozhi, N., Esau, D., Lamsal, R. P., Beauchemin, D. & Jerkiewicz, G. Structural Transformation of Monocrystalline Platinum Electrodes upon Electro-oxidation and Electro-dissolution. *ACS Catal* **8**, 6426–6439 (2018).

37. Parpot, P., Muiuane, V. P., Defontaine, V. & Bettencourt, A. P. Electrocatalytic oxidation of readily available disaccharides in alkaline medium at gold electrode. *Electrochim Acta* **55**, 3157–3163 (2010).

38. Mello, G. A. B., Cheuquepán, W., Briega-Martos, V. & Feliu, J. M. Glucose electro-oxidation on Pt(100) in phosphate buffer solution (pH 7): A mechanistic study. *Electrochim Acta* **354**, 136765 (2020).

39. Beden, B., Cetin, I., Kahyaoglu, A., Takky, D. & Lamy, C. Electrocatalytic Oxidation of Saturated Oxygenated Compounds on Gold Electrodes. *J Catal* **104**, 37–46 (1987).

40.   Dieterich, E., Kinkelin, S. J. & Bron, M. Comparative Study of the Synthesis of sub-10 nm Carbon-Supported Gold Nanoparticles and their Suitability for Methanol Electrooxidation in Alkaline Media. *ChemNanoMat* **8**, 6 (2022).

Supporting information

From Figure S4.1 the most conspicuous surface structures of the Pt mesh electrode are Pt(110) and (100)-type sites at 0.2 and 0.34 V *vs.* RHE.[36] Moreover, the onset potential for the oxidation of the Pt surface can be observed at 0.85 V *vs.* RHE.
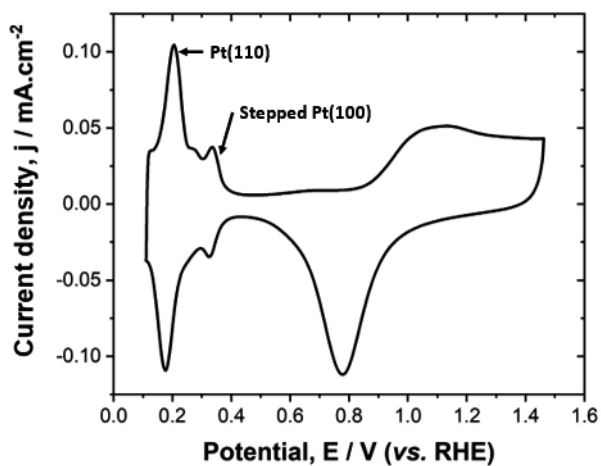
Figure S4.1. Cyclic voltammograms of polycrystalline Pt mesh electrode obtained under neutral conditions (0.2 M phosphate buffer) in an H-cell at 50 mV.s^{-1}.

From Figure S4.2 it can be observed that the current density (e.g., reaction rate) increases when convection is applied, meaning that the reaction rate is mass transport limited. Therefore, convection is required to minimize mass transport limitations to evaluate the intrinsic catalyst reaction rate.
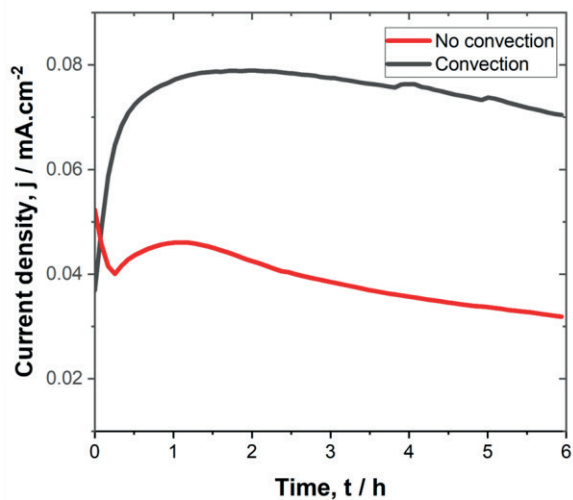
Figure S4.2. *Current-time curves for the electrocatalytic oxidation of 0.1 M glucose in 0.2 M PBS over PtO$_x$ in the absence and presence of convection.*

From Figure S4.3 it can be observed that a system with 0.2 M PBS retains a more stable pH, while that of 0.1 M PBS drops to ~4 after 6 h of reactions. This shows that 0.2 M PBS is required to retain a stable and neutral pH.
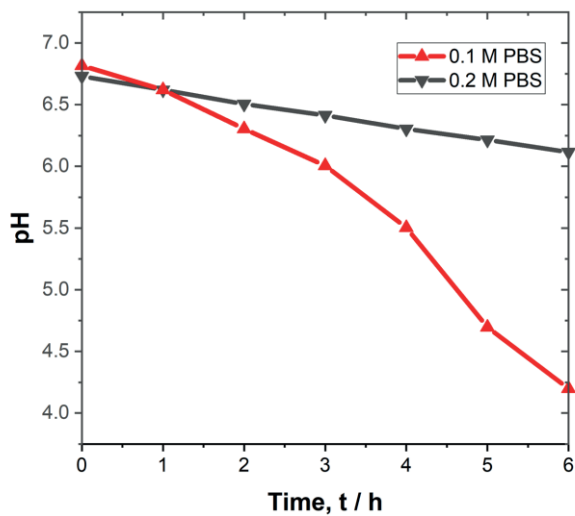
Figure S4.3. *pH-time curves for the electrocatalytic oxidation of 0.1 M glucose over PtO$_x$ buffered in 0.1 M and 0.2 M PBS.*

Figure S4.4 shows the current density for the electrocatalytic oxidation of glucose as a function of applied potential. For the electrocatalytic oxidation of glucose over Pt^0 (0.64 V *vs.* RHE) or PtO_x (1.2 V *vs.* RHE), illustrated by E_{ox} in Figure S4.3, the current density decreases over time, indicative that the catalyst deactivates over time as oxidized glucose species accumulate on the catalyst surface. These oxidized species are removed to reactivate the catalyst by applying two short successive pulses of E_{des} (2.0 V *vs.* RHE) and $E_{red/ads}$ (0.2 V *vs.* RHE).[15,19,30,37] At $E_{red/ads}$ a strong negative current followed by a negligible positive current was measured, indicative that the PtO_x first reduced to Pt^0 followed by a minor contribution of dissociative adsorption of glucose.[38]
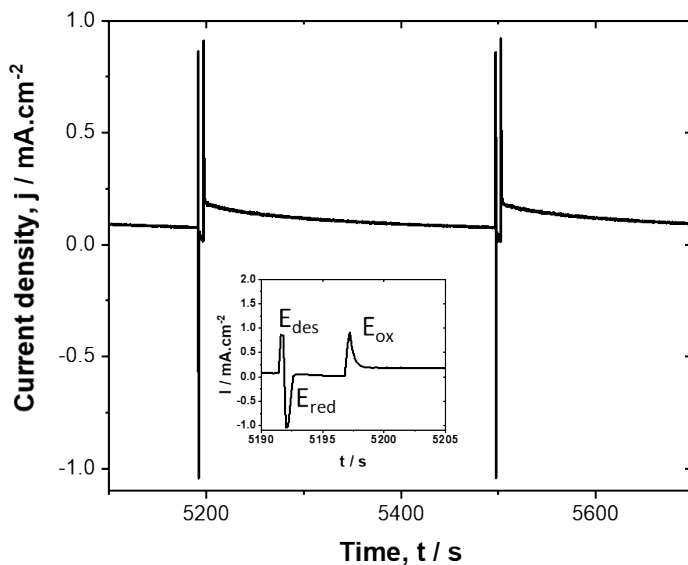
Figure S4.4. *The potential program and the related measured currents for the electrocatalytic oxidation of 0.1 M glucose in 0.2 M PBS over PtO_x with an inset to zoom in on the E_{des} and $E_{red/ads}$.*

The glucose oxidation products were analyzed by combining HPAEC-PAD (Figure S4.5A-B) and HPLC-UV-RI (Figure S4.6A-B). The approach is briefly described as follows.

The HPAEC chromatogram of MiliQ (Figure S4.5A) shows a gradual change in the PAD signal over time with a small peak 22.5 min. These changes in the PAD signal for a MiliQ can be attributed to a change in eluent composition over time during chromatographic elution. The HPAEC chromatogram of glucose and various glucose oxidation products (Figure S4.5B) shows a clear separation of arabinose, glucose, gluconate, 2-keto gluconate, glucose dialdehyde, guluronate, glucuronate, 5-keto gluconate, and glucarate. The PAD detector enables the quantification of products between 0.2-0.003 mM. In this study, glucose was not quantified by HPAEC-PAD since it was present in higher concentrations than 90 mM. Moreover, gluconate elutes with a change in PAD signal caused by a change in eluent composition, making its quantification by the chromatographic settings applied in this study impossible. Finally, the PAD detector uses a gold electrode, which cannot electrocatalytically oxidize oxalate and formate at 0.1 M NaOH,[39,40] and therefore cannot give an amperometric response.

The HPLC chromatograms of the individual components and their related UV and RI signals are given in Figure S4.6A-B. The HPLC-UV detector shows a good separation of oxalate, gluconate, and formate, enabling their quantification. The HPLC-RI detector shows that the peaks of gluconate, glucose, and glucose dialdehyde overlap. Yet, gluconate can be quantified by HPLC-UV and glucose dialdehyde can be quantified by HPAEC-PAD. As a result, it was possible to quantitatively analyze the glucose. In this case, the total RI signal, being the combination of gluconate, glucose, and glucose dialdehyde was corrected for the contribution of gluconate and glucose dialdehyde.[17,18]
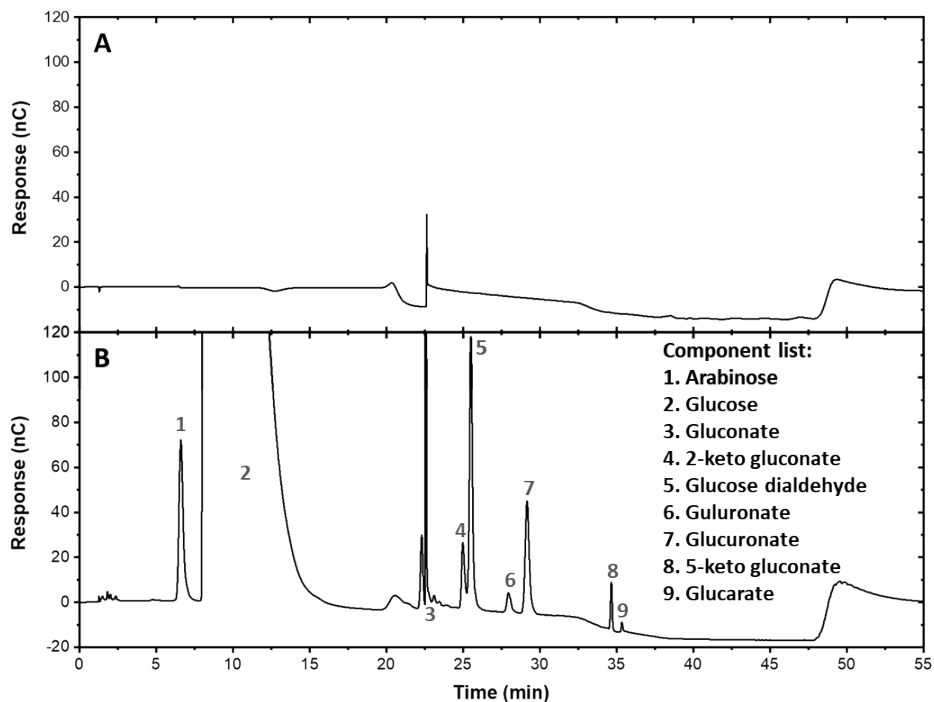
Figure S4.5. *HPAEC chromatograms and the corresponding PAD signal for a sample with A) MiliQ and B) 25 mM glucose, 50 mM PBS and different glucose oxidation products, namely 0.15 mM of formate, oxalate, arabinose, gluconate, 2-k-gluconate, glucose dialdehyde, glucuronate, glucose, 5-k-gluconate and glucarate, and 0.03 mM guluronate.*
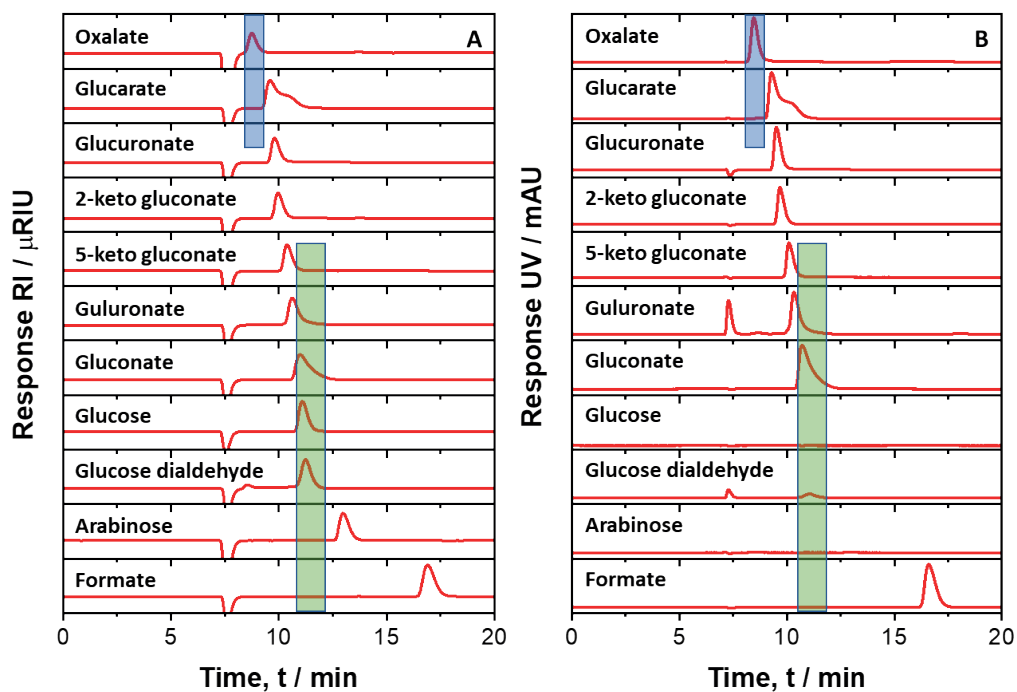
Figure S4.6. *HPLC chromatograms and the corresponding RI signal (A) and UV signal (B) for the pure components (2-5 mM), being oxalic acid, glucaric acid, glucuronic acid, 2-k-gluconic acid, 5-k-gluconic acid, guluronic acid, glucose, gluconic acid, glucose dialdehyde, and arabinose.*

Table S4.1 shows the measured charge related to the electrocatalytic oxidation of glucose, gluconate, and glucuronate measured at E_{des} and shows that all products that have been quantified were a result of their formation over Pt^0 and PtO_x (e.g., $C_x < C_{des}$) except for 5-keto gluconate over Pt^0. Therefore, it remains uncertain if Pt^0 can form 2-keto gluconate.

Table S4.1. *The measured charge at desorption potential (C_{des}) and the theoretical charge required to form a specific product (C_x) was obtained after 6 h chronoamperometry. The products with $C_x < C_{des}$ are highlighted in red. The description of the abbreviations of the (intermediate) products are given in the footnote.*

Reactant	Catalyst	C_{des} (C)	C_x (C)[a]						
			GA	GD	GUL	GLU	2-GA	5-GA	GAR
Glucose	Pt^0	1.2	16	5.4	0.8	2.0	-	0.0	0.3
GA	Pt^0	0.5	-	-	3.2	-	-	0.1	0.8
GLU	Pt^0	0.5	-	-	-	-	-	-	1.1
Glucose	PtO_x	1.2	114	3.0	5.0	5.8	0.1	0.7	3.1
GA	PtO_x	0.9	-	-	14	-	2.5	2.5	4.3
GLU	PtO_x	0.9	-	-	-	-	-	-	25.4

[a] GA = gluconate, GD = glucose dialdehyde, GUL = guluronate, GLU = glucuronate, 2-kGA = 2-keto gluconate, 5-kGA = 5-keto gluconate, GAR = glucarate

Figure S4.7 shows the product selectivities for the electrocatalytic oxidation of glucose at PtO_x as a function of initial glucose concentration. With a decrease in glucose concentration, the selectivity towards gluconate and glucose dialdehyde decreases, while the selectivity towards guluronate and glucuronate shows an optimum. This indicates that gluconate and glucose dialdehyde are primary products and guluronate and glucuronate are secondary products.
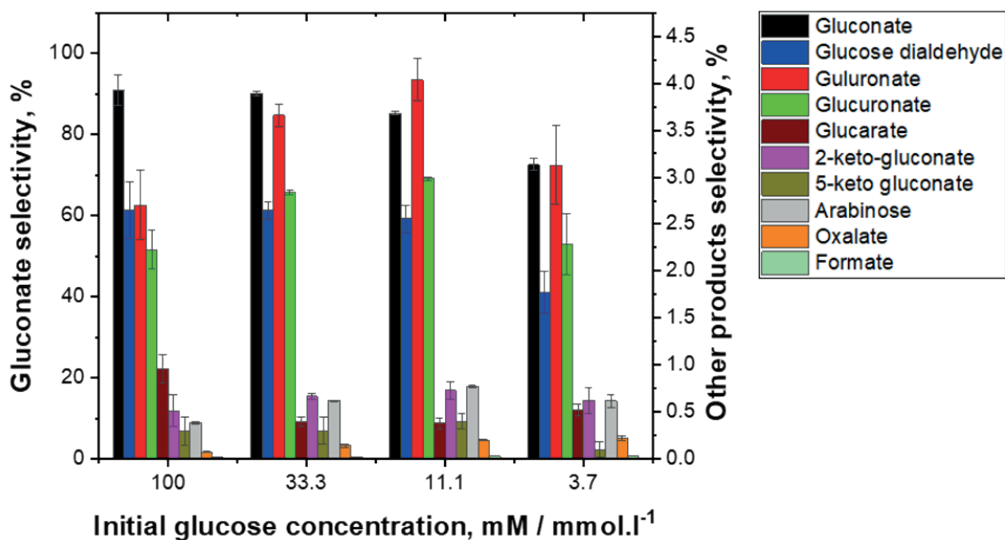
Figure S4.7. *Product selectivities as a function of initial glucose concentration obtained after 6 h of electrocatalytic oxidation of glucose over PtO_x in 0.2 M PBS.*

CHAPTER 5

Towards the electrocatalytic oxidation of starch

Authors: M. P. J. M. van der Ham, T. van Haasterecht, M. T. M. Koper, J. H. Bitter

Abstract

The electrocatalytic oxidation of starch, a high molecular weight polysaccharide, to anionic starch, is a promising method to replace the currently applied method of oxidation by hypochlorite, which is not sustainable. However, the feasibility of this electrocatalytic oxidation strongly depends on 1) the influence of low molecular weight polysaccharides and monomers (LMWPM) present in industrially derived starch feedstocks on the performance of the electrocatalyst and 2) a proper design of 3D electrocatalysts with good accessibility of the active sites for the large starch molecules. Therefore, these two issues will be studied here. Firstly, the role of LMWPM in industrially derived starch was evaluated by preparing starch samples with different contents of LMWPM. It was found that Pt at E = 0.6 V vs. RHE is more active towards the electrocatalytic oxidation of LMWPM than starch, which was confirmed by HPSEC, ^{1}H-NMR, and HPAEC, revealing that the starch neither oxidizes nor depolymerizes. Secondly, the electrocatalytic oxidation of starch was studied on a macroporous electrode synthesized by platinating a Ni foam. The Pt/Ni foam electrode had a high Pt ECSA, comparable to Pt black, and a high resistance to CO poisoning, which is crucial for the electrocatalytic conversion of organic molecules. It was demonstrated by potentiometric measurements that Pt/Ni foam can catalyze the electrocatalytic oxidation of unpurified starch. Our results demonstrate that 1) the electrochemical oxidation of starch is negatively influenced by the presence of low molecular weight polysaccharides and monomers and 2) Pt/Ni foam is a promising alternative electrocatalyst for starch oxidation and potentially also for other organic molecules in electrochemical reactors.
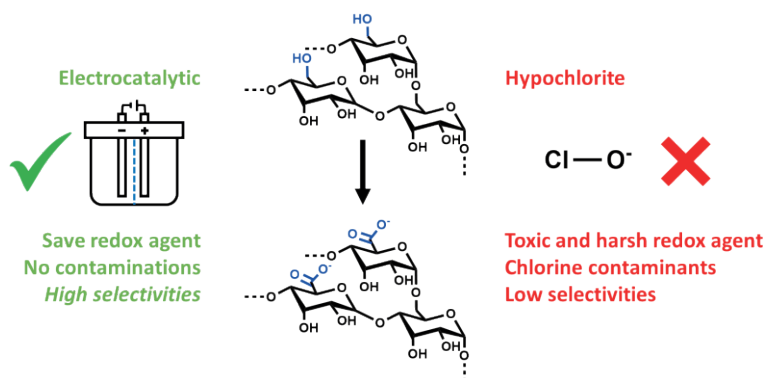
5.1. Introduction

Starch is a polysaccharide that holds great potential as biofeedstock for the production of polymeric,[1] oligomeric[2] and monomeric[3] platform chemicals and speciality chemicals. One of the polymeric materials that can be produced from starch is oxidized starch,[4] i.e. starch containing COOH/COO- groups. This oxidized starch can replace polyacrylates and is therefore an interesting sustainable alternative for the paper, textile, and food industries.[5] Currently the major process to produce anionic starch is by using hypochlorite as an oxidant. However, hypochlorite oxidation results in moderate selectivities, chloride contaminations, and chloride-containing by-products (salt).[5,6] Therefore, more environmentally benign oxidation approaches are desired. Electrocatalytic oxidation, when using renewable electricity, holds that potential since it does not require harsh oxidizing agents as it uses water as the oxidant and can be performed at ambient temperature and pressure.[7,8]

The bulkiness, polydispersity, and high number of functional groups of starch molecules (1-100 µm[9]) pose several challenges when designing 3D electrocatalysts with a supported active phases (the latter to make the most efficient use of the active phase). The challenges lie in the development of 3D electrocatalysts that 1) are selective towards the electrocatalytic oxidation of ~5% of the primary alcohol groups (highlighted in red in Figure 5.1) of starch to carboxylic acid groups (highlighted in green in Figure 5.1), 2) make efficient use of the catalytic phase i.e., not limited by mass transport phenomena of the large starch molecule and 3) can deal with all the differently sized molecules present in starch.[10,11]
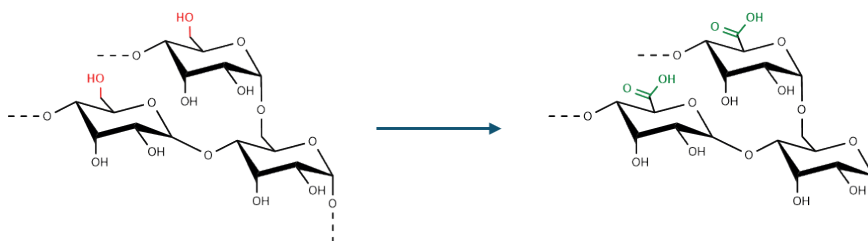
Figure 5.1. *Starch oxidation to anionic starch.*

The electrocatalytic oxidation of polysaccharides (e.g., cellulose) has been studied before under highly alkaline conditions. Sugano *et al.* used highly alkaline conditions to dissolve water-insoluble cellulose and to successively electrochemically oxidize it using a gold electrode, thereby introducing COO- groups.[12] However, these alkaline conditions also promote alkaline hydrolysis of polysaccharides,[13] generating monomers and oligomers. Kageshima *et al.* used highly alkaline conditions to solubilize and promote alkaline hydrolysis of cellulose,[14] generating monomers and oligomers, which were successively electrochemically oxidized by Pd or Au electrocatalysts in a fuel cell.[13] To the best of our knowledge, the direct, partial, electrocatalytic oxidation of polysaccharides while keeping the polymer chain (mainly) intact has not yet been demonstrated.

More recently, it was shown for the electrocatalytic oxidation of glucose, the monomer of cellulose and starch, that metallic Pt (at E = 0.64 V vs. RHE) promotes the electrocatalytic oxidation of the primary alcohol group under neutral conditions, thereby producing 23% glucose dialdehyde (based on product selectivity).[7] By contrast, Pt oxide (at E = 1.2 V vs. RHE) favors the electrocatalytic oxidation of the anomeric carbon group, resulting nearly exclusively in gluconic acid (91 %).[7] This indicates that metallic Pt may have the potential for the selective electrocatalytic oxidation of starch at the C6-OH group to produce anionic starch.

Native starch is polydisperse and water insoluble, where the latter property impedes its interaction with heterogenous electrocatalysts in aqueous media.[5] Therefore, native starch needs to be gelatinized first before it can be electrochemically oxidized. Gelatinization breaks down intermolecular bonds through heat and shear stress and can be achieved by drum-drying or extrusion.[15,16] However, these treatments also induce partial depolymerization,[15,16] thereby increasing the polydispersity of starch even further by the formation of low molecular weight polysaccharides and monosaccharides (LMWPM). It has been observed that the adsorption rate of starch and the adsorption constant of oligomers on activated carbon decreases with increasing molecule size.[10,17] Thus, LMWPM might therefore adsorb on the catalyst surface in competition with starch, thereby influencing the catalyst selectivity towards the desired starch oxidation.

Enhancing the activity of electrocatalysts can be achieved by designing electrocatalysts with a high surface to volume ratio of the active phase. Carbon supports decorated with nanosized metal particles are a popular and good choice. Carbon supports are inert, making them highly stable under various reaction conditions, and have tunable surface properties to improve the catalyst performance.[18] For example, we have shown that introducing support oxygen groups on the carbon promotes the adsorption of hydrophilic molecules like glucose in the perimeter of the Pt electrocatalyst, thereby enhancing the electrocatalyst activity.[19] However, these carbon supports are often mesoporous and therefore still susceptible to internal diffusion limitations when the aim is to electrochemically convert larger molecules like starch. To resolve this issue, metal foams, composed of Ni, Cu, or Ti, can be envisioned as supports as they are macroporous (pore size >100 μm).[13] The macroporous structure allows starch to diffuse into the support to the active phase of the catalyst, thereby reducing internal mass transport limitations.[13] Moreover, these foam structures are promising supports as they provide radial mixing, low-pressure drops, high heat transport properties (i.e., preventing hot spot formation in exothermic reactions),[20,21] excellent electrical conductivity, and high mechanical stress resistance.[22] To date, these foams have not been widely used in industry, which might be related to practical limitations as it is complicated to mount them in large-scale reactors.[21,23] However, for small-scale reactors, such as electrochemical reactors, these foams can provide excellent heat removal by thermal conduction

in the solid phase.[24] This is crucial for electrochemical reactors as ohmic resistance often causes high-temperature gradients in electrochemical reactors.[25]

Here, we aim to electrocatalytically oxidize starch by supported Pt catalysts under mild alkaline reaction conditions (pH = 11.5). First, we will focus on polycrystalline Pt electrodes and evaluate the role of the presence of LMWPM in industrially derived starch. Secondly, we will show the potential of a macroporous Pt on Ni foam catalyst for the electrochemical oxidation of starch.

5.2. Experimental section

5.2.1. Chemicals and material preparation

Hydrogen peroxide (30%) was acquired from VWR; Potassium permanganate (≥ 99%) and sulfuric acid (96%) were purchased from Sigma-Aldrich and used for cleaning the glassware. Sodium phosphate dibasic (≥ 99.99%), perchloric acid (99.999%), and sodium hydroxide (99.999%) were obtained from Sigma-Aldrich and used for preparing the electrolyte. Nickel foam (type 4753.005, pore size 0.4 mm, thickness 0.5 mm, specific surface area 5400 $m^2.m^{-3}$) was obtained from Racemat; chloroplatinic acid (99.9%) was acquired from Sigma-Aldrich and used for synthesizing the electrocatalyst. Glucose (≥ 99.5%) was acquired from Sigma-Aldrich; Industrially derived starch was obtained from Royal Avebe and was used for product analysis and as reactant. Deuterium oxide (99.96%) was obtained acquired from Euriso-top and used for ^{1}H-NMR analysis.

The electrochemical cell used in this study was stored in 0.5 M sulfuric containing 1 $g.l^{-1}$ permanganate. The cell was rinsed with dilute piranha solution and successively rinsed with MilliQ before use.[26]

The working and counter electrodes consisted of two identical 50·50 mm Pt gauzes (3600 mesh/cm2, 0.04 mm wire diameter, 99.9%) connected to a Pt wire (1 mm wire diameter, 99.95%) or two identical Pt/Ni foam electrodes (*vide infra* section 5.2.3 for the synthesis of Pt/Ni foam). The reference electrode was a reversible hydrogen electrode.

The electrochemical experiments were performed in an H-cell divided by an Aquivion membrane E87-05 (50 µm thick, >1.19 meq/g exchange capacity) equipped with a RHE electrode, separated from the work compartment by a Luggin capillary, unless stated otherwise. Each compartment contained 38 ml of 0.1 M phosphate buffer solution (pH = 11.5) and was purged for 30 min with Ar before conducting experiments.

5.2.2. Starch purification

The industrial derived starch was purified by centrifugal filtration by using 50 ml centrifugal tubes (Microsep™ Advance, MWCO 3 kD). 20 ml of 0.2 M industrially-derived starch was pipetted into the centrifugal tubes and centrifuged for 10 minutes at 7000 G and 15 °C in 4 consecutive steps. The tube was inverted between centrifugation steps to prevent the filter from clogging. After

such a series of centrifugation steps the starch filtrate containing the LMWPM was collected and MilliQ was added to the concentrated residue. This procedure was repeated 5 times to obtain a residue with purified starch. The solutions containing the LMWPM and purified starch were stored at -20 ˚C.

The concentrations of purified starch and LMWPM were determined by performing a chemical oxygen demand test. The COD was measured with a LCK514 kit (HACH GmbH, Germany) after appropriate dilution of the samples.[27] The measured COD values were used to calculate the starch and LMWPM concentrations, assuming the molecular composition to be $C_6H_{10}O_5$, thereby requiring 6 mol of O_2 for complete decomposition.

5.2.3. Pt/Ni foam synthesis

The nickel foam (Nif) was cut into 40*15 mm (length*width) pieces, sonicated consecutively in MilliQ and isopropanol, and finally thoroughly washed with MilliQ to remove any potential contaminants. The top part of the Nif was held in place with stainless steel clamps and placed between two Pt plates with a distance of 15 cm between the Nif and each Pt plate (*vide infra* Figure 5.7). The bottom part of the Nif (30 mm) was placed in an electrochemical bath containing 0.1 M $HClO_4$ and electrochemically treated by 30 consecutive cyclic voltammograms (CV) between -0.4 and 1.7 V *vs.* Ag/AgCl with a scan rate of 300 mV.s^{-1}. The electrochemically treated Nif together with the Pt electrodes were removed immediately after CV and the electrochemical bath was refreshed with 0.1 M $HClO_4$ and 1.5 mM H_2PtCl_6. The Nif and Pt electrodes were placed back in the electrochemical bath and held at E = 0.2 V *vs.* Ag/AgCl for 11 min to deposit the Pt precursor on the Nif, yielding a Pt/Nif electrocatalyst. After electrodeposition, the Pt/Nif electrode was immediately removed from the electrochemical bath and thoroughly rinsed with MilliQ.

5.2.4. Pt/Ni foam characterization

CO-stripping was performed to determine the electrochemical surface area (ECSA) of Pt of the Pt/Nif electrode before starch oxidation experiments. CO-stripping was conducted in 0.1 M phosphate buffer (pH = 11.5) in a three-electrode glass cell with a RHE reference electrode, separated from the working compartment by a Luggin capillary.[28] The Pt/Nif electrode was first cycled between 0.1 and 1.5 V *vs.* RHE at 50 mV.s^{-1} to obtain a stable CV. Successively, the electrode potential was held at E = 0.1 V *vs.* RHE, while purging the solution for 20 min with CO to saturate the Pt surface with CO. Successively, the solution was purged for 20 min with Ar to remove dissolved CO, followed by 4 CVs from 0.1 to 1.5 V *vs.* RHE at a scan rate of 5 mV.s^{-1}. The second scan was subtracted from the first scan to differentiate the contribution of CO oxidation from other electrochemical processes. The resulting coulombs were used to determine the ECSA,[29] assuming a charge of 420 mC.cm^{-2} for a monolayer of linearly adsorbed CO on Pt.[30]

Scanning Electron Microscopy (SEM) was performed with a FEI Magellan 400 to evaluate the surface structure of the catalyst. The SEM was coupled to Energy Dispersive X-ray Spectroscopy (EDS), an Aztec EDS system, that was operated at 15 keV to map the elemental distribution. Before analysis, the Pt/Nif was embedded with a Spurr Low-Viscosity Embedding Kit obtained from Sigma Aldrich and cut by a diamond knife to analyze the core of the Pt/Nif electrocatalyst.

XRD diffractograms were recorded with a Bruker D8 Advance equipped with a focusing X-ray Göbel Mirror to characterize the crystal structure of Pt and Ni foam and the potential formation of alloyed structures. The Sample was mounted on a XYZ stage and a rocking scan was performed to determine the incident angle. Thereafter, the measurement was performed in 2 theta mode (theta 2.188°), exit slit 0.6mm, from 30° to 90° with 0.05° and 1 s step size, equatorial soller slit of 0.3 and LYNXEYE detector in 0D mode fully opened at 14.325 mm.

5.2.5. Electrochemical measurements

Before each electrochemical experiment, the cleanliness of the cell was checked by performing 20 consecutive cyclic voltammograms (CV) with a Pt mesh electrode between 0.1 V and 1.5 V *vs.* RHE recorded at 20 mV.s^{-1}. The last CV was used to derive the electrochemical surface area of the Pt electrode by using the hydrogen underpotential deposition method from the hydrogen desorption peak.[31] Successively, a specific amount of reactant was added to the anode compartment and the solution was purged for 30 min with Ar to ensure oxygen-free conditions.

Linear sweep voltammetry (LSV) was performed from 0.1 to 1.5 V *vs.* RHE at a scan rate of 1 mV.s^{-1} to determine the peak potential for the electrocatalytic oxidation of 0.1 M purified starch (i.e. 0.1 M of glucose units). The derived peak potential (referred to as E_{ox}) was used for chronoamperometric measurements.

Chronoamperometry (CA) was performed with a Pt mesh electrode on 0.1 M purified starch (i.e. 0.1 M of glucose units) and with a Pt/Nif electrode on 0.1 M unpurified starch (i.e. 0.1 M of glucose units). CA was conducted with a potential program,[7,32,33] while mixing the solution with a stir bar at 900 rpm to induce convection. The potential program consisted of three repeating alternating potentials to remove oxidized species, thereby retaining an active electrocatalyst.[7,32,33] The first potential was the peak potential derived from the LSV and was held for a longer period of 50 seconds to electrocatalytically oxidize starch (E_{ox}). The successive two short potential pulses correspond to a desorption potential (E_{des}) and a reduction/adsorption potential ($E_{red/ads}$) of 1.7 V vs. RHE for 2 s and 0.2 V vs. RHE for 5 s respectively. The potential program was briefly optimized to maximize reactant oxidation at E_{ox} and minimize potential reactant oxidation at E_{des}. During CA measurements, 0.5 ml samples were collected each 30 min and diluted with 0.5 ml 0.2M H_2SO_4 and 20% methanol to neutralize the sample and prevent microbial contamination. After 6 h of reaction, a fraction of the remaining solution was purified

by centrifugal filtration, according to the "starch purification" method (see above), and freeze-dried.

5.2.6. Product analysis

High Pressure Size Exclusion Chromatography (HPSEC) was performed on the (oxidized) starch samples to assess the molecular weight distribution and formation of carboxylic acid groups (i.e. UV active groups). The system consisted of an OMNISEC resolve (OMNISEC, Malvern Panalytical Ltd., Malvern, United Kingdom) coupled to a multi-detector module OMNISEC reveal including an RI, a PDA, RALS (90°), LALS (7°), and a VISC detector. From the PDA detector, the UV data at λ = 253 nm was used for analysis. The separation was performed on an Aq Guard column (50x6 mm) coupled to an A4000 column (300x8 mm) with a 0.05 M Na_2SO_4 eluent at 35 ˚C and a 0.7 ml.min^{-1} flow rate. Dextran (Mw 70 kg.mol^{-1}) was dissolved in 0.05 M Na_2SO_4 to 2.4 mg.ml^{-1} and used as a standard solution. 25 µl of the sample was injected in duplicate and recorded for 17 ml.

^{1}H-NMR was performed on the purified (oxidized) starch samples to evaluate the formation of aldehyde groups. For this experiment 5 mg of freeze dried purified (oxidized) starch was dissolved in 250 µl of D_2O. The ^{1}H-NMR spectra were recorded with Bruker Advance III spectrometer operating at 600 MHz for ^{1}H equipped with a 2.5mm ^{1}H/^{13}C-NMR probe.[34]

High Performance Anion Exchange Chromatography (HPAEC) was performed to determine the presence of oxidized glucose products. The analysis was performed according to the procedure described by van der Ham *et al.*[7]

5.3. Results and discussion

The results and discussion section has been subdivided into two sections, which discuss: 1) how low molecular weight polysaccharides and monomers (LMWPM) in industrially derived starch affect the activity and selectivity of Pt electrocatalyst, and 2) the synthesis and characteristics of Pt/Nif electrodes and their potential to catalyze starch oxidation.

5.3.1. Presence of low molecular weight polysaccharides and monosaccharides

The industrially derived starch (i.e., unpurified starch) contains 90% water soluble starch and 10% smaller molecules mainly, consisting of low molecular weight polysaccharides and monosaccharides (LMWPM), as was determined by COD measurements. To investigate the role of the presence of LMWPM, the reactivity of the as-received unpurified starch sample will be compared to that of a sample where the LMWPM were removed.

Figure 5.2 illustrates the purification process of the industrially derived starch (i.e., unpurified starch), involving five sequential centrifugal filtration steps, resulting in a purified starch with a degree of polymerization (DP) greater than 18. Each purification step removed 50% of the LMWPM (i.e., DP < 18), leading to a high purity starch of 99%. This means that the purified starch

with DP ≥ 18 consists of starch molecules with one anomeric carbon (highlighted in red in Figure 5.2) accompanied by at least 18 C6-OH groups (highlighted in green in Figure 5.2).
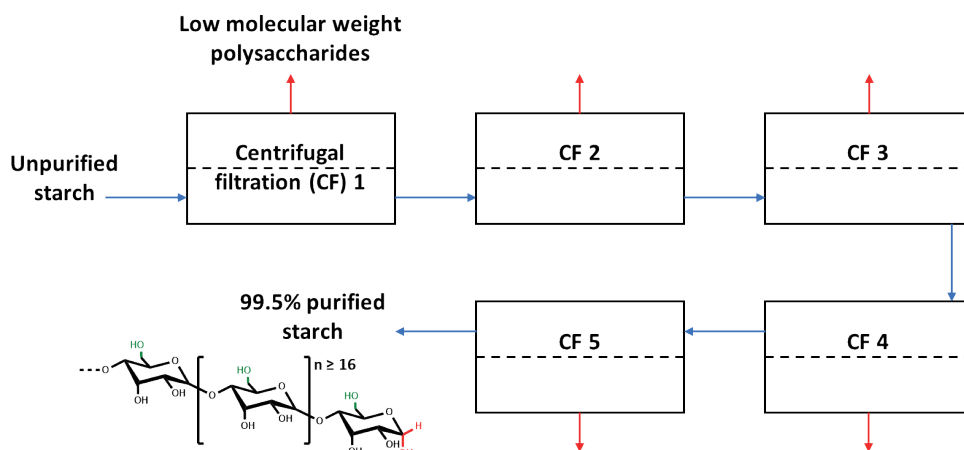

Figure 5.2. The purification process of industrial starch consists of 5 successive steps of centrifugal filtration steps to remove the low molecular weight polysaccharides from the starch and retain a high purity starch fraction with a degree of polymerization of ≥ 18.

The electrocatalytic oxidation of glucose was considered first for comparison with the electrocatalytic oxidation of starch (i.e., a polymer of glucose monomers). Figure 5.3A shows a cyclic voltammogram (CV) of Pt in a 0.1 M phosphate buffer solution (PBS, pH = 11.5) in the absence and presence of 0.1 M glucose. The blank CV of Pt, Figure 5.3A, shows typical features for a bare Pt electrode,[35] while the CV in the presence of glucose resembles the CVs obtained for saccharides such as glucose, mannose and xylose.[36–40] In the presence of glucose, two broad oxidative peaks at E = 0.5 to 0.9 V *vs.* RHE and at E = 0.9 to 1.4 V *vs.* RHE can be observed in the forward scan, which indicates two different oxidation processes. The first oxidation peak is below the surface oxidation potential of Pt (referred to as Pt^0, although Pt step sites and kinks are likely to be slightly oxidized[41]) and is therefore related to the electrocatalytic oxidation of glucose on Pt^0.[7] On the other hand, the second oxidation peak is above the surface oxidation potential of Pt and is therefore related to the electrocatalytic oxidation of glucose on platinum oxide (referred to as PtO_x).[7] Pt^0 is known to promote the electrocatalytic oxidation of both the anomeric carbon and the C6-OH group of glucose, while PtO_x strongly favors the electrocatalytic oxidation of the anomeric carbon of glucose.[7] At higher potentials, ~1.5 V *vs.* RHE, the current density drops significantly indicating that highly oxidized Pt surface species (likely a PtO_2 species[42,43]) are inactive for glucose oxidation. In the return scan a broad oxidative peak can be observed which is accompanied by a small dip at E = 0.87 V *vs.* RHE. This dip is related to the reduction of PtO_x/PtO_2.[44,45] Therefore, it is suggested that the oxidative peak in the return scan can be

attributed to the electrocatalytic oxidation of starch resulting from the reactivation of Pt oxide by its reduction.

Figure 5.3B shows the CVs of Pt in a 0.1 M PBS (pH = 11.5) in the absence and presence of 0.1 M (99 %) purified starch, 0.1 M unpurified (90 %) starch, and 0.01 M LMWPM, which was used to evaluate the effect of LMWPM in industrially derived starch feedstocks. In the presence of purified and unpurified starch, an increase in current density compared to the blank is observed on Pt^0 (at $E \leq 0.9$ V $vs.$ RHE), while only a minor increase in current density is observed on PtO_x (at $E = 1.1$ V $vs.$ RHE). This shows that Pt^0 is more active in catalyzing starch oxidation than PtO_x. To explain the observed difference in catalytic activity, the electrocatalytic oxidation of 0.1 M purified starch (i.e. 0.1 M purified starch contains 0.1 M of glucose units, Figure 5.3B) was compared first to the electrocatalytic oxidation of 0.1 M glucose (Figure 5.3A). Briefly, 0.1 M glucose and 0.1 M starch differ in the molecule size (i.e. adsorption strength/mode) and content of anomeric carbon groups as each glucose molecule has one anomeric carbon group and each starch molecule (e.g., glucose polymer of $\geq$ 18 glucose molecules) has one anomeric carbon group, while they have similar contents of primary alcohol groups. Interestingly, while PtO_x has a high catalytic activity for glucose oxidation, PtO_x is hardly active for catalyzing starch oxidation. PtO_x is known for its high activity in catalyzing the oxidation of anomeric carbon group present in glucose.[7,37] Therefore, the higher activity of PtO_x for catalyzing glucose oxidation than for starch oxidation can tentatively be attributed to the higher content of anomeric carbons present in glucose compared to starch and the effectiveness of PtO_x to catalyze these functional groups. Alternatively, the more oxidized surface of PtO_x than Pt^0 results in a weaker adsorption strength or different adsorption mode of larger molecules, thereby reducing the catalyst activity. On the other hand, Pt^0 was found to be catalytically active for both the electrocatalytic oxidation of glucose and starch, with a slightly higher activity towards glucose. The higher catalytic activity of Pt^0 can either be attributed to the electrocatalytic oxidation of the anomeric carbon group, which is present in a higher content in glucose than in starch, or a weaker adsorption strength/different adsorption mode for the larger starch molecules. Nonetheless, Pt^0 shows appreciable catalytic activity for converting starch, which can tentatively be attributed to the effectiveness of Pt^0 in catalyzing the oxidative dehydrogenation of the primary alcohol group of starch.[7,8]

The forward scan in Figure 5.3B shows that at $E < 0.9$ V $vs.$ RHE, Pt has a threefold lower current density for catalyzing the oxidation of 0.1 M purified starch than for 0.01 M LMWP, thereby revealing that the catalytic activity is higher for the more dilute LMWPM than for the ten times more concentrated purified starch. This higher activity of Pt towards the more dilute LMWPM can potentially be attributed to the higher content of anomeric carbon groups in LMWPM (DP $\leq$ 18) which are more reactive on Pt^0.[7,37] For Pt^0 the current density for catalyzing 0.1 M unpurified starch oxidation is higher than for the oxidation of 0.1 M purified starch. This shows that the catalytic activity of Pt^0 is higher for unpurified starch oxidation than for purified starch oxidation,

which can be related to the presence of smaller LMWPM in unpurified starch and thus a higher content of more reactive anomeric carbon groups. Hence, to steer the catalyst towards the electrocatalytic oxidation of starch and not to the LMWPM it is essential to remove LMWPM first.
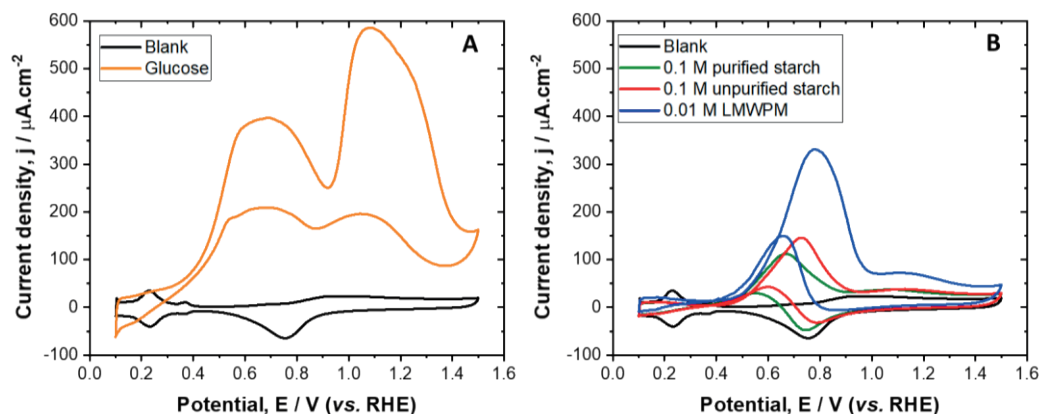

Figure 5.3. *CV of a polycrystalline Pt electrode in 0.1 M PBS (pH = 11.5) in A) the absence and presence of 0.1 M glucose and B) the absence and presence of 0.1 M unpurified starch, 0.1 M purified starch and 0.01 M LMWPM, recorded with stirring at a scan rate of 20 mV.s^{-1}.*

Figure 5.4A shows the linear sweep voltammetry of Pt in a 0.1 M PBS and 0.1 M purified starch solution, which was used to derive the optimum potential for catalyzing starch oxidation. A peak current density can be observed at E = 0.6 V *vs.* RHE (referred to as E_{ox}) and a second lower peak current density can be observed at E = ~1.1 V *vs.* RHE. The higher current density measured at E = 0.6 V *vs.* RHE shows that Pt^0 is more active for catalyzing starch oxidation than PtO$_x$ (at E > 0.9 V *vs.* RHE), confirming the results obtained by CV.

Electrocatalysts are known to deactivate by adsorbed oxidized products which is often resolved by applying a dynamic potential.[7,32,37] In such an approach, the oxidation potential of interest (E_{ox}) is followed by a short and strong oxidative pulse (E_{des}) to desorb (oxidized) products, which is followed by a short and low potential ($E_{red/ads}$) to reduce the catalyst and adsorb reactants.[7,32,37] Figure 5.4B shows the current density as a function of the dynamic potential for Pt in the presence of 0.1 M purified starch in 0.1 M PBS. During the first 50 seconds at E = 0.6 V *vs.* RHE (E_{ox} in Figure 5.4B), the current density rapidly decreases. This decrease in current density indicates that the catalyst deactivates quickly over time. After applying a short very positive pulse and successive low-potential pulse (e.g. not sufficient to reduce the (oxidized) molecule), the current density increases again at E_{ox} following a new potential cycle (illustrated by dashed green lines). This reveals that the dynamic potential reactivates the catalyst activity during starch oxidation and therefore is an effective strategy to retain an active catalyst for the electrocatalytic oxidation of large organic molecules.

A dynamic potential was also used to study the electrocatalytic oxidation of 0.1 M purified starch on Pt in 0.1 M PBS over longer times. Figure 5.4C shows the time curves for the average current density (i.e. average current of the individual potential cycles[7] derived from Figure 5.4B). From 0.5 to 6 h the current density gradually decreases from 70 $\mu A.cm^{-2}$ to <10 $\mu A.cm^{-2}$. The gradual decrease in current density indicates either a progressive decrease in reactant concentration and ultimately a depletion of reactant or the deactivation of the catalyst through the formation of poisoning species.[33] The total oxidation charge after 6 h reaction can be used to derive the maximum theoretical amount of oxidized groups formed,[46,47] assuming two and four electrons for the formation of an aldehyde and carboxylate, respectively. After 6 h, 33 coulombs of oxidation charge were generated, corresponding to the formation of 0.42 mmol aldehydes/0.21 mmol carboxylates.[49] Assuming that only the primary alcohol group of starch (38 mmol in solution) is catalytically oxidized, the amount of charge generated indicates that 5.7% of primary alcohol groups are oxidized to aldehydes or 3.7% of primary alcohol groups are oxidized to carboxylic acids.
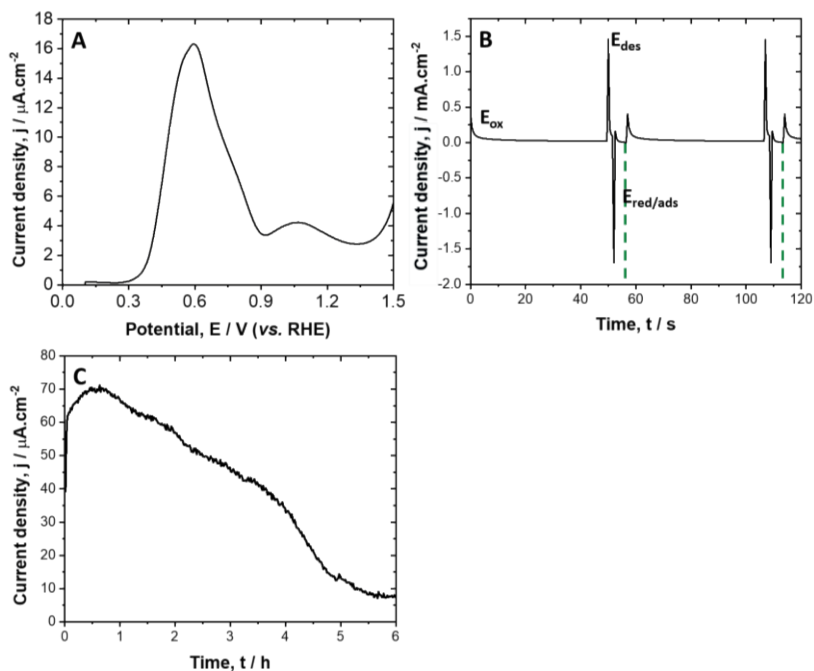
Figure 5.4. A) linear sweep voltammetry of Pt in 0.1 M phosphate buffer solution (pH = 11.5) and 0.1 M purified starch recorded at 1 mV.s^{-1}. B) Potential program used for the electrocatalytic oxidation of purified starch consisting of an oxidation potential (E_{ox} = 0.6 V vs. RHE, 50 s), a desorption potential (E_{des} = 1.7 V vs. RHE, 2 s) and a reduction/desorption potential ($E_{red/ads}$ = 0.2 V vs. RHE, 5 s). Dashed green drop down lines have been added to illustrate a single potential

cycle. C) Current-time curve for the electrocatalytic oxidation of purified starch on Pt[0] (at E = 0.6 V vs. RHE).

The electrochemically oxidized starch was characterized by high pressure size exclusion chromatography coupled to a refractive index (RI) detector (Figure 5.5A) and right-angle light scattering (RALS) detector (Figure 5.5B) to evaluate the degree of polymerization. HPSEC coupled to a UV detector was used to evaluate the formation of carboxylic acid groups (Figure 5.5B) and ^{1}H-NMR (Figure 5.5C) was used to evaluate the formation of aldehyde groups.

Figures 5.5A and 5.5B show the HPSEC chromatograms and the corresponding RI and RALS signal for the electrocatalytic oxidation of purified starch on Pt in 0.1 M PBS. The RI signal shows three peaks at 8.2, 10.8, and 12.4 ml, corresponding to starch, phosphate and methanol, while the RALS signal shows one peak at 8.2 ml, corresponding to starch. RALS is only able to detect larger molecules, like starch, and is therefore unable to detect smaller molecules like phosphate and methanol.

The unaltered RI and RALS signals in Figures 5.5A and 5.5B do not show any significant change over time for the electrocatalytic oxidation of starch. The unaltered RI and RALS signal indicate that the molecule is not being hydrolyzed and that the polymer chain remains intact implying that Pt[0] cannot catalyze hydrolytic reactions at pH = 11.5.

Figure 5.5C shows the HPSEC-UV chromatograms and Figure 5.5D shows the ^{1}H-NMR spectrum for the product formed during electrocatalytic oxidation of purified starch on Pt. The UV signal shows two main peaks at 9 and 10.8 ml (with a long tail), corresponding to starch and phosphate. The origin of the long tail remains unknown but is only present in samples containing starch and can therefore tentatively be attributed to a delayed elution of starch through in the UV detector since the RI and RALS detector did not give a tail. The UV signal does not show any significant change in signal over time for the electrocatalytic oxidation of starch. This indicates that Pt[0] does not catalyze the formation of carboxylic acid groups or that they remain below the detection limit of the UV sensor. The ^{1}H-NMR spectra, Figure 5.5D, of purified starch and oxidized starch show two regions of signals, namely from 3.5 to 4 ppm, and from 4.6 to 5.4 ppm. The lower range coincides with C-H bonds, while the higher range corresponds to C-OH bonds.[48] The spectra do not show a significant difference after electrochemical oxidation and therefore no appearance of an aldehyde peak can be observed. The ^{1}H-NMR has a sensitivity of ~9 ppm.[49] This indicates that the starch molecule is not electrochemically oxidized or that the degree of oxidation is below the detection limit of ^{1}H-NMR (<0.25 % C6-OH groups formed).
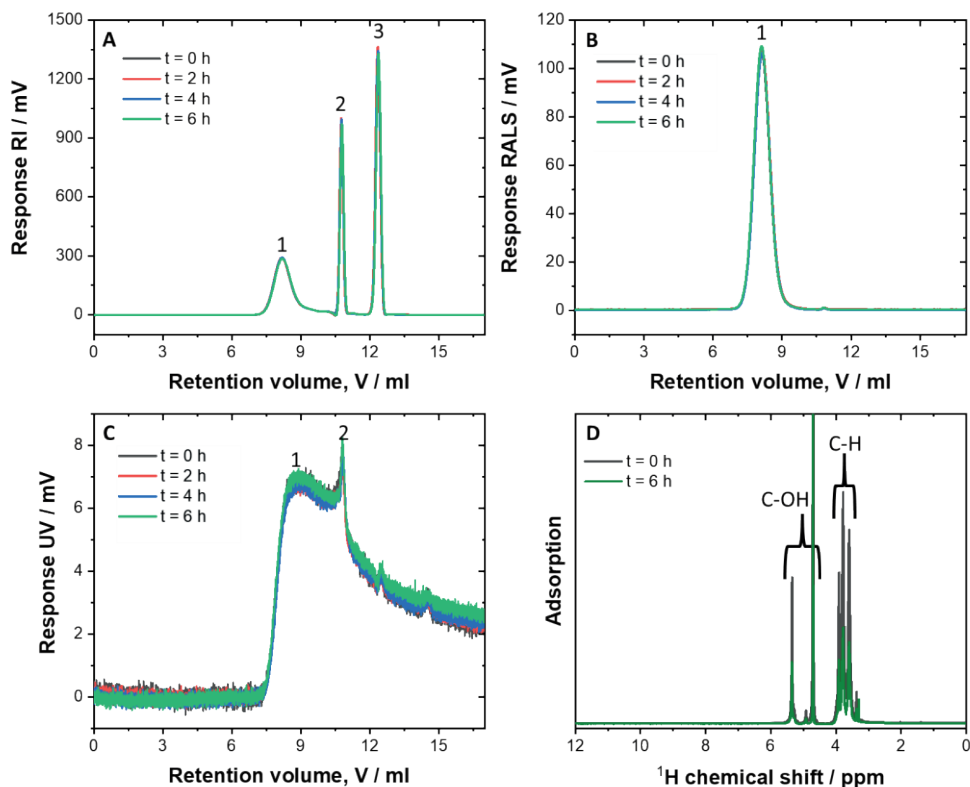
Figure 5.5. *HPSEC chromatograms and the corresponding A) RI signal, B) RALS signal, and C) UV signal, and D) ^{1}H-NMR spectra of electrocatalytically oxidized purified starch on Pt in 0.1 M phosphate buffer solution (pH = 11.5).*

Figure 5.6 shows the HPAEC chromatograms of electrochemically oxidized starch which was used to evaluate the role of the presence of LMWPM on the formation of LMWPM oxidation products. The first sample taken at t = 0, which has not been exposed to an electrochemical treatment, shows signals at 24.3 (~73 nC), 25.7 (~61 nC), 27.8 (~60 nC), 30.8 (~36 nC), and 33.8 min (~63 nC). These signals at 24.3, 25.7, 27.8, 30.8, and 33.8 can tentatively be attributed to LMWPM, consisting of maltose, maltotriose, maltotertaose, maltopentaose, and maltohexose respectively, which can easily be separated by HPAEC equipped with a CarboPac column.[50] The signal intensity, ranging between 36 and 73 nC, measured by the detector, corresponds to minor contents of LMWPM ranging between 0.16 and 0.08 mM. In the course of the reaction the signal at 24.3, 25.7, 27.8, 30.8, and 33.8 decreases, while before these peaks an increase in the signal can be observed at 23.8, 25.3, 27.3, 29.9, and 30.5 min. The decrease in signal intensity correlates with

the increase in signal intensity of the previous peak. This indicates that the LMWPM are slowly converted.
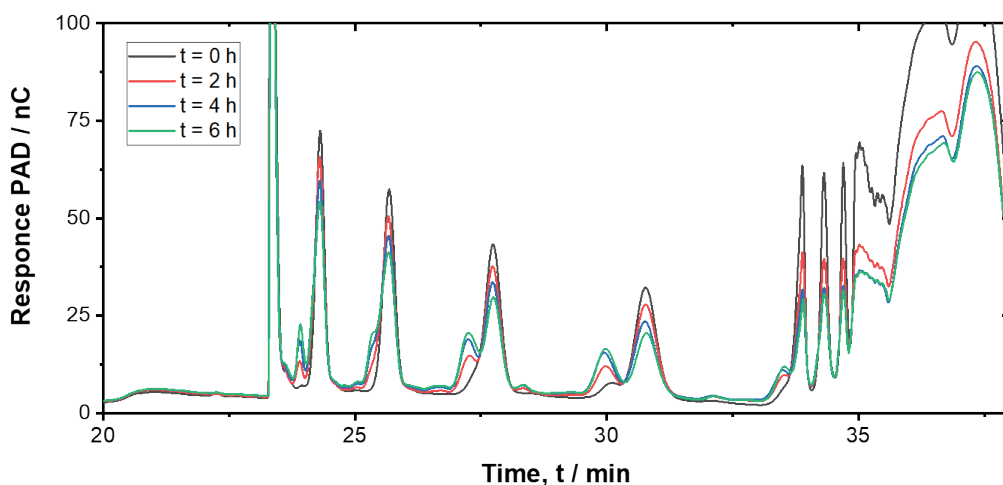
Figure 5.6. *HPAEC-PAD chromatogram of electrocatalytically oxidized purified starch on Pt in 0.1 M phosphate buffer solution (pH = 11.5).*

5.3.2. Pt/Ni-foam for electrocatalytic starch oxidation

Figure 5.7A shows the setup used for pretreating nickel foam (Nif) and for electrodepositing Pt (H$_2$PtCl$_6$) on the pretreated Nif. The Nif was partially submerged in the electrolyte and positioned at a 15 cm distance between two Pt plate counter electrodes to create a similar electric field on both sides of the Nif. This turned out to be essential for a homogeneous coating of Pt on Ni.[51] The electrochemical pretreatment of Nif consisted of 30 consecutive cyclic voltammetric cycles in 0.1 M HClO$_4$ to increase the Ni surface area and to remove potential contaminants present on the Ni surface.[52] The pretreatment also increased the concentration of α-Ni(OH)$_2$ surface species (Figure S5.1).[53,54] Successively, the pretreated Nif was placed in a fresh chemical bath containing 0.1 M HClO$_4$ and 1.5 mM H$_2$PtCl$_6$, while fixing the potential at 0.2 *vs.* Ag/AgCl at the Nif electrode. Figure 5.7B displays the resulting current-time curve. Initially, a small negative current was observed which is most likely the result of dipping the electrode in the solution. Next, an increase in current density was observed up to a current density of 2 mA.cm^{-2}. This is an anodic i.e. oxidative current. This anodic current was only observed during the electrodeposition of H$_2$PtCl$_6$ on Nif exposing α-Ni(OH)$_2$, as the electrodeposition of H$_2$PtCl$_6$ observed on Nif without α-Ni(OH)$_2$, surface resulted in a cathodic current (data not given). Therefore, this constant anodic current was ascribed to the continuous dissolution of a-Ni(OH)$_2$ species in an acidic electrolyte.[55] The constant dissolution of a-Ni(OH)$_2$ species indicates that the Pt is not covering the complete surface of the Nif. This anodic current overshadows the electrocatalytic reduction of H$_2$PtCl$_6$ during Pt deposition.[56] The catalyst obtained from the electrodeposition of Pt on Nif that has a high concentration of α-Ni(OH)$_2$

surface species was selected to continue this study as it has a high Pt ECSA (vide infra discussion on Figure 5.8C) and showed a good performance towards catalyzing starch oxidation. Figure 5.7C shows the catalyst obtained after platinating Nif with H_2PtCl_6. The part of Nif that was not in contact with the electrolyte retained its gray color, while the part of Nif submerged in the electrolyte obtained a black color, which was ascribed to a Pt layer covering the Nif (*vide infra* Figure 5.9).
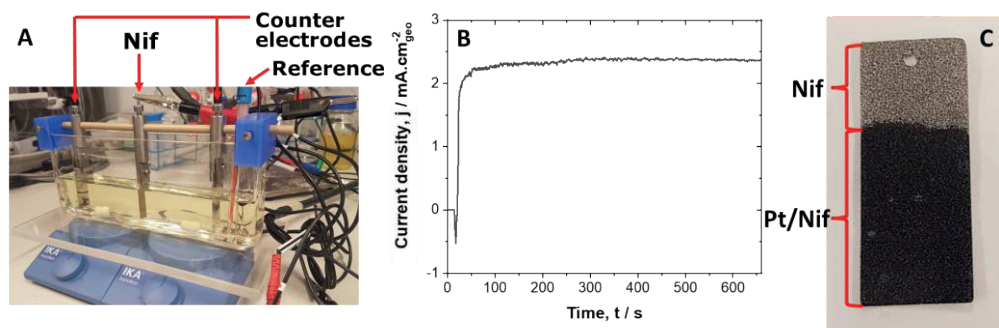

Figure 5.7. A) *Setup used to electrochemically deposit H_2PtCl_6 on a Nif electrode. B) The current-time of Nif in the presence of 1.5 mM H_2PtCl_6 and 0.1 M $HClO_4$ at a hold potential of 0.2 vs. Ag/AgCl and C) the resulting Pt/Nif electrocatalyst.*

The electrochemical properties of Nif, Pt mesh, and Pt/Nif were studied by cyclic voltammetry (Figure 5.8A-B) and by CO-stripping (Figure 5.8C). The CV of Nif, Figure 5.8A, shows a small constant current density in the forward scan between -0.1 and 1.45 V *vs.* RHE, which can be attributed to a pseudocapacitive background current.[53,54] At higher potentials, E = 1.45 V *vs.* RHE, a sharp increase in current density can be observed, caused by the electrochemical oxidation of Ni hydroxide to β-NiOOH.[53,54] In the return scan a cathodic current at 1.4 V *vs.* RHE can be observed, which is known to be related to the electrochemical reduction of β-NiOOH to β-Ni(OH)$_2$,[53,54] after which the current density returns to pseudocapacitive background levels to -0.1 V *vs.* RHE.

Figure 5.8B shows a CV of Pt mesh and Pt/Nif in a 0.1 M phosphate buffer solution (pH = 11.5). The CV of Pt mesh is similar to that of a polycrystalline Pt electrode.[35] In the forward scan, the anodic current between 0.1 to 0.4 V *vs.* RHE represents the desorption of hydrogen from specific facets on polycrystalline Pt (i.e. the peaks at E = 0.23 and 0.35 V *vs.* RHE correspond to Pt(110) and Pt(100)-type sites respectively),[35] while the increase in current density between 0.5 to 0.8 V *vs.* RHE represents the competitive adsorption of hydroxyl and phosphate ions on Pt.[57] The anodic current between 0.8 to 1.5 V *vs.* RHE is related to the electrochemical oxidation of Pt to Pt oxide.[35] In the return scan, the cathodic current from 0.9 to 0.6 V *vs.* RHE Pt relates to the reduction of Pt oxide to Pt, while below 0.4 V *vs.* RHE, the cathodic current represents the hydrogen adsorption

on Pt.[35] The features of the forward scan of Pt/Nif resemble the features of the Pt mesh electrode scan but are less defined. The less defined hydrogen desorption features indicate that Pt/Nif does not expose high contents of specific facets like the Pt mesh electrode.[58] Finally, in Figure 5.8B the features of the return scan of Pt/Nif are shifted by ~0.14 V to a lower potential compared to the features of the Pt mesh electrode. The lower potential required to electrochemically reduce Pt oxide to Pt on Pt/Nif than on Pt mesh shows that a higher driving force is needed to electrochemically reduce Pt oxide to Pt on Pt/Nif. This can tentatively be explained by the strong interaction of Pt with oxyphilic Ni domains ($NiO_x/Ni(OH)_y$).[58]

Figure 5.8C shows the first and second CV for a CO-stripping experiment on a Pt/Nif electrode which was used to determine the electrochemical surface area of Pt. In the first CV and between 0.1-0.35 V *vs.* RHE no current density related to hydrogen desorption can be observed.[35] The absence of hydrogen desorption can be attributed to the occupation of Pt active sites by CO.[58] Between 0.35 and 0.55 V *vs.* RHE a sharp increase in current density can be observed followed by a shoulder between 0.55-1.05 V *vs.* RHE. Rudi et al. showed that Pt in Ni rich environment has a low peak potential for CO oxidation at E = 0.5 V *vs.* RHE and attributed this to Pt domains being near oxyphilic $NiO_x/Ni(OH)_y$ domains, which activate and supply hydroxyl ions.[58] By contrast, Pt in Pt rich domains electrochemically oxidizes CO at $E \geq 0.65$ V *vs.* RHE.[58] Therefore, it is argued that the first anodic peak might be related to the electrochemical oxidation of CO on Pt in Ni rich environment, while the shoulder can be attributed to the electrochemical oxidation of CO on Pt in Pt rich environment.[58] The low CO oxidation potential is beneficial for the electrocatalytic oxidation of organic molecules as it is one of the main hurdles for Pt electrocatalysts at E < ~0.7 V *vs.* RHE, as adsorbed CO poisons the Pt surface.[59] The second CV of Pt/Nif shows a peak between 0.1-0.35 V *vs.* RHE which is ascribed to the desorption of hydrogen.[35] This indicates that the adsorbed CO has been electrochemically oxidized and desorbed, making Pt active sites available again for hydrogen adsorption. Lastly, based on the CO stripping experiments and the assumption that all the Pt precursor (e.g., 0.11 g Pt) was electrodeposited, a high Pt electrochemical surface area of 12 m^2.g Pt^{-1} was calculated, being comparable to the ECSA of Pt black.[60]
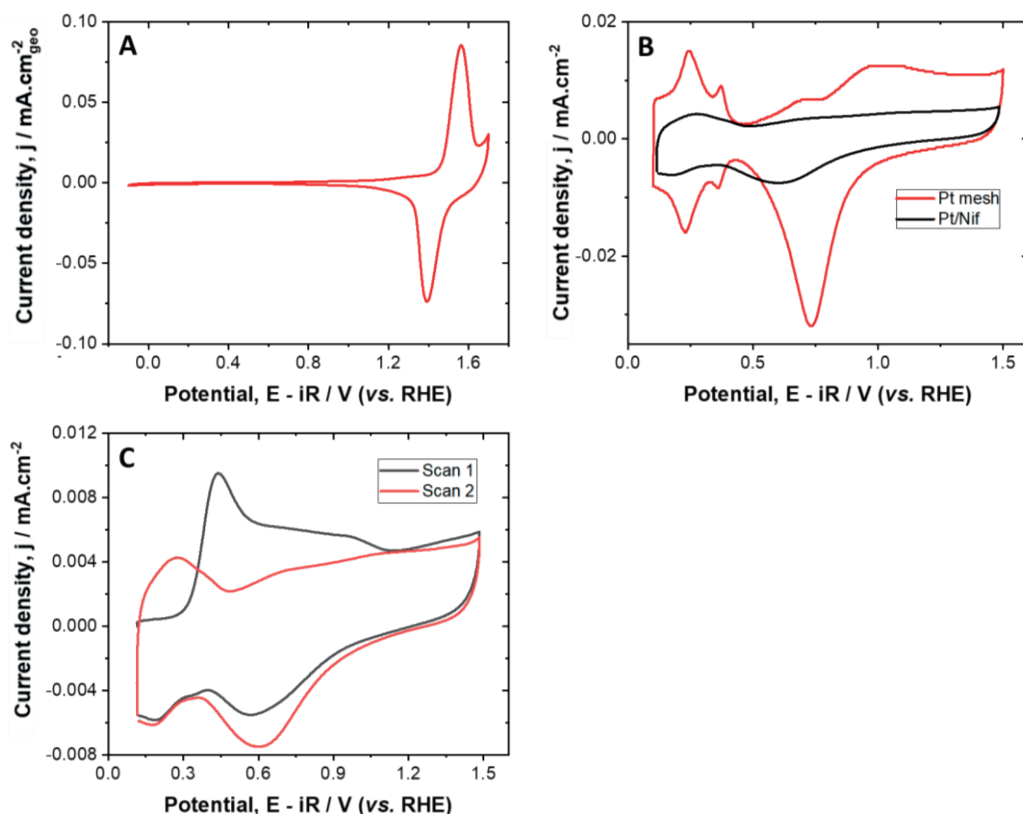
Figure 5.8. *Cyclic voltammograms of A) Nif and B) Pt mesh and Pt/Nif in 0.1 M PBS (pH = 11.5) at a scan rate of 5 mV.s^{-1}. C) Under similar experimental conditions, the CO-stripping and subsequent voltammogram of Pt/Nif.*

Figure 5.9A-B and Figure 5.9C-E show SEM images at different magnifications of Nif and Pt/Nif, respectively, and were used to evaluate the surface structure. Figure 5.9A-B shows that the Nif has a relatively smooth surface with a macroporous structure with pores in the range of a few 100 μm. Figure 5.9C shows that the macroporous structure remains intact after the electrodeposition of Pt on the Nif. At higher magnification for Pt/Nif (Figure 5.9D and E), a highly disordered structure with cracks can be seen. This disordered structure closely resembles that of electrochemically synthesized Pt black.[61] The cracks are likely to be related to the preferred deposition of Pt at defective Ni sites, thereby resulting in inhomogeneous coverage.[62] This can potentially be resolved by using polyvinyl pyrrolidine (PVP) during Pt electrodeposition on Ni foams since PVP can adsorb on the Ni surface and reduce the higher surface energy of defective sites.[62]

Figure 5.9F-H shows EDS images of Pt/Nif and was used to map the elemental distribution of Pt, Ni, and O. The oxygen species can be either attributed to the epoxy used to embed the Nif or to

oxidized Ni or Pt surface species. The metal elemental maps (Figure 5.9F-H) show two types of regions, namely one is composed of a high content of Ni and a low content of Pt, and one is composed of a high content of Pt and a low content of Ni. The region with a high content of Ni corresponds to a crack in the Pt layer thus we conclude that the Ni support is not completely covered by Pt. The Pt layer on the Nif is composed nearly exclusively of Pt and might contain highly dilute content of Ni. The high content of Pt indicates that the Nif is covered by a thick Pt layer since EDS has a typical penetration depth of ~0.4 μm at 15 keV, based on Castaing's formula.[63]

Figure 5.9I shows the X-ray diffractograms of Nif and Pt/Nif and was used to evaluate their crystal structure and the potential presence of alloy structures. The Nif shows three distinct peaks at 44.5˚, 52˚ and 76.5˚, corresponding to the (111), (200) and (220) crystal structures of Ni respectively.[64,65] The Pt/Nif shows similar peaks as Nif with 5 more peaks at 40˚, 46.6˚, 68.1˚, 82˚ and 86.5˚, corresponding to the (111), (200), (220), (311), (222) crystal structure of Pt respectively.[66] X-ray diffractograms did not show the existence of a PtNi alloy structure. However, since the X-rays also probe deeper layers of the Pt/Nif (i.e. are not surface sensitive), this PtNi alloy structure could not be excluded on the surface.
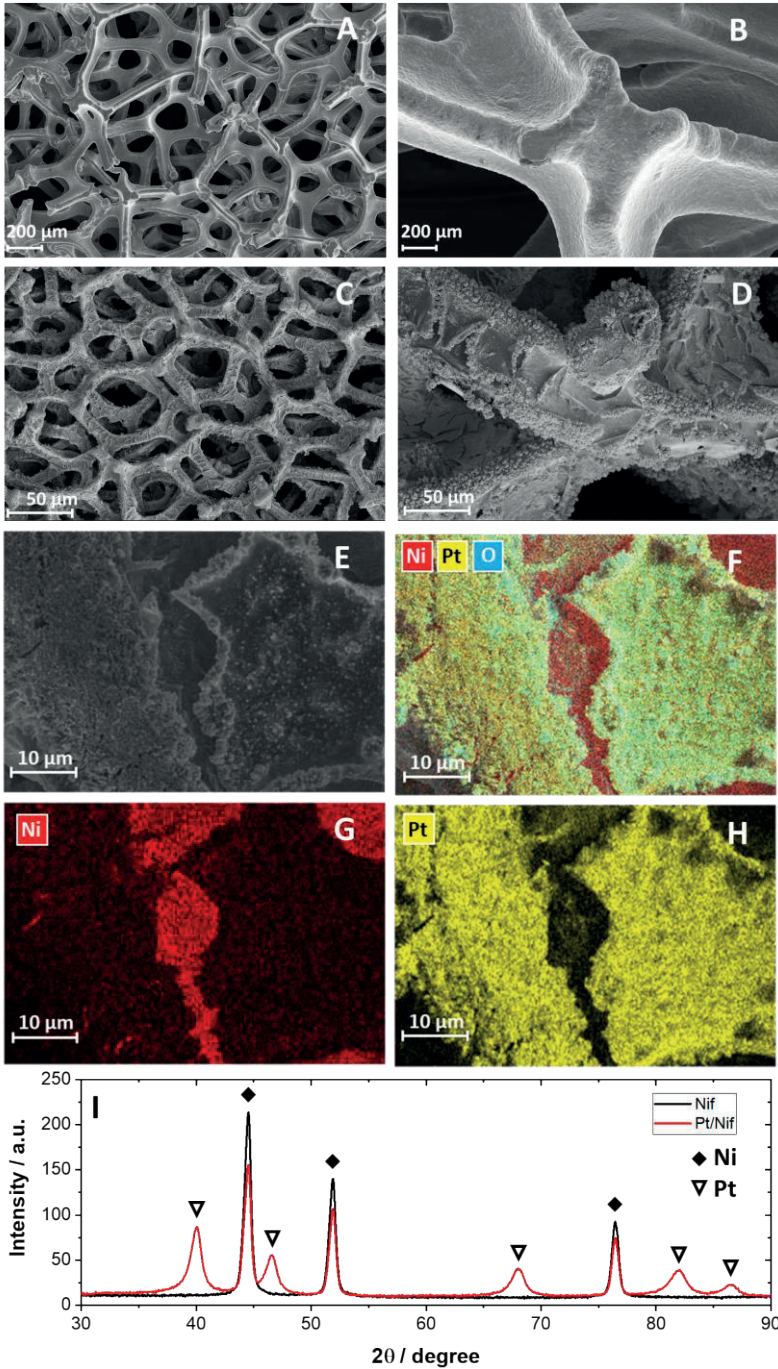
Figure 5.9. *SEM images of Nif (A and C) and Pt/Nif (B, D and E), the related EDS elemental map of Pt/Nif (F-H) and the X-ray diffractogram of Nif and Pt/Nif (I).*

The Pt/Nif electrocatalyst was tested for its potential to electrochemically oxidize unpurified starch. Figure 5.10A displays a LSV of Pt/Nif in the absence (blank) and presence of unpurified starch. The features in the blank LSV strongly resemble the features observed for Pt/Nif in the positive sweep measured during CV (Figure 5.8C second scan) with the exception that during LSV a strong increase in current at E = ~1.45 V *vs.* RHE was observed. The appearance of this feature for the Pt/Nif blank can result from the lower scan rate used during CV than during CV in Figure 5.8C. The lower scan rate results in more time for the electrochemical processes to equilibrate, thereby revealing processes that can be overlooked by fast scan rates. The increase in current at E = ~1.45 V *vs.* RHE might be attributed to the OER over Pt/Nif or the electrochemical oxidation of Ni hydroxide to Ni oxyhydroxide.[53,54]

The LSV of Pt/Nif in the presence of unpurified starch can be subdivided into three regions. In region 1, between 0.15 to 1.0 V *vs.* RHE, a stronger increase in current density can be observed in the presence of starch than in its absence (blank measurement). The small peak between 0.15 to 0.35 V *vs.* RHE in the presence of unpurified starch can be related to hydrogen desorption from Pt.[31] The faster increase in current density at E = 0.15 V *vs.* RHE in the presence of unpurified starch compared to the blank measurement indicates that starch is catalytically oxidized at very low potentials on Pt/Nif. For Pt/Nif and in the presence of unpurified starch, the highest increase in current density was observed in region 1 indicative that this potential window is the best region for Pt/Nif to electrocatalytically oxidize unpurified starch. In region 2, between 1.0 and 1.4 V *vs.* RHE, only a slightly higher increase in current density can be observed in the presence of purified starch than in the blank measurement. This indicates that Pt/Nif is hardly active in catalyzing starch oxidation in this region. The LSV of Pt/Nif in the presence of unpurified starch in regions 1 and 2 strongly resembles the results obtained with a Pt mesh electrode in the presence of purified starch (Figure 5.4A) except for the lower onset potential (E = 0.15 V vs. RHE) for starch oxidation on Pt/Nif. Finally, in region 3, at E > 1.4 V *vs.* RHE, Pt/Nif shows a steep increase in current density in the presence of unpurified starch, which is 0.05 V *vs.* RHE lower than in the absence of starch. This indicates that unpurified starch might have a promotive effect on the OER. Alternatively, the increase in current on Pt/Nif at E = ~1.45 V *vs.* RHE can be attributed to the electrochemical oxidation of starch on Ni (Figure S5.2) as was also observed for organic molecules like glycerol and mannose.[38,67]

Figure 5.10B shows the time response for the average current density (i.e. average current of the individual potential cycles[7], following the same procedure discussed in Figure 5.4C) for the electrocatalytic oxidation of 0.1 M unpurified starch on Pt in 0.1 M PBS. After 1.5 h the current density increases to 8 μA.cm^{-2} and successively decreases again to 2 μA.cm^{-2}, revealing a similar trend as for the electrocatalytic oxidation of purified starch on Pt mesh (Figure 5.4C). The loss in catalytic activity can tentatively be attributed to the depletion of the reactant over time or the deactivation of the catalyst. This indicates that Pt/Nif is well suited for the electrocatalytic

oxidation of starch. However, it still needs to be proven whether Pt/Nif can electrochemically oxidize starch and not only the saccharide oligomers and monomers.
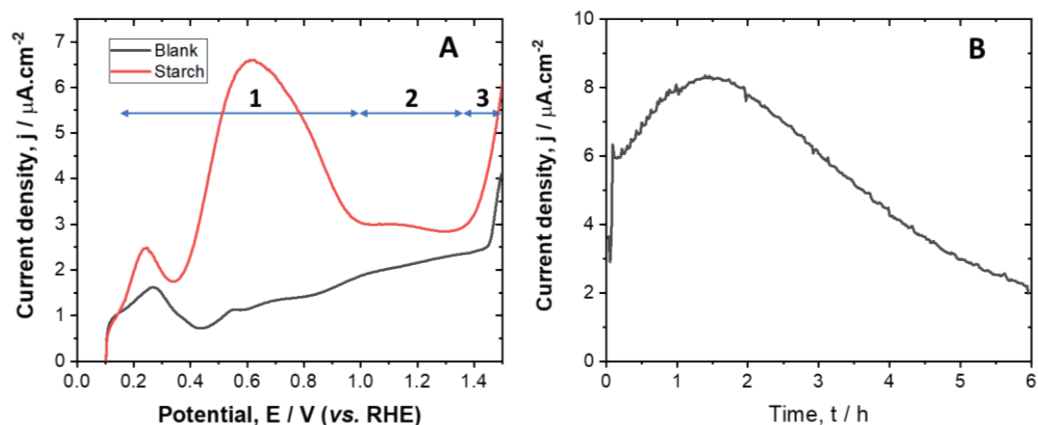

Figure 5.10. *A) Linear sweep voltammetry of Pt/Nif in the absence and presence of 0.1 M unpurified starch and B) the current-time curve for the electrocatalytic of 0.1 M unpurified starch in 0.1 M PBS (pH = 11.5) at a scan rate of 1 mV.s⁻¹.*

5.4. Conclusion

In this study we evaluated 1) the role of low molecular weight polysaccharides and monomers (LMWPM) present in industrially derived starch on the electrocatalytic oxidation of starch on polycrystalline Pt electrodes and 2) the potential for Pt/Nif to electrochemically oxidize unpurified starch.

Firstly, to evaluate the role of LMWPM, we prepared two samples of industrially derived starch: an unpurified starch sample (i.e. as received starch, containing LMWPM) and a purified starch sample (i.e. starch containing traces of LMWPM). It was observed that Pt at 0.6V *vs*. RHE is more active towards the electrocatalytic oxidation of unpurified starch than purified starch indicative that LMWPM are more reactive than starch. This was confirmed by the electrocatalytic oxidation of purified starch where starch remained unaffected (as determined by HPAEC and NMR), while the trace contents of LMWPM were converted (as determined by HPSEC). Therefore, we conclude that future research on the electrocatalytic oxidation of starch should take into account the role of the presence of smaller (poly)saccharides.

Secondly, we designed an electrodeposition setup that has a homogenous electric field during the electrodeposition of Pt on Ni foam and thereby assures the coating of both sides of the Ni foam. The Pt layer covering the Ni foam was not evenly distributed, thus still some Ni foam was exposed. Nonetheless, the Pt/Ni foam was found to have a high Pt ECSA, being comparable to Pt black, and was able to effectively remove CO at low potentials (E = 0.5 V *vs.* RHE), which is crucial for the electrocatalytic oxidation of organic molecules on Pt at lower potentials. The catalyst

activity evaluation showed that Pt/Nif is an effective catalyst for the electrocatalytic oxidation of unpurified starch.

References

1. Masina, N. *et al.* A review of the chemical modification techniques of starch. *Carbohydr Polym* **157**, 1226–1236 (2017).

2. Chronakis, I. S. On the molecular characteristics, compositional properties, and structural-functional mechanisms of maltodextrins: A review. *Crit Rev Food Sci Nutr* **38**, 599–637 (1998).

3. Todd Werpy & Gene Petersen. *Top value added chemicals from biomass: volume I--results of screening for potential candidates from sugars and synthesis gas*. http://www.osti.gov/bridge (2004).

4. Vanier, N. L., El Halal, S. L. M., Dias, A. R. G. & da Rosa Zavareze, E. Molecular structure, functionality and applications of oxidized starches: A review. *Food Chem* **221**, 1546–1559 (2017).

5. Hoogstad, T. M. *et al.* Environmental Impact Evaluation for Heterogeneously Catalysed Starch Oxidation. *ChemistryOpen* **11**, e202200029 (2022).

6. Whistler, R. & Schweiger, R. Oxidation of Amylopectin with Hypochlorite at Different Hydrogen Ion Concentrations. *Crit Rev Food Sci Nutr* **29**, 6460–6464 (1957).

7. van der Ham, M. P. J. M., van Keulen, E., Koper, M. T. M., Asadi Tashvigh, A. & Bitter, H. Steering the Selectivity of Electrocatalytic Glucose Oxidation by the Pt Oxidation State. *Angewandte Chemie International Edition* **62**, 33 (2023).

8. Kwon, Y., Schouten, K. J. P. & Koper, M. T. M. Mechanism of the Catalytic Oxidation of Glycerol on Polycrystalline Gold and Platinum Electrodes. *ChemCatChem* **3**, 1176–1185 (2011).

9. Fuentes, C. *et al.* Fractionation and characterization of starch granules using field-flow fractionation (FFF) and differential scanning calorimetry (DSC). *Anal Bioanal Chem* **411**, 3665–3674 (2019).

10. Hoogstad, T. M., Kiewidt, L., van Haasterecht, T. & Bitter, J. H. Size selectivity in adsorption of polydisperse starches on activated carbon. *Carbohydr Polym* **309**, 120705 (2023).

11. Hoogstad, T. M. *et al.* The effect of polydispersity on the conversion kinetics of starch oxidation and depolymerisation. *Chemical Engineering Science: X* **4**, 100044 (2019).

12. Sugano, Y., Latonen, R. M., Akieh-Pirkanniemi, M., Bobacka, J. & Ivaska, A. Electrocatalytic oxidation of cellulose at a gold electrode. *ChemSusChem* **7**, 2240–2247 (2014).

13. Kageshima, Y. *et al.* Insights into the Electrocatalytic Oxidation of Cellulose in Solution toward Applications in Direct Cellulose Fuel Cells. *Journal of Physical Chemistry C* **125**, 14576–14582 (2021).

14. Van Loon, L. R. & Glaus, M. A. Review of the Kinetics of Alkaline Degradation of Cellulose in View of Its Relevance for Safety Assessment of Radioactive Waste Repositories. *J Environ Polym Degrad* **5**, 2 (1997).

15. Roman, L., Walker, M. R., Detlor, N., Best, J. & Martinez, M. M. Pregelatinized Drum-Dried Wheat Starch of Different Swelling Behavior as Clean Label Oil Replacer in Oil-in-Water Emulsions. *Foods* **11**, 2044 (2022).

16. Ye, J. *et al.* Properties of Starch after Extrusion: A Review. *Starch/Staerke* **70**, 1700110 (2018).

17. Lee, J. W., Kwon, T. O. & Moon, I. S. Adsorption of monosaccharides, disaccharides, and maltooligosaccharides on activated carbon for separation of maltopentaose. *Carbon N Y* **42**, 371–380 (2004).

18. Gerber, I. C. & Serp, P. A Theory/Experience Description of Support Effects in Carbon-Supported Catalysts. *Chem Rev* **120**, 1250–1349 (2020).

19. Van der Ham, M. P. J. M. *et al.* Improved electrocatalytic activity of Pt on carbon nanofibers for glucose oxidation mediated by support oxygen groups in Pt perimeter. *Appl Catal B* **338**, 123046 (2023).

20. Kiewidt, L. & Thöming, J. Pareto-optimal design and assessment of monolithic sponges as catalyst carriers for exothermic reactions. *Chemical Engineering Journal* **359**, 496–504 (2019).

21. Sinn, C., Wentrup, J., Pesch, G. R., Thöming, J. & Kiewidt, L. Structure-heat transport analysis of periodic open-cell foams to be used as catalyst carriers. *Chemical Engineering Research and Design* **166**, 209–219 (2021).

22. Peng, Y., Liu, H., Li, T. & Zhang, J. Hybrid Metallic Foam with Superior Elasticity, High Electrical Conductivity, and Pressure Sensitivity. *ACS Appl Mater Interfaces* **12**, 6489–6495 (2020).

23. Montenegro Camacho, Y. S. *et al.* Development of a robust and efficient biogas processor for hydrogen production. Part 2: Experimental campaign. *Int J Hydrogen Energy* **43**, 161–177 (2018).

24. Kalz, K. F. *et al.* Future Challenges in Heterogeneous Catalysis: Understanding Catalysts under Dynamic Reaction Conditions. *ChemCatChem* **9**, 17–29 (2017).

25. Noël, T., Cao, Y. & Laudadio, G. The Fundamentals behind the Use of Flow Reactors in Electrochemistry. *Acc Chem Res* **52**, 2858–2869 (2019).

26. McCrum, I. T. & Koper, M. T. M. The role of adsorbed hydroxide in hydrogen evolution reaction kinetics on modified platinum. *Nat Energy* **5**, 891–899 (2020).

27. Contreras-Dávila, C. A., Carrión, V. J., Vonk, V. R., Buisman, C. N. J. & Strik, D. P. B. T. B. Consecutive lactate formation and chain elongation to reduce exogenous chemicals input in repeated-batch food waste fermentation. *Water Res* **169**, 115215 (2020).

28. Monteiro, M. C. O. *et al.* Absence of CO2 electroreduction on copper, gold and silver electrodes without metal cations in solution. *Nat Catal* **4**, 654–662 (2021).

29. Dix, S. T., Lu, S. & Linic, S. Critical Practices in Rigorously Assessing the Inherent Activity of Nanoparticle Electrocatalysts. *ACS Catal* **10**, 10735–10741 (2020).

30. Maillard, F. *et al.* Influence of particle agglomeration on the catalytic activity of carbon-supported Pt nanoparticles in CO monolayer oxidation. *Physical Chemistry Chemical Physics* **7**, 375–383 (2005).

31. Qiu, Y. *et al.* Anodic electrocatalytic conversion of carboxylic acids on thin films of RuO2, IrO2, and Pt. *Appl Catal B* **277**, (2020).

32. Kokoh, K. B., Léger, J. M., Beden, B., Huser, H. & Lamy, C. 'On line' chromatographic analysis of the products resulting from the electrocatalytic oxidation of d-glucose on pure and adatoms modified Pt and Au electrodes-Part II. Alkaline medium. *Electrochim Acta* **37**, 1909–1918 (1992).

33. Moggia, G., Schalck, J., Daems, N. & Breugelmans, T. Two-steps synthesis of D-glucaric acid via D-gluconic acid by electrocatalytic oxidation of D-glucose on gold electrode: Influence of operational parameters. *Electrochim Acta* **374**, 137852 (2021).

34. Berehova, N. *et al.* Nerve Targeting via Myelin Protein Zero and the Impact of Dimerization on Binding Affinity. *Molecules* **27**, 9015 (2022).

35. Sandbeck, D. J. S. *et al.* Particle Size Effect on Platinum Dissolution: Practical Considerations for Fuel Cells. *ACS Appl Mater Interfaces* **12**, 25718–25727 (2020).

36. Kokoh, K. B., Léger, J. M., Beden, B. & Lamy, C. 'On line' chromatographic analysis of the products resulting from the electrocatalytic oxidation of d-glucose on Pt, Au and adatoms modified Pt electrodes-Part I. Acid and neutral media. *Electrochim Acta* **37**, 1333–1342 (1992).

37. Moggia, G., Kenis, T., Daems, N. & Breugelmans, T. Electrochemical Oxidation of d-Glucose in Alkaline Medium: Impact of Oxidation Potential and Chemical Side Reactions on the Selectivity to d-Gluconic and d-Glucaric Acid. *ChemElectroChem* **7**, 86–95 (2020).

38. Parpot, P., Santos, P. R. B. & Bettencourt, A. P. Electro-oxidation of d-mannose on platinum, gold and nickel electrodes in aqueous medium. *Journal of Electroanalytical Chemistry* **610**, 154–162 (2007).

39. Kokoh, K. B. *et al.* Selective oxidation of D-gluconic acid on platinum and lead adatoms modified platinum electrodes in alkaline medium. *Electrochim Acta* **38**, 1359–1365 (1993).

40. Governo, A. T., Proença, L., Parpot, P., Lopes, M. I. S. & Fonseca, I. T. E. Electro-oxidation of D-xylose on platinum and gold electrodes in alkaline medium. *Electrochim Acta* **49**, 1535–1545 (2004).

41. Chen, X., McCrum, I. T., Schwarz, K. A., Janik, M. J. & Koper, M. T. M. Co-adsorption of Cations as the Cause of the Apparent pH Dependence of Hydrogen Adsorption on a Stepped Platinum Single-Crystal Electrode. *Angewandte Chemie - International Edition* **56**, 15025–15029 (2017).

42. Hersbach, T. J. P. *et al.* Base-Accelerated Degradation of Nanosized Platinum Electrocatalysts. *ACS Catal* **11**, 9904–9915 (2021).

43. Kusano, S., Matsumura, D., Ishii, K., Tanaka, H. & Mizuki, J. Electrochemical adsorption on Pt nanoparticles in alkaline solution observed using in situ high energy resolution X-ray absorption spectroscopy. *Nanomaterials* **9**, 642 (2019).

44. Shrestha, B. R., Yadav, A. P., Nishikata, A. & Tsuru, T. Application of channel flow double electrode to the study on platinum dissolution during potential cycling in sulfuric acid solution. *Electrochim Acta* **56**, 9714–9720 (2011).

45. Jerkiewicz, G., Vatankhah, G., Lessard, J., Soriaga, M. P. & Park, Y. S. Surface-oxide growth at platinum electrodes in aqueous H2SO 4 Reexamination of its mechanism through combined cyclic-voltammetry, electrochemical quartz-crystal nanobalance, and Auger electron spectroscopy measurements. *Electrochim Acta* **49**, 1451–1459 (2004).

46. Lemoine, C. *et al.* New insights on the selective electroconversion of the cellulosic biomass-derived glucose at PtAu nanocatalysts in an anion exchange membrane fuel cell. *Journal of Electroanalytical Chemistry* **887**, 115162 (2021).

47. Führer, A. M. *et al.* The synergetic effect of support-oxygen groups and Pt particle size in the oxidation of α-D-glucose: a proximity effect in adsorption. *ChemCatChem* **14**, 19 (2022).

48. Bunkerd, R. *et al.* Synthesis and Characterization of Chemically-Modified Cassava Starch Grafted with Poly(2-Ethylhexyl Acrylate) for Blending with Poly(Lactic Acid). *Starch/Staerke* **70**, 1800093 (2018).

49. Creasy, W. R., Mcgarvey, D. J., Rice, J. S., O'connor, R. & Dupont Durst, H. *STUDY OF DETECTION LIMITS AND QUANTITATION ACCURACY USING 300 MHZ NMR*.

50. Li, W., Corke, H. & Beta, T. Kinetics of hydrolysis and changes in amylose content during preparation of microcrystalline starch from high-amylose maize starches. *Carbohydr Polym* **69**, 398–405 (2007).

51. Rosa-Ortiz, S. M., Khorramshahi, F. & Takshi, A. Study the impact of CuSO4 and H2SO4 concentrations on lateral growth of hydrogen evolution assisted copper electroplating. *J Appl Electrochem* **49**, 1203–1210 (2019).

52. Bakar, N. A. A. *et al.* The effect different of hydrochloric acid concentrations on the cleaning of Ni foam substrate: Structural and morphological studies. *Mater Today Proc* **60**, 1036–1041 (2022).

53. Ferreira, E. B. & Jerkiewicz, G. On the Electrochemical Reduction of β-Ni(OH)2 to Metallic Nickel. *Electrocatalysis* **12**, 199–209 (2021).

54. Alsabet, M., Grdeń, M. & Jerkiewicz, G. Electrochemical Growth of Surface Oxides on Nickel. Part 3: Formation of β-NiOOH in Relation to the Polarization Potential, Polarization Time, and Temperature. *Electrocatalysis* **6**, 60–71 (2015).

55. Yin, J. *et al.* α-and β-Phase Ni-Mg hydroxide for high performance hybrid supercapacitors. *Nanomaterials* **9**, 1686 (2019).

56. Granados-Fernández, R., Montiel, M. A., Díaz-Abad, S., Rodrigo, M. A. & Lobato, J. Platinum recovery techniques for a circular economy. *Catalysts* **11**, 937 (2021).

57. Gisbert, R., García, G. & Koper, M. T. M. Adsorption of phosphate species on poly-oriented Pt and Pt(1 1 1) electrodes over a wide range of pH. *Electrochim Acta* **55**, 7961–7968 (2010).

58. Rudi, S. *et al.* pH-Induced versus Oxygen-Induced Surface Enrichment and Segregation Effects in Pt-Ni Alloy Nanoparticle Fuel Cell Catalysts. *ACS Catal* **7**, 6376–6384 (2017).

59. Santasalo-Aarnio, A. *et al.* Comparison of methanol, ethanol and iso-propanol oxidation on Pt and Pd electrodes in alkaline media studied by HPLC. *Electrochem commun* **13**, 466–469 (2011).

60. Zhao, H., Liu, R., Guo, Y. & Yang, S. Molten salt medium synthesis of wormlike platinum silver nanotubes without any organic surfactant or solvent for methanol and formic acid oxidation. *Physical Chemistry Chemical Physics* **17**, 31170–31176 (2015).

61. Stanca, S. E. *et al.* Optical Assets of in situ Electro-assembled Platinum Black Nanolayers. *Sci Rep* **7**, 14955-assembled Platinum Black Nanolayers (2017).

62. Wang, H., Zhang, L., Shen, H., Liu, L. & Li, L. Electrochemical fabrication of Pseudo Platinum foam and its application in methanol electrooxidation. *Int J Electrochem Sci* **12**, 11528–11539 (2017).

63. Paksoy, A. H. *et al.* Influence of alumina addition on steam corrosion behaviour of ytterbium disilicates for environmental barrier coating applications. *Corros Sci* **207**, 110555 (2022).

64. Hu, X., Tian, X., Lin, Y. W. & Wang, Z. Nickel foam and stainless steel mesh as electrocatalysts for hydrogen evolution reaction, oxygen evolution reaction and overall water splitting in alkaline media. *RSC Adv* **9**, 31563–31571 (2019).

65. Świrk Da Costa, K. *et al.* Syngas production from dry methane reforming over yttrium-promoted nickel-KIT-6 catalysts. *Int J Hydrogen Energy* **44**, 274–286 (2019).

66. Stanca, S. E. *et al.* Chemical and Electrochemical Synthesis of Platinum Black. *Sci Rep* **7**, 1–8 (2017).

67. Goetz, M. K. K., Bender, M. T. & Choi, K. S. Predictive control of selective secondary alcohol oxidation of glycerol on NiOOH. *Nat Commun* **13**, 5848 (2022).

Supporting information

Figure S5.1 shows the cyclic voltammograms of Ni foam recorded in 0.1 M HClO$_4$ at a scan rate of 200 mV.s^{-1} and was used to electrochemically polish and clean the Ni surface.[52] The CVs show three distinct regions in the forward scan, consisting of region 1 at E = 0.1 to 0.45 V *vs.* Ag/AgCl, region 2 at E = 0.45 to 1.0 V *vs.* Ag/AgCl, and region 3 at E >1 V *vs.* Ag/AgCl, and two regions in the return scan, consisting of region 4 at E = 1.7 to 0.8 V *vs.* Ag/AgCl, and region 5 at E < -0.25 V *vs.* Ag/AgCl. These regions can be assigned to different processes[53,54]: region 1 is the reversible formation of α-Ni(OH)$_2$ from Ni; region 2 is the irreversible formation of NiO and β-Ni(OH)$_2$; the third region is the reversible formation of β-NiOOH; the fourth region is the reduction β-NiOOH; and the fifth region is the reduction of α-Ni(OH)$_2$ to Ni.
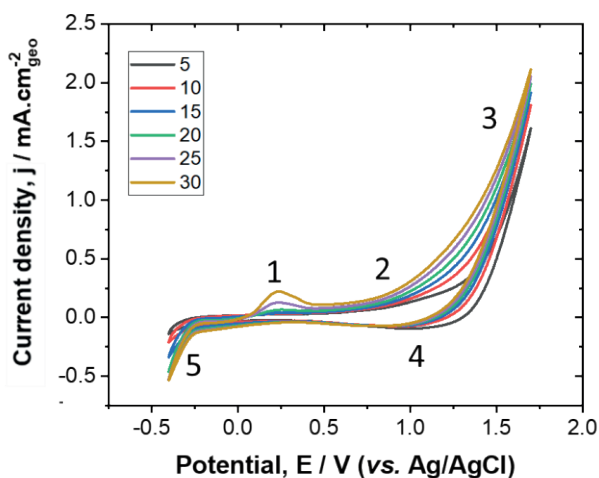
Figure S5.1. *Cyclic voltammetry of Nif was recorded in 0.1 M HClO$_4$ at a scan rate of 200 mV.s^{-1}.*

Figure S5.2 shows the cyclic voltammograms of Ni foam in the absence and presence of unpurified starch recorded in 0.1 M phosphate buffer solution. At ~1.5 V *vs.* RHE and in the presence of starch a stronger increase in current density can be observed in comparison to the blank measurement. This stronger increase in current density at ~1.5 V *vs.* RHE was also observed for the electrocatalytic oxidation of glycerol and mannose.[38,67] Therefore, Ni might be able to electrochemically oxidize starch at a potential higher than 1.5 V *vs.* RHE.
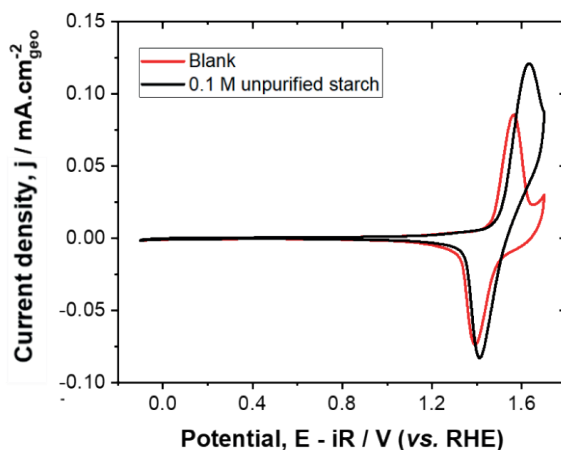
Figure S5.2. *Cyclic voltammetry of Nif was recorded in 0.1 M phosphate buffer solution (pH = 11.5) at a scan rate of 5 mV.s^{-1}.*
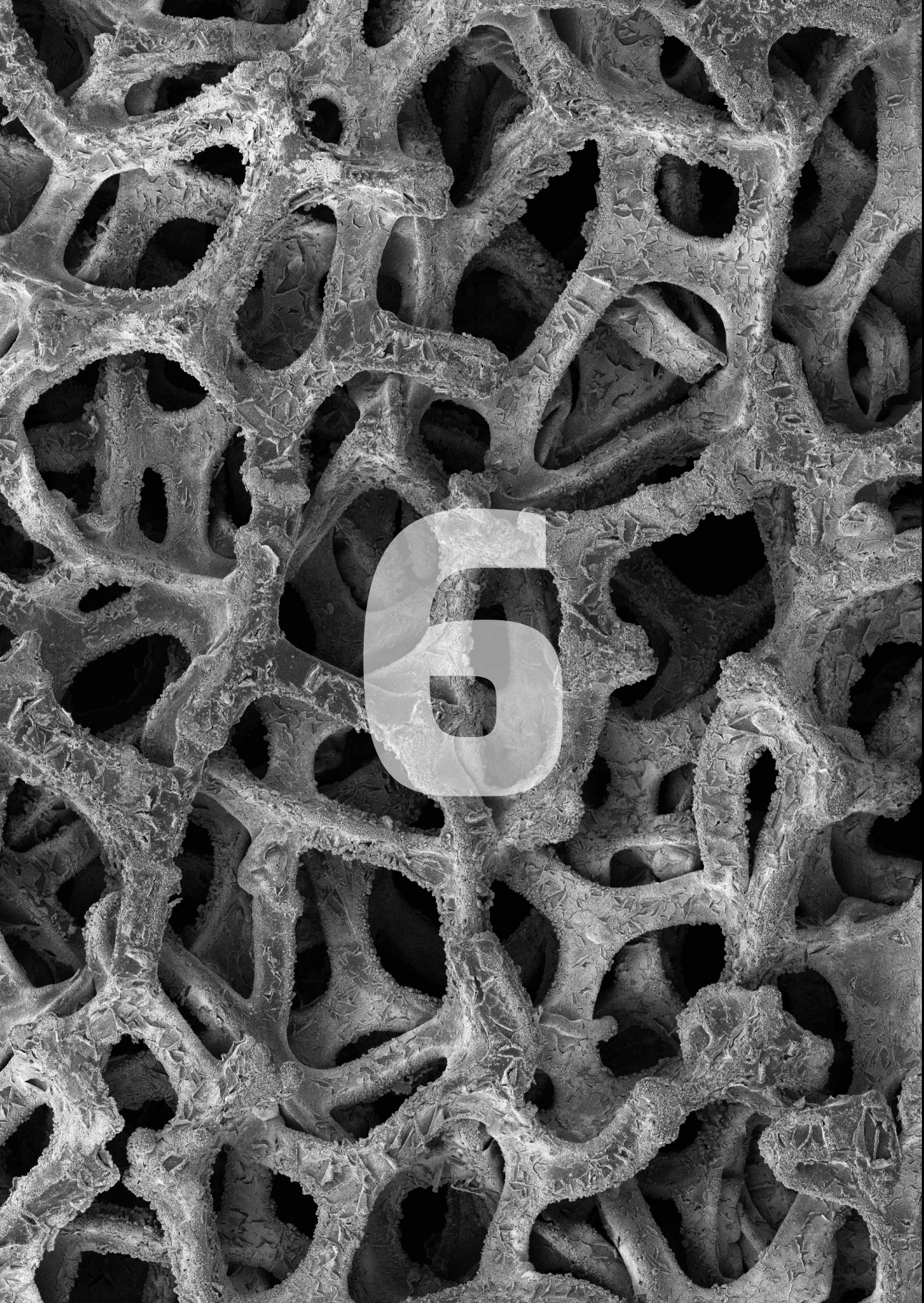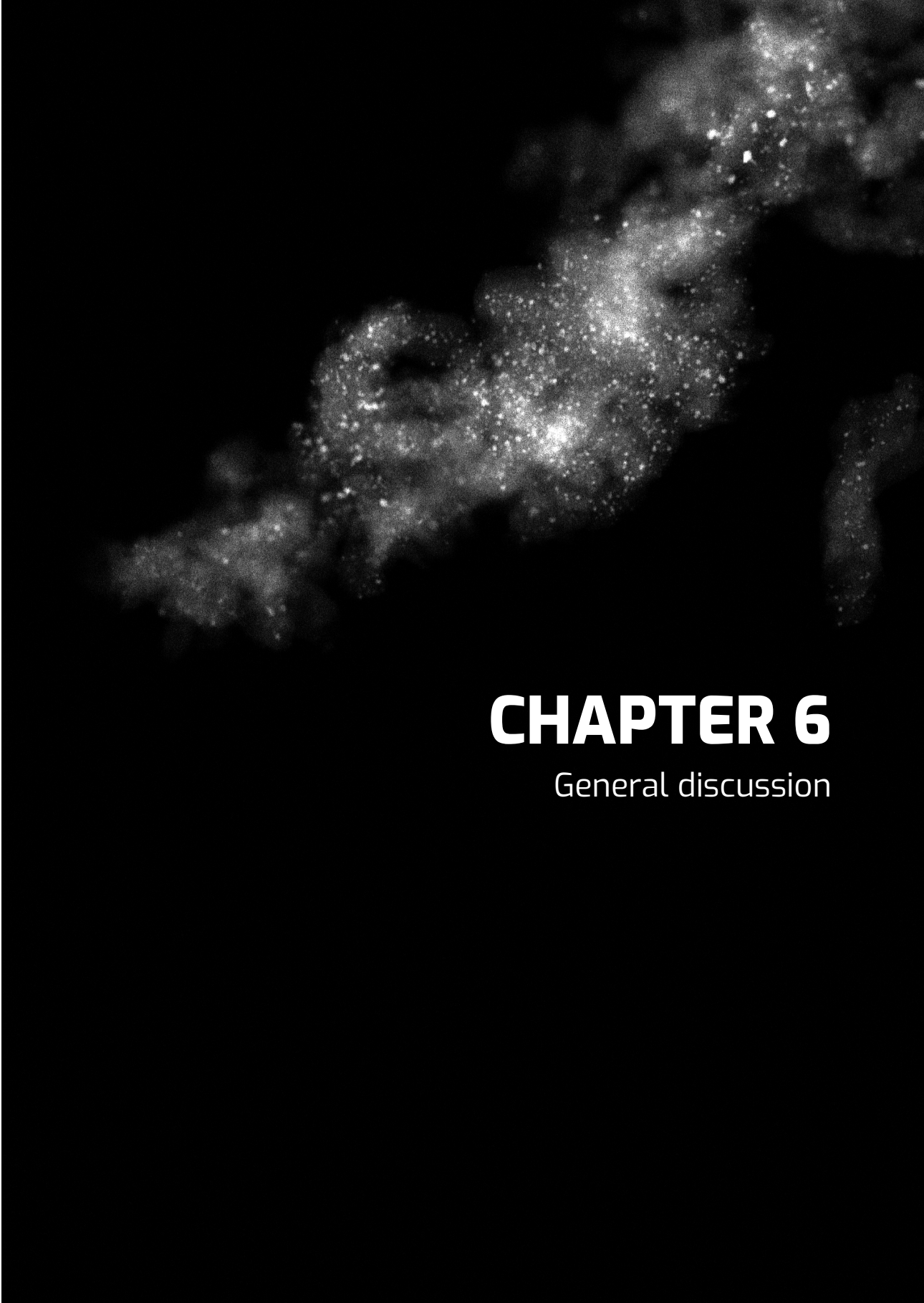
CHAPTER 6

General discussion

This thesis aims to design electrocatalysts for the electrocatalytic oxidation of saccharides and polysaccharides to platform molecules and speciality chemicals. Firstly, Section 6.1 discusses the thesis outline and the main outcomes of each chapter. Secondly, Section 6.2 puts the main outcomes of each chapter into perspective with the main challenges and considerations for future research on the electrocatalytic oxidation of glucose and starch. Thirdly, Section 6.3 gives a summary and outlines recommendations for future research on designing and studying electrocatalysts for the electrocatalytic oxidation of saccharides and polysaccharides.

6.1 Thesis overview

In this dissertation, a bottom-up approach was used to study the electrocatalytic oxidation of biofeedstocks for the synthesis of value-added platform and speciality chemicals. Therefore, the complexity of the biofeedstock was increased along the chapters. **Chapter 2** focuses on a literature study of the electrocatalytic oxidation of sugar alcohols and saccharides. Sugar alcohols are the most simple molecules that can be derived from biofeedstocks, composing of a carbon chain with a hydroxyl group attached to each carbon. Saccharides have an additional functional group when compared to sugar alcohols, being either an aldehyde or ketone. **Chapters 3 and 4** focus on the electrocatalytic oxidation of saccharides and **Chapter 5** discusses the electrocatalytic oxidation of starch, which is a (branched) polymer of saccharides.

In **Chapter 2** we found that most studies devoted to the electrocatalytic oxidation of biofeedtsocks, which closely resemble saccharides, have been conducted on sugar alcohols. From these studies, mechanistic information has been obtained which has been extended to the mechanism of electrocatalytic saccharide oxidation. Therefore, **Chapter 2** is a review that evaluates whether research conducted on the electrocatalytic oxidation of sugar alcohols and saccharides can be extrapolated to one another. For this review, the catalyst properties and reaction conditions were related to the catalytic performance for sugar alcohol oxidation (e.g., glycerol, erythritol, xylitol, and sorbitol) and (separately) saccharides (e.g., glyceraldehyde, xylose, and glucose). Successively, these trends were compared between sugar alcohols and saccharides. Our findings demonstrate that trends can partially be translated for the electrocatalytic oxidation of primary and secondary alcohol groups on sugar alcohols and saccharides. Several trends could not be translated which was attributed to the poor quantification of (intermediate) products of the glucose oxidation pathway, where several (intermediate) products are rarely quantified and therefore likely overlooked.[1] Moreover, studies performed at pH ≥ 10 should discriminate better between base-catalyzed reactions (e.g., isomerization and retro-aldol) and electrochemical reactions to gain better insights into the catalyst performance.[2,3] In addition, the type of electrolyte that is used needs to be considered more carefully, since many studies on non-noble metal catalysts use borax, which is known to form a complex with the reactant and thereby may affect the catalyst selectivity.[4] Briefly, the

trends show that Au can catalyze the electrocatalytic oxidation of the primary alcohol group and anomeric carbon, while Pt also catalyzes the electrocatalytic oxidation of secondary alcohol groups.[5] The electrocatalytic oxidation of secondary alcohol groups on Pt could be improved even further by modifying Pt with post-transition metals.[6]

In the field of thermocatalysis, it is well known that support oxygen groups affect the catalyst performance for different reactions,[7,8] while this is less studied in the field of electrocatalysis. Therefore, **Chapter 3** aims to evaluate whether and how support oxygen groups on Pt on carbon nanofiber (Pt/CNF) affect the electrocatalyst activity for the oxidation of glucose under acidic conditions (pH = 1). This study was conducted with a set of Pt/CNF electrocatalysts that bear different contents of support oxygen groups and different Pt particle sizes. A positive correlation was found between the content of support oxygen groups present on the CNF support and the activity of Pt for the electrocatalytic oxidation of glucose. *In-situ* XANES and *ex-situ* XPS showed that the Pt particle size nor the support oxygen groups on Pt/CNF affected the electronic properties of the Pt catalyst. Moreover, CO-stripping did not show distinguishable differences in Pt surface properties. Therefore, it was concluded that the support affects the adsorption of the reactant in the annulus of the Pt particle, being more significant for smaller Pt particles, which was mathematically substantiated. Hence, it was concluded that support oxygen groups in the Pt perimeter (e.g., Pt annulus) can be used to improve the electrocatalyst performance. The electrocatalyst performance of Pt/CNF was further improved by introducing more support oxygen groups by electrochemical oxidation, giving a new tool for electrocatalyst preparation.

The electrocatalytic oxidation of glucose can produce high-value chemicals,[9,10] but the selectivity of electrocatalysts needs to be improved. Therefore, in **Chapter 4** we have studied the relation between the Pt oxidation state and its activity and selectivity for catalyzing glucose oxidation, by using a new analytical approach that combines high-pressure liquid chromatography (HPLC) and high-pressure anion exchange chromatography (HPAEC) to quantify all glucose oxidation products. Chronoamperometry was performed at 0.64 and 1.2 V *vs.* RHE (corresponding to Pt^0 and PtO_x respectively)[11] to electrochemically oxidize glucose and partially oxidized glucose (gluconate and glucuronate) at neutral reaction conditions (pH = 7), thereby preventing base-catalyzed reaction (e.g. isomerization and retro-aldol reactions) and thus enabling us to discern between electrochemical and non-electrochemical reactions. Our results demonstrate that the Pt oxidation state affects the type of reaction, i.e., dehydrogenation of alcohol groups or oxygen transfer to aldehyde groups, for the electrocatalytic oxidation of glucose. PtO_x was found to be active for oxygen transfer reactions, while Pt^0 was largely inactive for this reaction. On the other hand, both PtO_x and Pt^0 promoted the dehydrogenation reactions, where it was found that PtO_x can dehydrogenate both the primary alcohol group (C6-OH) and secondary alcohol groups (C2-OH and C5-OH), while Pt is likely only able to dehydrogenate the primary alcohol group. This shows that the Pt oxidation state can be used to steer the type of reactions that are catalysed

and therefore be used to steer the catalyst selectivity. These insights could only be obtained by quantifying all (intermediate) products of the glucose oxidation pathway and therefore highlight the importance of using an analytical technique that enables this, such as a combination of HPAEC with HPLC.

Starch, a polymer of glucose, is oxidized in industry by hypochlorite to anionic starch,[12] where the aim is to oxidize ~5% of the primary alcohol groups (C6-OH) to carboxylates (C6-OOH). However, starch oxidation by hypochlorite results in stochiometric quantities of salt waste, chlorinated by-products and moderate selectivities.[13,14] In **Chapter 4** we have shown that Pt can oxidize the C6-OH group of glucose.[1] Therefore, the electrocatalytic oxidation of starch on Pt could potentially be used as a more selective and cleaner approach for the synthesis of anionic starch. Yet, starch is a bulky molecule and therefore easily susceptible to internal and external mass transport limitations, especially in 3D electrodes. These mass transport limitations reduce the overall catalyst activity and should therefore be avoided. To reduce external mass transport limitations for the electrocatalytic oxidation of starch highly macroporous electrocatalysts can be envisioned, such as a catalyst supported on a macroporous support like Ni foam. Thus, **Chapter 5** is a proof of principle study where we aimed to electrocatalytically oxidize water soluble starch to anionic starch with Pt on Ni foam (Pt/Nif) electrode.[15,16] Pt/Nif was synthesized by electrodeposition and was found to be highly resistant to CO poisoning and have a high Pt active surface area, being comparable to that of Pt black. The Pt/Nif was able to electrochemically oxidize industrially derived starch. Thereafter, the effect of purification of industrial-derived starch was evaluated, thereby removing low molecular weight polysaccharides (LMWP, with a degree of polymerisation < 18). Pt was found to be active towards the electrocatalytic oxidation of purified starch at 0.65 V and 1.1 V *vs.* RHE with the highest catalytic activity at 0.65 V *vs.* RHE. This indicates that Pt^0 (at E = 0.65 V *vs.* RHE), discussed in **Chapter 4**, is more active for the electrocatalytic oxidation of starch than PtO_x (at E = 1.1 V *vs.* RHE), which was likely attributed to the effectiveness of Pt^0 to catalyse the oxidation of the primary alcohol groups. However, product analysis revealed that only the small fraction of LMWP still present in the purified starch was electrochemically oxidized (as determined by HPAEC-PAD), while the starch itself remained unaffected as no aldehydes and carboxylic acids were detected (as determined by HPSEC-UV and ^{1}H-NMR).

6.2. Electrosynthesis of biomass-based chemicals from saccharides and polysaccharides

This section outlines a general picture of my views on what research should focus on, how our research contributes to this, and how state-of-the-art research can contribute to future developments.

6.2.1. Improving selectivities for electrocatalytic oxidation of glucose

Glucose oxidation can yield a wide variety of chemicals that have numerous applications. The wide variety of glucose oxidation products that can be obtained requires the development of catalysts with high selectivities to prevent a loss of value-added product and reduce downstream processing costs. Table 6.1 shows the products that can be obtained from glucose oxidation and their market price, market size and application. The most relevant glucose oxidation products are glucaric acid and gluconic acid, which have been noted as top value-added platform chemicals by the NREL.[10] The market size of gluconic acid (1.2 euro/kg)[17] is expected to grow to 120 kilo tons by 2024,[18] being relatively similar to glucaric acid (4.2 euro/kg)[19] with 70 kilo tons by 2024.[13] However, the difference in market price makes the market value of glucaric acid (370 million euro, Meuro) much bigger than that of gluconic acid (140 Meuro).[17,20] Moreover, the global gluconic acid market is only expected to grow to 170 Meuro, while glucaric acid is expected to grow to 1,060 Meuro.[17,19] Potentially this can be related to the numerous applications glucaric acid holds.[10] For example, glucaric acid has the potential to be used as a precursor for the synthesis of adipic acid, which is a precursor for nylon.[21] In addition, glucose oxidation can yield 2-keto gluconic acid[9] and 5-keto gluconic acid,[22] which are precursors to the platform chemicals tartaric acid and ascorbic acid. The market price and market size of 2-keto gluconic acid and 5-keto gluconic acid in Table 6.1 are based on tartaric acid and ascorbic acid, since they are platform chemicals that can be obtained from 2-keto gluconic acid and 5-keto gluconic acid respectively, thereby reflecting the potential these chemicals hold. Lastly, glucose oxidation can produce glucuronic acid,[23] which is a speciality chemical and can be a precursor for the synthesis of 5-keto gluconic acid. The market price of glucuronic acid was not considered as it is a speciality chemical and therefore much more expensive than the other platform chemicals that can be obtained through the electrocatalytic oxidation of glucose.

Table 6.1. *Glucose oxidation products and their market price, market size and application.*

Compound	Market price (euro/kg)	Market size (Meuro/year)	Application
Gluconic acid	1.2	70	Pharmaceutical, food, textile, and paper[24]
Glucaric acid	4.2	370	Biodegradable polymers, metal complexing agents, pharma, corrosion inhibitors[25]
2-keto gluconic acid	5.1[a]	1050[a]	Food, detergent, photographic developer and precursor to isoascorbic acid[26]
5-keto gluconic acid	2.3[b]	807[b]	Precursor to tartaric acid: food, pharma, cosmetics and textile[27]
Glucuronic acid	-	2[28]	Pharmaceutical intermediate,[23] precursor to 5-keto gluconic acid

[a] Market size[29] and market price[30] based on isoascorbic acid

[b] Market size[31] and market price[32] based on tartaric acid

Improving the catalyst selectivity in glucose oxidation reactions towards a desired product is relevant to reducing unwanted side reactions and producing less complex reaction mixtures, thereby reducing the loss of value-added products and preventing downstream processing costs. To date, glucose oxidation to gluconic acid, 2-keto gluconic acid, and 5-keto gluconic acid is performed via fermentation,[26,27,33] while glucose oxidation to glucaric acid is achieved by nitric acid.[25] However, fermentation processes result in slow kinetics, requiring large reactors, and complex down-stream processes.[33] On the other hand, glucose oxidation by nitric acid requires harsh redox agents and is mildly selective to glucaric acid (~60%), thereby resulting in complex downstream processes.[25] Therefore, alternative processes need to be studied that are more active and selective for glucose oxidation and do not require harsh redox agents. These issues can be resolved by electrocatalytically oxidizing glucose. Following this approach, options are given here below for future research to improve the selective electrocatalytic oxidation of glucose to gluconic acid, 2-keto gluconic acid, 5-keto gluconic acid, glucuronic acid, and glucaric acid.

These ideas listed here below are based on the findings discussed in **Chapter 2**. In these proposed studies it is strongly advised to quantify all (intermediate) products of the glucose oxidation pathway with our new analytical approach used in **Chapter 4**, thereby providing a better insight into the relation between the catalyst properties and its selectivity. This allows us to effectively develop pathways for the electrosynthesis of glucose oxidation products that can be used to replace less sustainable pathways currently used in industry for glucose oxidation (e.g., by fermentation or nitric acid).

1. Gluconic acid

Au can potentially be used for the selective electrocatalytic oxidation of glucose to gluconic acid or gluconate, depending on the pH of the electrolyte.[34–36] Gluconic acid and gluconate are both used in industry, depending on the application.[33] Hence, the production of gluconic acid and gluconate should both be considered to avoid the formation of salt waste if gluconate is converted to gluconic acid. The production of gluconate can be achieved under alkaline conditions (pH > 5), while the production of gluconic acid can be achieved under acidic conditions (pH ≤ 3, pK$_a$ of gluconate = 3.9).[34–36] Au can be considered an effective catalyst for this reaction as it only catalyzes the oxidation of the anomeric carbon and the primary alcohol group of glucose (**Chapter 2**).

For the selective production of gluconate, the electrocatalytic oxidation of glucose should be researched under alkaline conditions (pH = 13) on Au electrodes. At pH = 13, on Au, the electrocatalytic oxidation of glucose has an onset potential of 0.4 V *vs.* RHE and two peak potentials at 0.8 and 1.25 V *vs.* RHE.[34–36] By contrast, for the electrocatalytic oxidation of gluconate on Au the onset potential and peak potential are 0.8 V and 1.25 V *vs.* RHE respectively.[34–36] This indicates that the oxidation of the anomeric carbon of glucose proceeds at $E < 0.8$ V *vs.* RHE, while the oxidation of the primary alcohol group of glucose proceeds at $E > 0.8$ V *vs.* RHE.[37,38] As a result, under optimized reaction conditions (at $E = 0.4$-0.8 V *vs.* RHE) Au can selectively electrocatalytically oxidize glucose at the anomeric carbon to gluconate (85-100 %).[35,36,39] Yet, these studies are not likely to have considered the potential formation of glucose dialdehyde. Therefore, it is strongly suggested to study the electrocatalytic oxidation of glucose to gluconate on Au with our analytical approach used in **Chapter 4** to confirm the absence of glucose dialdehyde.

For the selective production of gluconic acid, the electrocatalytic oxidation of glucose should be researched under acidic conditions (pH = 1, 0.1M HClO$_4$) on Au electrodes. At pH = 1, the electrocatalytic oxidation of glucose on Au has an onset potential of 0.5 V *vs.* RHE and three peak potentials at 0.9, 1.4, and 1.6 V *vs.* RHE.[40,41] By contrast, the electrocatalytic oxidation of sugar alcohols on Au only takes place in alkaline conditions.[42] This indicates that Au can selectively electrocatalytically oxidize the anomeric carbon of glucose under acidic conditions. Yet, the activity of Au under acidic conditions (0.1 M HClO$_4$) at 0.9 V *vs.* RHE (0.2-0.6 mA.cm^{-2})[40,41] is much lower than under alkaline conditions (0.1 M NaOH) at 0.8 V *vs.* RHE (~3 mA.cm^{-2} and 40 mA.cm^{-2} for static and rotating electrodes respectively).[34–36,39] Moreover, when 0.1M H$_2$SO$_4$ is used as the electrolyte the activity of Au drops to 0 mA.cm^{-2}.[40,43] This indicates that mixing the solution and the type of electrolyte has a strong impact on the activity of Au for the electrocatalytic oxidation of glucose to gluconic acid. Despite these insights, the selective electrocatalytic oxidation of glucose on Au has rarely been studied, where to date only 60% gluconic acid has

been obtained at $E = 0.95$ V *vs.* RHE under nonoptimized reaction conditions.[41] Another effective approach would be to increase the temperature, thereby increasing the electrolyte conductivity, the mass transfer rate (i.e., decreasing the viscosity), and the reaction rate, which can also affect the catalyst selectivity.[44] The increase in conductivity can be used to reduce the electrolyte concentration, thereby reducing the concentration of adsorbed anions and increasing the concentration of reactant on the catalyst surface.[40,45,46] The increased concentration of reactant on the catalyst surface can improve the catalyst reaction rate and is likely to affect the catalyst selectivity.[46] However, a decrease in electrolyte concentration can also induce severe ohmic resistances, especially at industrially relevant current densities, and should therefore be considered. Therefore, more research on the effect of reaction conditions (e.g., type of electrolyte, temperature and convection) for the selective electrocatalytic oxidation of glucose to gluconic acid on Au electrodes under acidic conditions is required to further improve the catalyst activity and selectivity.

2. 2-keto gluconic acid and 5-keto gluconic acid

For the selective electrosynthesis of 2-keto gluconic acid and 5-keto gluconic acid, it is recommended to decouple the oxidation of glucose to gluconic acid from the oxidation of gluconic acid to 2-keto gluconic acid and 5-keto gluconic acid. For the production of 2-keto gluconic acid and 5-keto gluconate from gluconic acid bimetallic catalysts, such as Pt with Sb or Bi, can be considered. For example, under acidic conditions, Pt with Bi or Sb ad-atoms (at $E \leq 0.6$ V *vs.* RHE)[6,47,48] and alloyed structures of PtSb (at $E \leq 0.8$ V *vs.* RHE) and PtBi (at $E \leq 0.6$ V *vs.* RHE)[49,50] have proven to be highly selective in the dehydrogenation of the secondary alcohol group of various sugar alcohols (e.g., glycerol, erythritol, and sorbitol), reaching ~80% selectivity under unoptimized reaction conditions.[48,6] For the electrocatalytic oxidation of glucose, Kokoh *et al.* showed under unoptimized reaction conditions that lead adatom modified Pt electrodes in alkaline media can produce 33% 2-keto gluconate and 10% 5-keto gluconate.[51] By performing research on the electrocatalytic oxidation of gluconate on transition-metal (Bi, Sb, etc.) modified Pt electrodes, light might be shed on whether these catalysts have a preference for the electrocatalytic oxidation of 1) the secondary alcohol group adjacent to the carboxylate of gluconate to synthesize 2-keto gluconate or 2) the secondary alcohol group adjacent to the primary alcohol group of gluconate to synthesize 5-keto gluconate.

3. Glucuronic acid

Alternatively, a study devoted to the electrocatalytic oxidation of gluconate at the primary alcohol group could aid in the selective production of guluronate. For this, a catalyst with a high activity and selectivity for dehydrogenation reactions can be envisioned, such as Pt^0 (see **Chapter 4**). The activity of Pt^0 for the electrocatalytic catalytic dehydrogenation of the primary alcohol group of gluconate was relatively low at pH = 7, being 2.5 $\mu A.cm^{-2}$. The optimization of the

reaction conditions or the consideration of other catalysts that promote the dehydrogenation of the primary alcohol group can be considered.

4. Glucaric acid

So far, the electrocatalytic synthesis of dicarboxylates, such as glucarate from glucose and tartronate from glycerol, was predominantly achieved under harsh alkaline conditions (pH ≥ 13.7).[25,52–56] Yet, these harsh alkaline conditions catalyze homogeneous reactions of glucose, such as isomerization and retro-aldol reactions under anaerobic conditions, resulting in a loss of glucaric acid. Moreover, these alkaline conditions produce glucarate rather than glucaric acid, where the conversion of glucarate to glucaric acid results in salt waste production. To produce glucaric acid (pK_a = 2.8) the pH of the electrolyte should be after reaction ≤ 2. Therefore, we propose that future research on the synthesis of glucaric acid should either focus on 1) acidic conditions and alternative electrocatalysts or 2) alkaline conditions with short residence times of glucose in harsh alkaline electrolytes (e.g., by promoting its fast oxidation to dicarboxylates) and evaluate the additional purification costs of glucarate to glucaric acid.

Under acidic conditions, stronger oxidizing catalysts need to be considered for the electrocatalytic synthesis of glucaric acid from glucose. Bin *et al.* showed at pH = 2-4 that MnO_2 supported on a porous titanium electrode can electrocatalytically oxidize 91% glucose to 46% glucaric acid and 43% gluconic acid at 3 mA.cm^{-2}.[57] Likewise, Li *et al.* showed at pH = 1.3 that MnO_2 with TEMPO at *E* = 1.47 V *vs.* RHE can selectivity electrocatalytically oxidize 98% glucose to 85% glucaric acid.[58] In this case the oxygen vacancies on the MnO_2 surface were found to promote glucose oxidation reactions.[58] Considering the high selectivity of MnO_2 towards glucaric acid, it is also relevant to evaluate the selectivity of other metal oxides for glucose oxidation to glucaric acid. Alternatively, for noble metal catalysts the addition of highly oxidizing metals, such as Mn, Ce, or V, can change their electronic property.[59,60] Under acidic conditions, this approach resulted in higher catalytic activities and selectivities for the electrocatalytic oxidation of glycerol to tartronic acid and can therefore also hold the potential to improve the electrocatalytic oxidation of glucose to glucaric acid.

The electrocatalytic oxidation of glucose to glucarate needs to be studied under alkaline conditions on 1) noble metal catalysts, while considering 2) the additional purification costs to convert glucarate to glucaric acid and 3) the formation of degradation products via retro-aldol reactions. Under harsh alkaline conditions (pH ≥ 13.7) and in flow cells, the electrocatalytic oxidation of glycerol to dicarboxylates (~80% selectivity and 20% conversion at best [52]) was achieved at *E* = 0.5-0.7 V *vs.* RHE on Au[52,53] and Pt[54,55] electrodes. By contrast, in an H-cell, the electrocatalytic oxidation of glucose to glucaric acid (83% selectivity and 83% conversion) on NiFe oxide required much higher potentials, namely E = 1.3 V *vs.* RHE.[61] This indicates that noble metal catalysts require lower potentials to electrocatalytically oxidize glucose to glucaric acid and

therefore have a reduced energy consumption when compared to non-noble metal catalysts. Yet, the purification of glucarate formed under these harsh alkaline conditions should be considered as it can result in large amounts of salt wastes.[61] This salt waste could even be regarded as the main income for glucarate production. Moreover, blank experiments should be performed to prove the absence of base-catalysed degradation products that can be formed by retro-aldol reactions.

6.2.2. Considerations for support property modification of carbon-supported electrocatalysts

The performance of carbon-supported metal catalysts can be modified by changing the support properties. This concept has been widely applied in the field of thermocatalysis.[8] For example, for the catalytic oxidation of glucose to gluconate over Pt on carbon, the presence of support oxygen groups promotes the desorption of gluconate and thereby alleviates product inhibition caused by the strong interaction between Pt and gluconate.[62] Changing the support properties of carbon-supported metal electrocatalysts might therefore also be a promising approach to improve the electrocatalyst performance.

In **Chapter 3** we have shown that the presence of support oxygen groups on a carbon support in the perimeter (e.g., annulus) of Pt improves the catalytic activity towards the electrocatalytic oxidation of glucose at $E > 0.5$ V vs. RHE. CO-stripping and *in-situ* HERFD-XANES showed that the surface structure and the electronic properties of the Pt catalyst were not affected by the presence of support oxygen groups. Therefore, we hypothesize that the support oxygen groups improve the adsorption of glucose in the Pt annulus, thereby increasing the availability of glucose in the vicinity of the catalyst and consequently increasing the electrocatalyst activity. This indicates that support functionalities can play a significant role in the activity of supported electrocatalysts.

The support oxygen groups can also affect the catalyst selectivity during the electrocatalytic oxidation of glucose since it can change the coordination of the reactant to the catalyst.[7] Therefore, it is necessary to study the effect of support oxygen groups on the selectivity of the Pt/CNF catalysts for the electrocatalytic oxidation of glucose. Since Pt/CNF quickly deactivates during chronoamperometric measurements (**Chapter 3**), the catalyst needs to be reactivated by applying a dynamic potential (**Chapter 4**). This dynamic potential which requires a desorption potential ($E \geq 1.7$ V *vs.* RHE) is likely to cause the oxidation of the carbon support in the annulus of the Pt nanoparticles (**Chapter 3**). Therefore, this dynamic potential needs to be avoided to evaluate the effect of support oxygen groups on the selectivity of Pt/CNF for the electrocatalytic oxidation of glucose. Here we propose to combine LSV with online HPLC to collect products near the surface of the electrode to evaluate the product distribution for Pt/CNF catalysts with and without support oxygen groups.[63]

The support oxygen groups can also influence the catalyst stability during the electrocatalytic oxidation of glucose and therefore need to be researched. For example, the presence of support oxygen groups can facilitate Pt leaching and Ostwald ripening and thus decrease the stability of the Pt electrocatalyst.[64] This effect should be studied for carbon-supported catalysts with different contents of support oxygen groups decorated with ≤ 2 nm Pt particles by cycling between 0.1-1 V *vs.* RHE.[65] Leaching of Pt can be tracked by ICP-MS, while the growth of Pt particles can be tracked by using *in situ* electrochemical cell STEM.[66]

To improve the performance of the electrocatalyst for glucose oxidation even further, doping of the carbon support with different elements, such as sulfur,[67] iron,[68] or phosphorus must be researched. Doping the carbon support of electrocatalysts is a common practice to improve the catalyst performance.[8] For example, Pt on S-doped carbon nanotubes (Pt/SCNT) were found to have a twofold higher catalytic activity than Pt on carbon nanotubes (Pt/CNT) for the electrocatalytic oxidation of glycerol. Moreover, Pt/SCNT displayed improved catalytic stability and higher selectivity towards tartronate than Pt/CNT.[67] The higher catalytic selectivity towards tartronate indicates that this catalyst promotes the successive oxidation of glycerate. A similar effect was shown for Pt on iron and nitrogen co-doped carbon nanotubes (Pt/FeNC).[68] In this case the activity of Pt for the electrocatalytic oxidation of glycerol was 2.5-fold higher for Pt/FeNC than Pt/C. Moreover, Pt/FeNC promoted the successive oxidation of glycerate to tartronate, thereby increasing the selectivity towards tartronate 2.5 times to 50%. The FeNC support changed the electronic properties of the Pt catalyst by upshifting the d-band center, thereby increasing the interaction with glycerate and thus its successive oxidation to tartronate.[68] Hence, doping the carbon support holds the potential to improve the electrocatalytic oxidation of glucose to glucaric acid.

6.2.3. Techno-economic analysis of the electrocatalytic oxidation of starch

The economic feasibility of electrochemically oxidizing starch with Pt relies on its ability to compete with the well-established hypochlorite oxidation method. To assess this, a techno-economic analysis (TEA) must be conducted to evaluate the profitability of the electrocatalytic oxidation of starch, incorporating estimates of capital expenses (CAPEX) and operating expenses (OPEX). Additionally, a sensitivity analysis needs to be performed within the TEA to identify processes with the highest costs. This approach allows to identify essential research and development objectives that have the highest impact on the overall profitability of the process.

For the electrocatalytic oxidation of starch, a process design has been conceptualized, integrating upstream and downstream processes (DSP). Figure 6.1 shows this process design where granular starch is first solubilized by an extruder to obtain a solution of 10-40 wt.% starch (assuming it not to be too viscous) which is successively electrochemically oxidized in an electrochemical reactor. The oxidized starch is concentrated by a microfilter and successively

precipitated with 67 vol.% acetone as an antisolvent. The resulting slurry is consecutively filtered and dried by a drum filter. The retained solutions at the (micro)filters were recycled to recover the electrolyte and antisolvent. For the TEA the process was simplified into three unit blocks: starch modification block (highlighted in blue), electrochemical reaction block, and DSP block (highlighted in orange).
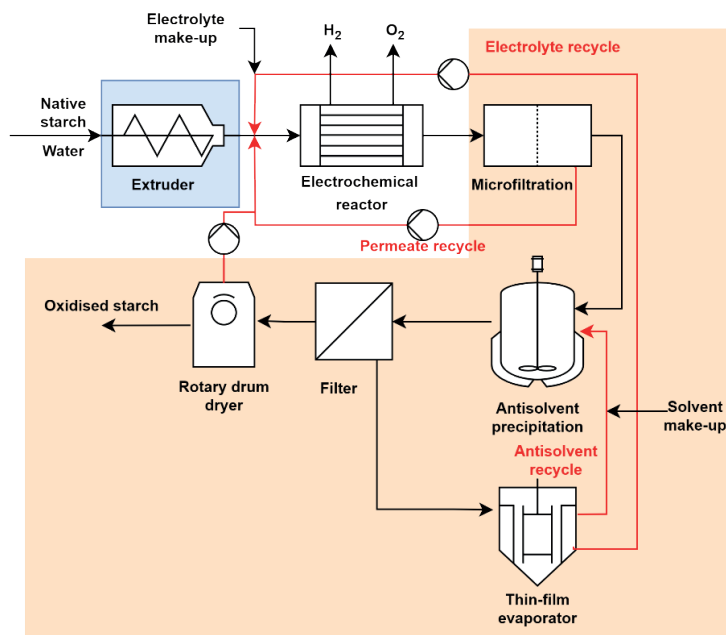

Figure 6.1. *A conceptual process design, simplified into three unit blocks, for the electrocatalytic oxidation of starch.*

Several assumptions were made for the TEA:

1) Reactions related to the buffering capacity of the electrolyte are ignored;

2) The mass balance consists of two flows: 5% reactive and 95% inert starch (e.g., based on 5% oxidized starch for commercial application);

3) Faradaic efficiency of 80% towards starch oxidation and chemical selectivity of 100%;

4) The electrochemical reactor is operated at 100 mA.cm^{-2};

5) At the cathode water is reduced to hydrogen;

6) Electrolyte and antisolvent (e.g., to precipitate starch) are 100% recycled, contributing to CAPEX rather than the OPEX;

7) The full plant size ranges from 1 to 5 kton.y^{-1} (varied during sensitivity analysis);

8) The starch concentration in the electrochemical reactor varies between 2 to 20 wt.%;

9) The complexity of the electrochemical reactor block scales with the square root of the number of cells in the electrochemical stack.

The overall methodology of TEA consisted of three major steps: 1) determining the feedstock and product prices (based on bulk prices), 2) assigning a complexity number to the overall system, 3) deriving the CAPEX and OPEX from the complexity number of the overall system by using the quick process economics approach by Frits M. Dautzenberg.[69] This methodology is a class 5 estimate, meaning that the expected accuracy range of actual costs ranges from -20 to -50 % (low range) and from +30 to +100% (high range).

The complexity number of the overall system is a summation of the fictive unit block sizes and the recycle factor. The fictive unit block sizes are based on the complexity and volume percent of each unit block which are an average of the complexity and volume percent of the processes in each unit block. The volume percent of an individual process is the feed volume of the individual process divided by the largest feed volume processed in the related unit block. The complexity number is based on engineering thumb of rules and best practices, except for the electrochemical reactor, where the complexity scales with the square root of the number of cells in the electrochemical stack. The recycle factor depends on all the recycle streams between the individual processes. The recycle factor is essentially a means of applying a penalty for operating at dilute concentrations in the process to avoid over-optimistic cost predictions. The more dilute the process, the larger the size of recycle streams and therefore, the CAPEX associated with handling them in the plant. The contributions of individual unit blocks and the recycle factor to the overall plant complexity number can already hint at the major cost contributors in the plant and therefore, opportunities to win back (part of) those costs through innovation and development.

The overall plant complexity is correlated to the capital intensity factor– M$ of annual product value generated per 1M$ invested in the plant. The capital intensity factor along with the generated annual product value is used to estimate the basic CAPEX, following the process economics described by F. Dautzenburg.[69] The basic CAPEX combined with the pressure and material factors (e.g., operating conditions requiring specialized materials), working capital, and start-up costs associated with a first-of-a-kind technology commissioning (estimated to be ~1 to 4 times the monthly operating costs) determine the required investment.[70] The annual OPEX consists of the annual feedstock cost, and estimates for labour and overheads (5.7% from basic CAPEX); interest, taxes, insurance (8% from basic CAPEX); utilities and energy (7.5% from total OPEX); maintenance costs; and depreciation (10 year payback period).[71]

The main conclusion that was drawn from the TEA is that the electrochemical production of oxidized starch is currently economically unviable. The main costs are associated with the basic CAPEX, resulting from the high complexity number of the overall system. More specifically, the high complexity of the overall system can be attributed to the large capacity of recycling streams resulting from operating at dilute concentration and the complexity of the electrochemical

reactor. However, the sensitivity analysis identified approaches for future research to improve the economics of the system. Firstly, reducing the size/capacity of recycling streams would greatly reduce the investment costs. The current concept assumes a feed stream of up to 20 wt.% starch for the electrochemical reactor. Increasing this concentration of the feed stream would reduce recycling flows. However, high concentrations might lead to increased viscosities, resulting in high ohmic drops. Secondly, it is advised to retain a simple configuration of the electrochemical reactor by reducing the number of stacks. This can be achieved by operating at high current densities > 100mA.cm^{-2} and increasing the active surface area of 3D electrodes or using an electrochemical mediator. For instance, the use of a mediator molecule can allow for decoupling the electrochemical reaction – activation/regeneration of catalytic amounts of mediator, from the target chemical reaction – mediated oxidation of starch. Consequently, the electrochemical reactor can be made smaller, with a minimum number of cell pairs and inexpensive electrode materials like carbon, resulting in lower CAPEX. A potential option for this would be to combine a homogenous binuclear manganese catalyst with H_2O_2 as they enable the production of oxidized starch with similar properties to that of hypochlorite oxidized starch.[72] The H_2O_2 can then be produced in-situ electrochemically with an oxidized carbon support.[73] Additionally, decoupling the chemical and electrochemical reactions can allow for larger plant capacities at which the annual product value generated can exceed the annual OPEX and generate profit. However, it must be noted that the cost of the mediator and mediator recovery in a separate DSP operation is expected to partially reduce the benefits arising from its use. Thirdly, pairing starch oxidation at the anode with a reduction reaction at the cathode for the synthesis of a chemical with a higher value than hydrogen and preferably, at least an equivalent value of the oxidised starch product. Finally, reduce the price of the feedstock.

6.3. Summary and recommendations

The electrocatalytic oxidation of biomass-based molecules can contribute to the sustainable synthesis of a large variety of platform and speciality chemicals.[1,74] We have shown that the electrocatalytic oxidation of glucose can be used to produce NREL-listed platform chemicals, such as gluconic acid and glucaric acid, while the electrocatalytic oxidation of starch can be used to produce speciality chemicals, such as anionic starch. Despite that to date, glucose oxidation to gluconic acid and glucaric acid is carried out by fermentation and nitric acid, respectively, while starch oxidation is carried out by hypochlorite. However, these approaches result in the formation of large amounts of salt waste and are mild selectivities.[13,25,33] Moreover, nitric acid and hypochlorite are harsh and toxic redox agents. By contrast, the electrocatalytic oxidation of glucose does not require harsh redox agents and can be performed, as we have shown in **Chapter 3**, under acidic conditions, avoiding the formation of salt waste. Furthermore, in **Chapter 4** we have shown by quantifying all (intermediate) glucose oxidation products that the selectivity for the electrocatalytic oxidation of glucose can easily be controlled by changing the applied

potential, thereby reducing the formation of side products and complex downstream process procedures.[1]

However, to date, no industrial application uses electrocatalysis to synthesize gluconic acid, glucaric acid, or anionic starch. Nonetheless, the interest in electrocatalytic oxidation reactions to convert molecules derived from biofeedstocks has significantly grown in the past decade,[75] since these reactions at the anode generate value-added products and can be coupled to hydrogen evolution reactions at the cathode to reduce energy consumption.[76,77] Here below 4 recommendations for further research are presented that could help achieve electrooxidation of glucose and starch on an industrial scale:

1) For the electrocatalytic oxidation of glucose, it is strongly recommended to **quantify all glucose oxidation products** in future research, as it will give a better insight into how the catalyst properties and reaction conditions affect the reaction pathway. Several catalysts, such as Au, Pt, PtSb, PtBi, and MnO_2, should be considered as they have shown to be highly selective and/or active towards specific products. These insights on the reaction pathway can be used to improve the catalyst selectivity towards desired products, thereby reducing the loss of value-added products and downstream processing costs.

2) **Support modification of carbon-supported catalysts**, such as support oxygen groups and nitrogen or sulfur doping, can be used to improve the catalyst performance for the electrocatalytic oxidation of glucose and starch. Further research on support oxygen groups can be devoted to their effect on the catalyst selectivity and stability by using online HPLC, ICP-OES, and *in situ* STEM. In addition, to improve the electrocatalyst performance even further the effect of nitrogen or sulfur doping could be considered.

3) **The design and evaluation of the physical and chemical properties of macroporous electrocatalysts** for the electrocatalytic oxidation of large biomass-based molecules like starch is recommended. Research on these macroporous catalysts can aid in establishing relations between catalyst pore size and reactant size to reduce internal mass transport limitations and thereby improve the overall reaction rate. Moreover, it is recommended to study these macroporous electrocatalysts in flow-through electrochemical cells to increase the turbulence for highly viscous concentrated starch solutions.

4) **The effect of temperature on the performance of electrocatalysts** should be researched more thoroughly since it also plays a crucial role in industrial electrochemical reactors. Currently, nearly all studies on the electrocatalytic oxidation of sugar alcohols and (poly)saccharides are conducted at room temperature, while an increase in temperature can have several positive effects. It can improve reaction rate

kinetics and reduce the viscosity of concentrated organic solutions, thereby reducing mass transport limitations and the resistance of the electrolyte.

References

1. van der Ham, M. P. J. M., van Keulen, E., Koper, M. T. M., Asadi Tashvigh, A. & Bitter, J. H. Steering the Selectivity of Electrocatalytic Glucose Oxidation by the Pt Oxidation State. *Angewandte Chemie International Edition* **62**, 33 (2023).

2. Li, L., Shen, F., Smith, R. L. & Qi, X. Quantitative chemocatalytic production of lactic acid from glucose under anaerobic conditions at room temperature. *Green Chemistry* **19**, 76–81 (2017).

3. Dai, C. *et al.* Electrochemical production of lactic acid from glycerol oxidation catalyzed by AuPt nanoparticles. *J Catal* **356**, 14–21 (2017).

4. Huang, X., Zou, Y. & Jiang, J. Electrochemical Oxidation of Glycerol to Dihydroxyacetone in Borate Buffer: Enhancing Activity and Selectivity by Borate-Polyol Coordination Chemistry. *ACS Sustain Chem Eng* **9**, 14470–14479 (2021).

5. Kwon, Y., Schouten, K. J. P. & Koper, M. T. M. Mechanism of the Catalytic Oxidation of Glycerol on Polycrystalline Gold and Platinum Electrodes. *ChemCatChem* **3**, 1176–1185 (2011).

6. Kwon, Y., Hersbach, T. J. P. & Koper, M. T. M. Electro-Oxidation of Glycerol on Platinum Modified by Adatoms: Activity and Selectivity Effects. *Top Catal* **57**, 1272–1276 (2014).

7. Toebes, M. L., Prinsloo, F. F., Bitter, J. H., Van Dillen, A. J. & De Jong, K. P. Influence of oxygen-containing surface groups on the activity and selectivity of carbon nanofiber-supported ruthenium catalysts in the hydrogenation of cinnamaldehyde. *J Catal* **214**, 78–87 (2003).

8. Gerber, I. C. & Serp, P. A Theory/Experience Description of Support Effects in Carbon-Supported Catalysts. *Chem Rev* **120**, 1250–1349 (2020).

9. Kokoh, K. B. *et al.* Selective oxidation of D-gluconic acid on platinum and lead adatoms modified platinum electrodes in alkaline medium. *Electrochim Acta* **38**, 1359–1365 (1993).

10. Todd Werpy & Gene Petersen. *Top value added chemicals from biomass: volume I--results of screening for potential candidates from sugars and synthesis gas*. http://www.osti.gov/bridge (2004).

11. Imai, H. *et al.* In situ and real-time monitoring of oxide growth in a few monolayers at surfaces of platinum nanoparticles in aqueous media. *J Am Chem Soc* **131**, 6293–6300 (2009).

12. Vanier, N. L. *et al.* Physicochemical, crystallinity, pasting and morphological properties of bean starch oxidised by different concentrations of sodium hypochlorite. *Food Chem* **131**, 1255–1262 (2012).

13. Broekman, J. O. P. *et al.* Dibasic Magnesium Hypochlorite as an Oxidant to Tune Pasting Properties of Potato Starch in One Step. *ChemEngineering* **7**, 24 (2023).

14. Hoogstad, T. M. *et al.* Environmental Impact Evaluation for Heterogeneously Catalysed Starch Oxidation. *ChemistryOpen* **11**, (2022).

15. Anil, A. *et al.* Effect of pore mesostructure on the electrooxidation of glycerol on Pt mesoporous catalysts. *J Mater Chem A Mater* **11**, 16570–16577 (2023).

16. Chen, A. Y. *et al.* Effects of pore size and residual Ag on electrocatalytic properties of nanoporous gold films prepared by pulse electrochemical dealloying. *Electrochim Acta* **153**, 552–558 (2015).

17. Gluconic Acid Market Size by 2030 - MarketWatch. https://www.marketwatch.com/press-release/gluconic-acid-market-size-by-2030-2023-04-11.

18. Gluconic acid Market Share - Industry Growth Forecast Report 2024. https://www.gminsights.com/industry-analysis/gluconic-acid-market.

19. 2023-2029 'Glucaric Acid Market' Highlights, With 122+ Pages By IRB - MarketWatch. https://www.marketwatch.com/press-release/2023-2029-glucaric-acid-market-highlights-with-122-pages-by-irb-2023-04-22.

20. Glucaric Acid Market Share Industry Growth Forecast Report 2018-2024. https://www.gminsights.com/industry-analysis/glucaric-acid-market.

21. Deng, W. *et al.* Efficient Catalysts for the Green Synthesis of Adipic Acid from Biomass. *Angewandte Chemie - International Edition* **60**, 4712–4719 (2021).

22. Luo, Z., Yu, S., Zeng, W. & Zhou, J. Comparative analysis of the chemical and biochemical synthesis of keto acids. *Biotechnol Adv* **47**, 107706 (2021).

23. Amaniampong, P. N. *et al.* Selective and Catalyst-free Oxidation of D-Glucose to D-Glucuronic acid induced by High-Frequency Ultrasound. *Sci Rep* **7**, 40650 (2017).

24. Sandu, M. P., Sidelnikov, V. S., Geraskin, A. A., Chernyavskii, A. V. & Kurzina, I. A. Influence of the method of preparation of the Pd-Bi/Al2O3 catalyst on catalytic properties in the reaction of liquid-phase oxidation of glucose into gluconic acid. *Catalysts* **10**, 3 (2020).

25. Liu, W. J. *et al.* Efficient electrochemical production of glucaric acid and H2 via glucose electrolysis. *Nat Commun* **11**, 265 (2020).

26. Zeng, W. *et al.* Efficient biosynthesis of 2-keto-D-gluconic acid by fed-batch culture of metabolically engineered Gluconobacter japonicus. *Synth Syst Biotechnol* **4**, 134–141 (2019).

27. Yuan, J., Wu, M., Lin, J. & Yang, L. Enhancement of 5-keto-d-gluconate production by a recombinant Gluconobacter oxydans using a dissolved oxygen control strategy. *J Biosci Bioeng* **122**, 10–16 (2016).

28. Glucuronic Acid Market Research | 2023-2030. *https://www.marketwatch.com/press-release/glucuronic-acid-market-research-2023-2030-2023-05-09*.

29. Ascorbic Acid Market Insights | 2023-2030. *https://www.marketwatch.com/press-release/ascorbic-acid-market-insights-2023-2030-2023-06-14*.

30. Vitamin C Price Trend and Forecast. *https://www.chemanalyst.com/Pricing-data/vitamin-c-1258*.

31. Tartaric Acid Market Insights | 2030. *https://www.marketwatch.com/press-release/tartaric-acid-market-insights-2030-2023-06-19*.

32. Tartaric Acid Price Trend and Forecast. *https://www.chemanalyst.com/Pricing-data/tartaric-acid-1126#:~:text=The%20price%20of%20tartaric%20acid%20for%20CFR%20Hamburg%20in%20September,the%20third%20quarter%20of%202022.*

33. Pal, P., Kumar, R. & Banerjee, S. Manufacture of gluconic acid: A review towards process intensification for green production. *Chemical Engineering and Processing: Process Intensification* **104**, 160–171 (2016).

34. Schlegel, N., Wiberg, G. K. H. & Arenz, M. On the electrooxidation of glucose on gold: Towards an electrochemical glucaric acid production as value-added chemical. *Electrochim Acta* **410**, 140023 (2022).

35. Arenz, M., Schlegel, N., Bagger, A. & Rossmeisl, J. Elucidating the reaction pathway of glucose electrooxidation to its valuable products: the Influence of mass transport and electrode potential on the product distribution. (2023) doi:10.26434/CHEMRXIV-2023-5ML1L.

36. Moggia, G., Kenis, T., Daems, N. & Breugelmans, T. Electrochemical Oxidation of d-Glucose in Alkaline Medium: Impact of Oxidation Potential and Chemical Side Reactions on the Selectivity to d-Gluconic and d-Glucaric Acid. *ChemElectroChem* **7**, 86–95 (2020).

37. Kwon, Y., Schouten, K. J. P. & Koper, M. T. M. Mechanism of the Catalytic Oxidation of Glycerol on Polycrystalline Gold and Platinum Electrodes. *ChemCatChem* **3**, 1176–1185 (2011).

38. Kwon, Y. & Koper, M. T. M. M. Combining voltammetry with HPLC: Application to electro-oxidation of glycerol. *Anal Chem* **82**, 5420–5424 (2010).

39. Moggia, G., Schalck, J., Daems, N. & Breugelmans, T. Two-steps synthesis of D-glucaric acid via D-gluconic acid by electrocatalytic oxidation of D-glucose on gold electrode: Influence of operational parameters. *Electrochim Acta* **374**, 137852 (2021).

40. Hsiao, M. W., Adzic, R. R. & Yeager, E. B. The effects of adsorbed anions on the oxidation of D-glucose on gold single crystal electrodes. *Electrochim Acta* **37**, 357–363 (1992).

41. Kokoh, K. B., Léger, J. M., Beden, B. & Lamy, C. 'On line' chromatographic analysis of the products resulting from the electrocatalytic oxidation of d-glucose on Pt, Au and adatoms modified Pt electrodes-Part I. Acid and neutral media. *Electrochim Acta* **37**, 1333–1342 (1992).

42. Kwon, Y., Lai, S. C. S., Rodriguez, P. & Koper, M. T. M. Electrocatalytic oxidation of alcohols on gold in alkaline media: Base or gold catalysis? *J Am Chem Soc* **133**, 6914–6917 (2011).

43.   Parpot, P., Santos, P. R. B. & Bettencourt, A. P. Electro-oxidation of d-mannose on platinum, gold and nickel electrodes in aqueous medium. *Journal of Electroanalytical Chemistry* **610**, 154–162 (2007).

44.   Noël, T., Cao, Y. & Laudadio, G. The Fundamentals behind the Use of Flow Reactors in Electrochemistry. *Acc Chem Res* **52**, 2858–2869 (2019).

45.   Valter, M. *et al.* Electrooxidation of Glycerol on Gold in Acidic Medium: A Combined Experimental and DFT Study. *Journal of Physical Chemistry C* **122**, 10489–10494 (2018).

46.   Del Colle, V. *et al.* The effect of Pt surface orientation on the oscillatory electro-oxidation of glycerol. *Journal of Electroanalytical Chemistry* **926**, 116934 (2022).

47.   Kwon, Y., De Jong, E., Van Der Waal, J. K. & Koper, M. T. M. Selective electrocatalytic oxidation of sorbitol to fructose and sorbose. *ChemSusChem* **8**, 970–973 (2015).

48.   Kwon, Y., Birdja, Y., Spanos, I., Rodriguez, P. & Koper, M. T. M. Highly selective electro-oxidation of glycerol to dihydroxyacetone on platinum in the presence of bismuth. *ACS Catal* **2**, 759–764 (2012).

49.   Lee, S. *et al.* Highly selective transformation of glycerol to dihydroxyacetone without using oxidants by a PtSb/C-catalyzed electrooxidation process. *Green Chemistry* **18**, 2877–2887 (2016).

50.   Guschakowski, M. & Schröder, U. Direct and Indirect Electrooxidation of Glycerol to Value-Added Products. *ChemSusChem* **14**, 5216–5225 (2021).

51.   Kokoh, K. B. *et al.* Selective oxidation of D-gluconic acid on platinum and lead adatoms modified platinum electrodes in alkaline medium. *Electrochim Acta* **38**, 1359–1365 (1993).

52.   Qi, J. *et al.* Electrocatalytic selective oxidation of glycerol to tartronate on Au/C anode catalysts in anion exchange membrane fuel cells with electricity cogeneration. *Appl Catal B* **154**, 360–368 (2014).

53.   Xin, L., Zhang, Z., Wang, Z. & Li, W. Simultaneous Generation of Mesoxalic Acid and Electricity from Glycerol on a Gold Anode Catalyst in Anion-Exchange Membrane Fuel Cells. *ChemCatChem* **4**, 1105–1114 (2012).

54.   Ahmad, M. S. *et al.* Electro-oxidation of waste glycerol to tartronic acid over Pt/CNT nanocatalyst: study of effect of reaction time on product distribution. *Energy Sources, Part A* 1–17 (2019).

55.   Ahmad, M. S., Cheng, C. K., Ong, H. R., Abdullah, H. & Khan, M. R. Electro-oxidation of renewable glycerol to value added chemicals over phosphorous-doped Pt/MCNTs nanoparticles. *Materials Science and Engineering* **702**, 012025 (2019).

56.   Zhao, L., Kuang, X., Sun, X., Zhang, Y. & Wei, Q. Synchronously Achieving Highly Efficient Hydrogen Evolution and High-Yield Synthesis of Glucaric Acid by MOF Nanorod Arrays. *J Electrochem Soc* **166**, H534–H540 (2019).

57.   Bin, D. *et al.* Controllable oxidation of glucose to gluconic acid and glucaric acid using an electrocatalytic reactor. *Electrochim Acta* **130**, 170–178 (2014).

58.   Li, J. *et al.* Efficiently Coupled Glucose Oxidation for High-value D-glucaric Acid with Ultradurable Hydrogen via Mn (III) in Acidic Solution. *Nano Res* **16**, 10748–10755 (2023).

59.   Li, J. *et al.* Tuning the Product Selectivity toward the High Yield of Glyceric Acid in Pt-CeO2/CNT Electrocatalyzed Oxidation of Glycerol. *ChemCatChem* **14**, e202200509 (2022).

60.   Liu, X. & Yang, C. Electrocatalytic selective oxidation of glycerol to glyceric acid over efficient Pt/CNTs-CeO2 catalysts. *Mater Lett* **324**, 132658 (2022).

61.   Liu, W. J. *et al.* Efficient electrochemical production of glucaric acid and H2 via glucose electrolysis. *Nat Commun* **11**, 265 (2020).

62.   Führer, A. M. *et al.* The synergetic effect of support-oxygen groups and Pt particle size in the oxidation of α-D-glucose: a proximity effect in adsorption. *ChemCatChem* **14**, 19 (2022).

63.   Kwon, Y., Schouten, K. J. P. & Koper, M. T. M. Mechanism of the Catalytic Oxidation of Glycerol on Polycrystalline Gold and Platinum Electrodes. *ChemCatChem* **3**, 1176–1185 (2011).

64.   Kim, J. H., Cheon, J. Y., Shin, T. J., Park, J. Y. & Joo, S. H. Effect of surface oxygen functionalization of carbon support on the activity and durability of Pt/C catalysts for the oxygen reduction reaction. *Carbon* **101**, 449–457 (2016).

65.   Sandbeck, D. J. S. *et al.* Particle Size Effect on Platinum Dissolution: Practical Considerations for Fuel Cells. *ACS Appl Mater Interfaces* **12**, 25718–25727 (2020).

66.   Beermann, V. *et al.* Real-time imaging of activation and degradation of carbon supported octahedral Pt–Ni alloy fuel cell catalysts at the nanoscale using in situ electrochemical liquid cell STEM. *Energy Environ Sci* **12**, 2476–2485 (2019).

67.   Ning, X. *et al.* Glycerol and formic acid electro-oxidation over Pt on S-doped carbon nanotubes: Effect of carbon support and synthesis method on the metal-support interaction. *Electrochim Acta* **319**, 129–137 (2019).

68.   Li, J. *et al.* High productivity of tartronate from electrocatalytic oxidation of high concentration glycerol through facilitating the intermediate conversion. *Appl Catal B* **317**, 121784 (2022).

69.   Dautzenberg, F. *The Catalyst Review*. vol. 27 (2014).

70.   Towler, G. & Sinnott, R. Capital Cost Estimating. in *Chemical Engineering Design* vol. 2 307–354 (2013).

71.   Towler, G. & Sinnott, R. Estimating Revenues and Production Costs. in *Chemicel Engineering Design* 355–387 (2013).

72.   Broekman, J. O. P. *et al.* Benign catalytic oxidation of potato starch using a homogeneous binuclear manganese catalyst and hydrogen peroxide. *Catal Sci Technol* **13**, 1233–1243 (2023).

73.   Perry, S. C. *et al.* Electrochemical synthesis of hydrogen peroxide from water and oxygen. *Nature Reviews Chemistry* vol. 3 442–458 Preprint at https://doi.org/10.1038/s41570-019-0110-6 (2019).

74.   Alaba, P. A. *et al.* A review of recent progress on electrocatalysts toward efficient glycerol electrooxidation. *Reviews in Chemical Engineering* **37**, 779–811 (2020).

75.   Li, T. & Harrington, D. A. An Overview of Glycerol Electrooxidation Mechanisms on Pt, Pd and Au. *ChemSusChem* **14**, 1472–1495 (2021).

76.   Li, Y., Wei, X., Chen, L. & Shi, J. Electrocatalytic Hydrogen Production Trilogy. *Angewandte Chemie International Edition* **60**, 19550–19571 (2021).

77.   Du, P., Zhang, J., Liu, Y. & Huang, M. Hydrogen generation from catalytic glucose oxidation by Fe-based electrocatalysts. *Electrochem commun* **83**, 11–15 (2017).
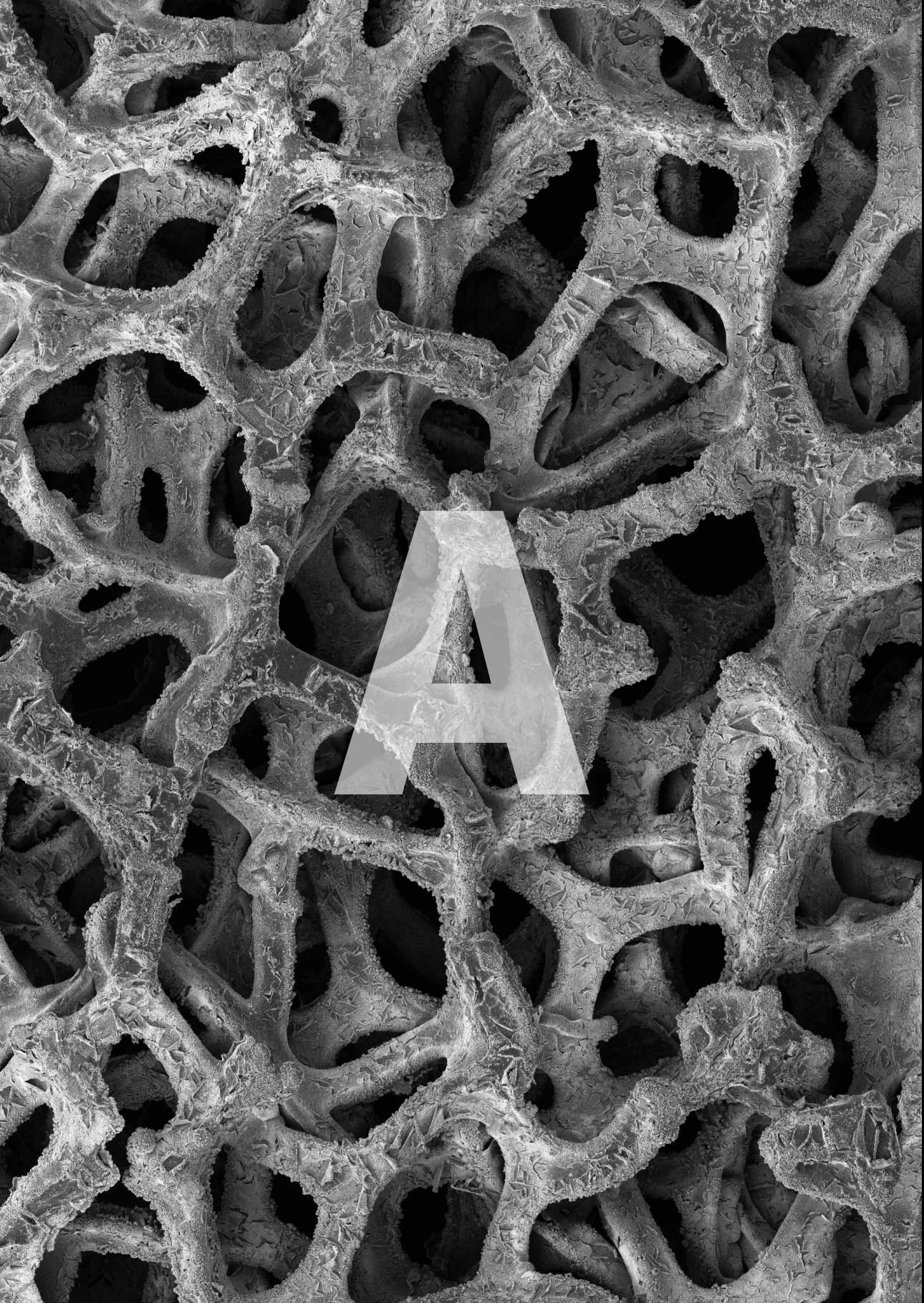
APPENDICES

Summary

Electrocatalysts that are driven by renewable electricity (e.g. wind and solar) can convert biofeedstocks (e.g. sugar alcohols, saccharides, and polysaccharides) for the production of sustainable chemicals that can replace unsustainable fossil-based chemicals. To apply these electrocatalysts in the chemical industry for the conversion of biofeedstocks, such as glucose and starch, improvements in their performance (i.e. activity, selectivity, and stability) are required first. This involves a better understanding of the property performance relation of electrocatalysts, as well as the design of porous electrocatalysts that are accessible for large biomass-based molecules to make effective use of the active phase of the catalyst. Therefore, this dissertation provides new insights into the design of different electrocatalysts for the oxidation of glucose and starch and gives a more profound understanding of the relation between catalyst properties and performance.

Chapter 1 provides a general introduction of the electrocatalytic oxidation of biofeedstocks to platform and specialty chemicals. First, the advantages of the electrocatalytic conversion of biofeedstocks are discussed. Thereafter, research gaps in the field of electrocatalytic conversion of biofeedstocks are presented, using a bottom-up approach by going from simple to more complicated molecules (i.e. from sugar alcohols to saccharides and finally to polysaccharides). This bottom-up approach is applied throughout this dissertation. The research gaps that were found are:

1) An evaluation that considers the translation of common trends between the electrocatalytic oxidation of sugar alcohols (e.g. glycerol) and related saccharides (e.g. glucose) in which the competition between electrochemical and non-electrochemical is considered, thereby giving valuable insights into catalyst design;
2) The effect of support oxygen groups on the activity of carbon-supported Pt catalysts for the electrocatalytic oxidation of glucose;
3) The role of Pt oxidation state on the catalyst activity and selectivity for the electrocatalytic oxidation of glucose;
4) The role of low molecular weight polysaccharides and monosaccharides on the electrocatalytic oxidation of glucose on Pt;
5) The design of a macroporous electrode, consisting of Pt supported on Ni foam, for the electrocatalytic oxidation of large starch molecules.

The most commonly studied biofeedstock in the field of electrocatalysis that resembles saccharides are sugar alcohols. These molecules have relatively similar chemical structures, since both molecules have primary and secondary alcohol groups, while saccharides also have an

aldehyde/anomeric carbon group. Therefore, we critically review in **Chapter 2** the electrocatalytic oxidation of sugar alcohols and related saccharides and evaluate whether common trends can be drawn between these molecules. For this purpose, we distinguish between reaction conditions (pH, type of electrolyte, temperature, and reactant concentration) and catalyst properties (type of metal, metal facets, metal oxidation state, and bimetallics) and evaluate how they affect the catalyst selectivity and activity. This approach enabled us to discuss the competition between electrocatalytic and non-electroataytic reactions.

We found that several common trends exist between the electrocatalytic oxidation of sugar alcohols and saccharides and identified several considerations for future research. Firstly, Au is likely only able to catalyze the oxidation of the primary alcohol group, while Pt is also able to catalyze the oxidation of the secondary alcohol group. Secondly, post-transition metals effectively change the selectivity of Pt electrocatalyst towards the secondary alcohol group, irrespective of the type of reactant. Thirdly, to date, the formation of dicarboxylic acids was only observed over MnO_2 under acidic conditions (pH = 1), while the formation of dicarboxylates was feasible over a wide range of electrocatalysts (e.g., based on Pt, Au, and $NiFeO_x$) under highly alkaline conditions (pH ≥ 13.7). Fourthly, the rate-limiting step for the electrocatalytic oxidation of sugar alcohols on Au electrodes is base-catalyzed. It is worthwhile to evaluate whether this also holds for the electrocatalytic oxidation of saccharides since that could be used to improve the catalyst activity and selectivity. Fifthly, studies on the electrocatalytic oxidation of saccharides (e.g. glucose) rarely report the formation of key intermediates such as glucose dialdehyde, 2-keto gluconic acid, guluronic acid, etc.), which are crucial to gain insight in the property performance relation of electrocatalysts. Finally and most importantly, we found that the competition between electrochemical and non-electrochemical reactions, induced by the type of electrolyte and pH, is often a neglected aspect that should be taken into account and optimized as it enables the efficient electrocatalytic conversion of sugar alcohols and related saccharides into valuable products.

In catalysis, it is well known that support oxygen groups on carbon-supported metal catalysts affect the performance of thermocatalysts, while this is not known in the field of electrocatalysis. Therefore, we investigate In **Chapter 3** the effect of support oxygen groups on Pt supported on carbon nanofibers (Pt/CNF) on the electrocatalytic oxidation of glucose at pH = 1. For this, four Pt/CNF catalysts were synthesized with different contents of support oxygen groups and different Pt particle sizes. The support oxygen groups and the Pt particle size were not found to affect the Pt electronic properties (*in-situ* XANES and *ex-situ* XPS), Pt surface structure (CO-stripping), and the ratio between adsorbates on the Pt surface (*in-situ* XANES). Nonetheless, a linear relation was found between the content of support oxygen groups and the catalytic activity of Pt. More specifically, after the electrochemical oxidation of Pt/CNF, oxygen groups were introduced in the annulus (i.e. perimeter) of the Pt particle, resulting in a series of Pt/CNF catalysts with different

Pt particle sizes and saturated contents of support oxygen groups in the annulus of the Pt particle. It was found that smaller Pt particles exhibited a higher catalytic activity, arguably due to the improved adsorption of reactants in the oxygen-rich annulus of smaller Pt particles.

Motivated by the lack of an analytical method to quantify all (intermediate) products in the glucose oxidation pathway, we developed a new analytical approach that combines high-pressure anion exchange chromatography with high-pressure liquid chromatography, thereby enabling the separation and quantification of all (intermediate) products formed during the electrocatalytic oxidation of glucose. With this tool in hand, we evaluate in **Chapter 4** the role of the Pt oxidation state on the electrocatalytic oxidation of glucose at neutral conditions. For this study, the surface oxidation state of Pt was found to have a significant influence on the type of oxidation reaction, i.e. dehydrogenative oxidation of the primary or secondary alcohol group or oxygen transfer to the aldehyde group. Pt^0 (at E = 0.64 V $vs.$ RHE) was found to promote dehydrogenative oxidation reactions of the primary alcohol group, thereby promoting the formation of glucose dialdehyde from glucose. By contrast, PtO_x (at E = 1.2 V $vs.$ RHE) is equally active in catalyzing dehydrogenative oxidation/oxygen transfer reactions, thereby promoting the conversion of the anomeric carbon of glucose and thus the formation of gluconate. Despite the high selectivity of PtO_x towards gluconate it also promotes the dehydrogenative oxidation of secondary alcohol groups of gluconate, resulting in the formation of complex reaction mixtures that contain 2-keto gluconate and 5-keto gluconate.

The insights from Chapter 4 motivated us to study the electrocatalytic oxidation of starch (e.g. a polymer of glucose) for the synthesis of anionic starch in **Chapter 5**. Electrocatalytic starch oxidation is a promising replacement for the current less sustainable industrial production of anionic starch through hypochlorite oxidation. Here we evaluate: 1) the role of low molecular weight polysaccharides and monosaccharides (LMWPM) present in industrially derived starch on the electrocatalytic oxidation of starch and 2) the potential use of highly accessible macroporous electrodes, consisting of Pt supported on Ni foam (Pt/Nif), for the electrocatalytic oxidation of the large starch molecules. To evaluate the role of LMWPM on starch oxidation, we prepared two samples: one with industrially derived starch as-received (i.e. containing high contents of LMWPM) and one with purified starch (i.e. containing minor contents of LMWPM). We showed that Pt^0 is more active toward the electrocatalytic oxidation of purified starch than PtO_x. However, Pt^0 favors the electrocatalytic oxidation of LMWPM over starch, which was confirmed by product analysis as starch did not hydrolyze nor did it show measurable changes in functional groups after electrocatalysis. For the synthesis of Pt/Nif, we designed an electrodeposition bath which ensures the electrodeposition of H_2PtCl_6 on both sides of the Ni foam. The Pt/Nif was found to have a high electrochemical surface area of Pt, being comparable to Pt black. It also demonstrated a high resistance to CO poisoning, which is crucial for organic synthesis.

Additionally, it was found to be active towards the electrocatalytic oxidation of industrially derived starch.

Chapter 6 provides a general discussion of the key accomplishments presented in this dissertation. Special attention is given to future research, including 1) the quantification of all (intermediate) products in the glucose oxidation pathway to gain better insight into the catalyst property performance relationship, 2) the modification of the support of carbon-supported metal electrocatalysts to improve the electrocatalyst performance for glucose oxidation, 3) the design and evaluation of the physical and chemical properties of macroporous electrocatalysts for the electrocatalytic conversion of large biomass-based molecules like starch, and 4) the effect of temperature on the electrocatalytic conversion of biofeedstocks.

Samenvatting

Elektrokatalysatoren die worden aangedreven door hernieuwbare elektriciteit (bijv. wind en zonne-energie) kunnen biogrondstoffen (bijv. suikeralcoholen, suikers en lange suikerketens) omzetten voor de productie van duurzame chemicaliën, waarmee niet duurzame fossiel gebaseerde chemicaliën vervangen kunnen worden. Voordat deze elektrokatalysatoren toegepast kunnen worden in de chemische industrie voor de omzetting van biogrondstoffen, zoals glucose en zetmeel, zijn verbeteringen in hun prestaties (d.w.z. activiteit, selectiviteit en stabiliteit) eerst vereist. Dit vergt een beter inzicht in de relatie tussen de eigenschappen en de prestaties van elektrokatalysatoren, evenals het ontwerp van poreuze elektrokatalysatoren die toegankelijk zijn voor grote, op biogrondstoffen gebaseerde moleculen om effectief gebruik te maken van de actieve fase van de katalysator. Daarom biedt dit proefschrift nieuwe inzichten in het ontwerp van verschillende elektrokatalysatoren voor de oxidatie van glucose en zetmeel en geeft het een diepgaander begrip in de relatie tussen de eigenschappen en de prestaties van de elektrokatalysator.

Hoofdstuk 1 geeft een algemene inleiding voor de elektrokatalytische oxidatie van biogrondstoffen naar specialistische chemicaliën en basischemicaliën (d.w.z. met een grote marktvraag). Eerst worden de voordelen van de elektrokatalytische omzetting van biogrondstoffen besproken. Daarna worden enkele cruciale maar nog onbeantwoorde onderzoeksvragen op het gebied van elektrokatalytische omzetting van biogrondstoffen gepresenteerd, waarbij de volgorde van onderzoeksvragen zich stapsgewijs richt op meer complexe moleculen (d.w.z. van suikeralcoholen naar suikers en uiteindelijk naar lange suikerketens). Dit proefschrift volgt deze aanpak van toenemende complexiteit in moleculen. De onderzoeksvragen die waren opgesteld zijn:

1) Een evaluatie die overeenkomstige trends bestudeert tussen het elektrokatalytisch oxideren van suikeralcoholen (bijv. glycerol) en gerelateerde suikers (bijv. glucose), waarbij de concurrentie tussen elektrokatalytische en niet-elektrokatalytische processen wordt meegenomen, en daarmee waardevolle inzichten geeft in het ontwerp van elektrokatalysatoren;

2) De relatie tussen zuurstofgroepen op koolstof van koolstofdragende metaalkatalysatoren en de activiteit voor het elektrokatalytisch oxideren van glucose.;

3) Het effect van de oxidatietoestand van Pt op de katalysatoractiviteit en selectiviteit voor het elektrokatalytisch oxideren van glucose;

4) Hoe de aanwezigheid van kleine suikerketens en suikers in industrieel verkregen zetmeel (d.w.z. lange suikerketens) het elektrokatalytisch oxideren van zetmeel beïnvloedt;

5) Het ontwerp van een macroporeuze elektrode, bestaande uit platina gedragen for nikkel-schuim, voor het elektrokatalytisch oxideren van de grote zetmeelmoleculen.

Suikeralcoholen zijn de meest bestudeerde organische stoffen binnen elektrokatalyse die vergelijkbaar zijn met suikers. Deze moleculen hebben relatief vergelijkbare chemische structuren, aangezien beide moleculen primaire en secundaire alcoholgroepen hebben, terwijl suikers ook een aldehyde/anomere koolstofgroep hebben. Daarom analyseren wij in **Hoofdstuk 2** grondig de literatuur over het elektrokatalytisch oxideren van suikeralcoholen en gerelateerde suikers, om te onderzoeken of er overeenkomstige trends bestaan tussen deze type moleculen. Deze benadering maakt het mogelijk om de competitie tussen elektrokatalytische en niet-elektrokatalytische reacties te bespreken.

Wij hebben vastgesteld dat er verschillende overeenkomstige trends bestaan tussen het elektrokatalyisch oxideren van suikeralcoholen en suikers, en wij hebben enkele overwegingen geïdentificeerd voor toekomstig onderzoek. Ten eerste lijkt goud enkel in staat te zijn om de primaire alcoholgroepen te katalyseren, terwijl platina ook in staat is om de secundaire alcoholgroepen te katalyseren. Ten tweede kunnen P-blokmetalen (metalen uit groep 13 t/m 17 van het periodiek systeem) de selectiviteit van platina effectief veranderen naar secundaire alcoholgroepen, ongeacht het type reactant. Ten derde is tot nu toe de vorming van dicarbonzuren alleen waargenomen over MnO_2 onder zure omstandigheden (pH = 1), terwijl de vorming van dicarbonzouten haalbaar is over verschillende elektrokatalysatoren (bijvoorbeeld op basis van platina, goud en nikkelijzeroxide) onder sterk alkalische omstandigheden (pH ≥ 13.7). Ten vierde is de traagste reactiestap in de reactieroute voor het elektrokatalytisch oxideren van suikeralcoholen over goud een base-gekatalyseerde reactiestap, in plaats van een reactiestap gekatalyseerd door goud zelf. Het is de moeite waard om te evalueren of dit ook geldt voor het elektrokatalytisch oxideren van suikers, aangezien dit kan worden gebruikt om de activiteit en selectiviteit van de katalysator te verbeteren. Ten vijfde, tonen onderzoeken naar het elektrokatalytisch oxideren van suikers (bijvoorbeeld glucose) zelden de vorming van essentiële tussenproducten zoals glucosedialdehyde, 2-keto gluconzuur, gulluronzuur, enzovoort, terwijl deze van cruciaal belang zijn om verbanden te leggen tussen de eigenschappen en de prestaties van katalysatoren. Als laatste en één van de belangrijkste punten hebben wij vastgesteld dat de competitie tussen elektrokatalytische en niet-elektrokatalytische reacties, die wordt veroorzaakt door het type elektrolyt en pH, vaak een verwaarloosd aspect is. Het is echter van cruciaal belang de balans tussen deze reacties te optimaliseren, omdat dit de efficiëntste manier oplevert voor het omzetten van suikeralcoholen en gerelateerde suikers naar waardevolle chemicaliën.

Het is algemeen bekend in de katalysewereld dat zuurstofgroepen op de koolstof van koolstofdragende metaalkatalysatoren een invloed hebben op de prestaties van de thermokatalysatoren, terwijl dit niet bekend is voor elektrokatalysatoren. Daarom hebben wij in **Hoofdstuk 3** onderzocht hoe de zuurstofgroepen op de platina dragende koolstofnanovezels

(Pt/KNV) katalysator de activiteit van de katalysator beïnvloedt bij het elektrokatalytisch oxideren van glucose bij pH = 1. Voor dit onderzoek hebben wij vier Pt/KNV katalysatoren gesynthetiseerd met verschillend hoeveelheden zuurstofgroepen op de koolstofdrager en verschillende Pt-deeltjesgroottes. De zuurstofgroepen op de kooldrager en de Pt-deeltjesgrootte bleken geen invloed te hebben op de elektronische eigenschappen van Pt (in-situ XANES en ex-situ XPS), de Pt-oppervlaktestructuur (CO-strippen) en de verhouding tussen de moleculen die aanwezig zijn op het Pt-oppervlak (in situ XANES). Desalniettemin blijkt er een lineair verband te bestaan tussen de hoeveelheid zuurstofgroepen op de koolstofdrager en de katalytische activiteit van Pt. Vervolgens hebben wij de Pt/KNV-katalysatoren elektrochemisch geoxideerd om zuurstof groepen in de cirkelring van de Pt-deeltjes aan te brengen. Dit resulteerde in een reeks Pt/KNV-katalysatoren met verschillende Pt-deeltjesgrootte en een verzadigde concentratie aan zuurstofgroepen op de kooldrager in de cirkelring van de Pt-deeltjes. Voor deze katalysatoren zagen wij een hogere activiteit voor Pt/KNV-katalysatoren met kleinere Pt-deeltjes, waarschijnlijk door een belangrijkere rol van adsorptie van reactanten in de zuurstofrijke cirkelring van kleinere Pt-deeltjes.

Het ontbreken van een analytische methode om alle (tussen)producten in de routes van glucose-oxidatie te kwantificeren heeft ons gemotiveerd om een nieuwe analytische aanpak te ontwikkelen. Om de scheiding en kwantificering van alle (tussen)producten, gevormd tijdens de elektrokatalytische oxidatie van glucose, te bewerkstelligen hebben wij hogedruk anionenuitwisselingschromatografie gecombineerd met hogedruk vloeistofchromatografie. Met behulp van deze analysemethode hebben wij in **Hoofdstuk 4** het effect van de Pt-oxidatietoestand op het elektrokatalytisch oxideren van glucose in neutraal milieu onderzocht. Uit deze studie kwam naar voren dat de oppervlakte-oxidatietoestand van Pt een significante invloed heeft op het type oxidatiereactie dat plaats vindt, dat wil zeggen dehydrogenatieve oxidatie van de primaire of secundaire alcoholgroep of zuurstofoverdracht naar de aldehydegroep. Metallisch Pt (Pt^0 bij E = 0,64 V *vs.* RHE) bleek de dehydrogenatieve oxidatie van de primaire alcoholgroep te bevorderen, waardoor de vorming van glucosedialdehyde uit glucose werd bevorderd. Daarentegen is platina-oxide (PtO$_x$ bij E = 1,2 V *vs.* RHE) even actief voor het katalyseren van dehydrogenatieve oxidatie- en zuurstofoverdrachtsreacties, waardoor de omzetting van de anomere koolstof van glucose en dus de vorming van gluconaat wordt bevorderd. Ondanks de hoge selectiviteit van PtO$_x$ voor gluconaat bevordert PtO$_x$ ook de dehydrogenatieve oxidatie van secundaire alcoholgroepen van gluconaat, wat resulteert in de vorming van complexe reactiemengsels die 2-ketogluconaat en 5-ketogluconaat bevatten.

De inzichten uit Hoofdstuk 4 motiveerden ons om in **Hoofdstuk 5** de elektrokatalytische oxidatie van zetmeel (oftewel lange ketens van glucosemoleculen) te bestuderen voor de synthese van anionisch zetmeel. Het elektrokatalytisch oxideren van zetmeel zou een veelbelovende vervanging kunnen zijn voor de huidige minder duurzame industriële productie van anionisch

zetmeel gemaakt met hypochlorietoxidatie. In dit onderzoek hebben wij onderzocht 1) hoe de aanwezigheid van kortere suikerketens en suikers (KSKS) in industrieel verkregen zetmeel het elektrokatalytisch oxideren van zetmeel beïnvloedt en 2) wat de potentie is van zeer toegankelijke macroporeuze elektrokatalysatoren, bestaande uit platina gedragen door nikkel-schuim (Pt/Nis), voor het elektrokatalytisch oxideren van de grote zetmeelmoleculen. Om de invloed van KSKS op de oxidatie van zetmeel te bestuderen, hebben wij twee monsters voorbereid: één met industrieel verkregen zetmeel (d.w.z. het bevat een hoog gehalte aan KSKS) en één met gezuiverd zetmeel (d.w.z. het bevat een laag gehalte aan KSKS). Onze resultaten lieten zien dat Pt^0 actiever is voor zetmeel oxidatie dan PtO_x. Echter bevordert Pt^0 het elektrokatalytisch oxideren van KSKS over zetmeel. Dit werd bevestigd door productanalyse waaruit bleek dat zetmeel na elektrokatalytisch oxideren niet gehydrolyseerd was en ook geen meetbare veranderingen in functionele groepen vertoonde. Voor het synthetiseren van Pt/Nis hebben wij een reactor ontworpen die de elektrodepositie van Pt-zout (H_2PtCl_6) aan beide zijden van het Ni-schuim verzekert. De gesynthetiseerde Pt/Nis katalysator bleek een hoog elektrokatalytisch oppervlak van Pt te hebben, vergelijkbaar met platinazwart. Bovendien had het een hoge weerstand tegen CO-vergiftiging, wat cruciaal is voor organische synthese. Tot slot bleek het actief te zijn voor het elektrokatalytisch oxideren van industrieel verkregen zetmeel.

Hoofdstuk 6 bestaat uit een algemene discussie van de belangrijkste doelen die in dit proefschrift zijn behaald. Extra aandacht wordt besteed aan toekomstig onderzoek, waaronder 1) de kwantificering van alle (tussen)producten in de routes van glucoseoxidatie om beter inzicht te krijgen in de relatie tussen de eigenschappen van de katalysatoren en de prestaties van de katalysator, 2) de modificatie van de koolstof van koolstofdragende metaalkatalysatoren om de prestaties van de katalysator te verbeteren, 3) het ontwerp en de evaluatie van de fysische en chemische eigenschappen van macroporeuze elektrokatalysatoren die kunnen dienen voor het elektrokatalytisch omzetten van grote op biogrondstoffen gebaseerde moleculen zoals zetmeel en 4) het effect van temperatuur op de elektrokatalytische omzetting van biogrondstoffen.

Acknowledgment

The last four years have been a fulfilling period of personal and professional development for me. I would like to acknowledge the invaluable contributions of those who have supported me along the way. Their guidance and assistance have been highly relevant in my achievements, and I am thankful for their contributions.

First of all, I would like to thank **Harry** for giving me the opportunity to perform a PhD on the electrocatalytic oxidation of biomass-based feedstocks at BCT. With your support I have been able to expand my knowledge and expertise in this previously unknown field of research. You guided me through these turbulent four years and taught me to keep an overview on the projects that I had been working on. I really appreciate that you always had your office door open, allowing me to drop by for a "brief" discussion. I also enjoyed your not so typical Wageningen mentality, which sparked interesting discussions at the coffee table. Lastly, I would like to thank you for being so hospitable in hosting all the Christmas dinners and barbecues of the BCT group at your place.

Marc, I really appreciate that you agreed with Harry for allowing me to perform this PhD. You thought me the fundamentals of electrochemistry and gave me the opportunity to learn the practical basics of electrochemistry in Leiden, playing a vital role in my development within this field. Your passion for education is well reflected in how you involve Benjamin at an early age in your complex research during our teams meetings or the conferences that we had attended. Moreover, I greatly appreciate your ability to actively listen to my concerns regarding research progress and offer straightforward solutions to the challenges I was facing. I'm also grateful that you gave me the opportunity to present my work at the electrochemical society in Stockholm.

Tomas, I appreciate that you were a helping hand in the lab whenever it was needed. It is unfortunate that we barley had the opportunity to educate agrotechnologist students in life courses due to the Corona pandemic. Yet, we had quite some fun and tough runs together where we tried to accomplish the 5 km within 20 min which we almost manages to achieve. Most of all, I enjoyed our talks about beer brewing and wine making.

Paolo and **Jordi**, thank for your collaboration on the review. Despite engaging in challenging discussions, our efforts have led to an extensive and high quality review. I would also like to thank the partners, **Paul**, **Michael**, **Dhruva**, **Kasper**, from the Electrons to Chemical Bonds for their contribution on scientific discussions.

About the author

Matthijs van der Ham was born in June 1994 in Borger, The Netherlands. He finished high school in 2012 at the Adelbert College in Wassenaar after which he moved to Wageningen to study Biotechnology at the Wageningen University & Research. During his student time he was engaged with the Student Association SSR-W where he did a full-time board member year. In 2017 he continued with his MSc where he specialized in bioprocess engineering. As part of his Master program, he conducted his MSc thesis at Biobased Chemistry & Technology with a focus on the extraction of cellulose from wheat straw by using molten salt hydrates and did an internship at the water board Aa en Maas with a focus on mitigating the emission of laughing gas (e.g. a potent greenhouse gas). After his internship, in 2019, he started his PhD research at Biobased Chemistry & Technology (Wageningen University & Research) and Catalysis and Surface Chemistry (Leiden University) under the supervision of Harry Bitter, Marc Koper, and Tomas van Haasterecht. Next to his scientific research he also devoted time professionalizing his skills for fruit wine making with the brand Hollandse FruitWijnerij. The most important results of the scientific work are presented in this dissertation.

Publication list

This thesis

M.P.J.M. van der Ham, T.J.P. Hersbach, J.J. Delgado, B.D. Matson, J. Lim, M. Führer, T. van Haasterecht, M.W.G.M. Verhoeven, E.J.M. Hensen, D. Sokaras, M.T.M. Koper, J.H. Bitter, Improved electrocatalytic activity of Pt on carbon nanofibers for glucose oxidation mediated by support oxygen groups in Pt perimeter. *Applied Catalysis B: Environmental*, **338** (2023)

M.P.J.M. van der Ham, E. van Keulen, M.T.M. Koper, A.A. Tashvigh, J.H. Bitter, Steering the Selectivity of Electrocatalytic Glucose Oxidation by the Pt Oxidation State. *Angewandte Chemie International Edition*, **62**, 6 (2023)

M.P.J.M. van der Ham, J. Creus, J.H. Bitter, M.T.M. Koper, P.P. Pescarmona, Electrochemical and non-electrochemical pathways in the electrocatalytic conversion of monosaccharides and related sugar alcohols into valuable products. (2023) *Manuscript in preparation*

Overview of completed training activities

Conferences, symposia and discipline specific activities

NIOK: Catalysis: An integrated approach	Schiermonikoog, The Netherlands	2019
NKCV: ElektroChemische Conversie & Materialen	Garderen, The Netherlands	2019
Electrochemistry and Bioelectrochemistry course	Leiden, The Netherlands	2020
NIOK: Photo- and Electrocatalysis – A hands-on workshop	Eindhoven, The Netherlands	2020
Electrochemical society conference[1]	Online	2020
ECCM conference	Den Haag, The Netherlands	2020
NCCC conference[2]	Noordwijk, The Netherlands	2021
ECCM conference	Online	2021
ISE conference[2]	Stockholm, Sweden	2022
NCCC conference[2]	Noordwijk, The Netherlands	2022
NWO: CHAINS[1]	Veldhoven, The Netherlands	2022
NCCC conference[1]	Noordwijk, The Netherlands	2023

General courses

VLAG PhD week - VLAG	Baarlo, The Netherlands	2019
Competence assessment - WGS	Wageningen, The Netherlands	2019
Scientific writing - WGS	Wageningen, The Netherlands	2020
The essentials of scientific writing and presenting - WGS	Wageningen, The Netherlands	2020
Efficient writing strategies - WGS	Wageningen, The Netherlands	2020
Career perspectives - WGS	Wageningen, The Netherlands	2022

Assisting in teaching and supervision activities

BPE-12806 and BCT-23306	Wageningen, The Netherlands	2019-2022
Supervision of BSc and MSc students	Wageningen, The Netherlands	2019-2022

Others

Preparation of research proposal	Baarlo, The Netherlands	2019
PhD study trip to France	Wageningen, The Netherlands	2022
Organisation of the PhD study trip to France	Wageningen, The Netherlands	2020-2022
Weekly meeting (electrochemistry meeting, group meeting, PhD meeting)	Wageningen, The Netherlands	2019-2023

[1]Oral presentation, [2]poster presentation